Characterization of protein complexes and photosynthetic performance of *Arabidopsis thaliana* mutant plants impaired in state transition, energy-dependent non-photochemical quenching, and cyclic electron flow

by

Stefanie Lackner

Thesis submitted in fulfillment of

the requirements for the degree of

PHILOSOPHIAE DOCTOR

(PhD)

Faculty of Science and Technology

Department of Chemistry, Bioscience and Environmental Engineering

2023

University of Stavanger
NO-4036 Stavanger
NORWAY
www.uis.no

ISBN: 978-82-8439-131-1
ISSN: 1890-1387
PhD: Thesis UiS No. 672

For my cousin Martin

"*But a plant on the edge of a desert is said to struggle for life against the drought, though more properly it should be said to be dependent upon the moisture."*

— *Charles Darwin, The Origin of Species*

Acknowledgment

My Ph.D. journey is coming to an end, and I would like to thank my family and friends for always being there for me, putting all their trust in me, and offering me more than anyone can expect. During my journey as a Ph.D. student, I have also met many more people I would like to express my gratitude. They were my guides, assessors, and motivators. I am very grateful to have met each one of them at the right time and place.

In the first place, I would like to thank my supervisor and mentor Lutz Eichacker. Through believing in me he gave me not only the opportunity to work on this interesting and electrifying topic, but I was also able to set foot in a foreign place far up north from home. Thank you for giving me the freedom and support to follow my interest, and for your never-ending energy (flow) when discussing the mysteries of photosynthesis and beyond. My lab group colleagues Ann Kristin Vatland, Astrid Mork-Jansson, and Julie Nikolaison I want to deeply thank for always listening to me when I was facing challenges inside and outside of the lab, and for always standing by my side with an open heart and helpful advice. I don't know if these lines of gratitude will ever be able to express how much I must thank Andrea Ramnath. By joining my project for her master thesis, she helped me with her competence, drive, and irresistible humor through the last and hardest year of my Ph.D. I further want to thank my Ph.D. companions Gunhild Fjeld and Tia Tidwell. Thank you for your mental support, most amazing lunch breaks, and after-work gatherings. I also want to deeply thank Mark A. Stewart for his hospitality and guidance during my research stay at the University of Groningen. Thank you, Markart Meckel, for your immense help on the method development in Munich. Your experience and assistance were indispensable to my work.

Thank you, Anne-Kathrin Pichler, Cornelia List, Andreea Cojocaru, Delphine Crappe, and Ann-Kristin Vatland for inspiring me with your dreams, plans, and actions you take in life, as well as for helping me with finding the right work-life balance. I am very grateful to have you in my life! Thank you, Mama and Papa, for always believing in

me and never having any doubts about the ideas and dreams I am pursuing. Most importantly, thank you, Hadle for your immense support and for motivating me to strive for success in my career and personal matters by unintentionally pushing me and making me exceed my self-imposed limits. But most of all thank you Hadle for being my place for retreat, my cornerstone. Thank you, Eirik for always being there for me embracing me with a smile and taking me with you on all your small and big adventures. And thank you Ida for being there and giving me little kicks of motivation during finalizing my thesis, but also once out in the world for reminding me every day of the beauty in this world. You three mean the world to me!

Stefanie Lackner, Stavanger 17.02.2023

Content

Abbreviations

AA, Antimycin A

AL, actinic light

A.thaliana, Arabidopsis thaliana (plant model organism)

β-DDM, detergent n-dodecyl-β-D-maltoside

CBB cycle, Calvin-Benson-Bassham cycle

CEF, cyclic electron flow

CO_2, carbon dioxide

curt1A, the gene coding for the curvature thylakoid 1A protein

crr2 or more specific crr-22, the gene for chlororespiratory reduction -22; *A. thaliana* mutant strain deficient in *crr2*/*crr-22* coding for the NdhB protein, impairing the accumulation and activity of the NDH complex

Cytb6f, the cytochrome b6f complex in the electron transport chain

e-, electron

ECL reaction, enhanced chemiluminescence reaction (for Western blotting)

ETC, electron transport chain

F_0, dark fluorescence yield when all PSII centers are open after dark preincubation

F_0', dark fluorescence yield during actinic light illumination calculated after Oxborough and Baker 1997 or measured after a short pulse of FR light is used to oxidize PSII

F_m, maximal fluorescence yield when all PSII centers are open after dark preincubation

Abbreviations

F_m', maximal fluorescence yield during illumination; lowered in respect to Fm due to NPQ

F or F_S, current fluorescence yield

Fd, ferredoxin

FR, far-red

h, hour(s)

Hiba, -2Hydroxyisobutyric acid (for FFE buffers)

HL, high light

IZE-FFE, interval zone free flow electrophoresis

kDA, kilodalton

LRE, light-response experiment with PAM spectroscopy (increasing light intensities)

LDS, Lithium dodecyl sulfate

LHCII, light-harvesting complex II (Lhcb1 and Lhcb2)

LEF, linear electron flow

LL, low light

ML, measuring light

Native-PAGE, Native- polyacrylamide gel electrophoresis

NDH, NADH dehydrogenase-like complex

Nm, nanometer

NPQ, non-photochemical quenching after Stern-Volmer approximation

Abbreviations

npq4, the gene for non-photochemical quenching 4; *A. thaliana* mutant strain deficient in *npq4* coding for the PSBS protein or PSII subunit S, impairing the fastest form of NPQ called qE

O_2, oxygen

OE CurtA, *A. thaliana* mutant strain overexpressing the protein-coding for the gene *Curt1a* leading to changes in the thylakoid membrane structure

pgr5, gene in proton gradient regulation 5; *A. thaliana* mutant strain deficient in the *pgr5* gene; impairing the protein PGR5 and thus impaired in PGR5/PGRL1-dependent CEF

P_0, P700 signal after dark preincubation

P_m, maximal P700 change

P_m', maximal P700 change during illumination; Pm' lowered in respect to P_m due to PSI acceptor side limitation

Pmf, proton motive force

Pc, plastocyanin

pph1, the gene for protein phosphatase 1 (or TAP38 Thylakoid associated phosphatase 38); *A. thaliana* mutant strain deficient in *pph1*, impairing the phosphatase PPH1 and thus state transition

PsbS, Photosystem II chlorophyll-binding protein (knocked out in the npq4 mutant)

PSII, photosystem II

PSI, photosystem I

PQ, plastoquinone (oxidized form)

PQH_2, plastoquinol (reduced form)

RC, reaction center

RCII, reaction center photosystem II

RCI, reaction center photosystem I

SP, saturation pulse (6000 µmol m-2 s-1 for 200 ms)

stn7, the gene for protein kinase stn7; *A. thaliana* mutant strain deficient in *stn7*, impairing kinase STN7 and thus state transition

TBS, solution containing 0.02 Tris-HCl pH 7.5 and 0.15M NaCl

WTcol, wild-type ecotype Columbia

WTgl1, wild-type ecotype Columbia gl1

WTler, wild type ecotype Landsberg erecta

Q_A, primary e- acceptor of PSII

Y(NA), PSI's acceptor side ferredoxin

Y(ND), PSI's donor side plastocyanin

µE, unit of light intensity equivalent to µmol m-2 s-1

µmol m-2 s-1, unit of light intensity

Note:

In the text, genes are written in lower-case letters and italics (e.g. *stn7*), proteins are written using upper-case letters (e.g. STN7) and mutants are written in lower-case letters, and mutant is added (e.g. the stn7 mutant).

Abstract

For optimal photosynthesis, the photosystem complexes in the plant leaf adapt to their light environment. In a process termed “state transition”, light energy distributes between photosystem II (PSII) and photosystem I (PSI), which is regulated by exchanging a mobile light-harvesting antenna complex termed LHCII. When light intensity rises, mobile LHCII is phosphorylated by the protein kinase state transition 7 (STN7), and the area of single membrane layered parts of the thylakoid membrane - termed stroma thylakoid membrane increases. The kinase STN7 was shown to localize in a complex with the cytochrome b6f (Cytb6f) complex. The regulation of the kinase activity correlated with the reduction state of the plastoquinone pool[1]. Also, a corresponding LHCII phosphatase termed phosphatase 1 (PPH1 or TAP38) has been identified as constitutively active. According to the established models for regulation of light energy distribution, two states have been defined: In state 1, non-phosphorylated LHCII is binding to PSII, and the number of grana layers is increased, whereas in state 2, phosphorylated LHCII is binding to PSI and the number of grana layers is decreased. Recently, it was found that the binding of phosphorylated LHCII to PSI and membrane biogenesis during state transition operate independently. Also, the shift between cyclic (CEF) and linear (LEF) photosynthetic e- flow was claimed to be independent of state transition but controlled by the dynamic thylakoid membrane changes[2]. According to one of the latest models, an increase in grana layers increases CEF based on a separation of the grana localized plastoquinone (PQ) pool(s) from the stroma thylakoid membrane, while more stromal thylakoid layers and decreased grana stacks facilitate an increase in LEF[3]. Another proposal assumes that at low-intensity light, in the stn7 mutant- with increased grana stacks decreases the capacity to perform CEF and LEF, while in the pph1 mutant- with a reduction in grana layers and increase in stroma thylakoid surface is increasing LEF and CEF[2]. In an attempt to differentiate between changes associated with the phosphorylation of LHCII and with the flow of electrons, mutants lacking STN7 (the stn7 mutant), PPH1 (the pph1 mutant), and mutants lacking a functional NADH dehydrogenase-like (NDH) complex (the crr-22

mutant referred later to as crr2) or proton gradient regulation 5 (PGR5) (the pgr5 mutant) were investigated. In addition, the role of qE- the fastest form of non-photochemical quenching (NPQ) was examined using the npq4 mutant, which lacks qE because the Photosystem II chlorophyll-binding protein (PsbS) is knocked out. Mutants were grown under standard light regimes. The composition of protein complexes in the stroma thylakoid membrane was examined, and the plant's capacity to adapt to low and close to growth light intensity and increasing light intensities was measured. We found that the mutants stn7 and pph1, as well as the npq4, crr2, and pgr5 mutants change the thylakoid distribution of photosystem complexes as well as the composition of electron flow.

In this study, we found an increase in higher molecular weight (HMW) complexes and phosphorylated LHCII molecules in the stroma thylakoid membrane in both the pph1 and the crr2 mutant. In contrast, fewer HMW complexes were found in the stn7 mutant characterized by an increase in grana stacking, and more PSI-Cytb6f complexes were present. When looking at the photosynthetic performance at actinic light close to growth light conditions, LEF was both enhanced in the pph1 and the crr2 mutant, while in the stn7 and the npq4 mutant, CEF was favored. We propose that both the pph1 and the crr2 mutant have a more balanced light utilization at PSII and PSI which is favoring LEF, while in the stn7 and the npq4 mutant, more light is utilized at PSI relative to PSII facilitating CEF. Therefore, our observations indicated that like in the state transition mutants, also the *npq4* mutation plays a role in the distribution of light between PSII and PSI. When NDH-dependent CEF is absent in the crr2 mutant, an increase in PGR5-dependent CEF was noticed, while in the pgr5 mutant, after the onset of actinic light when low or close to growth light conditions were used, the mutant was depending on LEF only. The amount of phosphorylated LHCII was increased in the pgr5 mutant, and a far-red (FR) light-induced state 2- to- state 1 transition was slower relative to WT indicating that the absence of PGR5/PGRL1-dependent CEF was facilitating LEF. After prolonged illumination with low (below growth light) actinic light, the plant switches from state 2- to- state 1 and increases NDH-dependent CEF relative to LEF. In both pgr5 and stn7 mutants, NDH-dependent CEF was enhanced. An increase in

Abstract

NDH-dependent CEF was absent in the crr2 mutant and reduced or missing in the pph1 mutant. In the crr2 mutant, we have observed an increase in phosphorylated LHCII at PSI. This observation lets us hypothesize that the arrested binding of phosphorylated LHCII to PSI in the pph1 mutant, interferes with the binding of the NDH complex. We hypothesize that a functional NDH-dependent CEF is established by NDH complex assembly with PSI in state 1- when the PQ pool is in an oxidized state. In contrast, under conditions such as after dark preincubation and under HL when the PQ pool is in a reduced state PGR5/PGRL1-dependent CEF is employed. On the opposite, when prolonged illuminated under growth light conditions the plant favors LEF over the performance of PGR5/PGRL1-dependent CEF.

1. Introduction

1.1 The chloroplast and its energy balance

A plant cell contains a ligneous wall and plasma membrane, which are surrounding an aqueous, cytosolic compartment. Inside the cell, a very interesting organelle resides, which is composed of a double membrane: the chloroplast. With its double membrane, it encloses an aqueous stromal compartment, which is composed of a complex network of thylakoid membrane structures, including proteins, pigments, and redox cofactors to transfer light energy into chemical forms of energy (i.e., NADPH and ATP) through the transfer of electrons (e-) along its electron transport chain (ETC) combined with the shuttling of protons through the membrane[4]. NADPH and ATP are in turn used, among many other processes, for fixation of CO_2 and synthesis of sugar phosphates[5]. The specific cell network in a leaf allows CO_2 to be taken up into the intracellular space through stomata before diffusing into the cell to serve photosynthesis. Light absorption in the visible part of the electromagnetic spectrum, mostly from the red and blue region empowers photosynthesis[6]. Absorption occurs within specialized pigment-binding protein complexes, such as photosystem II and I (PSII and PSI)[7], localized within the thylakoid membrane[8]. When working in series, photosystems are operating a linear electron flow (LEF), and electrons can be utilized e.g. to fix CO_2; whereas when LEF is not possible, cyclic electron flow (CEF) is employed. In both modes of operation, electron flow in photosynthesis is linked to the transfer of protons at the cytochrome b6f complex (Cytb6f) and it also drives the transport of ions across the thylakoid membrane[9,10]. Hereby, a trans-thylakoid proton motive force (pmf) is established, with both an electrical component (Δpsi) (especially K+ and Cl- ions)[11] and a chemical pH gradient (ΔpH)[12,13].

During LEF, the absorbance of four photons each is energetically required to drive photosynthesis at PSII and PSI. At PSII, four photons drive the oxidation of two H_2O molecules. Hereby one O_2 molecule is generated. Also, four protons (H^+) are released into the thylakoid lumen and four electrons are generated that are stored in two mobile

quinone molecules through fixation of another four protons from the chloroplast stroma (Fig. 1). At PSI, the four electrons released from PSII are technically sufficient for the parallel light-dependent reduction of two molecules of $NADP^+$. However, while flowing to PSI, the energy stored in the two quinones is also used by Cytb6f. The energy is utilized to establish a proton gradient across the thylakoid membrane through the release of the four stromal protons fixed at the stromal side of PSII into the lumen. Interestingly, only two of the four electrons from the two quinones are directly transported to PSI and are available for reduction of one $NADP^+$. The remaining two electrons are reutilized in an internal quinone cycle and formally synthesize one extra quinone and regenerate a semiquinone if the Q-cycle is preloaded (Q-cycle)[10,14–16]. Hence, an additional two photons are required at PSII to operate the Q-cycle and provide another two electrons required to synthesize the second NADPH molecule. In this state, a minimum of six photons at PSII and four photons at PSI accumulate a net of fourteen protons inside the thylakoid lumen. This number of protons establishes the minimum pmf[9] which is required to turn the ATPase membrane motor one full circle and enable the synthesis of three ATP. In *Arabidopsis thaliana*, the H^+/ATP ratio should hence be 4.66[17]. Although, the exact H^+/ATP ratio for ATP synthesis is still elusive[18], the high-resolution structure of the complete chloroplast ATP synthase with 14 c-subunits[19] supports the predicted ratio of 14 H^+/3 ATP, and hence the minimum of three ATP and two NADPH molecules as biochemical energy and redox capacity minimum, for fixation of one CO_2 molecule[5].

In conclusion, in *A. thaliana*, an energetic minimum of a total of 8 photons appears required for the synthesis of two NADPH in LEF. In addition to the utilization and the regeneration of the transient quinone and the synthesis of the second NADPH molecule, two extra photons are required at PSII to provide the additional quinone to supply PSI with the required electrons on its donor side and accumulate the extra protons required for the synthesis of three ATP molecules through LEF. Interestingly, the energetic minimum number of 10 photons and 14 protons required in Arabidopsis to achieve the corresponding minimum 3ATP/2NADPH stoichiometry for CO_2 assimilation is achieved at a photon ratio of 1.5 between PSII (six photons) and PSI (four photons). At

a higher photon flux, also a photon ratio of 1, with 6 photons at both PSII and PSI may be considered. At this state, both LEF and CEF processes may be working in parallel. At an equal absorbance of six photons at PSII and PSI, an accumulation of 16 protons can then be established. Here, the photon ratio is either at 1 contributing to LEF and CEF or maintained at 1.5 for the photons contributing to LEF. The additional two photons used at PSI in CEF may establish a CEF to LEF ratio of 2/10 or 20%. Hence, either LEF alone or a combination of LEF and CEF is regarded to meet the ATP/NADPH stoichiometry requirement in photosynthesis [20,21]. The two photons utilized in CEF only contribute with two protons to the overall pmf gradient and hence may be regarded as not essential to sustain ATP synthesis if the light intensity at PSII and PSI is equally distributed. However, it can be envisioned that CEF balances the use of different light intensities that may excite PSI in excess relative to PSII. Herein, the CEF-specific synthesis of quinone maintains the key redox cofactor to supply the donor side of PSI with electrons; whereby, an inhibition of PSI-dependent synthesis of NADPH in LEF is avoided, while the synthesis of ATP that is at large driven by the activity of PSII and the Cytb6f complex is maintained.

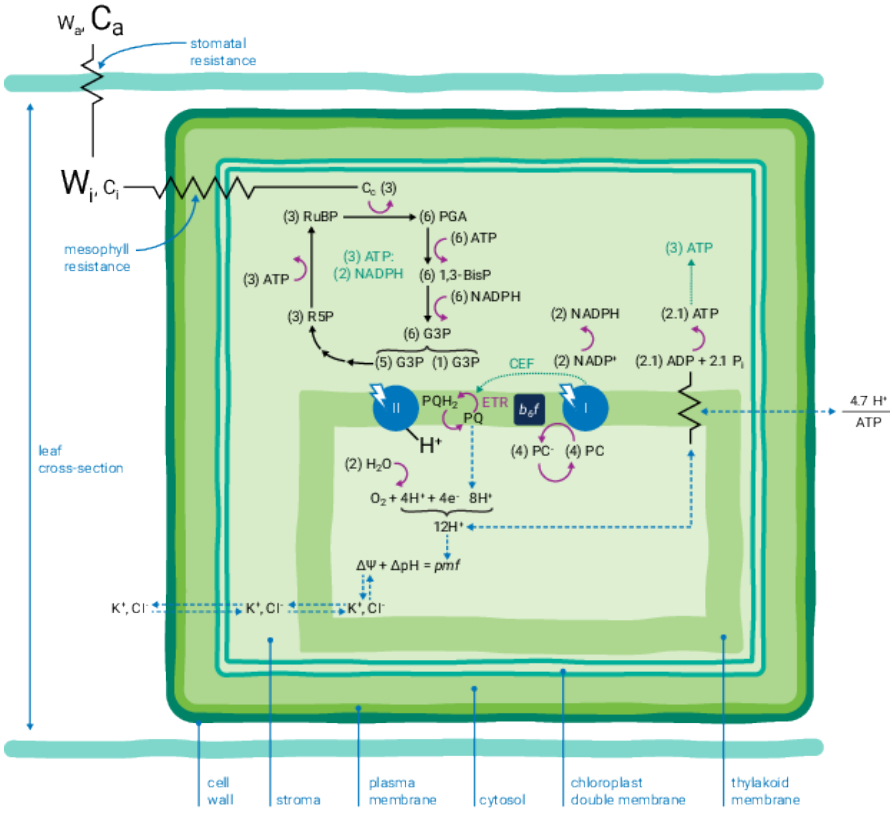

Figure 1. Simple schematic overview of key gas-, liquid-, and membrane-phase metabolic reactants of a photosynthetic chloroplast embedded in a leaf cell. The simplified scheme contains biophysical and biochemical photosynthetic reactions, such as the light reaction of the pigment-binding protein complexes PSII and PSI, the Calvin-Benson-Bassham (CBB) cycle, the ATP synthase and the formation of *pmf*, which are all depending on the interplay between e-flow inside the photosynthetic e- transport chain and the transfer of protons and ions from the lumen across the thylakoid membrane to the stroma. (Adapted from https://www.licor.com/env/support/LI-6800/topics/theory-gas-exchange.html)

The natural light energy supply for ATP and NADPH synthesis is the key element that must be coordinated dynamically by the biochemistry of photosynthesis to meet the changing light environment. For this purpose, the plant developed a couple of strategies to adapt light harvesting, e- transport, and carbon assimilation. In short, the plant tries to remain in balance to reduce the production of reactive oxygen species, being harmful to the photosynthetic machinery, and to balance photosynthetic input with metabolic output through regulating photosynthetic energy flow. This complex regulation

involves but is not limited to any feedback and feed-forward mechanisms such as the binding of light-harvesting complexes (LHC) to either PSII or PSI during the performance of state transition balancing light absorption and the regulation of photoprotective mechanisms such as non-photochemical quenching (NPQ) of excess light energy. Moreover, it includes the establishment of a proton gradient controlling e- transport, CBB cycle enzymes, redox control over CEF and ATP synthase and CBB cycle enzymes, ATP control of CBB cycle enzymes, and Pi control of ATP synthesis (Fig. 2). In short, the photosynthetic interplay between e- and proton transport and its influences on other mechanisms is very complex. Excessive research has been performed to unravel the plant's secret survival and adaptation mechanisms that happened since the divergence of land plants between 400 and 700 million years ago[22,23] when significant fluctuations in light intensity and quality, dehydration, and a life with gravity had to be overcome[24–26]. In the recent literature, a link between light adaptation mechanisms and the regulation of e- transport modes through controlling proton transport have been addressed. Still, a lot of open questions remain. In this introduction, a summary is presented on experimental findings and theoretical models on light absorption/quench and e- transport regulation and the impact on other regulatory pathways during a dark-to-low light transition and when the plant is acclimating to different light intensities and qualities.

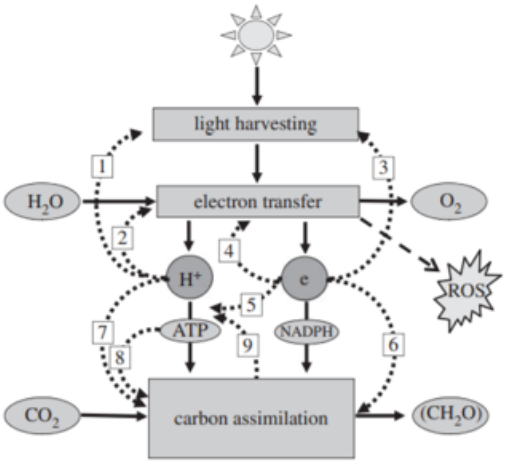

Figure 2. Regulatory feedback (arrows 1 – 4, 9) and feed-forward (5-8) mechanisms between light harvesting, e- transport, and carbon assimilation. 1. Proton gradient (H^+) control of photochemical quench, NPQ, 2. Proton gradient (H^+) control of e- transfer, 3. Redox control of state transition 4. Control of linear (LEF) and cyclic (CEF) transfer of electrons by redox state, 5. Redox control of ATPase activity, 6. Redox control of carbon assimilation, 7. Proton gradient (H^+) control of carbon assimilation 8. ATP control of carbon assimilation 9. ADP and Pi controlling ATPase. Adapted from Horton 2012[27].

1.2. Non-photochemical quenching (NPQ)

1.2.a Function, measurement, and different forms of NPQ

As already discussed in chapter 1.1, light energy is utilized by plants as an energy source that is driving the synthesis of NADPH and ATP, which are further used to fix CO_2 from the atmosphere. Solar energy is absorbed in LHC stacked inside chloroplast thylakoid membranes and is rapidly transferred to the photosynthetic reaction centers of each photosystem. When the absorbed light energy supply is not meeting the plant's energy demand, chloroplasts adjust the protein composition and especially increase the chlorophyll-containing antenna proteins in the LHC and rearrange the thylakoid membrane structure. However, when light supply exceeds its use in photosynthesis and the proton concentration in the thylakoid lumen is maintained high, a conformational change in the light-harvesting antenna is initiated resulting in non-photochemical

quenching (NPQ) of the absorbed light energy. Through this transformation, the antenna can turn from an efficient light-harvesting state into an efficient light-leaking state, transforming the captured light energy into heat, whereby damage to the photosynthetic machinery is prevented[28]. Many different forms of non-photochemical quenching exist, such as energy-dependent quenching qE, state transition-mediated quenching qT, zeaxanthin-dependent quenching qZ, and photoinhibitory quenching qI. These different forms are operating in different cellular locations and on various timescales. Without these mechanisms, the excitation "overload" of the reaction center capacity would lead to photoinhibition, leading to a decline in the electron transport rate and hence the plant's photosynthetic efficiency. It has been described that the oxygen-evolving photosystem II reaction center (PSII) is most vulnerable to excess light exposure, which in both its oxidized and over-reduced state can be damaging to pigment-containing protein complexes of the photosynthetic apparatus[29]. Through the initiation of NPQ and its major and rapid reversible component termed qE or energy-dependent quenching, the photosynthetic machinery is however able to prevent the accumulation of excess energy around the reaction center of PSII (RCII)[30–32]

The quenching of light energy in the form of heat, qE, is difficult to measure directly because it dissipates in time and space. However, it can be indirectly assessed using the fluorescence emission of chlorophyll[32]. When a leaf is exposed to a saturating short pulse of high-intensity light, a fast fluorescence maximum is determined that can be localized to originate at the level of PSII. If the light is applied as continuous illumination, a fast increase followed by a slow decrease in the level of fluorescence was found. It was concluded that in continuous light, the kinetic changes in the fluorescence intensity mirror the photochemical steady-state between light-dependent physical and light-independent biochemical reactions. In contrast, pulsed light triggers a change in the fast light-dependent reactions of the reaction centers and hereby affects the fluorescence signal, while no changes in the biochemical reactions can be expected within this timeframe that led to changes in the redox state of the reaction centers donor and acceptor sides. In the presence of continuous light, the decrease in fluorescence emission was ascribed to light quenched by photochemistry and transformed into heat

(by NPQ). NPQ is indicative of excessive light energy that can no longer be utilized by PSII but is discarded via heat[28]. NPQ can be readily observed when the plant leaf is dark-adapted before the continuous or actinic light (AL thereafter) is switched on. In the dark, two key fluorescent parameters F_0 and F_m can be determined. Using a pulsed non-photosynthetic measuring light (ML), the minimal fluorescence value, F_0, can be determined and taken as a measure of the reaction center number of PSII which is in an oxidized also termed open state. Upon application of a saturating pulse of light, a change in the fluorescence level when only ML is applied is determined. Its maximum is recorded as the maximal fluorescence value, F_m, that can be determined only when the plants are in a dark-adapted state. In this condition, F_m represents the total number of reaction centers of PSII that can change from an open into a closed state. The difference between the F_m and F_0 value represents the difference between the number of PSII in the open and the closed state and is also termed the variability of plant leaf fluorescence. Normalization of the variable fluorescence value $(F_m-F_0)/F_m$ (or F_v/F_m) is then taken as an estimate of the PSII quantum yield. This normalized value has been found of great value to compare the overall functional status of the photosynthetic machinery of a plant leaf and its metabolic status before experimental measurements are initiated. Also, continued measurement of maximal fluorescence can be conducted at different time points after AL has been switched on. In the presence of the photosynthetically active AL, the F_m' value, also mirrors the change of the ML in the presence of the saturating pulse (SP) or the total amount of PSII that is closed in the presence of both the actinic and the saturating light. It was found that F_m' which is always measured kinetically after the light has been switched on, is typically decreased relative to F_m. A decrease in the F_m' value relative to F_m in the presence of light-dependent photochemistry comes as a surprise because it indicates that the total number of open reaction centers that can be closed by the light pulse has been decreased already within a very short time frame after the induction of AL. The decrease in maximal fluorescence could indicate that the rate of photon utilization in photochemistry increased or/and that the number of photons that reach the reaction centers for photochemistry decreased (through NPQ). Interestingly, the decrease in the fluorescence peak can be viewed from two directions. Either the value of F_m' is

compared to the value of F_m relative to the basis of F_0, or the independent difference between the F_m' and the F_m value is analyzed and its normalized value $(F_m-F_m')/F_m'$ is used to compare the non-photochemical quench (NPQ) activity in different plant leaves.

Several different mechanisms for NPQ exist that differ in their induction and relaxation kinetics as well as in their dependence on known factors. The fastest mechanism, qE or energy-dependent quenching is induced and relaxed within minutes. The energy quench mechanism relies on the PsbS protein and the enzyme violaxanthin de-epoxidase (VDE) which converts violaxanthin to zeaxanthin[33–35]. qE is triggered through the formation of a proton gradient (ΔpH) across the thylakoid membrane[36–38]. It has been shown that the rate of PQ reduction by PSII is regulated by qE[39,40] (see paragraph 1.2.b). A second mechanism, which is relaxing over several hours is associated with damaged PSII centers and is termed qI or photoinhibitory quenching[41]. It has been shown that its recovery requires translation and assembly of D1 polypeptide with the PSII core[2]. However, not all qI-related changes can be explained by damage to RCs, and thus it is anticipated that the photoinhibitory quenching mechanism resulting in fluorescence quenching involves other components contributing to its slow relaxation[43]. This slowly reversible NPQ component qI has been shown to occur mostly at PSII through the exposure of the photosynthetic organisms to strong light due to an imbalance between the rate of photodamage to PSII and the rate of repair of damaged PSII[44–47]. Additionally, strong heat stress damages the oxygen-evolving complex in PSII directly[48]. Moreover, environmental stresses, such as limitation in CO_2[49,50], moderate heat[51], and low temperature[52] especially under high light exposure have been shown to inhibit the repair of PSII through suppression of the *de novo* synthesis of proteins. In contrast, PSI is more resistant to photoinhibition. PSI photoinhibition has been shown to occur in *A. thaliana* when exposed to high light under chilling temperatures[53]. Additionally, it was shown in sunflower leaves that short high-frequency light flashes of high light intensity applied to dark-adapted plants are leading to severe photodamage, especially in PSI centers when O_2 was present[54]. It has however been discussed that a plant under natural conditions does not encounter these high-frequency strong light pulses[55]. More recently, an experimental approach has been published to

induce PSI photoinhibition. PSII light from commercially available LED greenhouse lamps was applied at a lower intensity than growth light (hereby not inducing photochemical protection mechanisms), to overreduce the ETC. Then, by repetitively applying light flashes leading to the saturation of PSI, electron acceptors cause the production of reactive oxygen species that are leading to the photoinhibition of PSI by damaging its FeS centers[55].

During a dark to high light transition, both qE and qI can be estimated using pulse-modulated fluorescence spectroscopy through the induction and relaxation of NPQ (Fig. 3). For the determination of other quench parameters such as qZ and qT (described below), the right conditions for their induction must be chosen. For example, qT will be reflected in changes in F_m' during low light intensities, while in the case of qZ, high light exposure for a prolonged time is needed, leading to a decrease in F_m' that needs several minutes to relax/increase again when the light was turned off.

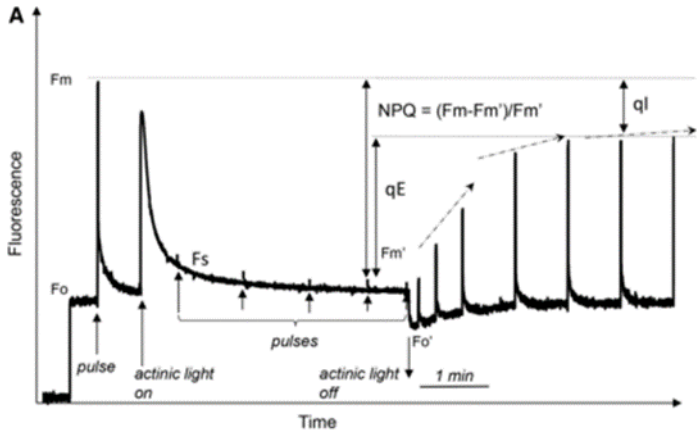

Figure 3. Induction and relaxation of NPQ during pulse-modulated spectroscopy of an *A. thaliana* leaf. In dark-preincubated leaves, F_0 and F_m are the minimal and maximum fluorescence levels before AL was turned on, whereas F_m' is maximal fluorescence during AL illumination (1000 µmol m-2 s-1). F_s is the steady-state fluorescence level. For the estimation of F_m and F_m', 10000 µmol m-2 s-1 saturating pulses of light were applied to close all RCIIs. qE is a quickly and qI is a slowly reversible component of NPQ, respectively. Adapted from Ruban 2016[28]

Another component termed qZ, or zeaxanthin-dependent quenching induces and relaxes within tens of minutes and depends on the formation of zeaxanthin[41,56]. In

contrast to ΔpH-dependent qE, qZ once zeaxanthin is synthesized is independent of ΔpH which was shown by lowering ΔpH through infiltrating leaves with the K^+/H^+ exchanger nigericin[35,56]. Another NPQ component is termed qT and describes a change in light energy distribution between PSII and PSI in a process termed state transition, which displays similar kinetics to qZ and is working within several minutes. Using the term quenching in the mechanism of state transition may be misleading because here quenching does not mean energy loss but rather energy transfer from one to another photosystem. The process balances the rate of light energy absorption at PSII and PSI through moving phosphorylated antenna molecules between the two photosystems. Phosphorylation of the antenna protein is depending on the kinase STN7 and phosphatase PPH1/TAP38 (referred to hereafter as PPH1)[31,36,57,58]. qT is operating at low light conditions and has been demonstrated to be inactivated at high light intensities through redox regulation mechanisms and a high ΔpH[59,60]. qT will be discussed in more detail in paragraph 1.2.c. Moreover, the plant also possesses the ability to move its chloroplasts within the cell leading to a decrease in fluorescence, termed qM[61]. Recently, also a slow relaxing component of NPQ termed qH was discovered[42,62]. The quenching component qH has been demonstrated to locate in the peripheral antenna of PSII[62,63] and is independent of PsbS, ΔpH, zeaxanthin formation, the activity of STN7, and photoinhibition of the D1 protein[63]. Moreover, qH is regulated by the suppressor of quencher protein 1 (SOQ1)[63]. The existence of further components and interaction between different mechanisms is likely. The next paragraphs will focus on the most thoroughly studied quench mechanism qE and the more unknown much slower energy transfer through qT. Both the lack of qT and qE showed a decrease in plant growth and influences the reduction state of plastoquinone (PQ) in fluctuating light and are concluded to play an important role under natural light conditions[64–66].

1.2.b Location, initiation, mechanism, and physiological role of qE

During the last decades, it has been excessively debated where the site of qE is located in the RC or antenna of PSII. A model was describing qE to take place in the RCII. On

the assumption that low lumen pH raises the redox potential of the acceptor side of PSII through releasing bound Ca^{2+}, charge recombination in the RC may be promoted and energy released as heat[67,68]. However, it was not clear if this process described qE or a stress-related photoinhibitory process in RCII[69]. In contrast to this model, it was further shown that also when RCII was completely open, qE was leading to a significant drop in fluorescence[30,69]. Moreover, qE was found to be activated at 77K when all photochemical processes, being the basis for RCII-mediated qE, were inhibited[70]. Evidence was presented that qE is originating at fluorescence bands showing quenching of fluorescence that were coming from LHCII complexes[70]. It was spectroscopically differentiated between bands quenched by RCII activity-termed photochemical quenching (qP) at 685 nm and 693 nm or quenched by qE at 680 nm and 700 nm associated with LHCII[71]. Moreover, through genetic manipulation studies, it was shown that when plants were missing LHCII antenna proteins qE levels dropped[72–74].

Eventually, it was shown that the fluorescence emission of isolated LHCII complexes could be lowered more than 10 times at low pH[1,2]. It was suggested that a low lumen pH resulted in an aggregation of LHCII and its importance for qE was supported by the findings that the addition of antimycin A (AA), which is decreasing ΔpH through inhibiting PGR5/PGRL1-dependent CEF, was inhibiting both qE and LHCII aggregation[75,76]. In addition, the LHC xanthophyll zeaxanthin was found to facilitate a stronger aggregation of LHCII than violaxanthin[75,76]. It was further proven that the de-epoxidation of violaxanthin to zeaxanthin is initiated during light exposure, with the responsible enzyme violaxanthin-de epoxidase (VDE) being activated when a high ΔpH is formed and qE being turned on in the presence of zeaxanthin[33,77]. Later it was also shown that qE can take place if zeaxanthin is missing but that the addition of zeaxanthin to isolated LHCII molecules at low pH increased the build-up of qE while adding violaxanthin retarded its formation[69,78,79]. This suggested that zeaxanthin is not needed for quenching per se but rather promotes its establishment[80]. It was further shown that around 80% of the violaxanthin/zeaxanthin transformation that is taking part in the xanthophyll cycle is found at the major LHCII complex. Moreover, these

xanthophylls were also detected in minor LHCII complexes (CP24, 26, and 29) but here it was found that violaxanthin was less efficiently de-epoxidated[81–83].

In an attempt to find the location and mechanism of the molecule(s) that dissipate the excess energy, the npq4 mutant lacking the PsbS protein was found to miss the rapid induction of qE[34]. This was determined through a qE-mediated light-induced conformational change in the thylakoid membrane that can be determined by a change in absorbance at 535 nm (ΔA_{535})[84,85]. In WT, an absorbance maximum is recorded at 505 nm and an absorbance shoulder to the peak is determined at 535 nm, which has been assigned to the transformation of violaxanthin into zeaxanthin by the xanthophyll cycle by comparison with the absorbance recorded from the npq4 mutant[86]. In the npq4 mutant, ΔA_{535} was absent. Additionally, the assessment of NPQ induction and relaxation kinetics showed that the npq4 mutant was defective in qE (Fig. 4)[34]. However, when treating intact chloroplasts with the protolytic agent diaminodurene (DAD), which enhances the formation of ΔpH by transferring protons into the chloroplast lumen, it resulted in the rapid and photoprotective induction of qE and ΔA_{535} in the *npq4* mutant[26]. With the induction of qE achieved without PsbS, this further indicated that the quenching process itself is independent of the PsbS protein but that it needs a larger ΔpH and hence acidic lumen to trigger a response, such as for example the reorganization of the PSII-LHCII structure. This data, therefore, provides experimental support for PsbS's role as a catalyst in qE.

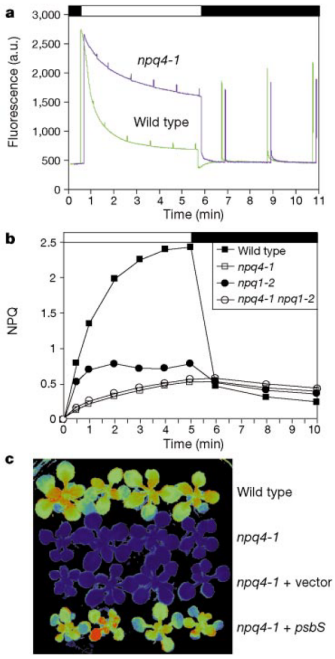

Figure 4. Chlorophyll fluorescence kinetics of *A. thaliana* leaves displaying a. Steady-state fluorescence F_S (offset by 10 sec in the npq4-1 mutant relative to WT), b. NPQ induction and relaxation kinetics (NPQ= $(F_m-F_m')/F_m'$) after 1250 µmol m-2 s-1 illumination (white bar) and darkness with only weak ML (black bar), and c. chlorophyll fluorescence video imaging after illuminating plants for 1 min with 800 µmol m-2 s-1. Adapted from Li et al. 2000[34].

It was further shown that PsbS, the protein missing in the *npq4* mutant[34] was independent of the RCII complex and did not bind any pigments[87]. Instead, PsbS was found to contain amino acids which can be protonated[88]. It was suggested that PsbS acts as a sensor that detects ΔpH. In addition, PsbS works independently of the xanthophyll cycle as the overexpression of PsbS in plants deficient in zeaxanthin synthesis enhanced qE[89]. Leaves were depleted of zeaxanthin when infiltrated with dithiothreitol (DTT), which inhibited violaxanthin de-epoxidation [89]. Moreover, at the onset of light, the overexpressor of PsbS (L17) was performing more qE (NPQ) than WT plants in the absence and presence of DTT corroborating PsbS's ability to promote qE and its independence of zeaxanthin. Furthermore, another mutant (npq1) that did

not possess zeaxanthin still performed qE[90]. More genetic studies, removing a single minor and or all LHC (No M plants) showed that qE requires the presence of the proton gradient, the PsbS protein, and LHCII trimers[91–94].

For understanding the operational mechanism of qE, structural analysis of LHCII complexes was conducted in intact membranes through freeze-fracture electron microscopy. Studies showed that in the qE state, the average distance between LHCII trimers became significantly shorter. This finding implied that LHCII trimers were establishing protein clusters that are resembling the LHCII aggregates studied *in-vitro*[95–97]. In addition, the cluster formation was reversible through dark incubation and was elevated when PsbS and zeaxanthin were present[96,97]. FRAP experiments revealed that zeaxanthin was inhibiting the mobility of LHCII inside the thylakoid membrane, while the presence of PsbS significantly enhanced LHC mobility[95,96]. However, when qE was initiated, LHCII clustering increased and kept the LHCII molecules less mobile[95,98]. It was further shown, that in the mutant overexpressing PsbS, LHCII clustering was increased relative to WT, and LHC mobility was decreased at the onset of light while the rate of state transition increased[95–98]. Next, it was tested what happens with the PsbS protein when ΔpH was formed and qE was turned on. It was found that in the dark, PsbS is a dimer, which is very non-specifically and weakly interacting with LHCII complexes (major and minor)[99,100]. When protonated through the build-up of ΔpH it monomerizes, changes its location, and increases its binding capacity to the antenna molecules[100]. This binding was further elevated through the assistance of zeaxanthin[100]. Through the changes in binding, the antenna becomes more clustered within the thylakoid membrane. On the contrary, deprotonated PsbS was found to promote the change back to an unquenched state and hence dissolving LHCII clusters, while zeaxanthin was in contrast found to facilitate aggregation[98,100]. Besides aggregation, quenching in isolated LHCII was achieved through initiating a conformational change in the structure by high hydrostatic pressure, in single fluorescence spectroscopy (SMS) experiments, when investigating the structure and function of the fluorescence spectral dynamics of single LHCII trimers close to room temperature on sub-second-to-second timescales, or when polymerized in

polyacrylamide gels[101–103]. Thus, results show that qE is initiated through structural changes within LHCII and both PsbS and zeaxanthin can facilitate its sensitivity to protons. Regarding the site of quenching with LHCII, lutein and chlorophyll dimers formed through the conformational change in LHCII have been discussed to operate as quenchers in an activated state[104,105]. However, the exact site of quenching is still elusive and different changes in pigment-pigment interaction (chlorophylls and xanthophylls) cannot be excluded as the details of changes leading to qE are still not known, as long as no structure of LHCII in a quenching state has been determined [106].

The physiological role of qE in removing excess light energy and preventing photosystem damage is well understood and accepted to be controlled by the level of ΔpH across the photosynthetic membrane[107]. However, it has to be kept in mind that ΔpH as a light exposure sensor is also involved in driving ATP synthesis, and when elevated also reduces e- flow at the Cytb6f complex and inhibits e- donation to PSII through suppressing the oxygen-evolving complex causing photoinhibition[108–111]. It is suggested that ΔpH must be regulated within very narrow limits, to regulate the degree of quenching especially at low light when light-dependent ΔpH levels are also required to regulate ATP synthesis. At the physiological level, lumen pH is around 5.8[112], and the pK of LHCII molecules which is around 4,0, is too low to initiate qE[81,112,113]. However, efficient qE, through protonating LHCII molecules at very low light intensities has been proven to be regulated through the presence of PsbS, and the activation of VDE which both are already protonated and activated at a pK of 6,0[87,114] (Fig. 5). Moreover, the formation of zeaxanthin when about 80% of violaxanthin is de-epoxidated, has been demonstrated to raise the luminal pK of LHCII from 4,5 to 6,5, facilitating the protonation and aggregation of LHCII molecules and thus allowing the protonation at moderate light levels and low ΔpH, hence amplifying qE[26,28,98,115]. When LHCII begins to aggregate, and their surrounding environment becomes more hydrophobic, increasing the affinity for protons is leading to a conformational change and the establishment of qE. It has been shown that the pKa of glutamate and aspartate are significantly increasing when hydrogen bonding is absent under hydrophobic conditions[116,117]. Therefore, it can be speculated that the pK of LHCII is influenced by

the protonation of glutamate and aspartate resulting in a structural change and its aggregation.

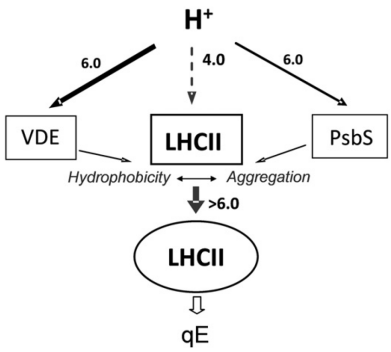

Figure 5. A model describing the effect of the xanthophyll cycle (VDE) and PsbS on the luminal pK of qE-active residues in LHCII. The pK of LHCII, around 4,0 is too low to activate qE at physiological pH values[81,112,113], but both PsbS and VDE (with a pH of around 6,0) get protonated and trigger the aggregation of LHCII molecules[87,114]. Through the aggregation, the hydrophobicity of the surrounding environment is increased, shifting the pK to 6,0 and enhancing the affinity for protons, hence activating qE at physiological lumen pH levels. Adapted from Ruban 2012[26].

In addition, while both zeaxanthin and PsbS facilitate the process of qE, the function of PsbS appears in regulating how many LHCII units are involved in the aggregated quenching. Thus, the limiting factors for qE are ΔpH, PsbS, and the major LHCII complex[94]. While zeaxanthin increases the sensitivity of qE for ΔpH-dependent changes, also sensing ΔpH by PsbS can work as a switch between the active and quenched state enabling the plant to adapt to fluctuations in the light intensity. In this direction, it has been shown that PsbS, violaxanthin de-epoxidase (VDE), and zeaxanthin epoxidase (ZEP) play an important role in plant productivity as their overexpression enhanced the biomass of tobacco plants by 15% under field conditions[18]. It suggests that NPQ induction lags alterations in light intensity, meaning that the plant does not always turn its protection mechanisms on and off fast enough to follow the changes in the light environment. Since these conditions can lead to harmful excitation of their photosynthetic machinery and a waste of energy when levels of light-harvesting remain low, due to a still elevated NPQ. Therefore, when proteins involved

in the NPQ mechanism were overexpressed, NPQ was able to follow light alterations more closely and enhance its biomass production through enhanced photosynthetic efficiency[119] (Fig. 6).

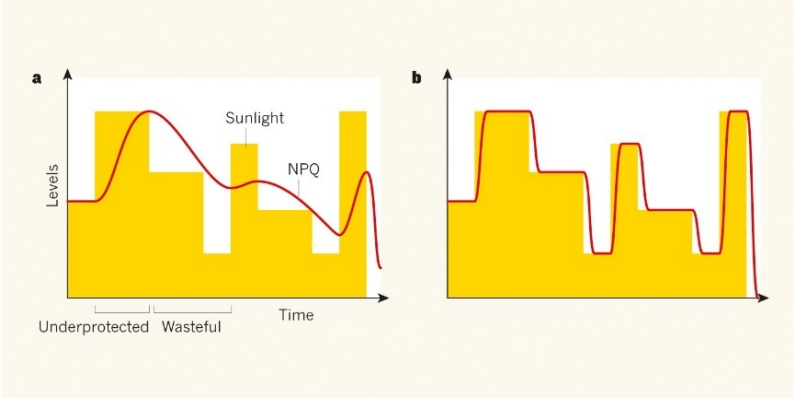

Figure 6. Correlation of normalized light intensity variations and NPQ measurement over time to throw excessive light energy away through the release of heat. a. In WT, NPQ lags the change in light intensity, leading to the wasteful and harmful utilization of incoming light energy. b. Genetically engineered plant overexpressing NPQ proteins follow light fluctuations more closely and increase biomass through enhanced photosynthetic efficiency[118]. The y-axis represents normalized light intensity levels (in µmol m-2 s-1) and normalized NPQ measurements and the x-axis represents time, which is not further defined. The model is simplified and do not reflect data points from the paper to illustrate NPQ kinetics upon changes in light intensity. Adapted from Ruban 2017[119].

1.2.c State transition, qT

The rapid initiation and relaxation of qE take place within seconds to minutes which fits the ΔpH changes that form and dissolve in seconds. In contrast, the phosphorylation/dephosphorylation of LHCII requires several minutes to establish state transitions, qT, making it responsive to changes in light intensity and quality over a longer period. As already mentioned above, using the term quenching in the mechanism of state transition may be misleading because here quenching does not mean energy loss but rather energy transfer from one to another photosystem. It is believed that both LHCB1 and LHCB2 subunits of LHCII are phosphorylated by the serine-threonine

kinase STN7. It is further demonstrated that the site of phosphorylation is at its N-termini facing the stroma[58]. When the plant is illuminated with low light, the kinase is activated through the binding of plastoquinol PQH_2 to the Cytb6f complex and deactivated at high light through an accumulation of reduced thioredoxin in the stroma or/and the formation of ΔpH[59,60]. Under high light and darkness, LHCII is dephosphorylated by the phosphatase PPH1[120,121]. As PPH1 has been suggested to be constitutively active, the rate of STN7 kinase activity is regulating the degree of phosphorylation of LHCII[120,121]. Both STN7 and PPH1 have been shown to localize in the thylakoid and to a lesser extent in stroma fractions, and after further fractionation PPH1 was shown to be stronger present in stroma lamellae relative to grana fractions[121]. In a different study, PPH1 has been found only in the thylakoid membrane but not in stromal fractions[120]. Two states have been defined: state 1 when LHCII is dephosphorylated and energetically coupled to PSII, and state 2 when phosphorylated LHCII is energetically coupled to PSI via the subunits PSAL, PSAH, and PSAO[122] (Fig. 7).

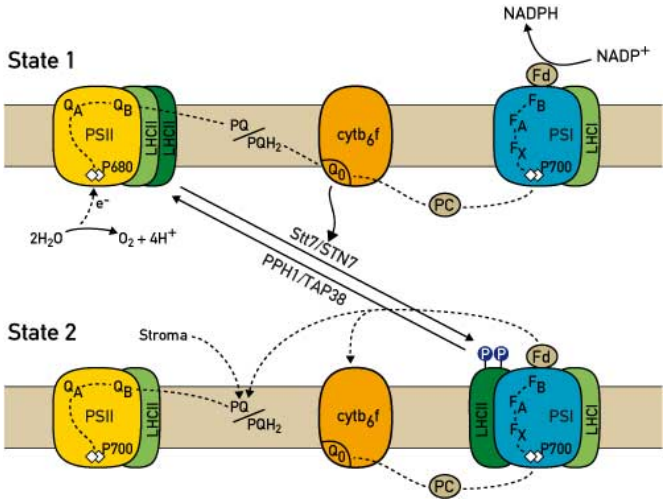

Figure 7. Scheme of state transition. When PSII is preferentially excited relative to PSI and the redox state of the PQ pool is reduced to PQH_2. PQH_2 binds to the Q_0 site of Cytb6f and activates the STN7 protein kinase. Subsequently, LHCII gets phosphorylated, and it disassociates from PSII and binds PSI (state 1-to-state 2 transition). However, differing from this illustration where LEF is indicated to be performed in state 1 and CEF in state 2, instead, it has been shown that CEF and LEF are regulated independently of state transition[123]. When PSI is preferentially

excited relative to PSII, or at HL or in darkness, STN7 (stt7 in Chlamydomonas) is deactivated and the PPH1 phosphatase dephosphorylates LHCII, which moves back to PSII (state 2- to- state 1 transition). Dotted lines show e- transport chains. P680, PSII reaction center chlorophyll dimer, Q_A, and Q_B are primary and secondary e- acceptors of PSII, P700 is the PSI reaction center chlorophyll dimer, F_X, F_A, F_B, 4Fe–4S centers acting as electron acceptors within PSI; PQ, plastoquinone pool; PC, plastocyanin; Fd, ferredoxin. Adapted from Rochaix 2007[124], version from https://molbio.unige.ch/en/research-group/jean-david-rochaix/objectives#section-3.

The mechanism of state transition has been demonstrated spectroscopically by using AL in different qualities (blue/red and far-red (FR)) to initiate phosphorylation/dephosphorylation and the shift of LHCII between both photosystems[58,120,121]. State transition can be demonstrated through initiating a shift in LHCII between PSII and PSI leading to a decrease/increase in fluorescence levels, which are representing the redox state of the PQ pool. Leaves were illuminated with low AL to activate the kinase and then FR light was supplemented, which is increasing the fluorescence signal by triggering a state 2- to- state 1 transition by moving LHCII from PSI to PSII (Fig. 7.)[121]. During an FR-induced state transition, LHCII moves from PSI back to PSII over several minutes and increases the fluorescence emission leading to a stronger reduction in PQH_2, while switching off FR light resulted in a stronger reduction of PQH_2 and movement of LHCII back from PSII to PSI and a decrease of fluorescence emission leading subsequently to an oxidation of PQH_2 (Fig. 8)[121]. This phenomenon was missing in both the stn7 and the pph1 mutant[58,120,121]. Additionally, when the stn7 mutant was grown at LL, the PSII's acceptor side Q_A was more strongly reduced relative to WT, during the illumination with low light intensities, suggesting that its PQ pool was more strongly reduced[58,66]. Moreover, in the stn7 mutant, a complex consisting of PSI-LHCI and phosphorylated LHCII was lost, which was formed in WT after illumination with low light intensities[123]. In contrast, the pph1 mutant showed this complex after dark preincubation and both when illuminated with low and FR light, whereas WT did not show it after darkness and prolonged illumination with FR light[120].

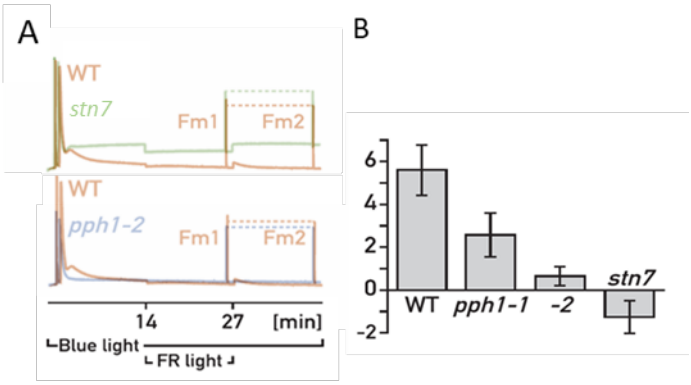

Figure 8. Chlorophyll fluorescence analysis of a state 2- to- state 1-to-state 2 transition in *A. thaliana* WT and stn7, and pph1 mutant leaves. A. Leaves were dark-adapted and exposed to blue light to induce state 2, then supplemented with FR light to promote a state 1 transition, then FR light was turned off and a return to state 2 was initiated if only blue light was provided. The y-axis is showing absolute fluorescence values and the x-axis is given in min and different light qualities (0-14 min and 27- end: blue light and 14- 27 min: blue and FR light). B. Quantification of state transition from A. with the formula qT= (F_m1-F_m2)/F_m1x100. The y-axis is given in not normalized arbitrary units of qT (which is calculated with the help of the formula). Adapted from Shapiguzov et al. 2010[121].

After having been grown at either PSII or PSI light, when acclimatizing the plant to the opposite light quality, with the *stn7* mutation the plant was not capable like WT to increase its Chla/b ratio when grown at PSI light and transferred to PSII light or decrease its Chla/b ratio when grown at PSII light and switched to PSI light in the leaf[123]. As the Chla/b ratio was interpreted to reflect the organization of the photosynthetic complexes, this finding was interpreted as an impairment in performing a state 1 – state 2 transition in the stn7 mutant relative to WT when not being able to adjust the binding of LHCII to the photosystems[120]. Additionally, the stn7 mutant was relative to WT keeping its F_s/F_m ratio increased when adapted to PSII light[120]. This finding was in agreement with the observation that in the stn7 mutant, the PSII acceptor side was more strongly reduced at low light intensities relative to WT[123]. Both an increase in F_s/F_m ratio and a stronger reduction of PSII‘s acceptor side might indicate that the PQ pool was more strongly reduced in the stn7 mutant relative to WT.

Similarly, plants lacking subunits of PSI (psad1-1 and psae1-3) that show a higher amount of phosphorylated LHCII at PSI but have a decreased capacity in performing state transition, did not change the ratio of Chl a/b nor the ratio of F_s/F_m when acclimatized to the opposite light quality[123]. Therefore, both a stable Chla/b content and F_s/F_m ratio are found when the mechanism of state transition is impaired.

Moreover, the STN7 kinase has been suggested to be an important regulator of long-term acclimation processes, regulating both chloroplast and nuclear-encoded gene expression, which is needed for adapting the photosynthetic protein complexes to changes in light quality. Hence, it suggests that besides the lack of state transition also protein complexes might be altered in the stn7 mutant relative to WT. Under controlled growth conditions, the stn7 mutant and both PSI subunit mutants (psad1-1 and psae1-3) showed retarded growth[123]. Moreover, the stn7 mutant suffered from a severe growth impairment when grown under fluctuating light intensities[58] and under field conditions[125]. In comparison to constant light, both fluctuating light and light under natural conditions is alternating light absorption in the grana/stroma thylakoid membrane leading to changes in light perception at PSII and PSI and hence affecting the reduction state of the PQ pool.

Moreover, when the stn7 mutant was grown under constant low, medium, or high light conditions, its PSII to PSI ratio was decreased relative to WT[126,127]. In contrast, at fluctuating light conditions the opposite result was obtained and the PSII to PSI ratio was clearly higher in the stn7 mutant than in WT[127]. Therefore, it was suggested that the redox state of the PQ pool, which is regulated through state transition-based balancing of light absorption at PSII and PSI, influences the stoichiometry of protein complexes[127]. It cannot be excluded that the higher PSII/PSI ratio under fluctuating light in the stn7 mutant relative to WT was caused through photoinhibition of PSI. It was further shown that when the stn7 mutant was grown at higher light intensities relative to growth light, the mutant increased the levels of NPQ and better tolerated high light stress relative to WT plants[128]. In contrast, to the stn7 mutant, there exists significantly less literature on the pph1 mutant. It has been reported that the pph1 mutant, when illuminated with light intensities below growth light has a more strongly

oxidized PSII acceptor side and increased e- flow through PSII, hence keeping the PQ pool more strongly oxidized[120].

In general, experimental data strongly indicated that through performing state transition, the plant is capable to balance light energy between PSII and PSI to ensure efficient operation of photosynthetic e- transport processes that lead to the reduction of $NADP^+$ to NADPH, fixation of CO_2, and production of sugars. Therefore, a role for state transition has been proposed to increase the plant's CEF to LEF ratio and hence ATP production when LHCII is phosphorylated and coupled to PSI[129–132]. However, it has been shown, that CEF works independently of state transition in both *Arabidopsis* and *Chlamydomonas*[123,133]. Moreover, the structure of the thylakoid membrane is influenced by the phosphorylation level of LHCII complexes, and when more dephosphorylated, grana stacking increases[134]. When illuminated under low white light intensities, growth light conditions, and PSII light, phosphorylation reduces the number of grana membrane layers and their diameter but is increasing the number of these smaller grana inside the chloroplast as well as the number of stroma lamellae compared to conditions promoting dephosphorylation such as darkness, FR light (or PSI light)[57,135] and high light[3,136–138] (Fig. 9). When illuminated with low light in the stn7 mutant, the grana diameter was smaller and the number of grana layers increased relative to both WT and the pph1 mutant, while under HL conditions the grana diameter was strongest increased in the stn7 mutant, followed by WT and did not change in the pph1 mutant relative to LL conditions always showing smaller grana stacks[137].

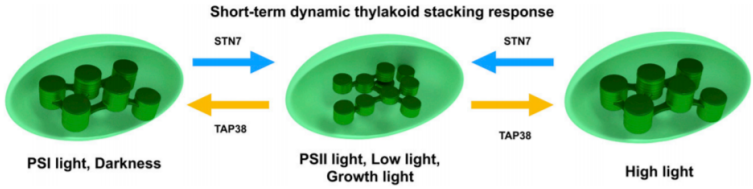

Figure 9. Model of dynamic thylakoid stacking in plants when exposed to different light intensities and qualities as well as darkness. When illuminated with low white light, growth light, and PSII light, the kinase STN7 is activated and phosphorylates LHCII molecules, resulting in a decrease in the grana diameter and an increase in the number of grana stacks per chloroplast hence increasing the area of stroma thylakoids relative to high-intensity light, FR light (PSI light)

illumination and darkness. In the dark, at high-intensity light, and at FR light (PSI light), STN7 activity is low, allowing PPH1 to dephosphorylate LHCII, leading to a rise in the grana diameter and lowering the number of grana stacks per chloroplast relative to low white light, PSII light and growth light. Adapted from Wood et al. 2019[137].

While recent work suggested that smaller grana facilitated the exchange of phosphorylated LHCII molecules between grana and stroma lamellae[134], using absorption flash spectroscopy indicated that a decrease in grana size (as in the pph1 mutant) increased the rate of PSI reduction, which was interpreted as an increase in LEF capacity[3]. In contrast, in larger grana (as found in the stn7 mutant) PSI reduction was enhanced after leaves were illuminated with FR light, suggesting that the capacity to perform CEF was increased[3,139]. Thus, under LL conditions dephosphorylated LHCII (in state 1) in the stn7 mutant and a more strongly reduced Q_A would indicate a decrease in LEF and increase in CEF[126–128], while in the pph1 mutant a more strongly oxidized Q_A would stand for an increase in LEF. This further indicated that thylakoid membrane dynamics might control the ratio between CEF and LEF[3].

Moreover, in a follow-up study, it was shown that the psal (LHC docking) mutant lacking a state 1-to-state 2 transition (indicated through 77K fluorescence emission spectroscopy) and hence behaving like the stn7 mutant locked in state 1, retained dynamic thylakoid stacking[122,137], and to regulate photosynthetic CEF and LEF modes[2]. These observations suggested that the regulation of e- transport depends on dynamic thylakoid stacking and is independent of state transition[2]. Additionally, it was shown that after LL illumination, CO_2 assimilation rates were higher in WT and the pph1 mutant relative to the stn7 mutant, whereas after HL irradiance in the pph1 mutant the rate of CO_2 assimilation was significantly lowered relative to WT and the stn7 mutant[2]. This was further shown to be caused by a more strongly reduced PSI acceptor side in the stn7 mutant under LL conditions as well as in the pph1 mutant under HL conditions, which was leading to a decrease in LEF. Additionally, the stn7 mutant was under LL showing the strongest reduction of Q_A (1-qL) (e- outflow at PSII was most strongly decreased) relative to WT and the pph1 mutant, while the pph1 mutant showed the highest reduction of Q_A (e- outflow at PSII was most strongly decreased) relative to WT and the stn7 mutant when transferred from LL to HL while having the strongest

oxidized Q_A (e- outflow at PSII was most strongly increased) when illuminated at LL[2]. Additionally, PSI's donor side was more strongly reduced (e- inflow was most strongly increased at the donor side of PSI) in the stn7 mutant under LL but not in the pph1 mutant under HL[2]. This finding was interpreted to be caused by a faster PQ/PQH_2 diffusion rate under LL and HL conditions in the pph1 mutant than in the stn7 mutant due to differences in the mutant's grana morphology (displayed in Fig. 10)[2]. Moreover, the pph1 mutant showed a 10-15% reduction in functional PSI after HL treatment, indicating that PSI suffers from photodamage at HL[2].

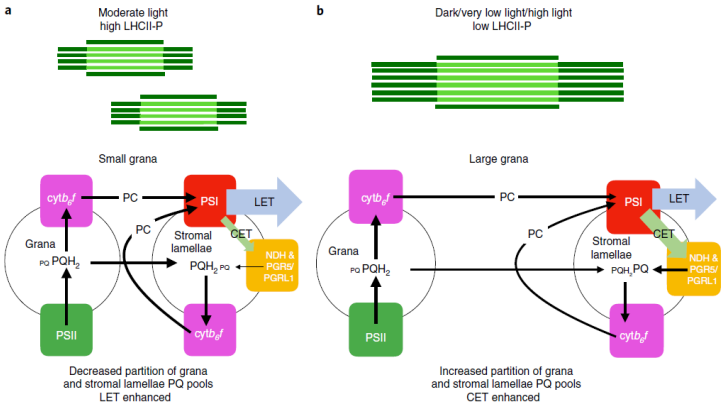

Figure 10. Model of grana stacking/de-stacking and its influence on the balance between CEF and LEF. a. Moderate light levels result in that LHCII phosphorylation and LHCII-LHCII interactions being weakened which is leading to more grana with fewer stacks, creating better-connected grana stacks and more stroma thylakoids. The diffusion of PC and the PQ pool between grana and stroma thylakoids is fast, and LEF is upregulated relative to CEF. b. After darkness or under LL and HL dephosphorylation of LHCII strengthens the binding of LHCIIs, leading to fewer and larger grana stacks and decreasing the contact area between grana membranes and the number of stroma thylakoids. If the diffusion of PC and PQ between the grana and stroma thylakoids is slow, this results in a stronger separation of the grana located PQ pool(s) to the stroma located PQ pool(s) leading to a more oxidized PQ pool which promotes CEF. Adapted from Wood et al. 2018[3].

Furthermore, based on evidence that CEF capacity was increased in WT and the stn7 mutant at LL relative to the pph1 mutant[2], the last model[3] (Fig. 10) was extended by explaining the influence of LL and HL on the dynamic thylakoid membrane regulation and its effect on e- transport (Fig. 11). It was proposed that when the STN7 kinase is turned off at HL when limited in CO_2, NADPH and accumulation of ATP increased,

the phosphatase PPH1 dephosphorylates LHCII and shifts the plant into state 1. Subsequently, in state 1 the thylakoid membrane transforms into larger grana stacks (like observed in the stn7 mutant). Through this adaptation, the plant increases its capacity to perform CEF. This is suggested to be caused by isolating the stromal PQ pool from the reduction power of PSII, hence poising for CEF[2]. However, the authors did not specify if the upregulation of CEF is located inside the grana or stroma thylakoid membrane. In contrast, at LL, STN7 is activated and LHCII phosphorylation triggers a transition to smaller grana and state 2 (like in pph1 mutant). It was further proposed that under LL conditions when the plant is in state 2, ATP production is insufficient to feed the CBB cycle, and increased PSI excitation relative to PSII increases the rate of CEF relative to LEF. Thus, in the latest model proposed by Hepworth et al. 2021, the stn7 mutant has an advantage at HL and a disadvantage at LL, while the pph1 mutant benefits from LL and shows a drawback under HL conditions (Fig. 11).

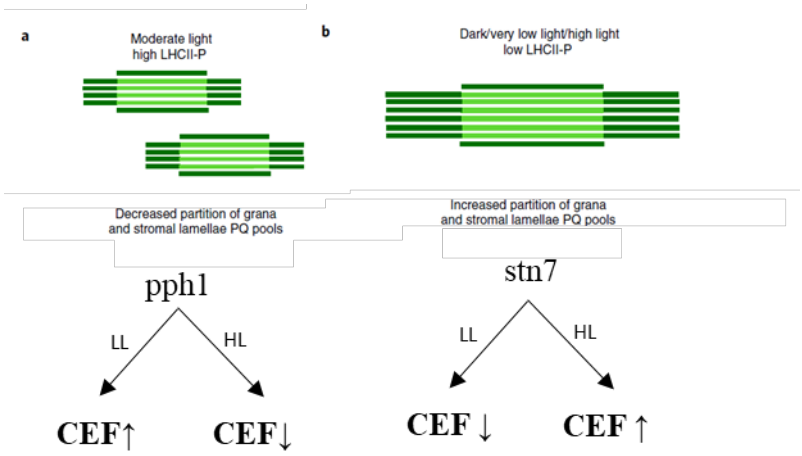

Figure 11. Model of grana stacking/de-stacking and its influence on the balance between CEF and LEF under LL and HL conditions. a. Under conditions promoting state 2 (in the pph1 mutant), where the diffusion of PC and the PQ pool between grana and stroma thylakoids is fast, CEF is upregulated under LL conditions through exciting PSI over PSII, keeping the stromal PQ pool more oxidized and decreased under HL conditions due to a stronger reduction of the stromal PQ pool by e- flow from PSII. b. Under conditions promoting state 1 (in the stn7 mutant), where the diffusion of PC and the PQ pool between grana and stroma thylakoids is slow, CEF is decreased under LL but upregulated at HL when the stromal PQ pool is isolated from PSII, thus poising CEF. The illustration was taken from Wood et al. 2018[3] and adapted according to the model proposed in Hepworth et al. 2021[2].

1.3. Cyclic electron flow (CEF)

1.3.a Different CEF modes and their regulation

The role of cyclic electron flow (CEF) around photosystem I (PSI) has been suggested to recycle electrons (e-) from ferredoxin (Fd) through plastoquinone (PQ), passing through the Cytb6f complex, generating ΔpH without net production of NADPH but generating ATP. In contrast, linear electron flow (LEF) is transporting e- from water to $NADP^+$ via photosystems II (PSII) and photosystem I (PSI) producing both NADPH and ATP[20]. Interestingly, CEF around PSI was discovered before the concept of LEF was known[140]. Arnon and coworkers showed already in 1954 that intact chloroplasts conducted O_2 evolution and CO_2 fixation from the atmosphere and performed photosynthetic phosphorylation[140]. They could show for the first time that isolated chloroplast had the capacity without adding other enzymes and compounds, to use light energy for adenosine triphosphate synthesis (through photosynthetic phosphorylation) and CO_2 fixation through the use of radioactive precursors labeled with isotopes ^{14}C and ^{32}P.

CEF consists of two pathways, namely the antimycin A (AA) sensitive pathway involving PROTON GRADIENT REGULATION5 (PGR5) and PGR5-LIKE PHOTOSYNTHETIC PHENOTYPE1 (PGRL1), and a minor pathway that is insensitive to AA mediated by the NADH dehydrogenase-like (NDH) complex (Fig. 12)[141–143].

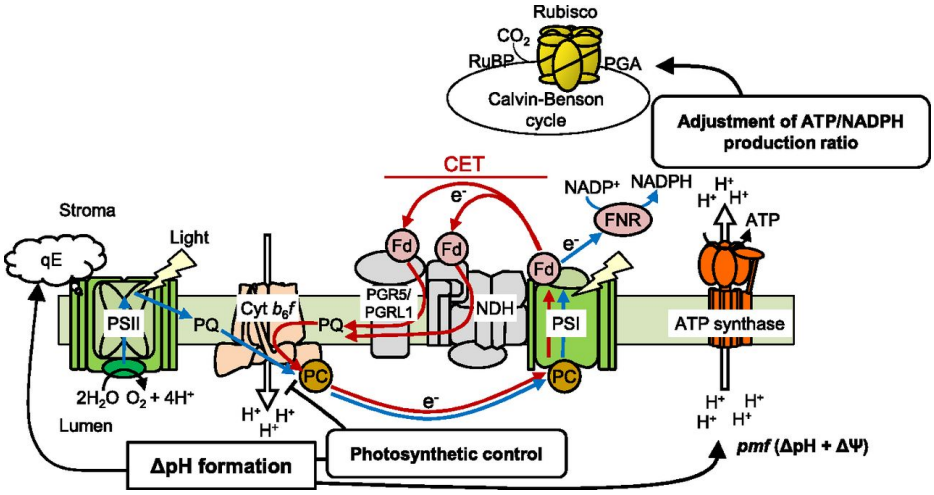

Figure 12. The photosynthetic ETC and its e- transport. Linear and cyclic e- flow are indicated by blue and red arrows. In angiosperms, CEF consists of two pathways: PGR5/PGRL1-dependent and NDH-dependent CEF. PGR5/PGRL1-dependent and NDH-dependent CEF shuttle e- from Fd at PSI to the PQ pool and generate ΔpH across the thylakoid membrane through the Q cycle in the Cyt6bf complex without the production of NADPH. The proton motive force (pmf) composed of ΔpH and ΔΨ is generating ATP at the ATP synthase. Through controlling the activity of the ATP synthase, the ATP/NADPH ratio is balanced, which is required for operating the CBB cycle and photorespiration, and increasing the e- sink capacity downstream of PSI. Additionally, ΔpH formation leads to luminal acidification which slows plastoquinol oxidation at the Cytb6f complex through photosynthetic control and prevents PSI from overreducing. Moreover, luminal acidification regulates the elimination of excess photon energy as heat through the induction of qE. Abbreviations: FNR, Fd:$NADP^+$ oxidoreductase; PC, plastocyanin; PGA, 3-phosphoglycerate; RuBP, ribulose 1,5-bisphosphate. Adapted from Hiroshi Yamamoto, Toshiharu Shikanai 2019[144].

It has been described that the PGR5/PGRL1-dependent CEF acts either as the AA-sensitive ferredoxin-plastoquinone reductase (FQR)[145,146] or regulates FQR activity by a Fd/$NADP^+$ reductase (FNR)-Cytb6f complex[139,147], produces ATP in ruptured chloroplast[148] and corresponds to the cyclic phosphorylation pathway[149]. When PGR5 is missing, the mutant cannot induce ΔpH-dependent NPQ under high light and due to impaired acidification of the thylakoid lumen cannot downregulate e- transport through Cytb6f termed photosynthetic control, which is indicated through a decrease in PSI donor-side limitation Y(ND) (increased e- inflow at the donor side of PSI)[139,141,144]. In contrast, in WT under HL conditions when the lumen acidifies[66], excess light energy

from PSII is thermally dissipated in a process termed NPQ[31,150,151] and e- transport gets downregulated at Cytb6f leading to a rise in PSI donor-side limitation Y(ND) (decreased e- inflow at the donor side of PSI)[139,141,144]. Since the pgr5 mutant is not capable to grow under fluctuating light intensities and is sensitive to high light, these protective mechanisms have been described to be important when light intensity varies and at high light[66,141,144,152,153]. Thus, the PGR5/PGRL1-dependent pathway was described as a stronger contributor to the generation of ΔpH than the NDH-dependent pathway[141,142]. Interestingly, in transgenic *Arabidopsis* plants over-accumulating PGR5, a delay in chloroplast development was caused, and NPQ was transiently increased when light intensities were increased[154]. Thus, it seems that PGR5 influences NPQ when the plant is challenged with a sudden increase in light intensities which was interpreted to be caused by elevated activity of PSI-dependent CEF.

The NDH complex in chloroplasts has been shown to accept electrons from Fd[155] and thus might compete with PGR5/PGRL1-dependent CEF, and with linear and other alternative e- transport mechanisms such as the Mehler-reaction. The NDH-mediated pathway was first discovered in cyanobacteria[156,157]. Thereafter, it was shown that NDH contributes to CEF around PSI in chloroplasts[158,159] and that it subtly contributes to the formation of ΔpH in the light[160–163]. Previous studies indicated that a dysfunctional NDH complex did not show a strong phenotype both in tobacco[158,159] and *Arabidopsis*[161] but was shown to be involved in stress resistance[160,164–167], at low light and under fluctuating light in rice[168,169]. However, a double mutant missing both the NDH complex and PGR5 protein has been shown to have a severe growth defect and an impairment in photosynthesis even under constant low light[162]. Thus, it has been suggested that NDH-dependent CEF is essential for growth in the pgr5 mutant[162,170]. It was further proven, that the NDH complex interacts with PSI and forms a complex that is required for NDH-mediated e- transport *in vivo* and for stabilizing the NDH complex[171–173]. It can therefore be imagined that NDH-dependent CEF is controlled through its interaction with PSI centers.

CEF and LEF have been demonstrated to share at least the PQ pool, Cytb6f, plastocyanin (Pc), PSI, and ferredoxin (Fd). Thus, both modes should be in constant

competition sharing several e- carriers. This could be regulated through a flexible spatial separation of CEF and LEF or a direct enzymatic control mechanism regulating their kinetic constants to maintain and regulate both e- flow modes. For example, this control mechanism could be a close association between Cytb6f and PSI which was observed both in algae[174] and recently in vascular plants[175]. Additionally, FNR movement and its binding to Cytb6f[176] were suggested to alter CEF to LEF ratios[139,177]. Different enzymes have been discussed in the literature to exert the role of a Fd:PQ oxidoreductase which is transferring e- from Fd to the PQ pool, namely PGRL1[145], the NDH complex[155], and the Cytb6f complex[178,179]. The NDH complex is the plant chloroplast homolog of mitochondrial Complex I and can use Fd or NADPH to reduce the PQ pool, and the Cytb6f has been shown to have PQ reducing activity when taking part in the Q-cycle[178,179]. Hence, partitioning between LEF and CEF can be regulated by environmental controlled regulations of the formation or activation/deactivation of various protein complexes inside the chloroplast's thylakoid membrane.

Moreover, the chloroplastic thioredoxin (Trx) system has also been proposed as a CEF-regulator[145,180,181]. Trx has been shown to be reduced by photo-reduced Fd via a Fd-Trx reductase (FTR)[182,183] and via the NADPH-Trx reductase C (NTRC) pathway, which utilizes NADPH and therefore can also operate in darkness[184,185]. A mutant defective in three Trx isoforms was suggested to enhance CEF around PSI[186] and the overexpression of NTRC stimulated the NDH-dependent pathway[181]. It was further proposed based on *in vitro* findings that Trx activated the PGRL1 protein[145]. Additionally, very recent findings indicated that thioredoxins were regulating PGR5/PGRL1-dependent plastoquinone reduction[153]. It was shown that a cysteine at PGRL1 is needed for forming a thioredoxin- PGRL1 complex[153]. Hence, it was proposed that thioredoxin directly regulates the PGR5/PGRL1-dependent CEF around PSI by forming a complex with PGRL1[153]. These findings are strongly indicating that the redox state of the photosynthetic e- transport chain is an important regulator of e- transport modes operated inside the chloroplast. This shows quite plainly that every mechanism that affects the plant's redox state is thus able to influence its CEF and LEF turnover directly.

1.3.b Characterization of CEF mutants and attempts to measure CEF activity

The *A. thaliana* pgr5 mutant was identified by its high fluorescence phenotype at high light intensities and by its decreased formation of ΔpH[141]. This made the mutant unable to induce the energy-depending (qE) component NPQ at increasing light intensities as shown during a dark-to-light transition (Fig. 13) and in a light-response experiment (LRE) (Fig. 14)[141]. Moreover, when analyzing the contribution of alternative e- modes in the presence of ambient air and under CO_2free (20% O_2), N_2 (0% O_2; 0% CO_2), or high CO_2 (0% O_2) conditions results showed that the oxidation of P700 was downregulated in the pgr5 mutant when $C0_2$ was limited and thus linear e- flow onto $NADP^+$ was inhibited[141]. In contrast, WT was able to oxidize P700 in CO_2free conditions only when oxygen was present[141]. This indicated a strong reliance of the pgr5 mutant on LEF compared to WT. Additionally, Kono et al. 2014 showed in an attempt to differentiate between the different NPQ components that during the recording of an LRE at high light intensities, the pgr5 mutant had decreased NPQ - namely the fast qE component, while at low light intensities the mutant lowered the performance of the medium phase of NPQ- namely state transition (qT)[187]. In agreement with less state transition (qT), in the pgr5 mutant, the ratio between Chl a to Chl b was increased by a value of 0.4 relative to WT, indicating that the mutant decreased the amount of LHCII molecules. In addition, at HL the pgr5 mutant failed to dephosphorylate LHCII[188]. Therefore, findings strongly suggest that when PGR5 was missing, and the mutant plant performed less state transition it was less adaptable to changing light intensities. This explanation was strengthened by the pgr5 mutant's lethal growth phenotype at fluctuating light[66].

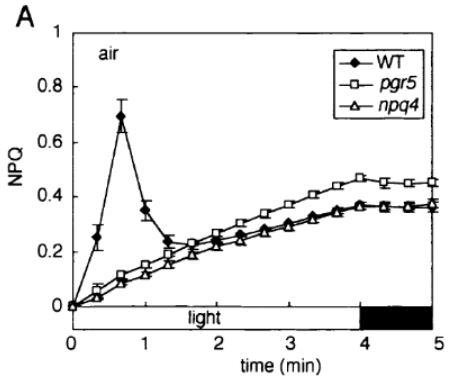

Figure 13. Induction of NPQ during a dark-to-light transition and in the dark in leaves of the WT, and npq4 and pgr5 mutant plants. White bar: 80 µmol m-2 s-1 and dark bar: darkness. Adapted from Munekage et al. 2002[141].

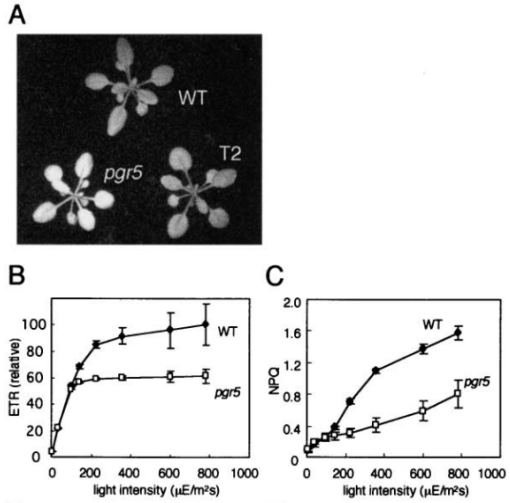

Figure 14. Characterization of the high-fluorescence phenotype when illuminated at 300 µmol m-2 s-1 (A), the relative e- transport rate through PSII (ETR) (B), and NPQ at increasing light intensity in the pgr5 mutant and WT leaves (C). ETR through PSII was calculated Y(II)x light intensity and NPQ after $(F_m-F_m')/F_m'$. Adapted from Munekage et al. 2002[141].

The pgr5 mutant, claimed to not form a ΔpH and acidify the lumen, is incapable of inducing photosynthetic photoprotection through downregulating e- flow through Cytb6f. This protection mechanism has been shown to play an important role in protecting PSI from photodamage[66,187]. In the pgr5 mutant, when illuminated for ten minutes at 1500 µmol m-2 s-1, both photosystems were significantly photoinhibited (PSII activity was decreased by 20% and PSI activity decreased by almost 70%) compared to WT leaves[141]. Additionally, it has been shown that the pgr5 mutant is very sensitive to fluctuating light, implying that both qE induction and photoprotection through Cytb6f are vital to adapt to changing light environments[144].

It was first proposed by Munekage et al. (2002) that the pgr5 mutant showed less CEF-PSI due to decreased activity of the ferredoxin-dependent plastoquinone reduction (FQR) in ruptured chloroplasts[141]. This observation was based on the observation of Endo et al. (1998) made in ruptured chloroplasts in the presence of Fd and NADPH during weak measuring light (ML) or only Fd at 10 µmol m-2 s-1 AL, as fluorescence levels were dropping when antimycin A (AA) was added[189]. Without AA, a rise in fluorescence indicated that e- were donated from reduced Fd to plastoquinone (PQ) via Fd $NADP^+$ reductase (FNR) and/or Fd plastoquinone reductase (FQR). Therefore, a drop in fluorescence through the addition of AA was interpreted as a decrease in e- donated from NADPH via Fd to the PQ pool during CEF. Interestingly, when adding Fd, the rise in fluorescence was only observed under weak ML when NADPH was added. On the contrary, when the light was turned on (at 10 µmol m-2 s-1), NADPH was not needed to yield the same fluorescence level as under weak ML when NADPH was supplemented to Fd. This observation might indicate that to perform AA-sensitive CEF, PSI's e- sink had to be in a reduced state. Indeed, it has been described several times that the redox state of the stroma regulates CEF and that a stronger reduction enhances CEF around PSI[190,191]. In contrast, when 10 µmol m-2 s-1 instead of weak ML (intensity not stated by authors) was used, PSI's acceptor side is ordinarily reduced, and NADPH was not needed to operate AA-sensitive CEF-PSI. Alternatively, it could also mean that under weak ML not enough photons are received at PSI. If this is the case, then PSI-based Fd reduction would be too low and then only NADPH can donate

e- for PQH_2 reduction. Subsequently, this would mean that if light increases to 10 µmol photons, PSI-based Fd reduction can substitute for NADPH supplementation.

In the experiment of Munekage et al. 2002, the presence of AA lowered the rate of fluorescence increase in WT, resembling the pgr5 mutant in the absence and presence of AA[141]. However, the total fluorescence yield was elevated in both WT and the pgr5 mutant with AA compared to measurements without the inhibitor[141]. While the same experimental setup was used as in Endo et al. (1989), the only difference was that the concentration of AA was increased from 1µM to 10-20µM in Munekage's study. In a follow-up study by Munekage et al. (2004) authors showed that when using only 2µM AA instead of 10-20µM, the fluorescence yield was decreased in WT chloroplasts treated with the inhibitor compared to its absence[162]. Therefore, it can be excluded that in the first study, not enough inhibitor was used to completely deactivate PGR5/PGRL1- dependent CEF at PSI. On the other hand, it suggests that an increased concentration of AA is leading to a stronger reduction of the chloroplasts PQH_2 pool and could therefore have a secondary effect on different e- and/or proton transport mechanism(s).

Additionally, also a newer study could confirm that without PGR5/PGRL1-dependent CEF, either knocking out *pgr5* or using AA caused a significant decrease in the rate of fluorescence changes upon Fd addition under the illumination with weak ML (Fig. 15). Hence, a decrease in PGR5/PGRL1-dependent CEF is decreasing the rate the PQ pool is reduced. However, also when only *the crr2 mutant* was knocked out, the rise in fluorescence levels showed the same pattern as it was observed in the pgr5 single mutant (Fig. 15)[162]. This observation made in crr2 mutant chloroplasts might suggest that during the first minute of illumination when NDH-dependent CEF was missing, PGR5/PGRL1-dependent CEF was also inhibited in the mutant and therefore resembling the pgr5 mutant measurements. It can be speculated that by changing the rate of LEF under this experimental setting, this is leading to a stronger reduction of the PQ pool when LEF is downregulated. If this was the case, then in addition to a decrease in LEF, PGR5/PGRL1-dependent CEF could be inhibited in crr2 when compared to WT.

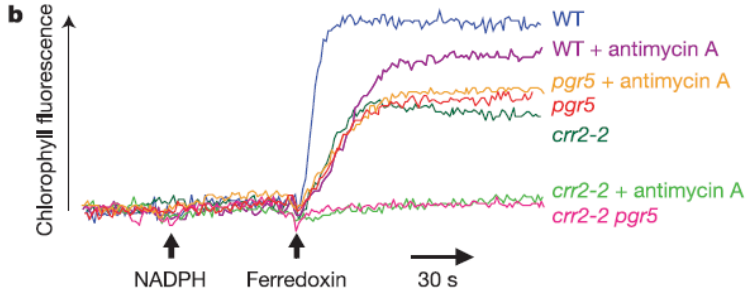

Figure 15. An increase of fluorescence emission in ruptured Arabidopsis chloroplasts indicated CEF activity by adding NADPH (0.25 mM) and ferredoxin (5 µM) under the illumination with weak measuring light (1 µmol m-2 s-1) of WT and different mutants in the absence or presence of 2 µM Antimycin A before measurement. Adapted from Munekage et al. 2004[162].

The lack of PGRL1 showed the same photosynthetic phenotype as the pgr5 mutant and it was further shown that it was essential for accumulating PGR5 in the so-called CEF complex containing PGR5, PGRL1, Cytb6f, PSI, and FNR in *Chlamydomonas reinhardtii* which was observed under conditions promoting CEF[133,174]. Both PGR5 and PGRL1 have been described to be sensitive to AA[145,189,192]. Additionally, PGRL1 was shown to accept e- from reduced ferredoxin (Fd) and to reduce quinones in an AA-sensitive and thus PGR5/PGRL1-dependent manner[145]. To show this, PQ reduction activity and hence CEF in ruptured chloroplasts from plants lacking both PGRL1 and PGR5 could only be restored when both recombinant PGRL1 and recombinant PGR5 were added to chloroplasts isolated from the pgrl1 pgr5 double mutant (pgrl1ab). Furthermore, both the lack of PGR5 and PGRL1 are similarly decreasing the formation of NPQ at the onset of light[142]. Therefore, it has been proposed that PGRL1 is the elusive ferredoxin-plastoquinone reductase (FQR) and that the PGR5/PGRL1 pathway corresponds to the cyclic phosphorylation discovered by Arnon et al.[140]. Moreover, experiments with ruptured chloroplasts of the pgr5 mutant displayed in addition to a decreased formation of a Fd-dependent proton motive force (pmf) also a diminished synthesis of ATP[148]. Interestingly, the activation of the ATPase during a dark-to-light transition happened more rapidly and to a greater extent in the pgr5 mutant compared

to WT[193]. Moreover, it was suggested that the activity of the ATP synthase was not fully downregulated in the dark in the pgr5 mutant relative to WT[193].

Moreover, the proton conductivity (g_{H^+}) of the ATP synthase (which is measuring the capacity of ATPase to transport protons across the membrane), was increased in the pgr5 mutant compared to WT[18,193]. The authors proposed a link between a low ΔpH and an increase in membrane conductivity through a stronger efflux of protons from the lumen through the ATPase. The ATPase activates in the light through the reduction of its gamma subunit by thioredoxin-f, which is reduced by Fd-thioredoxin reductase. A highly reduced PSI acceptor side in the pgr5 mutant[141] could therefore lead to an easier reduction of the gamma subunit in the pgr5 mutant relative to WT. However, Kanazawa and Kramer (2002) showed that the redox state of the thiols of the gamma unit of the ATP synthase is not affecting g_{H^+}[194]. Additionally, the activity of another thiol enzyme, namely NADP-malate dehydrogenase was increased in the pgr5 mutant relative to WT at low light levels[148,195]. Since this enzyme uses NADPH inside the chloroplast stroma to reduce oxaloacetate to malate, it supposes that the pgr5 mutant increasingly tries by these means to transform its NADPH to $NADP^+$. Especially, during a dark-to-light transition, when the mutant is not able to turn on the CBB cycle as the WT does, the increased activity of NADP-malate dehydrogenase is able to rise $NADP^+$ levels in the stroma. Thus, at the onset of light when the CBB cycle would be slower activated through a decrease in ATP synthesis[148] in the pgr5 mutant relative to WT, the mutant developed a mechanism to oxidize its PSI acceptor side and hence promote the performance of LEF.

However, Avenson et al (2005)[18] concluded that the higher proton conductivity (g_{H^+}) in the pgr5 mutant relative to WT was caused by alterations in steady-state substrate or effector concentration[194] due to a decrease in LEF in the pgr5 mutant relative to WT and loss of PSI e- acceptors leading to an increase in reduced intermediates in the ETC[141,162]. Based on their findings, Avenson et al. (2005)[18] concluded the following: When in the pgr5 mutant the rate of CEF is changed, the mutant will produce less ATP. Since the use of ATP and NADPH by the CBB cycle is coupled, an imbalance could result in an enhancement of ADP and [P_i] and NADPH in the mutant. Hence, LEF could

be lowered in the pgr5 mutant relative to WT due to a reduction in available PSI e-acceptor molecules ($NADP^+$). Similarly, in WT LEF was also decreased at CO_2-limiting conditions, but was in contrast leading in WT to a decrease in proton conductivity (g_{H^+}) , and elevated pmf and increased induction in qE, thus the opposite of what was observed in the pgr5 mutant[18]. Conclusively, a decrease in LEF in the pgr5 mutant relative to WT is not the reason for increased proton conductivity (g_{H^+}) in the mutant. It was therewith concluded by the authors that it is of great importance to correctly tune the activity of the ATPase and that excessive activity which could be the case in the pgr5 mutant could prevent the build-up of pmf and diminish qE, while on the opposite an uncontrolled decrease in its activity could lead to the over-acidification of the lumen and enormous formation of pmf leading to a pH-induced decline of the photosynthetic protein complexes[112,196].

Moreover, Rott et al. (2011) presented findings indicating that tobacco plants with diminished ATP synthase, decreased the capacity to establish a proton conductivity (g_{H^+}) across the thylakoid membrane already at low light intensities and behaved therefore opposite of the pgr5 mutant, which displayed an increase in proton conductivity (g_{H^+})[197]. Thus, this finding suggests a stronger activation of the ATP synthase in the pgr5 mutant relative to WT, which would propose that PGR5 plays a role in regulating the activity of ATPase molecules. Alternatively, an increased accumulation of H^+ protons in the pgr5 mutant relative to WT could result in the interpretation of an elevated ATP synthesis rate in the mutant due to the slow ATPase activity measurements. Therefore, PGR5 might not regulate ATPase molecules directly but control the accumulation of its substrate when regulating the rate of H^+ buildup inside the lumen instead. This could be achieved if the PGR5 protein would for example inhibit e- transport mechanisms which would lead to a decrease in the translocation of protons inside the chloroplast lumen. However, this model does not explain why in the pgr5 mutant, when following the last statement more H^+ protons would accumulate inside the lumen, and the formation of NPQ and execution of qE is decreased relative to WT. However, it has to be kept in mind that both components of pmf, namely proton conductivity (g_{H^+}) and ΔpH contribute to ATP synthesis[198]. It was shown that under

optimal conditions when ΔpH and NPQ are not needed, a fraction of pmf can be stored as Δpsi[12,18]. Thus, through an increase in proton conductivity (g_{H^+}) across the thylakoid membrane, a high pmf can result in less qE and high rates of ATP synthesis. On the opposite, under environmental stresses, such as low CO_2 or low O_2 conditions, when qE is of benefit pmf is predominantly stored as ΔpH[13]. Thus, pmf partitioning is regulating both photoprotection and ATP production. Hence, in the pgr5 mutant, an increase in H^+ accumulation could cause a drop in NPQ (namely qE) relative to WT when for example pmf is predominantly stored in Δpsi and not ΔpH.

There exists also a theoretical model that suggests that PGR5 is involved in the regulation of ATPase and that the pgr5 mutant is increasingly leaking H^+ from the thylakoid membrane, which is causing an increase in proton conductivity (g_{H^+}) [199]. This model is based on findings made in the overexpressor of the putative H^+/K^+ antiporter K+ efflux antiporter3 (KEA3), which through antiporting H^+ and K^+ most likely affect the partitioning of the pmf leading to an increase in proton conductivity (g_{H^+}) across the thylakoid membrane (Fig. 16). As both ΔpH and Δpsi contributes to driving ATP synthesis, a decrease in Δpsi through overexpressing KEA3 is suggested to decrease ATP synthesis. Moreover, overexpression of KEA3 decreased NPQ and maintained PSI's donor and acceptor sides more strongly reduced during a light-response experiment relative to WT in the same way as it was observed in the pgr5 mutant[200]. Additionally, during measurements where light intensities were alternated between HL and LL, PSI was more strongly reduced relative to WT and therefore the overexpression of KEA3 was again resembling the pgr5 mutant[200]. Thus, in the H^+ leakage model, PGR5 is expected to downregulate ATPase instead of CEF around PSI.

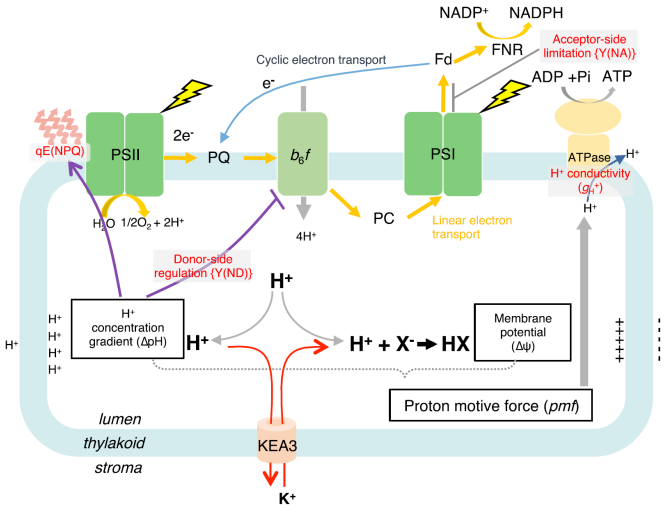

Figure 16. The influence of ion channels on the regulation of pmf and its partitioning in ΔpH and Δpsi to drive ATP synthesis during photosynthetic e- transport. In LEF (yellow arrow), at PSII (water splitting activity) and at Cytb6f (quinone cycle), and CEF (blue arrow) contribute to the H^+ translocation through the thylakoid membrane and formation of pmf. During H^+ translocation energy is stored as Δpsi. Ion channels (such as KEA3) are suggested to decrease the contribution of Δpsi, during H^+ accumulation in the lumen and the formation of ΔpH. Both ΔpH and Δpsi contributes to driving ATP synthesis. A decrease in Δpsi through overexpressing KEA3 is suggested to decrease ATP synthesis. The pmf is needed in addition to ATP synthesis, to induce qE, the dissipation of excessive energy at PSII through ΔpH-dependent luminal acidification of the lumen as well as downregulating e- transport through Cytb6f (monitored as an increase in Y(ND)). The latter is required to avoid damage at PSI when more e- are flowing in than can flow off. Thus, the regulation of pmf and ATP synthesis is of vital importance for the plant. Abbreviations: FNR, NADP1 oxidoreductase; PQ, plastoquinone; PC, plastocyanin. Adapted from Wang et al. 2019[200].

However, new evidence exists indicating that the pgr5 mutant is not leaking H^+ from the thylakoid membrane because increased H^+ conductivity across the thylakoid membrane could be complemented to WT levels through genetically introducing a transgenic flavodiiron (Flv) protein-dependent pseudo-CEF[201,202]. Flv reduces oxygen to water by accepting e- from NADPH or ferredoxin[203]. Adding this pathway to the *pgr5* mutation increased the pmf and decreased proton conductivity (g_{H^+}) levels when compared to WT levels[202]. Additionally, adding a mutation in the Rieske protein of the Cytb6f complex (*pgr1* mutation) into the pgr5 mutant background, was leading to a more sensitive response to luminal acidification and increased the photosynthetic

control at Cytb6f in the double mutant (pgr5 pgr1)[204,205] and also resulted in proton conductivity (g_{H^+}) levels like in WT[202] (Fig. 17). Interestingly, when introducing the gene facilitating pseudo-CEF, the pgr5 mutant was leading to an increase in pmf, whereas the double mutant pgr5 pgr1 showed a stronger decrease in pmf compared to WT[202]. Since adding the *pgr1* mutation in the pgr5 mutant was decreasing both proton conductivity (g_{H^+}) and pmf, it was therefore concluded that rising the pmf through adding the pseudo-CEF pathway was not directly causing a drop in the mutant's membrane conductivity. It rather suggests that the addition of a transgenic Flv protein is freeing Fd^+/$NADP^+$ molecules (through the reduction of oxygen to water when accepting e- from NADPH/Fd^-). Free Fd^+/NADP could cause an increase in LEF capacity in the pgr5 mutant containing the transgenic Flv protein relative to the pgr5 mutant without this artificial pathway. When LEF is upregulated, the plant is increasing its pmf but is decreasing proton conductivity (g_{H^+}) of the ATP synthase across the thylakoid membrane when utilizing more H^+ protons through increasingly producing ATP. On the contrary, when adding the *pgr1* mutation in the pgr5 mutant background, the double mutant is more sensitive to the formation of ΔpH which could cause a stronger upregulation of photosynthetic control at Cytb6f, hence discarding more energy, and decreasing e.g. the capacity to perform LEF in the double mutant relative to WT. Consequentially, proton conductivity (g_{H^+}) is formed like in WT, and a drop in H^+ accumulation inside the thylakoid lumen results in a decrease in pmf.

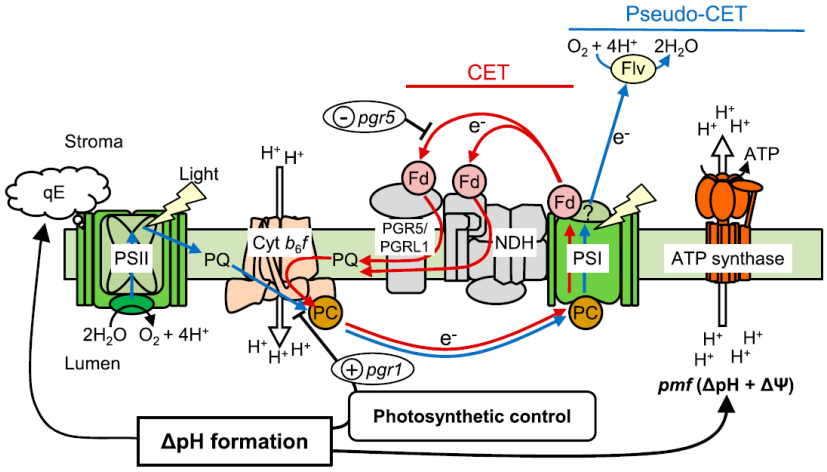

Figure 17. Model of photosynthetic e- and proton transport in genetically engineered *A. thaliana* pgr5 mutant plants. When a pseudo-CEF pathway (blue arrow) was introduced, ΔpH was formed through water splitting at PSII and the Q cycle at PSI when reducing O_2 to H_2O by accepting e- from x (Fd or NADPH) and Δpsi was decreased. Luminal acidification slows down plastoquinol oxidation at Cytb6f to stop damaging e- flow towards PSI as well as induces qE in the PSII antenna to discard excess energy as heat. Additionally, in the pgr5 mutant, the additional knock-out of *pgr1* was leading to a stronger response to ΔpH at Cytb6f increasing photosynthetic control. Adapted from Yamamoto et al. 2020[202].

In addition, when the formation of ΔpH was observed under illumination through monitoring the quenching of 9-aminoacridine fluorescence in ruptured chloroplasts, no difference was found in WT and the pgr5 mutant[202]. Additionally, when chloroplasts were treated with methyl viologen as a terminal e- acceptor, which is thought to function as an artificial e- acceptor from PSI, the pgr5 mutant restored the oxidation of PSI to WT levels, as already shown by Munekage et al. (2002)[141]. However, it has been shown by a different study in cyanobacteria that methyl viologen is partially inhibiting CEF and LEF[206]. Additionally, isolated intact chloroplasts supplemented with methyl viologen showed still ΔpH formation, measured through ΔpH-mediated 9-aminoacridine (AA) fluorescence quenching when AA was added and PGR5/PGRL1-dependent CEF-PSI was inhibited through most likely the performance of LEF[207]. Therefore, findings suggest, that the oxidation of PSI with the addition of methyl viologen in the pgr5 mutant resembles WT, due to the provision of artificial e- acceptor molecules and/or partial inhibition of CEF and/or LEF.

Moreover, it was suggested that the pgr5 mutant was still operating a type of CEF[147]. This was concluded while examining the capacity of WT, the pgr5 mutant and the crr4-2/pgr5 double mutant, lacking both PGR5 and the NDH complex, to oxidize P700 in dark-adapted leaves. When the PQ pool was saturated with a green light flash prior to the oxidation with FR light, all three plants showed a delay in P700 oxidation which was interpreted that both WT and the mutants were performing CEF at the start of illumination. This was possible because when applying a short pulse of saturating green light prior to measuring P700 oxidation with FR light the pulse is pre-reducing the electron donor pool without activating the CBB cycle. Thus, a delay in P700 oxidation resulted most likely from a closed PSI acceptor pool, hence e- transported in a cyclic manner. Under this experimental setup, it was observed that both the pgr5 mutant, and the crr4-2/pgr5 double mutant could accelerate the oxidation of P700 3 times (in the pgr5 mutant) and 7,5 times (in the crr4-2/pgr5 double mutant) relative to WT. It can be proposed that an acceleration in the oxidation of PSI is due to decreased CEF capacity in the mutants relative to WT, indicating that in the pgr5 mutant a mode of CEF was still present compared to the double mutant lacking both modes of CEF. Additionally, when the CBB cycle was light-activated prior to the measurement, the oxidation of P700 was generally increased indicating that LEF capacity was elevated. Interestingly, in the pgr5 mutant, when light-activated, P700 was more strongly oxidized relative to WT. Thus, when plants were dark- or light-preincubated before the measurement, CEF was increased in WT relative to the crr4-2 pgr5 double mutant and to a lesser extent compared to the pgr5 mutant. However, it also showed that in the pgr5 mutant a type of CEF was still operating.

Moreover, the same study also looked at the formation of NPQ which can be used as an indirect measurement of the plant's capacity to perform e- transport inside the chloroplast coupled to the translocation of protons inside the lumen hence turning on NPQ. Here, Nandha et al. (2007) showed that the pgr5 mutant was able to reach the same level of NPQ as WT, but needed a longer time for it (Fig. 18)[147]. The delay in NPQ formation in the pgr5 mutant relative to WT was shorter in the absence of CO_2 (10 minutes) than in its presence (20 minutes). This finding showed that under CO_2

limiting conditions the pgr5 mutant resembled WT faster relative to measurements with CO_2 because without CO_2 LEF is inhibited and both the pgr5 mutant and WT are performing CEF and/or alternative mechanisms to form ΔpH. Therefore, in the pgr5 mutant, either CEF and/or alternative e- transport pathways can be employed like in WT under LEF-inhibiting conditions. However, NPQ was formed in the pgr5 mutant at a reduced rate relative to WT. Therefore, the effect of the *pgr5* mutation is primarily of kinetic nature, and when long enough illuminated, the mutation has a smaller effect on NPQ than when only illuminated for short periods[147].

Moreover, after illumination with high AL in the presence of CO_2, the relaxation of NPQ in the dark was taking longer in the pgr5 mutant relative to WT. This finding was interpreted that the pgr5 mutant suffered stronger from photoinhibition when CO_2 is present and LEF can be performed relative to WT under the presence of CO_2. However, the slower relaxation of NPQ in the pgr5 mutant relative to WT was not observed under CO_2 limiting conditions. Thus, only under CO_2 limiting conditions, (when LEF was inhibited) other modes of e- transport could be increased in the pgr5 mutant relative to measurements with CO_2, leading to an increase in ΔpH and hence protecting the mutant from photoinhibition through the performance of NPQ.

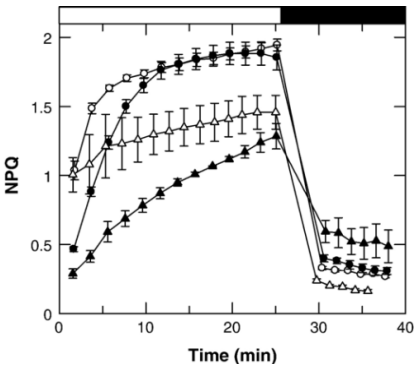

Figure 18. NPQ induction (AL, at 800 µmol m-2 s-1, the white bar at top of the graph) and relaxation (darkness, black horizontal bar) in WT (open symbols) and pgr5 mutant (closed symbols) Arabidopsis leaves exposed to 200 ppm (triangles) and 0 ppm CO_2 (circles). The y-axis represents arbitrary units of not-normalized NPQ values calculated through the formula F_m-F_m'/F_m'. Adapted from Nandha et al. 2007[147]

Furthermore, at the onset of low AL (below GL) when AA is added (inhibiting PGR5/PGRL1-dependent CEF) in WT and in the ndhB mutant, insufficient in the NDH complex, fluorescence quenching through NPQ was decreased, and steady-state fluorescence emission F_s was elevated (Fig. 19)[208]. Interestingly, NPQ was already strongly decreased in the ndhB mutant relative to WT without the addition of AA. Additionally, an increase in F_S in both WT and ndhB with AA was indicating that the PQ pool was more strongly reduced relative to measurements without AA. It can be imagined that in both cases when lacking NDH-dependent CEF or a combination of NDH-dependent CEF and PGR5/PGRL1-dependent CEF are decreasing the performance of CEF which is responsible for the translocation of H^+ protons through the thylakoid membrane and the formation of NPQ. However, only when AA is supplemented to WT and the ndhB mutant, fluorescence emission levels F_S are significantly higher compared to measurements without the inhibitor. Therefore, results suggest that PGR5/PGRL1-dependent CEF is after darkness at the onset of low AL the main contributor to NPQ, which is needed for the regulation of the redox state of the PQ pool through controlling light distribution between PSII and PSI which is in turn affecting the efficiency of photosynthetic performance.

Moreover, in WT the induction rate of photochemical quenching (qP) decreased with AA relative to measurements without the inhibitor, hence keeping Q_A for a longer time more strongly reduced (e- outflow at PSII decreased) but oxidizing it after prolonged illumination. In contrast to WT, when the NDH complex was missing, both the induction rate and the formation of qP were decreased, thus keeping PSII‘s acceptor side Q_A more strongly reduced during the whole measurement (e- outflow at PSII decreased) (Fig. 19). These findings strongly indicated that in WT and the NDH mutant, the supplementation of AA is showing the same Q_A reduction phenotype at the onset of light like in the pgr5 mutant. However, in WT, but not in the NDH mutant, PQH_2 was oxidized after prolonged illumination. This finding proposes that the oxidation of the PQ pool is enhanced in WT when PGR5/PGRL1-dependent CEF is missing because NDH-dependent CEF is present. Hence, after prolonged illumination NDH-dependent

CEF in WT- not inhibited by AA, might facilitate the performance of LEF leading to the oxidation of PSII's acceptor side.

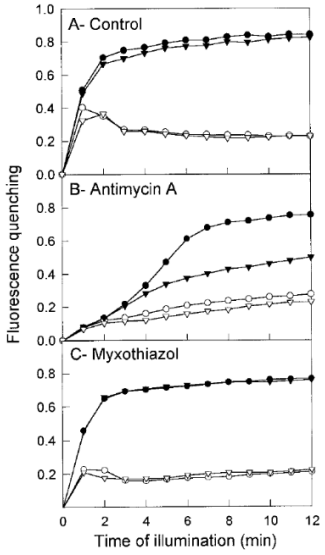

Figure 19. Dark-to-light kinetics in WT (circle) and the ndhb mutant (triangle) on stripped tobacco leaves. A. control, B. treated with 5 µM Antimycin A and C. with 10 µM myxothiazol. Photochemical qP (black symbols) and non-photochemical qN quenching (white symbols) were determined at low AL 230 µmol m-2 s-1 (growth light was 350 µmol m-2 s-1). Adapted from Joet et al. 2001[208].

1.4. Regulating the onset of photosynthesis in low light

1.4.a. The challenge to find a link between CEF, ATPase activity, PMF, NPQ, and thylakoid membrane changes at the onset of photosynthesis in low light

During the first minutes of light exposure after a dark preincubation, LEF has been suggested to be decreased due to a delay in CO_2 assimilation capacity. In this condition, the plant could switch on alternative e- flow routes, such as the reduction of molecular O_2[209], the generation of $NADP^+$ through the synthesis of malate, or employ triose phosphate transporters (reviewed 23); although, shuttles that transport electrons around

PSI via CEF[210] have been described to be the dominant form of alternative electron-flow. This alternative pathway should lead to a PSII- independent proton accumulation in the lumen and if these protons cannot be used in the synthesis of ATP for CO_2 assimilation at the onset of low light exposure, their accumulation should transiently turn on NPQ (see paragraph 1.3.b). In contrast, inhibition of CEF at PSI during the onset of photosynthesis in low-light, namely inhibition of the PGR5/PGRL1-dependent CEF mode using AA, was shown to inhibit NPQ (qE) in leaves (Fig. 19)[208].

In isolated thylakoid membranes, a linear relationship could be found between the energy-dependent quench qE and the pH or proton concentration of the intra-thylakoid space[31,211,212]. It was further shown that NPQ was linked to alterations in the trans-thylakoid pmf, consisting of a chemical (ΔpH) and electric component (Δpsi)[37,38]. Δpsi and ΔpH were suggested to keep the pH of the thylakoid lumen between pH 7.0 and 6.5[213]. A change in the use of pmf for ATP synthesis and imbalances in proton translocation into the lumen can result in lowering the pH of the lumen below 6.5. When lowering luminal pH, the plant initiates photoprotective responses such as NPQ and photosynthetic control of electron flow at the Cytb6f complex, whereby the reoxidation rate of PQ and hence of LEF is decreased[112,214].

Moreover, it has been shown that the chloroplast ATP synthase, which is redox regulated[215,216] undergoes a conformational change upon illumination that enables it to increase its activity at a lower proton concentration threshold than under dark conditions[198]. It was shown that already 4 µmol m-2 s-1 AL led to rapid activation of ATPase due to a very high redox potential of its thiols[217,218]; whereas in the dark, ATPase is reoxidized and inactivated. Kohzuma et al. (2017) showed that *Arabidopsis* mutants with ATPases that are redox-insensitive, are equally active when illuminated or dark-incubated. Mutants showed a lower transient increase in NPQ relative to WT at the onset of low AL, when the plants were incubated for a prolonged time in darkness (Fig. 20)[219,220]. In agreement with Cardol et al. (2010)[150], it has been suggested that this decrease in NPQ formation was due to the lower concentration of proton accumulation in the lumen, and a lower pmf upon a dark-to-low light transition in the presence of the constitutively active ATPase strains relative to the WT. The loss of pmf in the mutants

with redox-insensitive ATPases has been further described to enhance the turnover and repair of various photosynthetic complexes, such as the D1 protein, OEC33, and Pc[215,221]. Thus, the right interplay between CEF and LEF and the activity of the ATP synthase at the onset of light is of crucial importance when regulating the proton concentration of the intra-thylakoid space and consequential pmf formation and NPQ response. Moreover, the interplay between ATPase inactivation and activation as well as pmf formation might be a critical regulatory pathway in protecting the plant from photodamage.

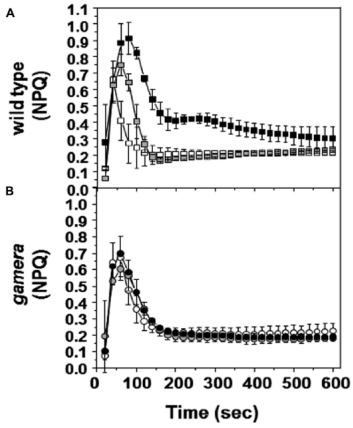

Figure 20. Dark-to-low light transition influencing NPQ in Arabidopsis WT (A) and the gamera mutant (B) (redox-insensitive ATPases which is constitutively switched on) after different dark-adaptations (1 min =white square/circle, 1 h (gray square/circle) and 10 h =black square/circle) when illuminated with 20 µmol m-2 s-1. When ATPase is constantly on, the proton-dependent induction of NPQ is released faster relative to WT upon prolonged incubation of plants in darkness. Adapted from Kohzuma et al. 2017[220].

However, it is still unknown which mechanism(s) affect(s) the relaxation of NPQ during a dark-to-low light transition. Experimental evidence indicates that CO_2 assimilation is initiated at the onset of low light, once NPQ formation relaxes (Fig. 21 A and C)[222]. However, based on a more careful but unpublished kinetic analysis the authors of the study stated that the initiation of e- flow through PSII (Y(II)) precedes the relaxation of NPQ. This would imply that the increased utilization of ATP for the CBB cycle through the performance of LEF is not fully controlling the relaxation of

NPQ and/or pmf[194,222]. Moreover, there was no correlation between the start of CO_2 assimilation and the relaxation of NPQ after dark preincubation, when very high light intensities were applied (Fig. 21 B and D), which indicated that when a stable and high ΔpH/pmf was maintained at higher irradiances, the NPQ mechanism, which resulted in the deepoxidation of violaxanthin to zeaxanthin differed from the NPQ mechanism used at low light[222]. Indeed, when leaves were illuminated at higher light intensities relative to lower light levels before a dark preincubation, when illuminated at low light, NPQ relaxation was delayed keeping NPQ levels elevated due to a higher content of zeaxanthin formed during the pretreatment with HL irradiances[223]. Additionally, at the onset of low and high light illumination, NPQ was diminished when scratched leaves were infiltrated with the inhibitor nigericin[222] or when isolated intact chloroplasts were treated with nigericin. Nigericin treatment led to the collapse of ΔpH and the inhibition of violaxanthin deepoxidation to zeaxanthin[212].

In isolated intact chloroplasts, the strongest decrease in NPQ was obtained even at low concentrations of nigericin when it was combined with AA, which was inhibiting PGR5/PGRL1-dependent CEF[212]. Interestingly, treating intact chloroplasts with nigericin increased the chloroplast's uptake of oxygen[212]. Additionally, Cardol et al (2010) showed that inhibiting mitochondrial complex III by myxothiazol and silencing complex I through directed-gene deletion (CMSII mutant) is leading to a slower and decreased formation in NPQ and delayed its relaxation [150]. It was further shown that in the CMSII mutant that was light-adapted for 15 min and subsequently illuminated with FR light, PSI oxidized slower relative to WT. It was concluded that due to the lack of mitochondrial complex III and complex I more CEF occurred through a delayed switch from CEF to LEF, causing the slow-down of P700 oxidation. In agreement, the CMSII mutant decreased Y(II) during the first minutes of illumination relative to WT. It was therefore concluded that in the mutant, a slower relaxation of the pmf and thus NPQ was due to delayed activation of the CBB cycle. Additionally, the mutant showed a smaller pool of PSI metabolic acceptor molecules at the onset of illumination. It was therefore hypothesized that the malate-oxalacetate shuttle pathway between chloroplast

and mitochondria may influence the metabolic e- acceptor pool and/or the ATP to ADP ratio, which in turn was affecting the LEF to CEF ratio.

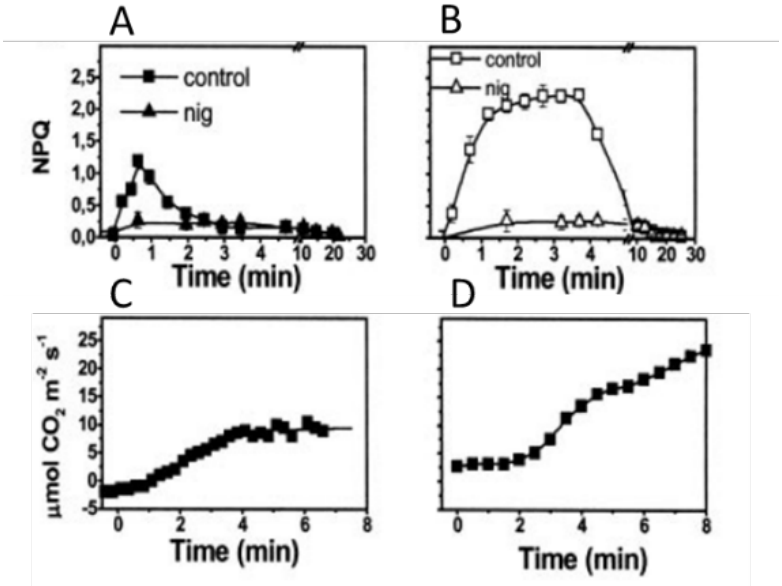

Figure 21. Dark-to-light transition in barley leaves and NPQ formation and CO_2 assimilation rates under low (A (squares) and C) and high (B (squares) and D) photon flux. Low light = 100 µmol m-2 s-1, high light= 1000 µmol m-2 s-1 and, in A. and B. leaves were scratched and treated with nigericin (triangle). Adapted from Cardol et al. 2010[150].

Moreover, while in many different knockout mutants NPQ induction was enhanced at the onset of low light, the exact role for increased NPQ is often elusive. For example, by reducing the activity of the water-splitting complex at PSII to only 20% in the Δ5 mutant, NPQ induction at the onset of low light was enhanced and needed more time to relax (Fig. 22). The same phenotype was observed in the Δ5/crr-23 double mutant, when in addition to the OEC also the NDH complex was not functional (Fig. 22). The authors concluded that the decrease in LEF when the water-splitting complex at PSII was decreased, increased the rate of CEF, which resulted in the induction of a very strong NPQ response at the onset of light[224].

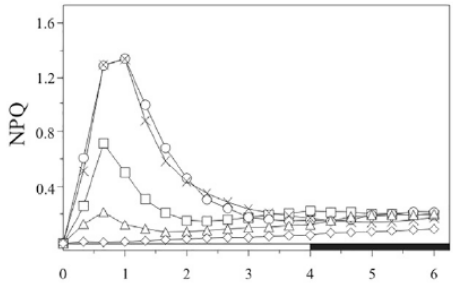

Figure 22. NPQ induction during a dark-to-light transition in WT (square) and mutant plants (Δ5= circle, Δ5 pgr5= triangle, Δ5 crr4-3= cross, and Δ5 npq4-1= diamond) at 53 µmol m-2 s-1 (white bar) for 4 min followed by a 2 min dark period (black bar). Adapted from Suorsa et al. 2016[224].

As already discussed in paragraph 1.2.c, very recent data indicated that at the onset of light, the thylakoid membrane dynamics strongly affect e- and proton transport pathways in the chloroplast[3]. During a dark-to-light transition, the activation of the protein kinase STN7 leads to a reduction in grana membrane layers and diameter and enlargement of the surface of stroma lamellae[2]. This adaptation has been suggested to upregulate both the rate of LEF and CEF[2]. This mechanism was shown to depend on thylakoid membrane changes but was independent of state transition or binding of phosphorylated LHCII molecules to PSI[2]. Contradictory to other findings, where an increase in NPQ was interpreted to be caused by an increased rate of CEF, in this model an increase in NPQ, when more protons were accumulating in the luminal space was interpreted as a decrease in ATPase activity through a decrease in LEF which is further resulting in a decrease in CEF activity.

One of the main challenges in this field of study is that no direct method exists to measure the activity of certain pathways such as the proton gradient formation or ATPase activity *in vivo*, leading scientists to perform indirect measurements on mutant strains that are incapable of or show reduced capacity performing certain regulatory mechanisms. Unfortunately, due to the complexity of analysis, investigations can usually only be conducted with a limited number of mutants, making it very difficult to draw conclusions on the interconnection of certain signaling pathways and regulatory

mechanisms. The objective of this study was to investigate a link between the state transition mutants (stn7 and pph1 mutants) as well as the npq4 mutant and the regulation of e- transport at the onset of light, after prolonged illumination at low actinic and light levels close to GL and during increasing light irradiance levels. Therefore, chlorophyll fluorescence and absorption changes of state transition mutants and the npq4 mutant were compared under the same growth conditions and experimental setup with two cyclic e- transport mutants, namely one lacking PGR5/PGRL1-dependent (pgr5 mutant) and the other NDH-dependent-CEF (crr2 mutant) around PSI. Additionally, state transition mutants were compared with cyclic mutants on the level of protein complexes present in the stroma thylakoid membrane.

2. Material and methods

2.1 Materials

Chemicals and consumables used during the conductance of the experiments are listed in table 1 and table 2 and the name of all instruments is collected in table 3. Additionally, the software used by the instruments and for data analysis is listed in table 4. A detailed description of the plant nutrient "Hoagland" solution can be found in tables 5 and 6.

Table 1. Chemical directory

Full name	**Common name**	**Company**
-2Hydroxyisobutyric acid, 99% (dry wt.), water <2%	HiBa	Alfa Aesar
Acetic acid (glacial) 100%, anhydrous		Merck
Acetone		VWR chemicals
Aluminium sulphate-(14-18)-hydrate, 97+%, crystalline		Alfa Aesar
Bis-tris propane or 1,3 bis(tris(hydroxymethyl)methylamino)propane	Bis -Tris	VWR chemicals
Boric acid		Roth
Bromphenol blue		Merck
Calcium Chloride		Merck
Calcium nitrate tetrahydrate, 98%, extra pure		Acros organics
Coomassie Brilliant Blue G250		Serva
Copper sulphate pentahydrate		Sigma-Aldrich
D(-)-Sorbitol	Sorbitol	VWR chemicals
Digitonin, high purity		Merck Calbiochem
Dimethyl sulfoxide	DMSO	Lab-Scan analytical sciences
1,4 Dithiothreitol	DTT	Biomol

EDTA Disodium salt dihydrate	EDTA	Amresco
Ethanol		Solveco
Ferric EDTA	Fe-EDTA	VWR chemicals
Glycerol anhydrous		PanReac AppliChem
Glycine		Merck
Hydrochloric acid fuming 37%		Merck
Hydrogen peroxide		VWR chemicals
Hydroxypropyl methylcellulose	HPMC	BD (Becton, Dickinson and Company)
Lithium dodecyl sulphate	LDS	Sigma-Aldrich
Luminol		PanReac AppliChem
Magnesium Chloride anhydrous		Merck
Magnesium sulphate heptahydrate		VWR chemicals
Manganese Chloride Tetrahydrate		ICN Biomed
-2Morpholinoethanesulphonic acid	MES	VWR chemicals
Methanol		Merck
Monopotassium phosphate		Roth
n-Dodecyl β-D-maltoside	β-DDM	Sigma-Aldrich
o-Phosphoric acid		Roth
p-Coumaric acid		Sigma-Aldrich
Ponceau S		Sigma-Aldrich
Potassium chloride		Roth
Potassium nitrate		Merck
Skim milk powder		VWR chemicals
Sodium chloride		VWR chemicals

Sodium dodecyl sulphate	SDS	Merck-Schuchardt
Sodium molybdate		Merck
2,7-Naphthalenedisulfonic acid, 4,5-dihydroxy-3-[(4-sulfophenyl)azo]-, trisodiumsalt	SPADNS	
Tricine buffer		Amresco
Tris-(hydroxymethyl) aminomethane	Tris	VWR chemicals
Triton X-100		VWR chemicals
Zinc sulphate heptahydrate		VWR chemicals

Table 2. Consumable directory

Consumable	**Company**
Amicon Ultra 0.5mL 100K centrifugal filters	Millipore
Antibodies (PetB, D2)	Agrisera
Anti-Rabbit IgG F (ab)2 fragment HRP	Sigma Life Science
Filter paper 3mm CHR	Whatman, GE Healthcare
MagicMark XP western protein standard	Invitrogen by Thermo Fisher Scientific
Microplate 96 well, UV-STAR, COC, F-bottom (chimney well), µClear	Greiner Bio-one
NativeMark unstained protein standard	Invitrogen by Thermo Fisher Scientific
NativePAGE 3-12% Bis-Tris gel (1mm x 10 well)	Invitrogen by Thermo Fisher Scientific
Nitrocellulose blotting membrane 0.45µm	Amersham Protran
NuPAGE 4-12% Bis-Tris gel (1.5mm x 15 well)	Invitrogen by Thermo Fisher Scientific
SeeBlue Plus2 prestained protein standard	Invitrogen by Thermo Fisher Scientific
Vivaspin 500 100K centricons	Sartorius Stedim Biotech
Planting soil (plantejord)	Tjerbo
Agra-vermiculite	LOG AS

Table 3. Instrumentation list

Instrument	Description	Manufacturer
Blotter	PierceG2 Fast Blotter	Thermo Scientific
Centrifuge 1	Centrifuge 5430 R	Eppendorf
Centrifuge 2	Centrifuge 5415 R	Eppendorf
Chemiluminescence imager	ChemiDoc™ Touch Imaging System	BioRad
DUAL-PAM-100 Measuring system	Pulse-modulated fluorescence and P700 assessment device	Walz
Electrophoresis gel tank	Novex Mini Cell, Xcell SureLock	Invitrogen
Fluorescence imager	Odyssey® CLx	Licor
Fluorescence imager	Typhoon™ Variable Mode Imager	Amersham Biosciences
Free Flow Electrophoresis system	FFE advanced	FFE service GmbH, Munich, Germany
Heating block 1	HBT 130	HLC
Heating block 2	Thermoblock 220 V	Störk-Tronic
Microplate reader	SpectraMax Paradigm Multi-Mode Microplate Reader	Molecular Devices
Mili-Q water filtration machine	Arium mini	Sartorius
pH-meter	pH 210 microprocessor pH meter	Hanna instruments
Pipettes	Pipetteman	Gilson
Scanner (white-light)	CanoScan 9950F	Canon Solutions
Shaker 1	CH-4103 Bottmingen	Infors AG
Shaker 2	PMR-30 Mini Rocker-Shaker	Grant-bio
Spectrometer	UV-2401PC Spectrometer	Shimadzu
Voltmeter 1	Electrophoresis power supply - EPS 600	Pharmacia Biotech
Voltmeter 2	Electrophoresis power supply - EPS 301	Pharmacia Biotech
Water distiller	Aqua Purificator G 7795	Miele

Table 4. List of software used at different machines/tasks

Instrument/task	**Software**
Fluorescence image Odyssey® CLx; Licor/ Gel scan analysis	Image studio lite Version 5.2
ChemiDoc™ Touch Imaging System; Biorad/ Gel scan analysis Typhoon scan and Western Blot analysis	Image lab Version 6.1
DUAL-PAM-100 Measuring system; Walz/ Chlorophyll fluorescence and absorption spectroscopy	PAM software Version 1.19
Mass spectrometry analysis	Scaffold_version 4.8.6, Proteome Software Inc., Portland, OR
PAM data analysis	Origin Pro 2018b

Table 5. Stock solution plant nutrients "Hoagland"

Chemical	1 L 10x solution	Final 1x concentration
1 M KH_2PO_4	10 ml	1 mM PO_4^{-2}
1 M KNO_3	50 ml	5 mM NO_3^-
1 M $Ca(NO_3)_2 : 4H_20$	50 ml	10 mM NO_3^- 5 mM Ca^{2+}
1 M $MgSO_4 : 7H_20$	20 ml	2 mM Mg^{2+} 2 mM SO_4^{-2}
1 % Fe-EDTA	10 ml	
Micronutrients	10 ml	

Table 6. Micronutrient solution for Hoagland stock solution in table 5.

Chemical	Amount (g)
H_3BO_3	2.86
$MnCl_2 : 4H_2O$	1.81

$CuSO_4 : 5H_2O$	0.089
$ZnSO_4 : 7H_2O$	0.22
$Na_2MoO_4 : 2H_2O$	0.029

2.2 Methods

2.2.a Plant material, growth conditions, and growth monitoring

A. thaliana (L.) mutant plants of stn7, pph1, and npq4 and corresponding WT ecotype Columbia-0, and mutant plants crr-22, pgr5-1, and the corresponding WT ecotype Columbia gl1, and overexpressor CurtA (OE CurtA) and its corresponding WT ecotype Ler-0 were grown in the laboratory under light intensities around 80- 90 µmol m-2 s-1 under a 8 h:16 h light: dark photoperiod at 22 °C for about 10- 13 weeks. As a light source, Philips de Luxe Pro TL5 HC 49W/965 lightbulbs were used. Plants were grown in commercially available soil (plantejord Tjerbo) in combination with agra-vermiculite 3:1. Plants were watered -23 times a week and fertilized once a week with Hoagland solution (detailed recipe see 2.1. materials table 5 and 6). *A. thaliana* seeds were graciously provided by: Jean-David Rochaix, Department of Molecular Biology, the University of Geneva, Switzerland for the stn7 mutant and WT ecotype Col-0, Toshiharu Shikanai from the Department of Botany, Kyoto University, Japan for crr-22, pgr5-1 and WT ecotype Ler, Matthew P. Johnson, Department of Molecular Biology and Biotechnology at University of Sheffield, Great Britain for the npq4 mutant and Mathias Pribil, Department of Plant and Environmental Sciences at University of Copenhagen, Denmark for WT ecotype Columbia-0, OE CurtA (overexpressor of CurtA) and WT ecotype Ler seeds. The pph1 mutant (SALK_025713) was purchased from the SALK institute. For analysis of growth curves in WT Col-0, images of the mutant plants stn7 and pph1 were recorded over 9 weeks using raspberry pi, and the area of the plants was collected by analysis of images via ImageJ.

2.2.b Isolation of chloroplasts and protein complexes

For the analysis of protein complexes, 13- to 15-week-old plant leaves were harvested after 2 h of light pre-incubation. Leaves were cut in cold isolation media (10 mM Hiba (-2Hydroxyisobutyric acid), 300 mM Sorbitol, 5 mM $MgCl_2$, 5 mM KCl, 5 mM $CaCl_2$(x2H_2O), titrated with BisTris to pH 6.8), filtered through nylon gauze (22 µM) and chloroplasts were pelleted through a 2 min centrifugation step at 2000 g at 10 °C. To lyse the chloroplasts and remove unwanted cell debris, chloroplasts were incubated in 1x cold TMK (0.1 M Tris-HCl pH 8.5, 0.1M MgCl2, 0.2 M KCl) buffer for 10 min on ice and then centrifuged for 3 min at 5700 g at 10 °C. The pellet was further washed three times in 1x TMK buffer. The pellet was taken up in buffer that was used to inject the sample into the FFE chamber (separation buffer 4: 250 mM Sorbitol, 10 mM Acetic Acid, with Tris to pH 7.5) and proteins of the chloroplasts were solubilized according to chlorophyll concentration of the chloroplast extracts as determined by Porra et al. (1989)[225]. For the solubilization, each chloroplast isolation was adjusted to a chlorophyll concentration of 1,4 µg/µl in a total volume of 350 µl (equivalent to 490 µg chlorophyll), then 16 mM digitonin was used for solubilization. The solubilization mix was first incubated 10 min at 10 °C and then spun for 30 min at 30300 rcf at 10 °C. Only the top 200 µl of the solubilization mix was applied for FFE.

2.2.c Analysis of protein complexes via interval zone free flow electrophoresis (IZE-FFE) and LDS-Native-PAGE

Interval zone free flow electrophoresis (IZE-FFE) provides a novel approach in proteomics to separate membrane protein complexes in an aqueous medium, at low temperatures (10 °C) and through fast (<4 min) and highly reproducible processing. Moreover, by not inducing any solid matrix, such as polyacrylamide, the size of supramolecular arrangements is not restricted. In contrast, the molecular mass entry limit of high-resolution polyacrylamide gel matrices is according to the protein standard of about 1,5 MDa[226]. When keeping supercomplex structures in a liquid phase many additional steps are needed to analyze the complex that compromises complex stability can be circumvented. Using this methodology, the separation of membrane protein

complexes has been achieved within 235 seconds (Fig. 23). Protein complexes are separated according to their native charge of the complexes, and resolution is obtained through mobility differences in defined pH zones. Separated protein complexes are collected in 96-well microtiter plates. In this study, membrane protein structures of *A. thaliana* were separated via IZE-FFE and then further analyzed via LDS-Native-PAGE. While many membrane supercomplex structures separated through IZE-FFE were too large to enter the native gel and thus could not be resolved in detail, still, differences in the thylakoid membrane protein structure of different mutant plants could be derived. Additionally, by adding β-DDM to the liquid fractions, proteins located in the higher molecular weight complexes (HMW) could be solubilized and analyzed.

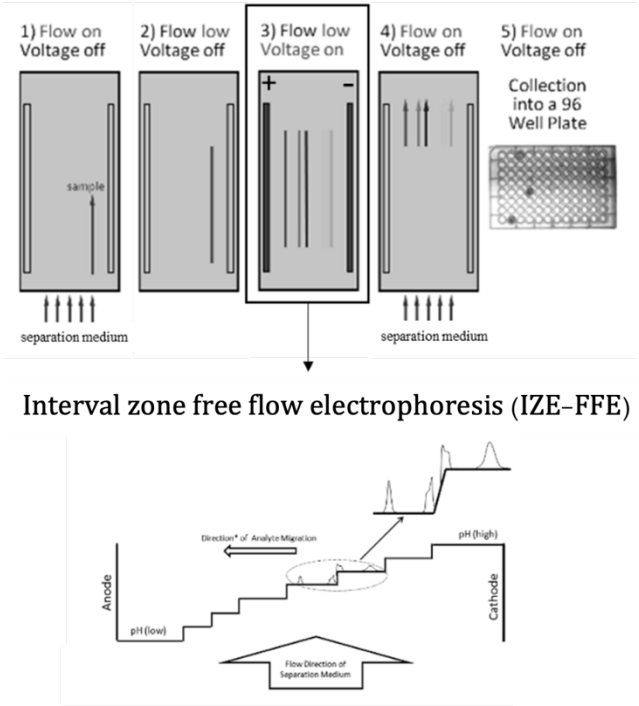

Figure 23. Separation of thylakoid membrane supercomplex protein structures via interval zone free electrophoresis (IZE-FFE). Solubilized proteins of the thylakoid membrane were separated in a liquid separation medium over 235 seconds. First, the sample was injected (1), then the high voltage (1599 V) was turned on (2), the protein supercomplexes were separated at low speed of the separation media with defined pH zones (4), and protein complexes were eventually pooled

and collected 96-wells. Illustration modified from FFE service GmBH (https://www.ffeservice.com/).

All IZE-FFE separations were performed on a free-flow electrophoresis (FFE) advanced system (FFE Service GmbH, Germany) with a gap size of 0.2 mm. Before the operation, 1. the uniform tube flow was tested through the application of a chemical color solution (SPADNS), 2. the chamber was coated with 0,2 % HMPC, and 3. pH steps were controlled by separating a mix of chemicals with known PI's. As electrode buffers and anodic and cathodic stabilization buffers (inlet 1 and 9) 200 mM acetic acid and 200 mM tris, adjusted with acetic acid to pH 7.5 were used. Separation buffer 1 (inlet 2) contained 20 mM Tris, 10 mM acetic acid, 250 mM sorbitol, and 150 µM β-DDM and was adjusted with acetic acid to pH 6.5; separation buffer 2 (inlet 3) contained 10 mM tris, 10 mM acetic acid, 250 mM sorbitol, 150 µM β-DDM and was adjusted with acetic acid to pH 6.5; separation buffer 3 (inlet 4 and 5) contained 10 mM Tris, 10 mM Acetic acid, 250 mM sorbitol and was adjusted with Tris to pH 7.0; separation buffer 4 (inlet 6, 7 and 8) contained 10 mM Tris, 10 mM acetic acid, 250 mM sorbitol and was adjusted with tris to pH 7.5. The separation media was diluted at the end of the separation with a counter-flow solution composed of 250 mM sorbitol. Samples were applied via inlet 7 at pH 7.5, on the cathodic side of the separation chamber. For the separation, the sample was applied continuously at a sample pump rate of 1700 µl/h and separated at a buffer flow rate of 120 ml/h at a high voltage setting of 1500 V, 150 mA, and 150 Watt. Separated protein complexes were collected in 96-well polyethylene microtiter plates (Greiner Bio-One UV-STAR; 655801). With each sample, IZE-FFE was repeated three times.

Samples in microtiter plates were processed for LDS-Native-PAGE as followed. Selected fractions were up-concentrated in 100 K cut-off filters (Millipore; Amicon Ultra 0.5 mL) and the same volume of up-concentrated sample was solubilized a second time with 5 mM digitonin. When stated the third solubilization with 1,25 mM or 2,5 mM with β-DDM was done. Samples were run in 1x sample buffer (0,05 M BisTris, 1,5 N HCl, 10 % (w/v) Glycerol, 0,05 M NaCl, 0,0125 mM PonceuS) on Native-PAGE 3-12 % BisTris gel (1mmx 10 well; Invitrogen by Thermo Fisher Scientific) in a native

buffer (50 mM BisTris and 50 mM Tricine) containing if specified 80 µM LDS to the cathode buffer. For 2D-Native-PAGE analysis, cut gel bands were loaded in 4x sample buffer containing 2 mM β-DDM. Native-PAGE gels were run cooled overnight at 17 V and 2D-NativePAGE gels at 5 V. After 13-15 h to finish the run the voltage was increased to 30V. Gel bands were stained using colloidal Coomassie stain[227]. Stained and unstained gels were scanned at ex 685 nm/ em 700 nm and ex 785 nm/ em 800 nm (Odyssey® CLx; Licor). Bands were cut and frozen at -80 °C before MS analysis.

2.2.d Immunoblot analysis of protein complexes' subunits

Immunoblot analyses were performed using equal volumes of up-concentrated sample fraction derived from IZE-FFE. Samples were loaded with 6x sample buffer (30 % Glycerol, 0.56 M Tris-HCl pH 6.8, 6 mM EDTA, 10 % Sodium dodecyl sulphate (SDS), 179.11 µM Bromphenol blue and freshly added 100 mM DTT) on NuPAGE 4-12% BisTris gels (1,5 mm x15 well; from Invitrogen by Thermo Fisher Scientific) and run at 200 V with 1x SDS-PAGE MES-Tris running buffer pH 7.3 (50 mM MES, 50 mM Tris Base, 0.1 % SDS,1 mM EDTA). The gels were semi-dry electroblotted (PierceG2 Fast Blotter; Thermo Scientific) onto a nitrocellulose membrane using transfer buffer (96 mM Glycine, 10 mM Tris, and 10% freshly added methanol) and incubated for 45 min gently shaking in 5 % milk containing 1x TBS (0.02 Tris-HCl pH 7.5, 0.15M NaCl). Membranes were incubated in the first antibody in 1x TBS gently shaking in the cold room overnight at concentrations according to the manufacturer (www.agrisera.com) and then washed 5 min in 1x TBS, incubated in anti-rabbit-IgG for 1 h and 20 min and washed 5 min in 1x TBS. Chemiluminescence was detected (ChemiDoc™ Touch Imaging System; BIORAD) using a home-made ECL (enhanced chemiluminescence) reaction mix (0.1 M Tris-HCl pH 8.3, 2.5 mM Luminol, 9 mM p-Coumaric acid, 0.1 M Tris-HCl pH 8.3, 0.0183 % H_2O_2) and exposing images between 40-120 sec. The antibodies were commercially bought at Agrisera (https://www.agrisera.com) and the first antibodies were used in a dilution

recommended by the manufacturer, while the secondary antibody (anti-rabbit-IgG) was used in a dilution 1:5000 always.

2.2.e Mass spectrometry analysis

Mass spectrometry analyses were performed at Cambridge's Centre for Proteomics, UK. Gel pieces were reduced with DTT and alkylated with iodoacetamide. Then samples were subjected to enzymatic digestion with sequencing grade trypsin (Promega, Madison, WI, USA) overnight at 37 °C. After digestion, the supernatant was pipetted into a sample vial and loaded onto an autosampler for automated LC-MS/MS analysis.

All LC-MS/MS experiments were performed using a Q Exactive Orbitrap mass spectrometer (Thermo Fisher Scientific Inc, Waltham, MA, USA) and a Dionex Ultimate 3000 RSLC nanoUPLC (Thermo Fisher Scientific Inc, Waltham, MA, USA) system. Separation of peptides was performed by reverse-phase chromatography with a Thermo Scientific reverse-phase nano Easy-spray column (Thermo Scientific PepMap C18, 2 µm particle size, 100A pore size, 75 µm i.d. x 50cm length) at a flow rate of 300 nL/min. Peptides were loaded with 0.1% formic acid for 3 minutes at a flow rate of 10 µL/min onto a pre-column (Thermo Scientific PepMap 100 C18, 5 µm particle size, 100A pore size, 300 µm i.d. x 5mm length) from the Ultimate 3000 autosampler. After this period, the column valve was switched to allow elution of peptides from the pre-column onto the analytical column. Solvent A was water + 0.1% formic acid and solvent B was 80% acetonitrile, 20% water + 0.1% formic acid and the linear gradient employed was -240% B in 30 minutes. Further wash and equilibration steps gave a total run time of 60 minutes.

The LC eluant was sprayed into the mass spectrometer by means of an Easy-Spray source (Thermo Fisher Scientific Inc.) and subsequently all m/z values of eluting ions were measured in an Orbitrap mass analyzer (was scanned between m/z 380-1500 and set at a resolution of 35000). Data dependent scans (Top 20) were employed to

automatically isolate and generate fragment ions by higher energy collisional dissociation (HCD, NCE:25%) in the HCD collision cell. The measurement of the resulting fragment ions was performed in the Orbitrap analyzer (set at a resolution of 17500). Singly charged ions and ions with unassigned charge states were excluded from being selected for MS/MS and a dynamic exclusion window of 20 seconds was employed.

Post-run, the data was processed using Protein Discoverer (version 2.3., ThermoFisher). Briefly, all MS/MS data were converted to mgf files, and the files were then submitted to the Mascot search algorithm (Matrix Science, London UK, version 2.6.0) and searched against a common contaminants database (125 sequences) and the UniProt Arabidopsis thaliana database (CCP_Uniprot_Arabidopsis_thaliana_20180514, 41675 entries). Mascot was searched with a fragment ion mass tolerance of 0,100 Da and a parent ion tolerance of 20 PPM. Carbamidomethyl of cysteine was specified in Mascot as a fixed modification. Deamidated of asparagine and glutamine, oxidation of methionine and phosphorylation of serine, threonine and tyrosine were specified in Mascot as variable modifications.

Scaffold (version Scaffold_4.10.0, Proteome Software Inc., Portland, OR) was used to validate MS/MS based peptide and protein identifications. Peptide identifications were accepted if they could be established at greater than 95,0% probability by the by the Scaffold Local FDR algorithm. Protein identifications were accepted if they could be established at greater than 99.0% probability and contained at least 2 identified peptides. Protein probabilities were assigned by the Protein Prophet algorithm[228]. Proteins that contained similar peptides and could not be differentiated based on MS/MS analysis alone were grouped to satisfy the principles of parsimony. Proteins sharing significant peptide evidence were grouped into clusters.

2.2.f Chlorophyll fluorescence and absorption measurements through pulse-modulated spectroscopy

For PAM spectrometry, chlorophyll (Chl) fluorescence (> 700 nm) when excited with actinic light (AL) (at 635 nm) and absorption changes (absorption difference spectra of 830 nm and 875 nm) were measured simultaneously using DUAL-PAM 100 (Walz). First, the dark fluorescence yield (F_0) was determined after µsec-pulses of measuring light (ML; 620 nm at 5 µmol m-2 s-1) were applied. Then, saturation pulses (SPs) from red LEDs (635 nm) with 6000 µmol m-2 s-1 were applied for a duration of 200 ms every 30 sec to determine the maximum Chl fluorescence with closed PSII centers after 15 min dark preincubation (F_m) and during illumination (F_m') with red LEDs (635 nm). The dark fluorescence yield (F_0') was calculated when AL was turned on by the approximation of Oxborough and Baker (1997)[229] $F_0'=F_0/(F_v/F_m+F_0/F_m')$ (Fig. 24).

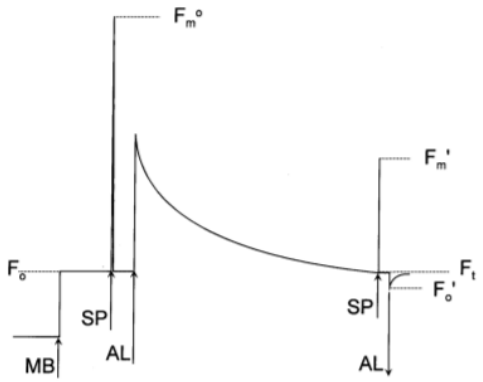

Figure 24. Sequence of a typical fluorescence trace determined by pulse-modulated fluorescence spectroscopy. First, the ML is switched on (↑MB) and the dark fluorescence yield (F_0) is measured. Through the application of a saturation light pulse with high intensity (↑SP) the maximal fluorescence yield in the dark (F_m) is determined. Then AL, driving photosynthesis, is applied (↑AL). After a defined time interval, another SP allows measuring of the maximal fluorescence in the light (F_m'). In addition, the fluorescence level before the SP is applied is termed F_t (or F_s). Turning off the AL (↓AL), typically in the presence of far-red light or in the case of this study after the calculation of F_0' after Oxborough and Baker (1997)[229] allows estimating the dark fluorescence yield (F_0') when the leaf was illuminated. The x- axis is given in minutes and the y-axis is showing arbitrary fluorescence units. Adapted from Maxwell and Johnson 2000[230].

The effective quantum yield of PSII [Y(II)] in AL was calculated as (F_m'-F_s)/F_m'[40]. Fluorescence F_s is the steady-state Chl fluorescence level in the presence of red AL from LEDs. qL, a parameter estimating the fraction of open PSII centers (redox state of Q_A) providing an approximation of the photochemical quench performed by the plant, was calculated according to the lake model using qL= (F_m'-F)/(F_m'-F_0') x F_0'/F)). The lake model assumes perfect connectivity between PSII reaction centers across the membrane, through being connected by LHCs. Alternatively, the membrane can be described as a collection of disconnected "puddles" of light-harvesting complexes that each contain one reaction center (defined as qP). This means that in the lake model it is estimated that excitation energy is very likely transferred from closed to neighboring open centers. In contrast, when estimating qP, it is considered that pigments are separated from one another and each antenna cluster contains one reaction center[231]. It is regarded that in the lake model the pigment antenna organization is more realistically described than in the puddle model and that in the latter the fraction of open PSII centers is overestimated. Y(NPQ), the quantum yield of regulated energy dissipation was calculated according to Kramer et al. (2004)[232] by the equation: Y(NPQ)= 1-Y(II)-1/(NPQ +1+qLx(F_m/F_0-1). Additionally, to derive the quantum yield of regulated energy dissipation NPQ without assuming that the PSII pigments are organized to the lake model principle based on a Stern-Volmer approach[232], Fm and F_m' values were interpreted (after Holzwarth et al. 2013[233]). In the latter, F_m'(t) is showing a decreasing function, starting from the unquenched F_m to F_m' at a certain AL intensity with the lowest level of fluorescence indicating the state of fully operative quenching mechanism(s). Those F_m'(t) values represent the quenched fluorescence level at different AL intensities when all PSII RCs are closed (for reviews see[234,235]). Therefore, F_m'(t) is giving us directly the measurable signal that defines quenching. Instead of transforming F_m'(t) into a so-called Stern-Volmer quenching function in Y(NPQ), the decay in F_m' was measured directly. According to Holzwarth et al. 2013[233], NPQ would only have a theoretical base in Stern-Volmer quenching in the very unlikely situation when the concentration of quencher would increase linearly with time after the onset of actinic radiation.

The level of oxidized P700 was monitored as the absorption difference was at 875 nm minus 830 nm. In analogy to the quantum yields of PSII, the quantum yields of PSI were determined using the SP method[236]. The maximum oxidizable P700 (P_m), was determined after dark preincubation by application of an SP in the presence of FR light at approx. 720 nm. To oxidize the entire system, FR light (25.6 Wm-2) was applied from 200 ms before the start of the saturation pulse to its cessation. The complete reduction of P700 is induced after the cessation of FR light and SP application defined as the dark P700 signal (P_0). Moreover, P_m' represents the maximal change of the P700 signal during illumination determined by the application of an SP. When AL is turned on, the part of P700 centers that is oxidized (donor-side limited closed centers ($P700^+A$)) is estimated with the help of the determination of a transitional P700 level (P) (Y(ND) = P-P_0 or Y(ND) =1- P700 red.). After the P level is reached, the application of an SP leads to the oxidation of the active P700 fraction, and when knowing the maximal change of the P700 signal during illumination is determined by the application of an SP (P_m') the active fraction of P700 can be determined (P_m'-P). Additionally, the part of the P700 center that cannot be oxidized (acceptor-side limited closed centers ($P700^-A$) is estimated (Y(NA)

= P_m - P_m'/P_m) (Fig. 25). All parameters with corresponding equations are collected in table 7.

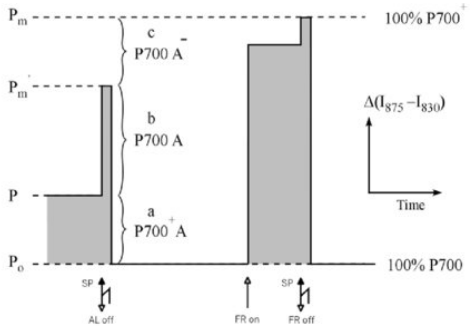

Figure 25. Illustration of the principle of pulse-modulated spectroscopy (PAM) methodology to determine the efficiency of energy conversion in PSI. P700 is determined by

the difference of 875 nm and 830 nm pulse-modulated measuring light reaching the photodetector. Complete P700 oxidation (characterized through a positive signal change) is induced through a short saturating pulse of high intensity (SP), in the presence of far-red light (FR) and defined as the maximal P700 signal (P_m). In contrast, complete reduction of P700 is induced after the cessation of FR light, and SP application defined as the dark P700 signal (P_0). When AL (AL) is turned on, a fraction of P700 centers (a), which represents donor-side limited closed centers $P700^+A$ is oxidized and estimated through a transitional P700 level (P). When this level is reached, the SP-induced signal indicates the further oxidation of the active P700 fraction (b), which represents open P700 centers through determining the maximal P700 signal (P_m') subtracted from the transitional P700 level (P) during AL illumination. Additionally, the fraction of closed P700 centers (c), which represents acceptor-side limited closed centers that cannot be oxidized corresponds to the difference between P_m and P_m'. Adapted from Klughammer and Schreiber 2008[237].

Table.7. Parameters and corresponding equations determined in pulse-modulated spectroscopy.

parameter	formula
Y(II)	$(F_m'-F_s)/F_m'$
Y(NPQ) (after Stern-Volmer approach)	1-Y(II)-1/(NPQ +1+qLx(Fm/F_0-1)
qL	$(F_m'-F)/(F_m'-F_0')$ x $F_0'/F)$)
NPQ (after Holzwarth 2013[233])	F_m'/F_m
F_0'	$F_0/(F_v/F_m+F_0/F_m')$
Y(I)	1-Y(NA)-Y(ND) or P_m'-P
Y(ND); PSI donor side limitation	1-P700 red. or P-P_0
Y(NA); PSI acceptor side limitation	$(P_m-P_m')/P_m$

During a dark preincubation period, the whole plant was incubated in darkness for 15 min. Plants were taken for measurements after the night when adapted at least for 1h to growth light (85 µmol m-2 s-1) conditions. Measurements were performed on cut leaves. For each measurement, two leaves were put on top of each other. Light intensities were used during the measurements as indicated in the text and figures.

In the case of light-response experiments (LREs) light intensities steps (11, 18, 27, 58, 100, 131, 221, 344, 536, 830 µmol m-2 s-1) were applied for 30 seconds to reach the steady-state at each light irradiance level and parameters were determined through the application of an SP at the end of each illumination step. In the case when light preincubation was used, F_m, $F_{0,}$ and P_m were determined after the whole plant was incubated for 15 min in darkness, subsequently, leaves were cut and incubated for another 15 min at 75 µmol m-2 s-1 red AL (635 nm) inside the leaf chamber. When FR light (approx. 720 nm) was added during kinetics if no other was indicated 70 µmol m-2 s-1 FR light was used and when supplemented during LRE 132 µmol m-2 s-1 FR light was applied.

3. Results

For ease of reading all figures of the result, discussion and supplements can be found in a bigger size in a separate document named “Appendix A figures and figure text”.

3.1. Pulse-modulated spectrometry results: state transition mutants (stn7 and pph1 mutants) and the npq4 mutant

3.1.1 A kinetic analysis at the onset of low light close to GL conditions in stn7, pph1, and npq4 mutant leaves

The distribution of light energy and the electron transport rate between PSII and PSI is affected in a process termed state transition by phosphorylation of LHCII. The change in e- transport was studied at the onset of illumination after a dark preincubation. State transitions were investigated in *A. thaliana* mutant plants in which LHCII is coupled to PSII (in the stn7 mutant), and LHCII is coupled to PSI (in the pph1 mutant). Also, the npq4 mutant plant was studied as the mutant performs state transition but lacks PsbS, a protein discussed in the regulation of a process termed qE in which light energy is discarded in the form of heat at PSII.

At first, the contribution of light energy harvesting through LHC and its utilization at one of the photosystem reaction centers to release electrons into the photosynthetic electron chain was analyzed. Here, the effective photosynthetic quantum yield at PSII (Y(II)) and PSI (Y(I)) was determined, and the ratio of Y(I) to Y(II) was analyzed (Fig. 26). This allowed determining the relative contribution of the reaction centers to the overall photosynthetic e- flow (Fig. 26 C and D). During the first minute of the onset of illumination, electron outflow from the acceptor side of PSII and PSI was activated, leading to an oxidation of PSI’s acceptor side (decrease in the level of Y(NA)) and a lesser extent of PSII‘s acceptor side (decrease in Q_A levels) (Fig. 26 A, D, C, and F). At the same time, e- flow between photosystems was slowed through minor and transient

oxidation of PSI's donor side (increase in Y(ND) levels) (Fig. 27 B and E). A constant light intensity correlates to a continuous rate of electron inflow into the electron transfer chain (ETC). At the same time, a decrease in the reduction level of the photosystems acceptor-side represents an increase in the rate of electron outflow from the ETC relative to a continuous electron inflow at its donor site. A change in the rate of electron outflow from PSI is termed LEF and is considered in contrast to CEF, in which electrons circulate PSI. With this understanding in mind, electrons circulating PSI in CEF reduce the acceptor-sides of PSII and PSI. At PSII, this requires a distinction between light-dependent electron inflow and CEF. Both PSII and PSI are coupled in the ETC. A change in the rate of electron outflow at PSII could directly affect the rate at which electrons reduce the donor side at PSI. Therefore, the PQ pool at the acceptor side of PSII buffers the rate of electron delivery to the donor side of PSI to sustain the photon-dependent rate of PSI reduction at its acceptor site. However, rate changes in the photon-dependent reduction of the acceptor-side of PSII or PSI should well affect the filling or reduction state of the PQ and $NADP^+$ buffer. A change in the two buffers' filling state can also affect the enzymatic rate of electron unloading at the acceptor-sides of PSII and PSI. According to this understanding, a reduction state of 50% means that the rate of electron outflow from the acceptor-sides relative to electron inflow is balanced at 50% of the two capacities regulating electron flow. If the value is higher or lower than 50%, the balanced difference between inflow and outflow rates has decreased or increased. Moreover, the rate of PSII acceptor side oxidation or e- outflow through LEF and of PSI donor side reduction or e- inflow through CEF is under the additional control of the rate of proton pumping at the Cytb6f complex. The rigid coupling of electron and proton flow means that the rate of proton usage by the ATPase complex is an essential element in regulating the rate of electron flow through the Cytb6f complex. The critical regulatory position of the Cytb6f complex for coupling the rate of electron flow between PSII and PSI has found a special recognition in the term "photosynthetic control." It is suggested in the literature that the rise in PSI donor side oxidation is caused by an increase in the proton gradient after dark preincubation at the onset of light when the ATPase is not fully activated[108,109,238–243].

Our data showed that through the outflow of electrons into the metabolic pool, Y(I) increased about Y(II) (Fig. 26 A and B). The relative contribution of electron flow through PSI (Y(I)) was higher than through PSII (Y(II)) in WT and the stn7 mutant, while the pph1 and the npq4 mutant showed a more balanced e-flow indicated by an about 1:1 ratio of Y(I)/Y(II) (Fig. 26 A and B). This observation showed that both dark-adapted WT and stn7 mutant plants decreased e- flow through PSII relative to PSI. In contrast, the pph1 mutant - in state 2 with phosphorylated LHCII at PSI - showed a more balanced e- flow through both photosystems relative to WT and the stn7 mutant. Also, e- flow between PSII and PSI was more balanced in the npq4 mutant. Thus, an increase in light absorption at PSII mediated by the lack of qE in the npq4 mutant did not lead to a more substantial reduction in PSII relative to PSI. Surprisingly, a more balanced e- flow through PSI and PSII in the npq4 mutant was achieved by decreasing e- turnover not only at PSII but also at PSI. In the next step, Y(I), Y(II), and the ratio of the two were analyzed in more detail and complemented with Chl fluorescence and absorption studies of PSII's acceptor side Q_A and PSI's donor side represented by Y(ND) levels and acceptor side represented by Y(NA) levels.

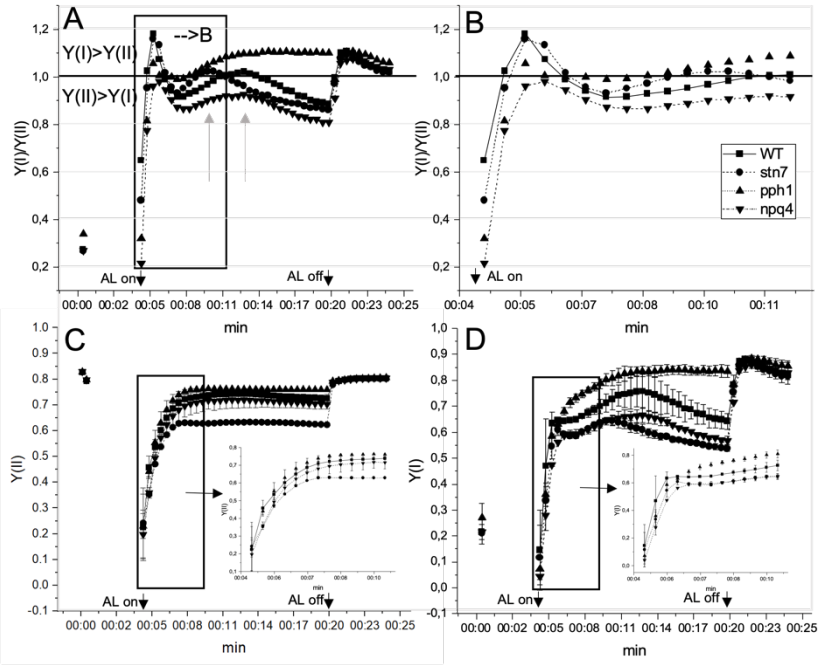

Figure 26. Photosynthetic performance of PSII and PSI during a dark-to-low light transition and when the light was switched off in *A. thaliana* WT (■) and mutants stn7 (●), pph1(▲), and npq4 (▼). A kinetic steady-state analysis of e- flow at A. the ratio of Y(I)/Y(II), B. the ratio of Y(I)/Y(II) during the first six minutes of illumination (indicated with a black box in A.), C. PSII (Y(II)) and D. PSI (Y(I)) were determined via pulse-modulated spectroscopy. Both in C. and D., the first six minutes (indicated with a black box) of illumination were magnified and displayed as a small inset. When during the measurement AL was turned on and off as indicated by small black arrows and "AL on" or "AL off". In addition, the switch in WT and stn7 from a balanced Y(I)/Y(II) towards Y(II)>Y(I) was labeled by grey arrows. The x-axis refers to time (in min) and the y-axis to normalized arbitrary units (calculated according to method section 2.2.f). The AL used in the measurement was 58 µmol m-2 s-1 and plants were grown at 85 µmol m-2 s-1. Average values from three to five different plants are shown for each genotype and bars indicate standard deviation.

Kinetic analysis of the first minute after the onset of low light showed that the rate of Y(II) increase was slower in both stn7 and npq4 mutants relative to WT and the pph1 mutant (Fig. 26 C inset). The slower rate in Y(II) increase (Fig. 26 C) was caused by a slower decrease in the Q_A level (determined through 1-qL), hence e- outflow at the acceptor side PSII was lowered in the stn7 and the npq4 mutant relative to WT, and the pph1 mutant (Fig. 27 A and D). We concluded that Q_A and the directly coupled PQ

pool stayed more strongly reduced in both the stn7 and the npq4 mutant relative to WT and the pph1 mutant. This observation originated either from the mutant's increased light absorption at PSII and/or a decrease in linear e- transport and a rise in e- inflow through cyclic e- transport relative to WT and the pph1 mutant.

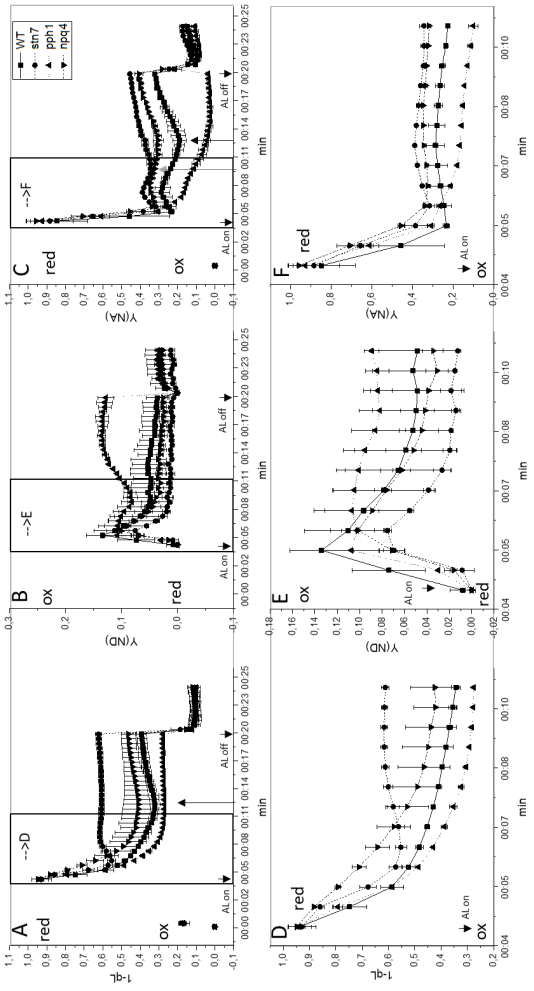

Figure 27. The oxidation state of PSII's acceptor side Q_A (1-qL) and PSI's donor and acceptor side during a dark-to-low light transition and when the light was turned off in WT (■), stn7 (●), pph1 (▲), and npq4 (▼) *A. thaliana* leaves. Kinetic steady-state analysis of the

redox state of Q_A (1-qL) (A and D), PSI's donor side limitation Y(ND) (B and E), and PSI's acceptor side limitation Y(NA) (C and F) were determined via pulse-modulated spectroscopy. The x-axis refers to time (in min) and the y-axis to normalized arbitrary units (calculated according to method section 2.2.f). The AL used in the measurement was 58 µmol m-2 s-1 and plants were grown at 85 µmol m-2 s-1. Average values from three to five different plants are shown for each genotype and bars indicate standard deviation.

During the first minute of illumination, the rate of Y(I) increase in the stn7 mutant was comparable to WT and the pph1 mutant. In addition, PSI's donor side was more strongly reduced (Y(ND) value decreased), while the decrease of PSII's acceptor side limitation was slowed down (Q_A levels increased) (Fig. 27. A, B, D, and E), indicating that e- inflow at PSI's donor side was increased and e- outflow at the acceptor side of PSII was decreased. Hence, it can be speculated that not linear but cyclic e- supply to PSI was increased. Also, PSI's acceptor side limitation was enhanced (Y(NA) levels increased), further strengthening that the rate of e- outflow into the metabolic pool was decreased relative to WT (Fig. 26 E and F), supporting that in the stn7 mutant more e- were flowing from PSI towards the PQ pool through CEF.

Another important observation was that at the very onset of AL, NPQ (measured through Y(NPQ) and F_m'/F_m) was increased in WT, stn7 and pph1 mutants but not in the npq4 mutant (Fig. 28 and 29). It was extensively discussed in the literature that a decrease in F_m' at the onset of light was caused by the formation of a proton gradient before the ATPase is fully activated, leading to the acidification of the lumen and initiation of PsbS-dependent quench qE. qE is the fastest form of NPQ and enables the plant to discard photons by dissipating heat (for review see Ruban 2018[107]). Furthermore, it was shown that qE works independently of zeaxanthin formation[89]. Interestingly, the transient increase in NPQ needed a longer time to relax in the stn7 mutant relative to WT, whereas in the pph1 mutant it was like in WT (Fig. 28 A and B). These observations indicated that the proton gradient was longer elevated in the stn7 mutant relative to WT and the pph1 mutant. It can be speculated that in the stn7 mutant when e- outflow at PSI is decreased, the proton gradient takes a longer time to relax. This could be caused by a slower activation of the ATP synthase. Alternatively, at low light conditions, an increased performance of CEF relative to LEF in the stn7

mutant could cause a rise in the proton gradient relative to WT, which is maintaining NPQ for a prolonged timespan.

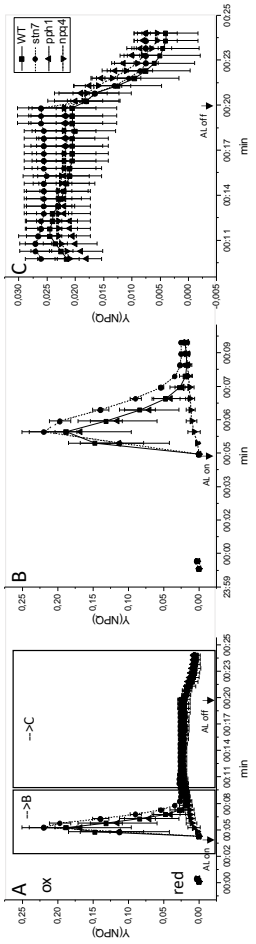

Figure 28. Chlorophyll fluorescence quench analysis during a dark-to-low light transition and when the light was turned off in WT (■), stn7 (●), pph1 (▲), and npq4 (▼) *A. thaliana* leaves. A., B, and C. Kinetic steady state analysis of the yield of non-photochemical quenching (Y(NPQ)) was determined via pulse-modulated spectroscopy. The x-axis refers to time (in min) and the y-axis to normalized arbitrary units (calculated according to method section 2.2.f). The AL used in the measurement was 58 µmol m-2 s-1 and plants were grown at 85 µmol m-2 s-1.

Average values from three to five different plants are shown for each genotype and bars indicate standard deviation.

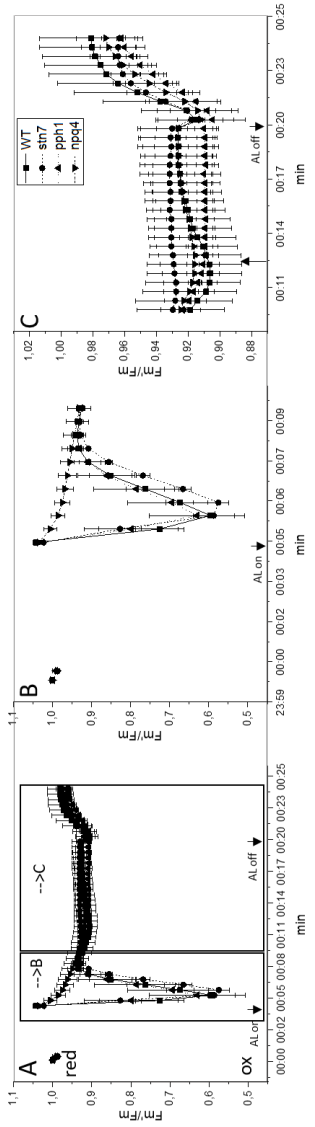

Figure 29. Chlorophyll fluorescence quench analysis during a dark-to-low light transition and when the light was turned off in WT (■), stn7 (●), pph1 (▲), and npq4 (▼) *A. thaliana* leaves. A., B, and C. Kinetic steady-state analysis of maximal fluorescence F_m' during light

treatment normalized to the maximal fluorescence F_m after dark preincubation (F_m'/F_m) was determined via pulse-modulated spectroscopy. The x-axis refers to time (in min) and the y-axis to normalized arbitrary units (calculated according to method section 2.2.f). The AL was 58 µmol m-2 s-1 and plants were grown at 85 µmol m-2 s-1. Average values from three to five different plants are shown for each genotype and bars indicate standard deviation.

In the npq4 mutant, the increase in Y(I) was slower relative to WT, stn7, and pph1 mutants which resulted in a lower Y(I)/Y(II) ratio in this mutant (Fig. 26 A and D insets). Y(I) values were found to be lowest in the npq4 mutant, which was indicated by Y(NA) values that were more increased relative to WT and the pph1 mutant during the first minute (minute 4,5 to 5,5 in Fig. 26 D and Fig. 27 C and F), hence e- outflow at the acceptor side of PSI was decreased in the mutant. Additionally, Y(ND) levels were decreased (Fig. 27 B and E), while Q_A levels were elevated in the npq4 mutant relative to WT and the pph1 mutant (Fig. 27 A and D), indicating that e- inflow at the donor side of PSI was increased and e- outflow at the acceptor side of PSI was decreased. These observations indicated that like in the stn7 mutant, less e- were flowing into the metabolic pool, and instead the npq4 mutant increased e-flow between PSI and the PQ pool through CEF. Interestingly, PSII's acceptor side, Q_A (1-qL) was elevated in the npq4 mutant relative to the stn7 mutant (Fig. 27 A and D**).** This observation suggested that during the first minute, when qE was missing in the npq4 mutant, e- outflow at PSII was decreased relative to the stn7 mutant. An explanation for this could be that in the npq4 mutant when qE was completely lost, while in the stn7 mutant it was still functional the npq4 mutant needed to increase its CEF to LEF ratio relative to the stn7 mutant.

Thereafter, we found that in WT, in the stn7 mutant, and to a lesser degree in the npq4 mutant that the Y(I)/Y(II) ratio decreased, due to a decrease in Y(I) (Fig. 26 A and D). In WT, stn7, and npq4 mutants, the decrease in Y(I) (Fig. 26 D) correlated with an increase in Y(NA) and decrease in Y(ND) levels, hence e- inflow at the donor side of PSI was increased and e- outflow at the acceptor side of PSI was decreased. Additionally, this was accompanied by a slowdown in the decrease in Q_A levels (measured by 1-qL) (Fig. 27 A, B, and C), indicating that e- outflow at the acceptor side of PSII was decreased. This observation, therefore, showed that the outflow of e- from both PSII and PSI was decreased. However, in the pph1 mutant, Y(I)/Y(II) stayed

stable and did not show a drop as we observed in WT, and both the stn7 and the npq4 mutant (Fig. 26 A). Furthermore, in the pph1 mutant a balanced Y(I)/Y(II) ratio was already reached between minutes 1,5 and 2,5 (between minutes 6 and 8 in Fig. 26 A) (Fig. 26 A), hence, 7,5 minutes earlier relative to WT. In the pph1 mutant, Y(NA) and Q_A levels continued to decrease, and Y(ND) levels stayed elevated relative to WT, and the stn7 and the npq4 mutant (Fig. 27 A, B, and C). These findings suggest that in WT, and the stn7 and the npq4 mutant, e- outflow from PSII into the PQ pool and from PSI into the metabolic pool was decreased, while e- inflow at the donor side of PSI was increased, whereas in the pph1 mutant we observed the opposite. It further suggested that the binding of phosphorylated LHCII to PSI in the pph1 mutant facilitated LEF, while in WT, and the stn7, and the npq4 mutant stronger binding of LHCII towards PSII decreased levels of LEF and increased the performance of CEF.

But after about 3,5 minutes of illumination, when Y(ND) stayed at the same level, Y(NA) levels dropped (Fig. 27 C and F, minute 7) and Y(I) increased leading to a 1:1 balance between Y(II) and Y(I) in WT and the stn7 mutant (Fig. 26 C and F). A drop in Y(NA) and a more balanced Y(I) to Y(II) ratio levels in WT, in both the stn7, and in the npq4 mutant suggested that linear e- outflow into the metabolic pool was increased. Interestingly, when Y(NA) levels were dropping and causing a rise in the Y(I) to Y(II) ratio (Fig. 27 C and Fig. 26 A), in WT, a 1:1 ratio of Y(I)/Y(II) was reached after about 9 minutes of illumination (Fig. 26 A minute 12,5), whereas in the stn7 mutant, equilibrium was established after about 5,5 minutes of illumination (Fig. 26 A minute 8,5), thus 3,5 minutes earlier relative to WT (Fig. 26 A). In the stn7 mutant, Y(I) levels were decreased, and Y(NA) levels were increased relative to WT, hence the e- outflow from the acceptor side of PSI into the metabolic pool was lowered relative to WT (Fig. 26 D and Fig. 27 C and F). However, in the stn7 mutant, also Y(ND) levels were decreased relative to WT, leading to an increase in Y(I) when e- inflow at the donor side of PSI was elevated (Fig. 26 D and Fig. 27 B and E). Therefore, a 1:1 ratio in Y(I)/Y(II) was established faster in the stn7 mutant compared to WT due to a lower level of Y(II) relative to WT (Fig. 26 A and C). This was caused in the stn7 mutant by a decrease in Q_A levels relative to WT (Fig. 27 A and D), indicating that e- outflow

from PSII was decreased. Thus, it can be speculated that when LHCII was bound at PSII in the stn7 mutant e- outflow from both PSII and PSI was decreased, while e- inflow at the donor side of PSI was elevated when for example CEF is enhanced relative to LEF. In the npq4 mutant, Y(NA) levels were increased leading to a drop in e- outflow at PSI (Y(I)) and resulting in a decrease in the Y(I)/Y(II) ratio relative to WT (Fig. 26 A, C, and D and Fig. 27 C and F). On the other hand, in the npq4 mutant, Y(II) was only marginally decreased (Fig. 25 C) reflected by slightly elevated Q_A levels relative to WT (Fig. 26 A and D). These observations displayed that while PSII was not showing a significant difference in the npq4 mutant and hence LEF was just a little bit lowered but stayed close to WT, e- outflow of the acceptor side of PSI was decreased, while e- inflow at its donor side was increased relative to WT, and the pph1 and the stn7 mutant. These observations suggested that CEF was enhanced relative to LEF in the npq4 mutant relative to WT, and the pph1 and the stn7 mutant. However, while in the stn7 mutant a decreased e- outflow at PSI correlated with a decreased e- outflow at PSII, in the npq4 mutant it did not. It indicated that in the npq4 mutant the upregulation of CEF restricts LEF, while in the stn7 mutant when LEF is already restricted to a stronger extent than in the npq4 mutant an enhancement in CEF does not compromise LEF any further. After about 3,5 min of illumination when a drop in Y(NA) was observed in WT, in the stn7, and the npq4 mutant, Y(NA) levels were rising again (Fig. 27 C). It can be speculated that when Y(NA) levels were rising again that the plant reduces LEF, hence restricting e- outflow at the acceptor side of PSI. The rise in Y(NA) was leading to a drop in Y(I) and thus decreasing the Y(I)/Y(II) ratio (Fig. 26 A and D). Interestingly, in the stn7 mutant, Y(NA) increased after about 7 minutes of illumination (minute 9,5 in Fig. 27 C), hence two minutes earlier relative to WT and the npq4 mutant. In both WT and the npq4 mutant, in addition to Y(NA) also Q_A levels increased after about 9 minutes of illumination (minute 12,5 in Fig. 27A and C), whereas in the stn7 mutant Q_A remained at the same level and stayed significantly more increased relative to WT and the npq4 mutant (Fig. 27 A and C). Moreover, Y(NA) levels in WT and the npq4 mutant were showing the same trend as observed in the stn7 mutant, however, both differed in kinetics. In contrast, in the pph1 mutant Y(ND) levels increased after 7 minutes of illumination (from minute 9,5 in Fig. 27 B) (Fig. 27 B), while Q_A and

Y(NA) remained at the same level and were thus both significantly more decreased than in WT (Fig. 27 A and C), indicating that e- inflow at the donor side of PSI was decreased, while e- outflow at both PSII‘s and PSI‘s acceptor side was elevated in the mutant. Consequently, opposite to WT and the other mutants, the Y(I)/Y(II) ratio was increased in the pph1 mutant (Fig. 26 A). Since Y(NA) and Y(ND) levels showed the same trend in state transition performing WT and the npq4 mutant relative to stn7 mutant, the redox change observed at PSI was most properly caused by changes in the mode of e- transport and not during state transition and light distribution to PSII/PSI via LHCII. The reason why Q_A levels stayed stable in the stn7 and pph1 mutants, while they did change in WT and the npq4 mutant can be explained by the phosphorylation/dephosphorylation and binding of LHCII to PSII /PSI during state transition in WT and the npq4 mutant.

Interestingly, when Y(NA) and Q_A levels increased in WT and the npq4 mutant, hence e- outflow at the acceptor side PSII and PSI decreased (Fig. 27 A and C), F_m’/F_m values shifted from a value resembling the pph1 mutant towards values seen in the stn7 mutant (Fig. 29 C). The value of F_m’ indicates the amount of PSII centers that can be reached by a short saturating pulse (SP) of very high-intensity light making them fluoresce. In principle, not only PSII centers but also PSI centers can fluoresce. However, it is believed that at room temperature variations in the fluorescence signal are coming mostly from PSII while the signal from PSI is ignored[244–246]. Thus, it can be assumed that the change in F_m´ levels showed that during the illumination in both WT and the npq4 mutant, more PSII centers were shifting into an SP-inducible fluorescing state. On the opposite, the number of fluorescent photosystems in the stn7 and the pph1 mutant did not change. Furthermore, when FR light was applied in addition to AL, F_m’/F_m values increased in both WT and the npq4 mutant (Fig. 30 C section 2). In contrast, in both the stn7 and the pph1 mutant when continuously illuminated with AL the addition of FR light did not change F_m’/F_m values (Fig. 30 A and B; section 2). Thus, it strongly proposes that the change in F_m’/F_m levels seen in WT and in the npq4 mutant and change in e- outflow at PSII (through modulating Q_A levels) is regulated by the performance of state transition. Moreover, during the continuous illumination with low

AL, the outflow of e- at both the acceptor side of PSII and PSI was decreased (Q_A levels and Y(NA) levels elevated (Fig. 27 A and C) in WT and the npq4 mutant and were thus closer resembling the stn7 mutant than the pph1 mutant. It can be speculated that after prolonged illumination with low AL state transition (from state 2- to state 1) was performed in WT and the npq4 mutant, leading to a downregulation in LEF and upregulation of CEF, hence shifting towards a stn7-mutant phenotype.

However, the addition of FR light to AL instantly lowered F_m'/F_m values in the stn7 mutant, while it did not have any effect in the pph1 mutant (Fig. 30 A and B; section 2). It showed that the addition of FR light decreased the amount of fluorescent PSII centers in the stn7 mutant, while in the pph1 mutant no change was recognized (Fig. 30 A and B). In WT and the npq4 mutant, supplementing FR light caused only a very small lowering of F_m'/F_m values relative to the stn7 mutant (Fig. 30 C). Thus, FR light showed the strongest effect on F_m'/F_m values in the stn7 mutant and the smallest in the pph1 mutant. It can be speculated that an increase in LEF would lower PSII‘s and also PSI‘s fluorescence signal and result in a drop in the F_m'/F_m value. If this was the case, it would suggest that the addition of FR light was causing the strongest increase in LEF in the stn7 mutant and the smallest increase in the pph1 mutant. The reason why in both WT and the npq4 mutant F_m'/F_m levels decreased only marginally might be caused by the fact that both were more resembling the pph1 mutant than the stn7 mutant. Thus, in WT, in the npq4 mutant, and in the pph1 mutant already without the addition of FR light more LEF was performed at this stage relative to the stn7 mutant.

After 20 minutes of illumination, in total Y(II) and Y(I) values were most strongly decreased in the stn7 mutant, followed by the npq4 mutant and WT, whereas in the pph1 mutant we observed the strongest increase in both values (Fig. 26 C and D). In the stn7 mutant, elevated Q_A levels were accompanied by increased Y(NA) values, hence e- outflow at the acceptor side of both PSII and PSI was decreased (Fig. 27 A, B, and C) and decreased Y(ND) levels caused by an increase in e- inflow at the donor side of PSI. In contrast, in the pph1 mutant decreased Q_A levels were accompanied by decreased Y(NA) values and significantly increased Y(ND) levels when compared to WT, leading to an elevation in the e- outflow at both the acceptor side of PSII and PSI,

while e- inflow at the donor side of PSI was significantly decreased (Fig. 27 A, B and C). Therefore, the phosphorylation of LHCII and binding to PSI (in the pph1 mutant) facilitated the outflow of e- of the acceptor side of both photosystems, while e- inflow at the donor side of PSI was decreased. In contrast, dephosphorylated LHCII not binding to PSI (in the stn7 mutant) decreased e- outflow at both acceptor sides and increased e- inflow at the donor side of PSI.

Interestingly, when Y(ND) levels were in the npq4 mutant similarly to WT, Y(NA) levels were elevated in the npq4 mutant, hence e- outflow at the acceptor side of PSI was decreased in the mutant, resulting in a drop in Y(I) (Fig. 27 C and 26 D). In contrast, Q_A values were only marginally elevated in the npq4 mutant relative to WT (Fig. 27 A), indicating that e- outflow at the acceptor side of PSII was only slightly decreased. Thus, after prolonged illumination at low AL, e- outflow at PSII and e- inflow at the donor side of PSI were in the npq4 mutant like in WT, whereas e- outflow at PSI was decreased when compared to WT. These observations showed that at low AL close to GL condition, when PsbS is absent in the npq4 mutant, PSI was more strongly affected relative to PSII. It can be speculated that in the npq4 mutant a drop in e- outflow at the acceptor side of PSI was caused by an increase in CEF and decrease in LEF relative to WT. In contrast, in WT when less CEF is performed more LEF was operated, which can increase the e- outflow at the acceptor side of PSI relative to the npq4 mutant. Thus, Y(ND) levels, resembling e- inflow at the donor side at PSI are not especially different between WT and the npq4 mutant, suggesting that the mutant compensates for the lack to perform LEF by increasing CEF and keeping e- inflow at a WT-like level.

3.1.2 After dark preincubation illumination with low actinic light and supplementing FR light in stn7, pph1, and npq4 mutant plants

After the onset of 25 µmol m-2 s-1 AL, NPQ (measured by a decrease in F_m'/F_m and rise in Y(NPQ) levels) was transiently induced in WT, and the pph1 and stn7 mutants (Fig. 30). In contrast, in the npq4 mutant, the initial transient rise in NPQ was missing (Fig. 30 C and D). This observation agreed with our previous findings made at the onset

of 58 µmol m-2 s-1 AL (Fig. 29) and showed that in the npq4 mutant, qE - the fastest known form of NPQ - was lacking.

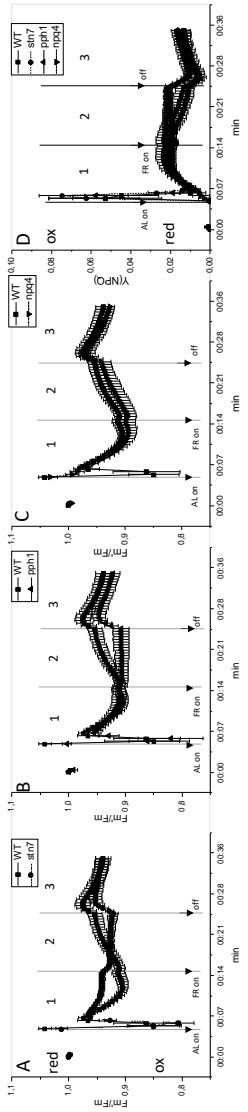

Figure 30. Chlorophyll fluorescence quench analysis during a 1. dark-to-low light transition, 2. a state 2- to- state 1 transition when FR light was added, and 3. in darkness in

WT (■), stn7 (●), pph1 (▲), and npq4 (▼) *A. thaliana* leaves. A., B, and C. Kinetic steady-state analysis of maximal fluorescence Fm' during light treatment normalized to the maximal fluorescence Fm after dark preincubation (Fm'/Fm) and D. of the yield of non-photochemical quenching (YNPQ) were determined via pulse-modulated spectroscopy. The x-axis refers to time (in min) and the y-axis to normalized arbitrary units (calculated according to method section 2.2.f). The AL was 25 µmol m-2 s-1 and the FR light was 70 µmol m-2 s-1. Plants were grown at 85 µmol m-2 s-1. Average values from three to five different plants are shown for each genotype and bars indicate standard deviation.

After the transient rise in NPQ, when F_m'/F_m levels first decreased and then increased, F_m'/F_m values continued to decrease (Fig. 30). In addition, Q_A (measured through 1-qL) and Y(NA) values decreased leading to the oxidation of the acceptor side of PSII and PSI, while Y(ND) levels decreased indicating that e- inflow at the donor side of PSI increased after photosynthetic control at Cytb6f (caused through the acidification of the thylakoid lumen when ΔpH rises and downregulates e- transport) is reversed (through the activation of the ATPase leading to a decrease in ΔpH) (Fig. 32 and Fig. 33). This observation suggested that when ATPase was activated and the proton gradient lowered, e- inflow at the donor side of PSI increased (decreased Y(ND) levels), and both outflow of e- at the acceptor side of PSII and PSI into the metabolic pool increased (decreased Q_A and Y(NA) levels). The course of F_m'/F_m decrease was very similar in WT and in pph1 and npq4 mutants (Fig. 30 B and C; section 1). In contrast, after three minutes of illumination in the stn7 mutant, F_m'/F_m values stopped decreasing relative to WT and the pph1 and npq4 mutant plants (Fig. 30). Additionally, in the stn7 mutant Q_A and Y(NA) levels halted their decrease, and Y(ND) stayed decreased leading to a stronger reduction state of all PSII's acceptor side and PSI's donor and acceptor side relative to WT, hence decreasing the e- outflow at PSII and PSI, lowering both Y(I) and Y(II) (Fig. 31 A and B) and increasing e- inflow at PSI's donor side (Fig. 30, Fig. 32 and Fig. 33). This observation indicated that under low light illumination in the stn7 mutant more PSII centers fluoresce (higher F_m'/F_m levels) because more light is absorbed. However, stronger PSII fluorescence in the stn7 mutant is causing a decrease in linear e-flow, while the cyclic e- flow was increased relative to WT. In contrast, in the pph1 mutant F_m'/F_m continuously decreased, and Q_A decreased like in WT, hence e- outflow at PSII's acceptor side was in mutant and WT alike (Fig. 30 and Fig. 32). However, both Y(ND) and Y(NA) were more decreased in the pph1 mutant relative to

WT, and the stn7 and the npq4 mutant, indicating that e- outflow at PSI's acceptor side was increased, while e- inflow at PSI's donor side was decreased (Fig. 33). In concert with measurements at 58 µmol m-2 s-1 AL, in the stn7 mutant, the oxidation of PSII's (decrease in Q_A) and PSI's acceptor side (decrease in Y(NA)) was lowered relative to WT and the pph1 mutant, whereas in the pph1 mutant both e- acceptors were more strongly oxidized relative to WT and the stn7 mutant (Fig. 26 A, B, and C vs. Fig 32; section 1 and 33; section 1). Results, therefore, suggest that under low AL conditions in the pph1 mutant when LHCII is phosphorylated at PSI, fewer PSII centers fluoresce relative to the stn7 mutant, and linear e-flow is increased, while the cyclic e- flow is lowered.

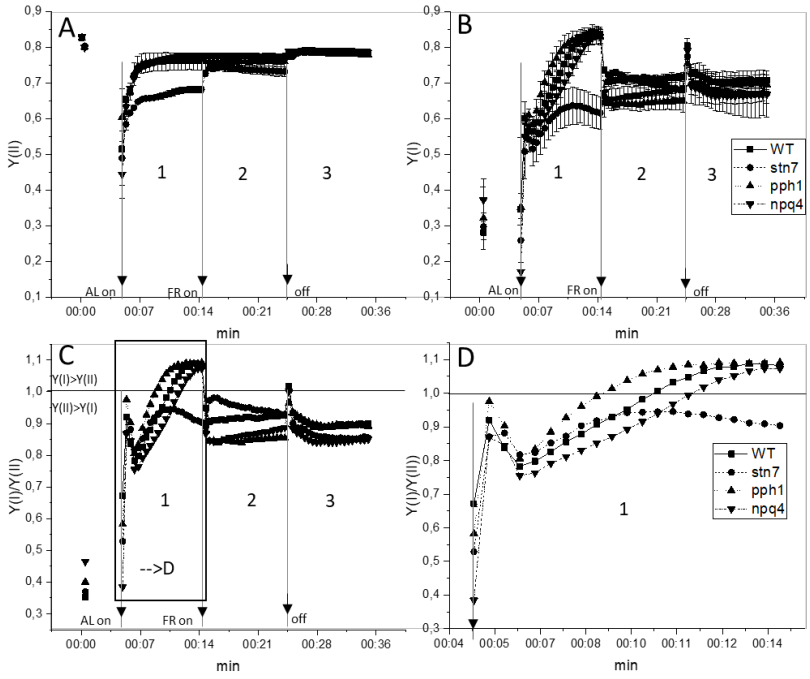

Figure 31. Photosynthetic performance of PSII and PSI during a 1. dark-to-low light transition, 2. a state 2- to- state 1 transition when FR light was added, and 3. in darkness in WT (■), stn7 (●), pph1 (▲) and npq4 (▼) *A. thaliana* leaves. A kinetic steady-state analysis of e- flow at A. PSII (Y(II)), B. PSI (Y(I)), C. and D. the ratio of Y(I)/Y(II) was determined via pulse-modulated spectroscopy. The x-axis refers to time (in min) and the y-axis to normalized

arbitrary units (calculated according to method section 2.2.f). The AL was 25 µmol m-2 s-1 and the FR light was 70 µmol m-2 s-1. Plants were grown at 85 µmol m-2 s-1. Average values from three to five different plants are shown for each genotype and bars indicate standard deviation.

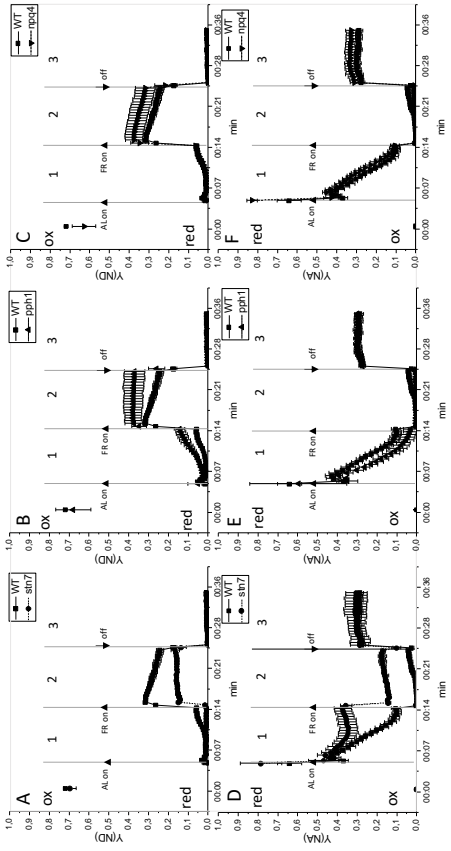

Figure 32. The oxidation state of PSI's donor and acceptor side during a 1. dark-to-low light transition, 2. a state 2- to- state 1 transition when FR light was added, and 3. in darkness in WT (■), stn7 (●), pph1 (▲) and npq4 (▼) *A. thaliana* leaves. A kinetic steady-state analysis of the redox state of A., B., and C. PSI's donor side limitation Y(ND) and D., E., and F. PSI's acceptor side limitation Y(NA) were determined via pulse-modulated spectroscopy. The x-axis refers to time (in min) and the y-axis to normalized arbitrary units (calculated according to method section 2.2.f). The AL was 25 µmol m-2 s-1 and the FR light was 70 µmol m-2 s-1. Plants were grown at 85 µmol m-2 s-1. Average values from three to five different plants are shown for each genotype and bars indicate standard deviation.

Interestingly, in the npq4 mutant, Q_A levels were slower reduced, hence the rate of e- outflow at PSII's acceptor side was lowered, while Y(NA) levels were only slightly more decreased leading only to a marginal decrease in e- outflow at PSI relative to WT (Fig. 32 C and F and Fig. 33 C). These observations differed from findings made at 58 µmol m-2 s-1 AL, where both Q_A and Y(NA) levels were in the npq4 mutant like in the stn7 mutant significantly more decreased relative to WT, hence e- outflow at both PSII's and PSI's acceptor side was decreased in the mutant (Fig. 26 A and C).

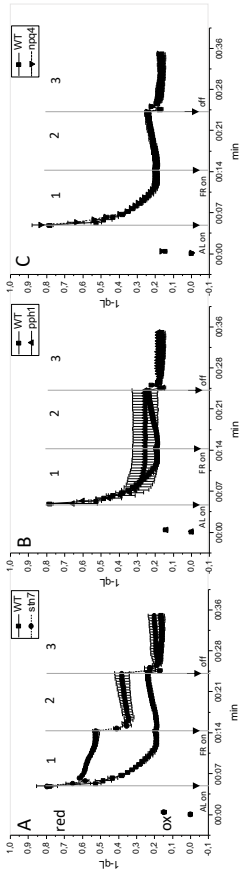

Figure 33. The oxidation state of PSII's acceptor side Q_A (1-qL) during a 1. dark-to-low light transition, 2. a state 2- to- state 1 transition when FR light was added, and 3. in darkness in WT (■), stn7 (●), pph1 (▲) and npq4 (▼) *A. thaliana* leaves. A kinetic steady-state analysis of the redox state of A., B., and C. PSII's acceptor side Q_A (1-qL) was determined

via pulse-modulated spectroscopy. The x-axis refers to time (in min) and the y-axis to normalized arbitrary units (calculated according to method section 2.2.f). The AL was 25 µmol m-2 s-1 and the FR light was 70 µmol m-2 s-1. Plants were grown at 85 µmol m-2 s-1. Average values from three to five different plants are shown for each genotype and bars indicate standard deviation.

These findings suggested that at 25 µmol m-2 s-1 AL, e- outflow at PSII and PSI was more equal in the npq4 mutant relative to 58 µmol m-2 s-1 AL. It suggests that at 25 µmol m-2 s-1 AL, light quanta were more equally absorbed at PSII and PSI, while at increasing light intensities (at 58 µmol m-2 s-1) light absorption when not accurately balanced between PSII and PSI, causing a decrease in e- outflow at both the acceptor side of PSII and PSI (leading to more decreased Q_A and Y(NA) levels). It can be speculated that when light is not balanced accurately between PSII and PSI it is causing a decrease in linear and increase in cyclic e- flow. In contrast to the npq4 mutant where e- transport mechanisms differed between both low light conditions, e- outflow at the acceptor side of PSI was decreased at both tested low light conditions in the stn7 mutant relative to WT. This further suggested that while in the npq4 mutant CEF is only increased in light environments that show an increased induction of NPQ, in the stn7 mutant CEF is increased at all low light conditions in an NPQ-independent manner. Hence, an increase in CEF could substitute in the npq4 mutant for the lack of a functional NPQ response.

Furthermore, after about 7 minutes of illumination (at 25 µmol m-2 s-1 AL), F_m'/F_m values increased in WT and the npq4 mutant but not in the pph1 mutant nor the stn7 mutant (Fig. 30 B; section 1). This indicated that light absorption at PSII was increased in WT and the npq4 mutant but not in the pph1 and the stn7 mutant, which could be interpreted as a state 2- to- state 1 transition being performed. Simultaneously, in WT and the npq4 mutant Y(ND) levels halted their increase and both Y(NA) and Q_A (measured through 1-qL) values did not decrease any longer, hence e- outflow at the acceptor side of PSII and PSI as well as at the donor side of PSI was halted (Fig. 32; section 1 and Fig. 33; section 1). The latter was most properly mediated through an increased e- inflow at PSI's donor side. Interestingly, in the stn7 mutant Y(NA) levels were increasing and Y(ND) levels stayed completely decreased, whereas in the pph1 mutant Y(ND) levels kept on the rise and Y(NA) levels continued to decrease (Fig. 32

B, D, and E). Therefore, in the stn7 mutant, the outflow of e- at the acceptor side of PSI was decreased and the inflow of e- at the donor side of PSI was elevated, while in the pph1 mutant it was the opposite. Hence, both state transition mutants did not behave like the WT nor the npq4 mutant. It can be speculated that both WT and the npq4 mutant acclimatized during the continuous illumination with low AL to a state where they decreased the rate of linear e- flow and enhanced cyclic e- transport and therefore moved from a pph1 mutant-like behavior to a stn7 mutant-like one. Hence, we propose that in both WT and the npq4 mutant when performing a transition into state 1 led to an upregulation of CEF and downregulation of LEF.

By supplementing FR light to low AL in WT and the npq4 mutant, F_m'/F_m continued to rise (Fig. 30 B; section 2). This indicated that in WT and the npq4 mutant the simultaneous illumination with FR light and AL increased the number of PSII centers that were fluorescing when illuminated by an SP. In contrast, F_m'/F_m values stayed constantly elevated in the stn7 mutant and constantly decreased in the pph1 mutant relative to WT and did not change throughout FR and low AL illumination (Fig. 30 A and B). It can be proposed that this increase is initiated through a state 2- to- state 1 shift, increasing the binding of LHCII at PSII relative to PSI. Additionally, when FR light was added to low AL, the Y(I)/Y(II) ratio decreased in WT, and in pph1 and npq4 mutants instantly due to a stronger increase in the levels of Y(ND) and decrease in Y(NA), indicating that e- inflow at the donor side was lowered and e- outflow at the acceptor side of PSI was enhanced, while Y(II) stayed constant (Fig. 31 section 2 and Fig. 32 C and F). FR light directly excites the PSI reaction center and thus leads to its oxidation. In the pph1 and the npq4 mutant plant the addition of FR light showed the strongest decrease in the Y(I)/Y(II) ratio through the strongest increase of Y(ND) levels relative to WT and the stn7 mutant (Fig. 31 C; section 2 and Fig. 32 B and C). However, in the npq4 mutant and WT but not in the pph1 mutant it was possible to increase its Y(I)/Y(II) ratio again by increasing Y(ND) levels by increasing e- inflow at PSI's donor side, hence increasing Y(I) for several minutes (Fig. 31 B and C). This adaptation was taking place in WT and the npq4 mutant in about seven minutes. Thus, changes observed in F_m'/F_m levels, PSII's acceptor side Q_A and PSI's donor and acceptor side

strongly suggested that in WT and the npq4 mutant the illumination with 25µmol m-2 s-1 AL with the addition of FR light initiated state transition, namely the dephosphorylation of LHCII and its binding to PSII. In addition, this LHCII switch increased e- inflow at the donor side of PSI and decreased e- outflow at both PSII‘s and PSI‘s acceptor side through enhancing CEF relative to LEF.

Moreover, the addition of FR light to AL was causing the strongest decrease in Y(ND) levels in the npq4 mutant relative to WT and the other mutants (Fig. 32 C; section 2). This further indicated that FR light had the strongest effect on the npq4 mutant and was decreasing e- inflow at the donor side of PSI the strongest. In addition, when AL light was supplemented with FR light the continuous rise of Y(NA) levels over time was absent, hence e- outflow at the acceptor side of PSI was increased in the npq4 mutant relative to WT (Fig. 32 F; section 2). This indicated that in contrast to WT in the npq4 mutant less CEF and more LEF was performed. However, the addition of FR light to low AL was decreasing Y(ND) levels and increased F_m'/F_m levels throughout illumination in the npq4 mutant like in WT, indicating that the mutant was increasing CEF relative to LEF during the performance of a state -2 state 1 transition (Fig. 32 C and Fig. 30 C)). It, therefore, suggests that when in the npq4 mutant low AL is used and FR light was supplemented more LEF relative to CEF was performed when compared to WT.

Interestingly, in the stn7 mutant, the supplementation of FR light showed an increase in the Y(I)/Y(II) ratio relative to WT, by keeping Y(ND) levels more decreased (Fig. 31 B and Fig. 32 A). It suggests that e- inflow at the donor side of PSI was elevated in the stn7 mutant in comparison to WT causing an increase in Y(I). However, when exposed for 7 minutes with low AL supplemented with FR light, the Y(I)/Y(II) ratio decreased in the stn7 mutant and reached WT levels (Fig. 31 C; section 2). The decrease in the stn7 mutant in Y(I)/Y(II) was reflected by a slight decrease in Y(II) through more strongly decreasing Q_A levels and a stronger decrease in Y(I) by more strongly decreasing Y(NA) levels relative to WT (Fig. 31 A and B; section 2 and Fig. 32 D and Fig. 33 A). It, therefore, indicated that in addition to a stronger inflow of e- at PSI‘s donor side e- outflow at both the acceptor side of PSII and PSI was decreased.

Therefore, it was noted that also in the stn7 mutant prolonged illumination with low AL and FR light was leading to an increase in CEF relative to LEF.

3.1.3 Increasing light irradiance levels in dark-adapted stn7, pph1, and npq4 mutant leaves

Next, we investigated how WT and mutant stn7, pph1, and npq4 *A. thaliana* leaves adapt photosynthesis to increasing light intensities during the recording of a light-response experiment (LRE). Light irradiance levels were elevated every 30 seconds, and the photosynthetic performance was determined at the end of each light step by a SP. In the pph1 mutant, Y(ND) and Y(NA) levels were between 18 and 131 µmol m-2 s-1 like WT (Fig. 35 B and E). However, Q_A (measured through 1-qL) was decreased at 11 µmol m-2 s-1, hence e- outflow at the acceptor side of PSII was increased in the pph1 mutant relative to WT and was thereafter not different from WT values (Fig. 34 B). In addition, PSI‘s donor side Y(ND) was more increased at 11 µmol m-2 s-1, hence e- inflow at PSI was lowered in the pph1 mutant relative to WT (Fig. 35 B). In total, the pph1 mutant was able to keep the redox state of PSI and PSII like WT, except from the first measurement point at 11 µmol m-2 s-1. When FR light was added to the LRE, the pph1 mutant reassembled WT Q_A levels (measured through 1-qL) but more increased Y(ND), and also Y(NA) was kept marginally more decreased between 27 and 58 µmol m-2 s-1, hence e- outflow at PSII was the same but e- inflow at the donor side of PSI was decreased, while e- outflow at PSI was increased relative to WT (Fig. 34 B and Fig. 35 B and E). Thus, adding FR light in WT had the same effect on the outflow of e- at PSII’s acceptor side as the *pph1* mutation. However, the supplementation of FR light decreased e- inflow at PSI‘s donor side and elevated e- outflow at PSI‘s acceptor side in the pph1 mutant relative to WT leaves. It can be speculated that when FR light was added LEF is the same, but that CEF is decreased in the pph1 mutant relative to WT.

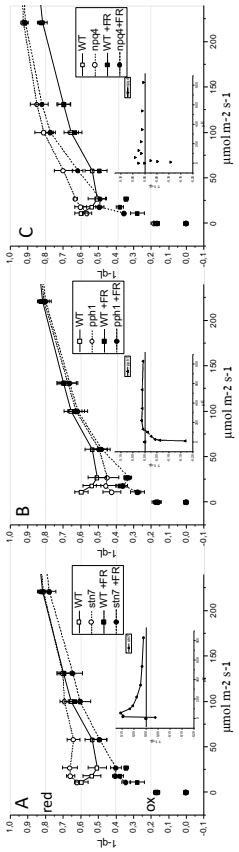

Figure 34. The oxidation state of PSII's acceptor side Q_A (1-qL) in *A. thaliana* mutant leaves A. stn7, B. pph1, and C. npq4 compared to WT during the recording of a light-response experiment with increasing light irradiance levels determined via pulse-modulated spectroscopy. The graph in the inset shows the difference of measurements performed with AL minus measurements performed with AL supplemented with FR light (131 µmol m-2 s-1), subsequently, mutant difference graphs were subtracted from WT graphs (insert). In these difference spectra negative values indicated that FR light was less effective, positive values indicated more effective and values around zero indicated that FR light made no difference in the oxidation of Q_A (1-qL) relative to WT. The x-axis refers to increasing light intensities (in µmol m-2 s-1) and the y-axis to normalized arbitrary units (calculated according to method section 2.2.f). Plants were grown at 85 µmol m-2 s-1. Average values from three to five different plants are shown for each genotype and bars indicate standard deviation.

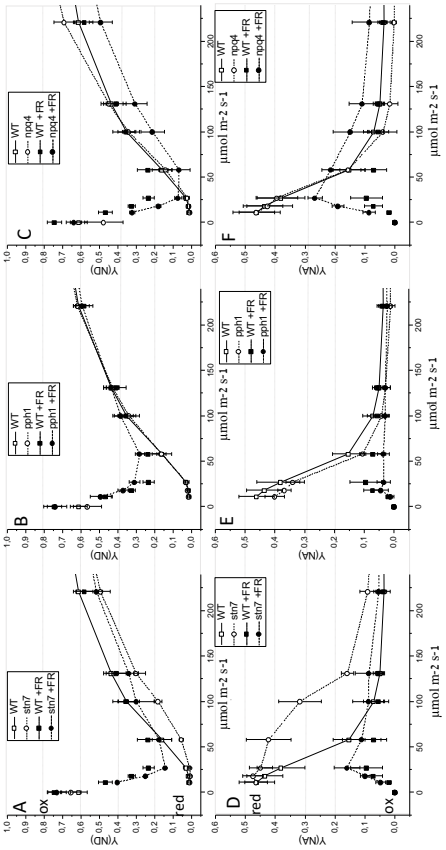

Figure 35. The oxidation state of PSI's donor and acceptor side in *A. thaliana* WT and stn7, pph1, and npq4 mutant leaves during the recording of a light-response experiment with increasing light irradiance levels was determined via pulse-modulated spectroscopy. PSI donor side limitation Y(ND) in A. the stn7 mutant, B. the pph1 mutant and C. the npq4 mutant and PSI acceptor side limitation in D. the stn7 mutant, E. the pph1 mutant, and F. the npq4 mutant during the recording of light-response experiments with increasing light irradiance levels were determined via pulse-modulated spectroscopy. FR light at 131 µmol m-2 s-1 was supplemented. The x-axis refers to increasing light intensities (in µmol m-2 s-1) and the y-axis to normalized arbitrary units (calculated according to method section 2.2.f). Plants were grown at 85 µmol m-2 s-1. Average values from three to five different plants are shown for each genotype and bars indicate standard deviation.

In contrast, Q_A levels were more elevated between 18 and 58 µmol m-2 s-1, indicating that e- outflow at the acceptor side of PSII was decreased in the stn7 mutant relative to WT (Fig. 34 A). When exiting the stn7 mutant with AL of 100 µmol m-2 s-1 and more, the reduction state of Q_A was in the stn7 mutant like WT, which indicated that at increased light irradiance levels both plants showed the same reduction in the acceptor side of PSII/the PQ pool. However, while above 100 µmol m-2 s-1 Q_A levels were in the stn7 mutant like WT, both Y(ND) were decreased, and Y(NA) levels were increased from 58 until 240 µmol m-2 s-1 showing that e- inflow at the donor side of PSI was increased, while the e- outflow at PSI was decreased relative to WT (Fig. 34 A and Fig. 35 A and D). Thus, in the stn7 mutant more than 100 µmol m-2 s-1 AL was needed to show similar Q_A values but more than 340 µmol m-2 s-1 to show similar Y(NA) levels relative to WT (Fig. 34 A and Fig. 35 D; and data not shown for >240 µmol m-2 s-1). These observations indicated that the stn7 mutant was above growth light conditions more strongly behaving like WT than below growth light conditions. Interestingly, WT and the stn7 mutant never reached similar Y(ND) values (Fig. 35 A). As a matter of fact, Y(ND) values were decreased during the recording of the complete LRE, indicating that e- inflow at the donor side of PSI was always elevated through for example increasing CEF in the stn7 mutant relative to WT (from 11 until 830 µmol m-2 s-1) (Fig. 35 A and data not shown for >240 µmol m-2 s-1).

To test if decreased Y(ND) levels were caused by an increase in light absorption at PSII relative to PSI in the stn7 mutant compared to WT, we added 131 µmol m-2 s-1 FR light during the LRE. When FR light was added, it showed the strongest effect on Q_A in the stn7 mutant, followed by the npq4 mutant, and had the smallest influence in the pph1 mutant (Fig. 34 A, B, and C; small inset). In pph1 and npq4 mutants, FR light showed less effect at LL intensities (negative values in difference spectra), while in the stn7 mutant, FR light was at LL more effectively (positive values in difference spectra) decreasing Q_A levels (1-qL) and hence increasing e- outflow at PSII‘s acceptor side relative to WT (Fig. 34 A, B, and C; small inset). From light intensities above 58 µmol m-2 s-1, the effect of FR light was lost in the pph1 mutant (values around zero in difference spectra), while in the stn7 mutant and to a lesser extent in the npq4 mutant,

FR light showed a stronger oxidative effect on Q_A (positive values in difference spectra) in comparison to WT (Fig. 34 A, B and C; small inset). Interestingly, through the addition of FR light Q_A levels were between 11 and 27 µmol m-2 s-1 to a small degree more decreased in the stn7 mutant relative to WT levels, and only resembled WT measurements from 58 µmol m-2 s-1 (Fig. 34 A). Thus, the addition of FR light when low AL was given did not increase e- outflow at the acceptor side of PSII in the stn7 mutant. Furthermore, Y(NA) levels resembled through the addition of FR in the stn7 mutant WT levels from >18 µmol m-2 s-1 AL, whereas Y(ND) levels stayed more decreased between 11 and 27 µmol m-2 s-1 AL in the same way as Q_A values were more decreased in the stn7 mutant relative to WT (Fig. 34 A and Fig. 35 A and D). Hence, with FR light only from 58 µmol m-2 s-1, both Y(ND), and Q_A values were in the stn7 mutant resembling WT values (Fig. 34 A and Fig. 35 A). This observation showed that in the stn7 mutant the supplementation of FR light kept Q_A, Y(ND) and Y(NA) from light irradiance levels of 58 µmol m-2 s-1 until 131 µmol m-2 s-1, like WT (Fig. 34 A and Fig.35A and D). However, when low light (11-27 µmol m-2 s-1) was applied in the stn7 mutant, FR light had a decreased effect on Y(ND) and to a smaller degree on Q_A and Y(NA) levels relative to WT (Fig. 34 A and Fig. 35 A and D). Therefore, observations indicated that at the first low light steps increasing light absorption at PSI through adding FR in the stn7 mutant did not help to resemble WT values. The addition of FR light showed a decreased capacity to decrease e- inflow at the donor side of PSI in the stn7 mutant when compared to WT. When FR light was supplemented, Q_A and Y(NA) levels were in the stn7 mutant closer to WT levels than Y(ND) levels were (Fig. 34 A and Fig. 35 A and D). This observation suggested that under low light conditions FR light had less capacity to decrease e- inflow at the donor side of PSI, while the difference in e- leaving from the acceptor side PSII and PSI into the metabolic pool was more similar in the stn7 mutant when compared to WT. This could be the case when CEF was enhanced in the stn7 mutant versus WT. On the other hand, it can be assumed that less influence of FR light on Y(ND) levels at LL indicates that in the stn7 mutant more light was already utilized at PSI relative to PSII relative to WT. However, when FR light was added to increasing AL intensities (>58 µmol m-2 s-1) the stn7 mutant‘s Q_A, Y(ND) and Y(NA) levels were like WT. Thus, at increasing

light irradiance levels e- transport modes were more similar in WT and the stn7 mutant. Interestingly, the addition of FR light had above >240 µmol m-2 s-1 in the stn7 mutant no influence on Y(ND). Like at low AL, from 240 µmol m-2 s-1, Y(ND) levels decreased in the stn7 mutant stronger, hence e- inflow at the donor side of PSI was elevated relative to WT and was resembling an LRE without FR light (data not shown). Therefore, FR light in the stn7 mutant had not only less influence on Y(ND) below 58 µmol m-2 s-1 but also above 131 µmol m-2 s-1 relative to WT. Interestingly, under both low and high light conditions, e- inflow at the donor side of PSI was increased relative to WT. It can be speculated that when AL conditions differed from growth light conditions when the light was more utilized at PSI relative to PSII and more CEF is performed in the stn7 mutant the addition of FR light had less effect in increasing LEF over CEF when compared to WT.

Additionally, the supplementation of FR light lowered NPQ values in both the stn7 mutant and WT (measured through Y(NPQ) and $1-F_m'/F_m$) relative to measurements performed without FR light (Fig. 36), whereas in the stn7 mutant from >18 µmol m-2 s-1 until 830 µmol m-2 s-1, NPQ values were elevated when supplemented with FR light relative to WT with FR light (Fig. 36 A and D, 230-830 µmol m-2 s-1 data not shown). This finding, therefore, indicated that the addition of FR light to increased AL enhanced NPQ in the stn7 mutant relative to WT. It can be assumed that an increase in NPQ in the stn7 mutant relative to WT is an indication that the supplementation of FR light increased the mutant's transthylakoid proton gradient. It can be speculated that during the performance of an LRE an increased rate of CEF in the stn7 mutant relative to WT caused a rise in NPQ in the mutant.

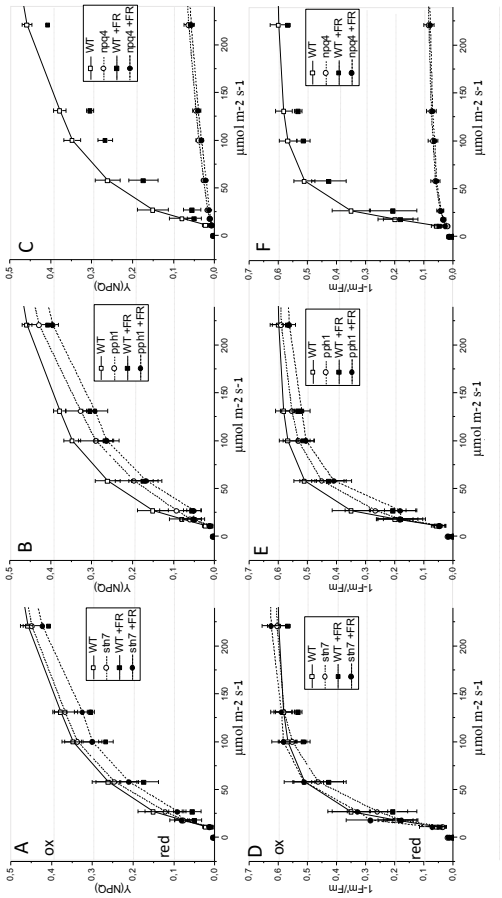

Figure 36. Chlorophyll fluorescence quench analysis in *A. thaliana* WT and stn7, pph1, and npq4 mutant leaves during the recording of a light-response experiment with increasing light irradiance levels was determined via pulse-modulated spectroscopy. The yield of non-photochemical quenching Y(NPQ) in A. the stn7 mutant, B. the pph1 mutant, and C. the npq4 mutant and the maximal fluorescence F_m' during light treatment normalized to the maximal fluorescence F_m after dark preincubation (1-F_m'/F_m) in D. the stn7 mutant, E. the pph1 mutant, and F. the npq4 mutant during the recording of light-response experiments with increasing light irradiance levels were determined via pulse-modulated spectroscopy. FR light at 131 µmol m-2 s-1 was supplemented. The x-axis refers to increasing light intensities (in µmol m-2 s-1) and the y-axis to normalized arbitrary units (calculated according to method section 2.2.f). Plants were grown at 85 µmol m-2 s-1. Average values from three to five different plants are shown for each genotype and bars indicate standard deviation.

In contrast, Q_A levels (1-qL) were more elevated in the npq4 mutant relative to WT with or without FR light, indicating that e- outflow at the acceptor side of PSII was decreased in the npq4 mutant (Fig. 37). In detail, Q_A levels without FR light were increased in the npq4 mutant from 27 µmol m-2 s-1 and with FR light from 11 µmol m-2 s-1 relative to WT (Fig. 34 C). At increasing light irradiance levels, WT quenches incoming light through the NPQ mechanism qE, which is missing in the npq4 mutant. Indeed, in the npq4 mutant, the initiation of NPQ (qE) (measured through Y(NPQ) and 1-F_m'/F_m) was significantly decreased relative to WT (Fig. 36 C and F). Moreover, the supplementation of FR light at low AL did not increase e- outflow at the acceptor side of PSII in the npq4 mutant like in WT. Like in the stn7 mutant at LL and HL intensities, FR light showed a decreased capacity to increase e- outflow at the acceptor side of PSII in the npq4 mutant relative to WT. This could be caused by a decrease in the turnover in LEF and an increase in CEF in the npq4 mutant relative to WT. Since also the addition of FR light showed no effect, it can be speculated that like in the stn7 mutant a stronger absorption and utilization of light at PSI relative to PSII is fueling CEF in the npq4 mutant when compared to WT. However, between 11 and 131 µmol m-2 s-1 when no FR light was supplemented, both Y(ND) and Y(NA) levels were in the npq4 mutant like in WT. In contrast, when FR light was added, Y(NA) was decreased between 11 and 131 µmol m-2 s-1, hence e- outflow at the acceptor side of PSI was decreased, and Y(ND) levels were decreased between 58 µmol m-2 s-1 to 131 µmol m-2 s-1, indicating that e- inflow at the donor side of PSI was elevated in the npq4 mutant relative to WT (Fig. 35 C and F). Thus, FR light had a decreased capacity to increase e- outflow at the acceptor side of PSI and instead increased e- inflow at the donor side of PSI (Y(ND)) decreased and Y(NA) levels elevated in the npq4 mutant relative to WT) (Fig. 35 C and F). Hence, it can be speculated that under these light conditions the addition of FR light increased CEF relative to LEF in the npq4 mutant when compared to WT. Interestingly, from 240 µmol m-2 s-1 AL without the addition of FR light, Y(ND) levels were elevated, and Y(NA) values decreased in the npq4 mutant relative to WT, indicating that e- outflow at the acceptor side PSI was increased and e- inflow at the donor side of PSI was decreased at very high light (Fig. 37). However, when adding FR light to AL above 240 µmol m-2 s-1 AL both Y(ND) and Y(NA) levels were

similar in the npq4 mutant like in WT when no FR light was used (Fig. 37). This observation strongly suggested that at HL (above 240 µmol m-2 s-1 AL) without FR light, less LEF (more increased Q_A levels) and less CEF was performed in the npq4 mutant compared to WT.

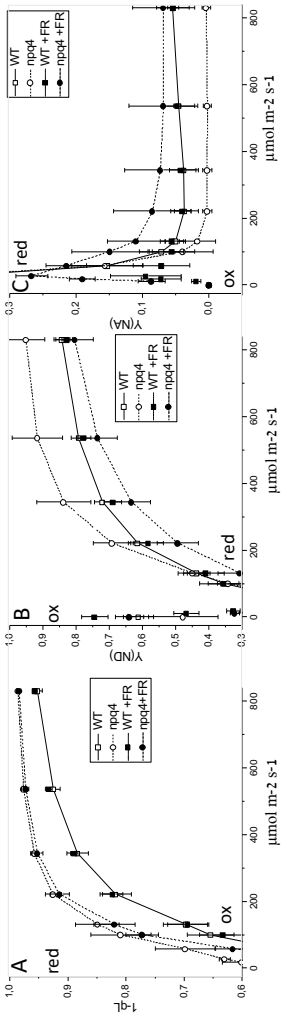

Figure 37. The oxidation state of PSII's acceptor side Q_A (1-qL) and PSI's donor and acceptor side during increasing light irradiance levels (LRE) in WT (square) and npq4 (dot)

***A. thaliana* leaves.** A. Redox state of Q_A (1-qL), B. PSI donor side limitation Y(ND), and C. PSI acceptor side limitation Y(NA). and D. Q_A (1-qL), B. and E. PSI's donor side limitation Y(ND), and C. and F. PSI's acceptor side limitation Y(NA) were determined via pulse-modulated spectroscopy. FR light at 131 µmol m-2 s-1 was supplemented. The x-axis refers to increasing light intensities (in µmol m-2 s-1) and the y-axis to normalized arbitrary units (calculated according to method section 2.2.f). Plants were grown at 85 µmol m-2 s-1. Average values from three to five different plants are shown for each genotype and bars indicate standard deviation.

In addition, Y(I) levels from 53 µmol m-2 s-1 did not differentiate between the npq4 mutant with or without the supplementation of FR light (data not shown). Thus, data indicated that when light intensities above 240 µmol m-2 s-1 were used adding FR light caused an increase in CEF relative to LEF in the npq4 mutant when compared to measurements without FR light. Findings, therefore, displayed that in the npq4 mutant, when lacking excitation quench at PSII, different light intensities and qualities changed the mode of e- transfer through PSII and PSI relative to WT. Under both LL and HL conditions LEF is decreased, while under low to medium conditions CEF was in the npq4 mutant like in WT. In contrast, under HL the mutant decreased LEF and CEF relative to WT. Interestingly, when FR light was supplemented CEF was elevated, and LEF was decreased under all tested light intensities in the npq4 mutant when compared to WT.

It can be speculated that when the plant is not able to use this mechanism of photoprotection the mutation counteracts by decreasing the amount of light absorbed at both PSII and PSI relative to WT to protect its photosystems from photodamage. Interestingly, when the performance of LEF is generally decreased in the npq4 mutant relative to WT increasing the absorption of light at PSI through adding FR light causes a rise in CEF in both the npq4 and stn7 mutant plants relative to WT. In contrast, in the pph1 mutant LEF can be more facilitated relative to the stn7 and npq4 mutant plants. Hence, data indicated that the npq4 mutant is in fact like the stn7 and the pph1 mutant affected by light energy absorption and distribution at PSII and PSI.

3.2. Pulse-modulated spectroscopy results: CEF mutants (pgr5 and crr2 mutants)

3.2.1 A kinetic analysis at the onset of low actinic light close to GL in pgr5 and crr2 mutants

Next, the influence of missing PGR5/PGRL1-dependent or NDH-dependent CEF on e- transport was investigated after dark preincubation at the onset of low light. Additionally, proton transport was indirectly determined by measuring NPQ (at 58 μmol m-2 s-1). *A. thaliana* mutant plants crr2 –insufficient in the NDH complex and pgr5 mutant- lacking PGR5 and thus not able to perform NDH-dependent and PGR5/PGRL1-dependent CEF were studied via pulse-modulated spectroscopy. The influence on e- flow through PSII and PSI when missing one of the two CEF modes was first examined by determining the effective photosynthetic quantum yield at PSII (Y(II)) and PSI (Y(I)) (Fig. 38 A and B). The ratio of Y(I) to Y(II) was determined to show the relative contribution of the reaction centers to photosynthetic e- flow (Fig. 38 C).

At the onset of illumination, during the first-minute electron outflow from the acceptor side of PSI was activated, Y(NA) levels decreased (Fig. 39 C and F), hence e- outflow at the acceptor side of PSI increased, and Y(I) levels increased compared to Y(II) (Fig. 38 A and B). Interestingly, the relative contribution of electron flow through PSI was increased in WT and in the crr2 relative to the pgr5 mutant (Fig. 38 B). In the pgr5 mutant, the effective quantum yield at PSI (Y(I)) was significantly decreased relative to WT but the effective quantum yield at PSII (Y(II)) was WT-like, leading to a strongly decreased Y(I)/Y(II) ratio relative to WT (Fig. 38). Only after about 5 minutes of illumination (minute 9,5 in Fig. 38 B), Y(I) the pgr5 mutant reached WT levels, leading to a 1:1 ratio of Y(I) to Y(II) (Fig. 38 C). Thus, when the light was turned on in the pgr5 mutant, the increase in Y(I) required more time in comparison to WT. In addition, the decrease of Y(NA) levels was slower relative to WT, which indicated that the outflow of e- through the acceptor side of PSI was slowed down relative to WT (Fig. 38 B and Fig. 39 C and F). On the other hand, Y(II) levels in the pgr5 mutant were like

in WT, and Q_A levels (measured through 1-qL) stayed at the same level indicating that e- outflow at the acceptor side of PSII was similar (Fig. 38 A and Fig. 39 A and D). This finding strongly suggested that LEF was at the immediate onset of light in the pgr5 mutant the same as in WT. However, during the first minutes of illumination, a decrease in Y(I) initiated through a slower outflow of e- at the acceptor side of PSI strongly indicated less CEF and a slower activation of the CBB cycle in the pgr5 mutant relative to WT. Additionally, during the first four minutes of light, the PSI donor side Y(ND) was decreased in the pgr5 mutant relative to WT (Fig. 39 B and E), hence e- inflow at the donor side of PSI was decreased. More decreased Y(ND) levels at the immediate onset of light in the pgr5 mutant relative to WT are indicative of increased e- inflow at the donor side of PSI in the pgr5 mutant relative to WT, which could result from a decrease in ΔpH when less LEF and/or CEF is performed in the mutant leading to a decrease the photosynthetic control at Cytb6f relative to WT. In concert, at the onset of light, the transient rise in NPQ (determined through F_m'/F_m or Y(NPQ)) was significantly decreased in the pgr5 mutant relative to WT (Fig. 40), indicating that fewer protons were translocated inside the lumen in the mutant leading to a smaller ΔpH in the mutant. Therefore, lower photosynthetic control at Cytb6f and lower NPQ levels indicated that at the onset of low AL when PGR5/PGRL1-dependent CEF was missing generally less e- transport was performed in the pgr5 mutant relative to WT.

What is more, between 7 and 10 minutes of illumination (between minutes 12,5 and 15,5 in Fig. 38 A and B), Y(II) and Y(I) were slightly decreased in the pgr5 mutant relative to WT (Fig. 38 A and B). Moreover, in the pgr5 mutant, Y(II) levels were lowered due to more increased Q_A levels, hence less e- were flowing out from the acceptor side of PSII (Fig. 38 A and Fig. 39 A) and Y(I) was decreased due to elevated Y(NA) levels, indicating that also e- outflow at the acceptor side of PSI was decreased (Fig. 38 B and Fig. 39 C). A decrease in Y(II) is indicative of a decrease in linear e- flow capacity in the pgr5 mutant relative to WT. Moreover, elevated Q_A levels and Y(NA) levels could suggest that after prolonged illumination, when LEF is decreased CEF mediated through the NDH complex was increased in the pgr5 mutant relative to WT.

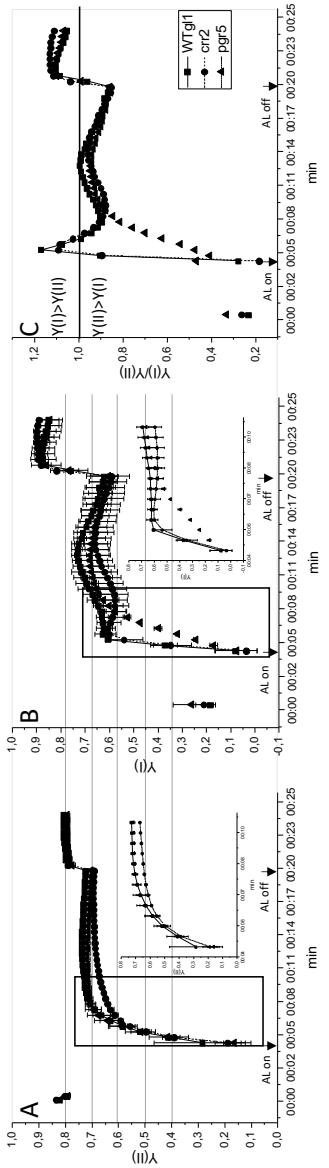

Figure 38. Photosynthetic performance of PSII and PSI during a dark-to-low light transition and when the light was turned off in WT gl1 (■), crr2 (●), and pgr5 (▲) *A. thaliana* leaves. A kinetic steady-state analysis of e- flow at A. PSII (Y(II)), B. PSI (Y(I)), and C. the ratio of Y(I)/Y(II) were determined via pulse-modulated spectroscopy. The x-axis refers

to time (in min) and the y-axis to normalized arbitrary units (calculated according to method section 2.2.f). The AL used in the measurement was 58 µmol m-2 s-1 and plants were grown at 85 µmol m-2 s-1. Average values from three to five different plants are shown for each genotype and bars indicate standard deviation.

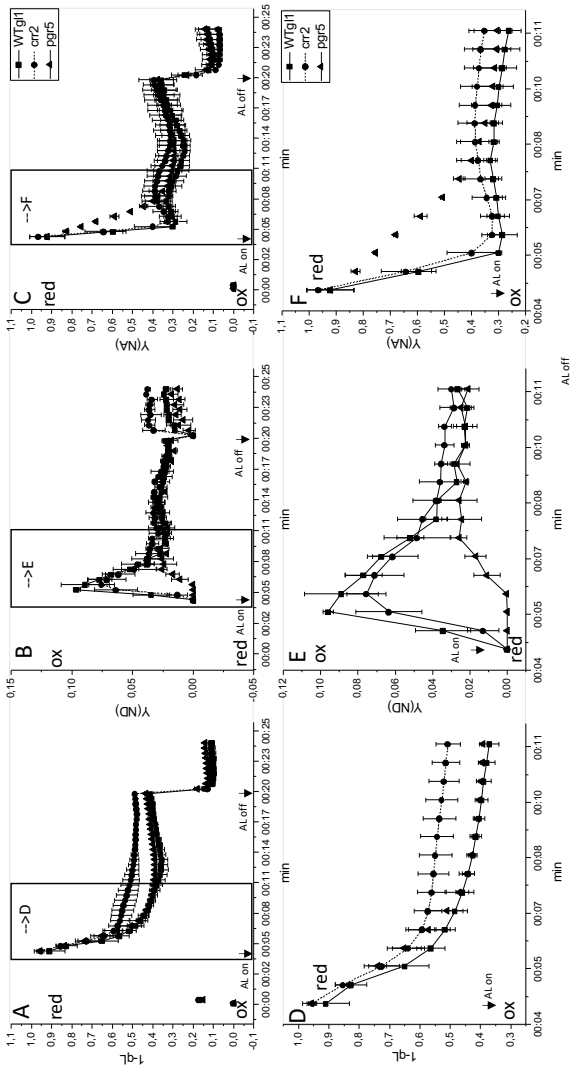

Figure 39. The oxidation state of PSII's acceptor side Q_A (1-qL) and PSI's donor and acceptor side during a dark-to-low light transition and when the light was turned off in WT gl1 (■), crr2 (●) and pgr5 (▲) *A. thaliana* leaves. A kinetic steady state analysis of the redox

state of A. and D. Q_A (1-qL), B. and E. PSI's donor side limitation Y(ND), and C. and F. PSI's acceptor side limitation Y(NA) were determined via pulse-modulated spectroscopy. The x-axis refers to time (in min) and the y-axis to normalized arbitrary units (calculated according to method section 2.2.f). The AL used in the measurement was 58 µmol m-2 s-1 and plants were grown at 85 µmol m-2 s-1. Average values from three to five different plants are shown for each genotype and bars indicate standard deviation.

In contrast, in the crr2 mutant, after the second minute of illumination (from minute 6,5 in Fig. 38 A), Y(II) levels significantly decreased caused by increased Q_A levels (measured through 1-qL) relative to WT, indicating that e- outflow at the acceptor side of PSII was decreased, while Y(I) was like in WT (Fig. 38 A and B and Fig. 39A and D). Interestingly, Q_A levels in crr2 and stn7 mutants were both elevated relative to WT (Fig. 39 A and Fig. 27 A), while Y(I) was not significantly different in the crr2 mutant from WT levels (Fig. 38 B). Unlike in the crr2 mutant, Y(I) levels were decreased in the stn7 mutant relative to WT (Fig. 26 D). If in the stn7 mutant CEF was increased while LEF was decreased leading to increased Q_A levels compared to WT, it could indicate that CEF was increased in the crr2 mutant relative to WT. However, at the same time Y(I) levels were in the crr2 mutant WT-like, and thus elevated relative to levels in the stn7 mutant (Fig. 26 D). Hence, in the crr2 mutant more e- were able to exit linearly into the metabolic e- pool relative to the stn7 mutant. It can be speculated that in addition to stn7 mutant-like upregulation of CEF in the crr2 mutant when compared to WT, more e- were able to be released from PSI in a linear manner relative to the stn7 mutant. Hence, when the NDH complex was missing in the crr2 mutant, it enhanced its capacity to perform LEF relative to the stn7 mutant. This difference in the capacity to perform LEF in crr2 and stn7 mutants could be based on differences in the thylakoid membrane structure. For example, when the crr2 mutant would be able to increase light absorption and subsequently the turnover of e- at both PSII and PSI it could lead to an increase in LEF and CEF in the crr2 relative to the stn7 mutant, while the stn7 mutant only increases e- turnover at PSI and not PSII.

Moreover, Y(I) decreased more between minutes 5,5 and 10,0 of light exposure (from minute 9,5 until 14,5 in Fig. 38 B) in the crr2 mutant relative to WT (Fig. 38 B), due to a transient stronger increase in Y(NA) levels relative to WT (Fig. 39 C and F), indicating that after prolonged illumination e- outflow at the acceptor side of PSI was

decreased. A decrease in e- outflow at PSI into the metabolic pool could be mediated through changes in the mode of e- transport in the crr2 mutant relative to WT. During this time interval when lacking NDH-dependent CEF in the crr2 mutant, it also caused an increase in Q_A levels relative to WT, indicating that e- outflow at the acceptor side of PSII was decreased and hence LEF was diminished relative to WT plants (Fig. 39 A). It can be speculated that after prolonged illumination with LL when NDH-dependent CEF is missing the performance of PGR5/PGRL1-dependent CEF is increased and LEF is decreased relative to WT. However, Y(ND) levels were in the crr2 mutant and WT alike, hence e- inflow at the donor side of PSI was similar (Fig. 39 B). It can be speculated that both NDH-dependent CEF (upregulated in WT) and PGR5/PGRL1-dependent CEF (upregulated in the crr2 mutant) are increasing e- inflow at the donor side of PSI to the same extent.

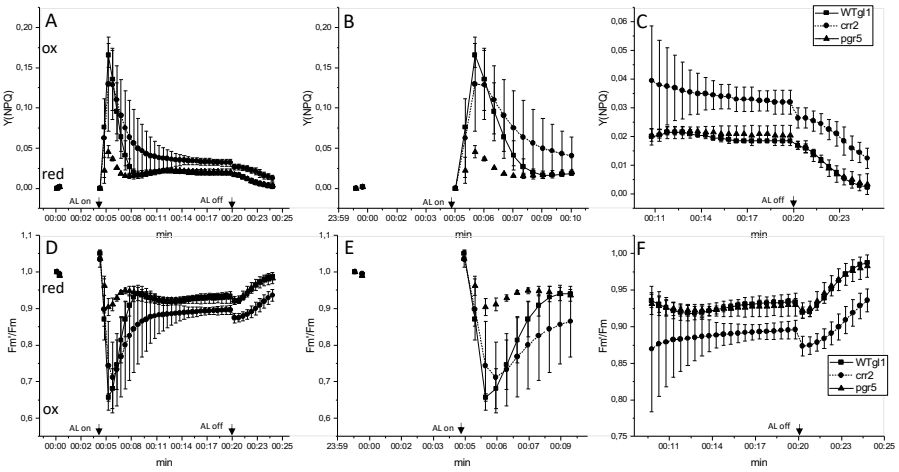

Figure 40. Chlorophyll fluorescence quench analysis during a dark-to-low light transition and when the light was turned off in WT gl1 (■), crr2 (●), and pgr5 (▲) *A. thaliana* leaves. A., B., and C. Kinetic steady state analysis of the yield of non-photochemical quenching (Y(NPQ)) and D., E., and F. of maximal fluorescence F_m' during light treatment normalized to the maximal fluorescence F_m after dark preincubation (F_m'/F_m) were determined via pulse-modulated spectroscopy. The x-axis refers to time (in min) and the y-axis to normalized arbitrary units (calculated according to method section 2.2.f). The AL used in the measurement was 58 µmol m-2 s-1 and plants were grown at 85 µmol m-2 s-1. Average values from three to five different plants are shown for each genotype and bars indicate standard deviation.

Additionally, in the crr2 mutant the transient increase in NPQ (measured through F_m'/F_m or Y(NPQ)) was not able to relax like in WT after about 7 minutes of low light exposure and was still present at the end of illumination and when the light was turned off (Fig. 40). This observation indicated that after prolonged illumination the proton gradient was elevated in the crr2 mutant relative to WT. An enhanced proton gradient is caused by an increase in protons translocated into the luminal space. Similarly, but to a smaller extent when compared to the crr2 mutant, in the stn7 mutant the transient increase in NPQ took a longer time to relax relative to WT. Hence, it suggested that after dark preincubation an increase in LEF and CEF in the crr2 mutant relative to WT and the stn7 mutant resulted in a rise in the proton gradient and performance of NPQ**.** Since after prolonged illumination LEF seems to be decreased in the crr2 mutant relative to WT, a stronger NPQ might be caused by a rise in PGR5/PGRL1-dependent CEF. In contrast, under these light conditions in WT LEF was decreased and NDH-dependent CEF was increased. It can be speculated that through the performance of NDH-dependent CEF and decreasing LEF the plant can better control its proton gradient, while the upregulation of PGR5/PGRL1-dependent CEF and LEF is leading to an increase in protons inside the luminal space that cannot be utilized by the ATPase, and is therefore elevating NPQ levels in the crr2 mutant relative to WT.

Moreover, we observed an increase in NPQ after prolonged exposure to darkness (Fig. 40 C), which was accompanied by more increased Y(ND) levels and decreased Y(NA) levels (Fig. 39 B and C), leading to increased Y(I) levels in the crr2 mutant relative to WT (Fig. 38 B). These observations were indicating that e- inflow at the donor side of PSI was decreased, while e- outflow was increased at the acceptor side of PSI. Therefore, e- outflow from PSI into the metabolic pool was under only ML through the application of short saturating pulses of AL elevated in the crr2 mutant relative to WT. It indicated that after prolonged illumination with low AL, switching off the light increased LEF in the crr2 mutant relative to WT. It can be speculated that when lacking NDH-dependent CEF in the crr2 mutant, it is increasing its LEF turnover relative to WT instead.

3.2.2. A kinetic analysis at the onset of low actinic light and when FR light was added in the crr2 and in the pgr5 mutant

Next, we investigated the mutant plant's lacking PGR5 and the NDH complex (the pgr5 and crr2 mutant) ability to perform state transition, through increasing light absorption at PSI by adding FR light. During the addition of FR light, a state 2- to- state 1 shift was induced. In this experiment, the AL was set to 25 µmol m-2 s-1. As noticed above, when examining the state transition in the mutant(s) (in paragraph 3.2), a state 2- to-state 1 adaptation mechanism was already observed when leaves were exposed to prolonged illuminated with low AL without the supplementation of FR light. However, for making a statement about the mutant's capacity to perform state transition, the section of AL supplemented with FR light was analyzed here.

First, when determining the effective photosynthetic quantum yield at PSII (Y(II)) and PSI (Y(I)) at low AL, we observed that after about 9 minutes of illumination the ratio of Y(I) to Y(II) was increased in the crr2 mutant relative to WT, while in the pgr5 mutant the ratio was like in WT (Fig. 41 B). This change in Y(I)/Y(II) correlated with the efficiency to decrease Y(NA) levels, hence increasing e- outflow at PSI's acceptor side throughout illumination (Fig. 42 E and F). In the crr2 mutant, Y(NA) levels were lowered at a faster rate (Fig. 42 E), whereas in the pgr5 mutant the rate decreased slower relative to WT (Fig. 42 F). This lets us conclude that at the onset of low AL, e- outflow at the acceptor side of PSI was elevated in the crr2 and decreased in the pgr5 mutant. It can be speculated that in the crr2 mutant more LEF was performed relative to WT and the pgr5 mutant.

When illuminated with 25 µmol m-2 s-1, the plant was able to activate the outflow of e- from the acceptor side of PSII and PSI, decreasing both Q_A (measured through 1-qL) and Y(NA) levels (Fig. 42 A, B, E, and F). In WT, Y(NA) levels were after an initial decrease increasing again during the first two minutes and at the same time, the decrease in Q_A was slowed down (minute 6,5 until 7 in Fig. 42 B and F). In contrast, both the increase of Y(NA) levels and slow-down of decreasing Q_A levels was missing

in the pgr5 mutant relative to WT (minute 6,5 until 7 in Fig. 42 B and F). Therefore, in the pgr5 mutant, the Y(I)/Y(II) ratio increased exponentially, while in WT the ratio showed a drop before increasing again (Fig. 41 A and B).

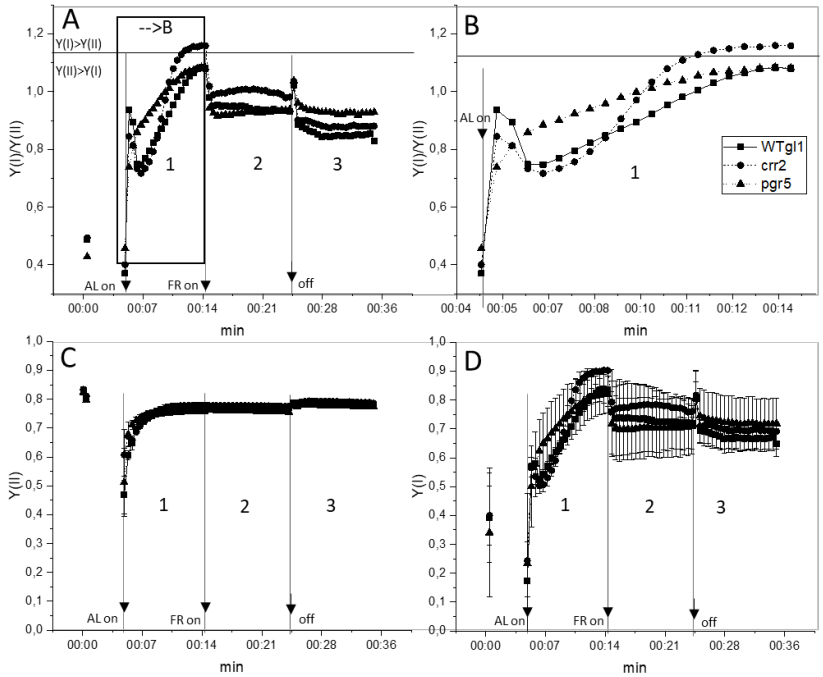

Figure 41. Photosynthetic performance of PSII and PSI during a 1. dark-to-low light transition, 2. a state 2- to- state 1 transition when FR light was added, and 3. in darkness in WT (■), crr2 (●) and pgr5 (▲) *A. thaliana* leaves. A kinetic steady-state analysis of e- flow at A. and B. the ratio of Y(I)/Y(II), C. PSII (Y(II)), and D. PSI (Y(I)) were determined via pulse-modulated spectroscopy. The x-axis refers to time (in min) and the y-axis to normalized arbitrary units (calculated according to method section 2.2.f). The AL was 25 µmol m-2 s-1 and the FR light was 70 µmol m-2 s-1. Plants were grown at 85 µmol m-2 s-1. Average values from three to five different plants are shown for each genotype and bars indicate standard deviation.

Results, therefore, suggest that in WT a halt in the decrease in Q_A levels and a short increase of Y(NA), which was leading to a drop in e- outflow at both the acceptor side of PSII and PSI during the first two minutes depending on PGR5/PGRL1-dependent CEF. It can be speculated that when the ATPase is not fully activated during the first two minutes of illumination, the plant decreases LEF and operates PGR5/PGRL1-dependent CEF instead. In contrast in the pgr5 mutant, the lack of PGR5/PGRL1-

dependent CEF, resulted in a slower but continuous decrease of Q_A levels and Y(NA) levels relative to WT (Fig. 42 B and F), indicating that the pgr5 mutant showed a slower outflow of e- at the acceptor side of PSII and PSI when compared to WT. This could be the case if the mutant is not able to operate PGR5/PGRL1-dependent CEF and thus relies solely on LEF for the translocation of protons inside the thylakoid lumen and production of ATP, which is needed to turn on the CBB cycle. It can be speculated that without PGR5/PGRL1-dependent CEF the pgr5 mutant plant has a decreased capacity to perform LEF. Moreover, at the onset of light, the lack of PGR5/PGRL1-dependent CEF in the pgr5 mutant caused a decrease in NPQ relative to WT (Fig. 43). This is another piece of evidence showing that in the absence of PGR5/PGRL1-dependent CEF, the capacity to establish a proton gradient was diminished in the pgr5 mutant compared to WT plants.

In the first 1-2 minutes, Y(NA) and Y(ND) levels in the crr2 mutant and in WT were alike (Fig. 42 C and E). However, the Q_A levels decreased slower in the crr2 mutant relative to WT (Fig. 42 A) suggesting that e- outflow at the acceptor side of PSII was lowered in the mutant. Hence, the slower decrease in Q_A levels in the crr2 mutant suggests that the mutant‘s PQ pool was more strongly reduced compared to WT. When comparing Q_A levels to the pgr5 mutant it can be proposed that in the crr2 mutant a decrease in e- outflow at the acceptor side of PSII was caused by an upregulation of PGR5/PGRL1-dependent CEF in the crr2 mutant relative to WT and the pgr5 mutant. After about 3,5 minutes of illumination, Q_A levels were in WT like in the crr2 mutant, showing that e- outflow at PSII was alike in WT and the crr2 mutant at this time point. At the same time, the transient increase in NPQ stopped in both the crr2 mutant and WT leading to similar F_m‘/F_m levels (Fig. 43 A and D). These observations suggested that at this stage LEF was performed similarly in WT and the crr2 mutant.

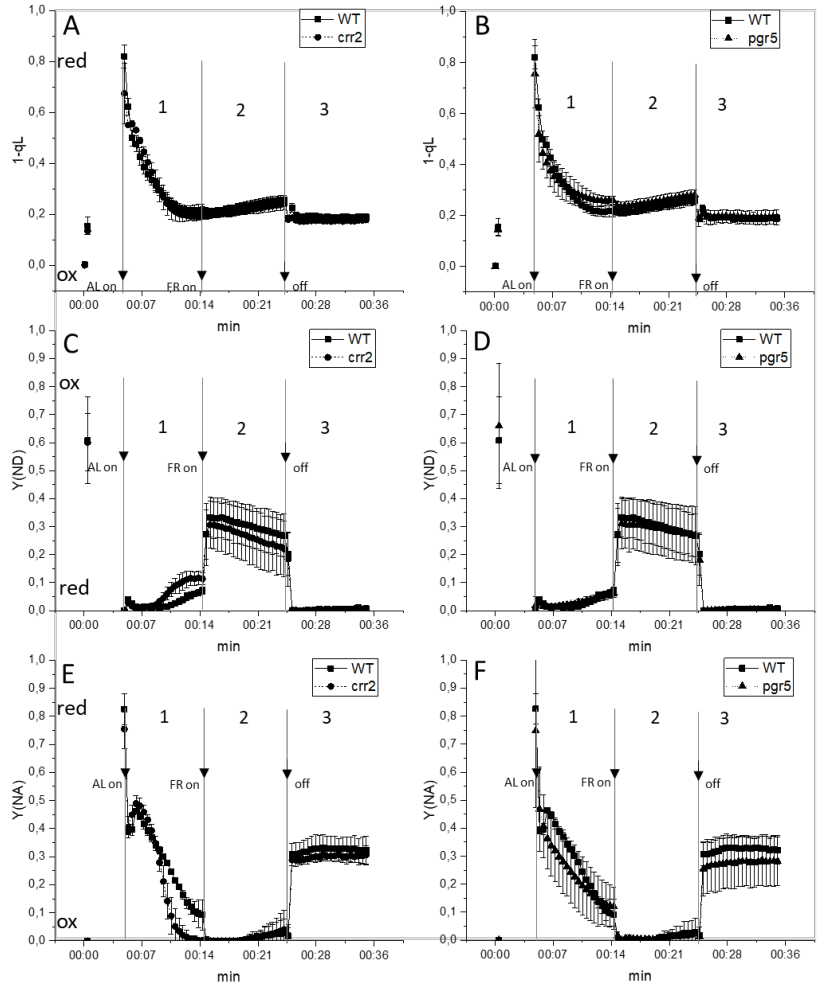

Figure 42. The oxidation state of PSII's acceptor side Q_A (1-qL) and PSI's donor and acceptor side during a 1. dark-to-low light transition, 2. a state 2- to- state 1 transition when FR light was added, and 3. in darkness in WT (■), crr2 (●) and pgr5 (▲) *A. thaliana* leaves. A kinetic steady-state analysis of the redox state of A. and B. Q_A (1-qL), C. and D. PSI's donor side limitation Y(ND) and E., and F. PSI's acceptor side limitation Y(NA) were determined via pulse-modulated spectroscopy. The x-axis refers to time (in min) and the y-axis to normalized arbitrary units (calculated according to method section 2.2.f). The AL used in the measurement was 25 µmol m-2 s-1 and the FR light was 70 µmol m-2 s-1. Plants were grown at 85 µmol m-2 s-1. Average values from three to five different plants are shown for each genotype and bars indicate standard deviation.

After about 7 minutes of illumination (from minute 10 in Fig. 42 B) Q_A levels were increased in the pgr5 mutant relative to WT (Fig. 42 B), indicating that e- outflow at the acceptor side of PSII was lowered. Additionally, Y(ND) levels were alike during the whole measurement in the pgr5 mutant and WT (Fig. 42 D). This observation indicated that prolonged illumination with low AL resulted in a more strongly reduced PQ pool in the pgr5 mutant relative to WT. This could be linked to elevated Y(NA) levels in the pgr5 mutant relative to WT, which are indicative of a decrease in e- outflow at the acceptor side of PSI when for example less LEF and more CEF are performed in the mutant relative to the WT.

In contrast, when deprived of NDH-dependent CEF in the crr2 mutant, Y(NA) was significantly decreased and Y(ND) levels significantly elevated after prolonged illumination compared to WT and the pgr5 mutant ((from minute 10 in Fig. 42 C and E)), indicating that e- inflow at the donor side of PSI has decreased and that e- outflow at its acceptor side of PSI was increased. Thus, lacking NDH-dependent CEF and/or missing the NDH complex in the crr2 mutant tremendously influenced the redox state of PSI. Additionally, when illuminated for about 7 minutes (from minute 10 in Fig. 41), Y(I) relative to Y(II) was increased, leading to a rise in the Y(I)/Y(II) ratio in the crr2 mutant when compared to WT (Fig. 41 A, C, and D). A rise in Y(I) in the crr2 mutant relative to WT was accompanied by a stronger decrease in Y(NA) levels (Fig. 42 E), by increasing the outflow of electrons into the metabolic pool while increasing Y(ND) levels and hence decreasing e- inflow at PSI‘s donor side (Fig. 42 F). This could be achieved through example increasing the capacity to perform LEF while decreasing CEF in the crr2 mutant relative to WT. In contrast, in WT LEF is decreased and CEF increased at this stage. It can therefore be speculated that the type of CEF used in WT under these conditions is depending on the NDH-complex.

By illuminating WT and mutant plants that were adapted to light with low AL and FR light we investigated the capacity to perform state transition. When AL was supplemented with FR light, we recorded a decrease in the rate of how fast F_m'/F_m increased in the pgr5 mutant relative to WT gl1 (Fig. 43 H). In contrast in both pph1 and stn7 mutants, except for a small drop in F_m'/F_m, which was also seen in WT, F_m'/F_m

was kept stable (Fig. 18 A, B, and C), while crr2 and npq4 mutants showed rates like their corresponding WTs (Fig. 43 A, D, E, F, and all rates compared in H).

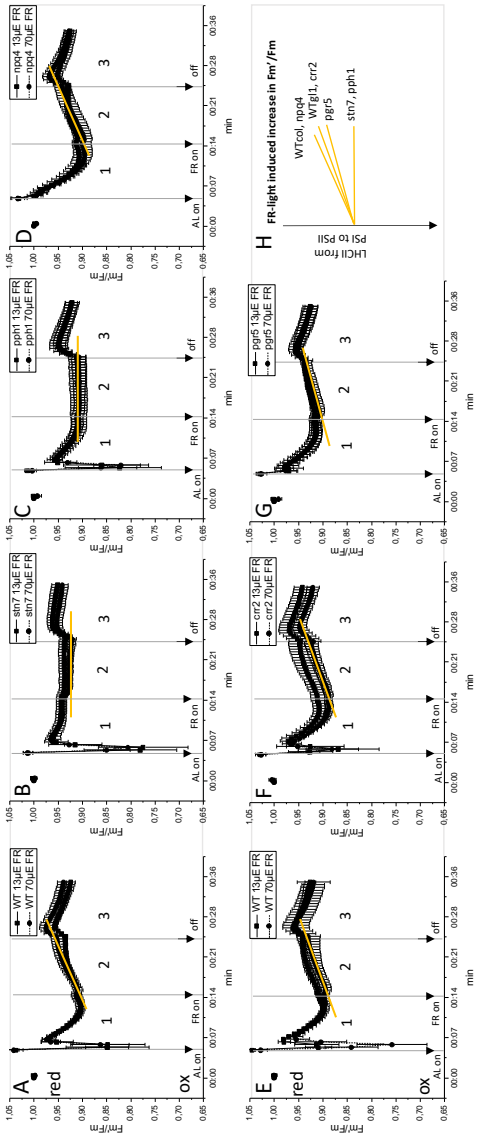

Figure 43. Chlorophyll fluorescence quench analysis during a 1. dark-to-low light transition, 2. a state 2- to- state 1 transition when FR light was added, and 3. in darkness in

A. WT col, B. stn7, C. pph1, D. npq4, E. WT gl1, F. crr2, and G. pgr5 *A. thaliana* leaves. A kinetic steady-state analysis of maximal fluorescence F_m' during light treatment normalized to the maximal fluorescence F_m after dark preincubation (F_m'/F_m) was determined via pulse-modulated spectroscopy. In H. the different rates of FR light induced change in F_m'/F_m when 70 µmol m-2 s-1 FR light was supplemented to 25 µmol m-2 s-1 were compared. The AL used in the measurement was 25 µmol m-2 s-1 and FR light with either 13 µmol m-2 s-1 (indicated with 13 µE) or 70 µmol m-2 s-1 (indicated with 70µE) was supplemented in phase 2. The x-axis refers to time (in min) and the y-axis to normalized arbitrary units (calculated according to method section 2.2.f). Plants were grown at 85 µmol m-2 s-1. Average values from three to five different plants are shown for each genotype and bars indicate standard deviation.

When comparing F_m'/F_m values between the stn7 mutant- showing increased values, and the pph1 mutant- showing decreased values relative to each other, only a small difference between them was observed (Fig. 43B and C). Therefore, findings suggested as already seen under 58 µmol m-2 s-1 that when FR light was added in WT the rise in F_m'/F_m was induced through increasing the number of photochemically reduced and hence fluorescing PSII centers. In contrast, both in the stn7 and in the pph1 mutant it was not possible to increase the number of those PSII centers throughout illumination. We therefore, suggest that the rise in F_m'/F_m values is linked through the phenomena of state transition, in detail a state 2- to- state 1 transition when light absorption at PSII was increased when LHCII molecules were dephosphorylated and detached from PSI centers. The lower rate in increasing the F_m'/F_m values in the pgr5 mutant relative to WT could therefore be an indication of a decreased capacity to perform state transition. In accordance, also the rate of how fast Y(ND) levels were lowered through performing a state 2- to- state 1 transition when increasing e- inflow at the donor side of PSI was decreased in the pgr5 mutant relative to WT gl1 (Fig. 44 H). It was concluded in paragraph 3.1.2 (After dark preincubation illumination with low AL when supplementing FR light in stn7, pph1, and npq4 mutant plants) that increased e- inflow at the donor side, which coincided with a decrease in e- outflow at the acceptor side of PSII and PSI is caused by an increase in CEF relative to LEF. In contrast, in the stn7, and in the pph1 mutants no change in Y(ND) levels was observed (Fig. 44 B and C; H) and in the npq4 mutant levels resembled WT (Fig. 44 H). This finding therefore strongly indicated that during low light conditions the mechanism of a state 2- to- state 1 transition was missing in the stn7 and pph1 mutants, and was decreased in the pgr5 mutant relative to WT while the npq4 mutant was like WT.

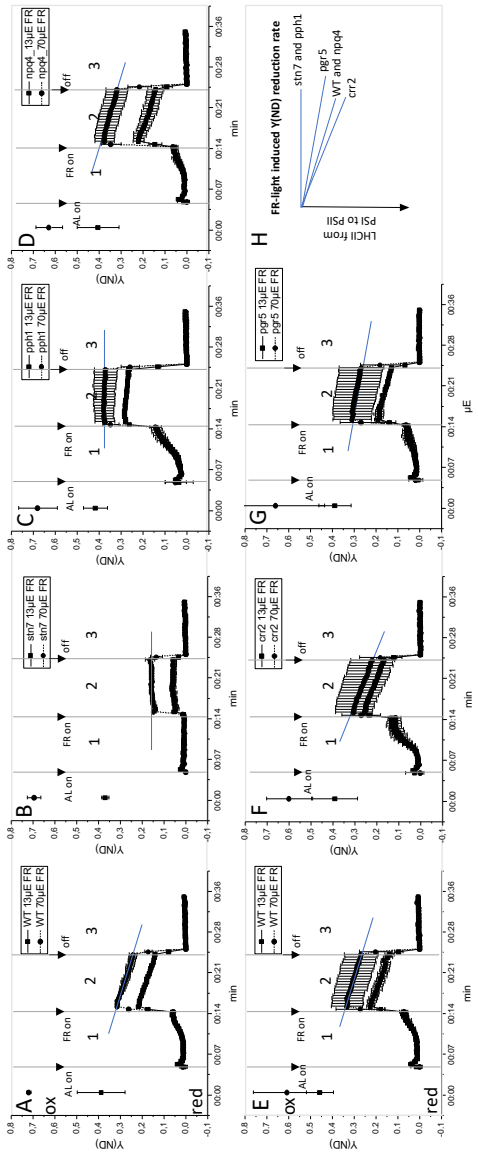

Figure 44. Oxidation state PSI's donor side during a 1. dark-to-low light transition, 2. a state 2- to- state 1 transition when FR light was added, and 3. in darkness in A. WT col, B. the stn7, C. the pph1, D. the npq4, E. WT gl1, F. crr2, and G. pgr5 *A. thaliana* leaves. A., B., and C. A kinetic steady-state analysis of PSI donor side limitation Y(ND) was determined via pulse-modulated spectroscopy. In H. the different rates of FR light induced change in Y(ND) when 70 µmol m-2 s-1 FR light was supplemented to 25 µmol m-2 s-1 were compared. The AL

used in the measurement was 25 µmol m-2 s-1 and FR light with either 13 µmol m-2 s-1 (indicated with 13 µE) or 70 µmol m-2 s-1 (indicated with 70 µE) was supplemented in phase 2. The x-axis refers to time (in min) and the y-axis to normalized arbitrary units (calculated according to method section 2.2.f). Plants were grown at 85 µmol m-2 s-1. Average values from three to five different plants are shown for each genotype and bars indicate standard deviation.

Moreover, in the crr2 mutant, the addition of FR light showed the same rise in F_m'/F_m values when compared to WT (Fig. 43 H), indicating that the mutant adapted to the change in the light like WT. However, during the illumination with low AL and FR light, Y(ND) levels were faster decreased in the crr2 mutant relative to WT gl1 (Fig. 44 H), indicating that e- inflow at the donor side of PSI was increased. In contrast, Y(NA) levels, were increasing in the crr2 mutant like in WT (Fig. 42 E). Similar Y(NA) levels but differences in Y(ND) levels between the crr2 mutant and WT can either result from differences in light absorption at PSII through the performance of state transition and/or through variations in e- transport. For example, when more CEF is performed in the crr2 mutant relative to WT, Y(ND) would be faster lowered because the inflow of e- at the donor side of PSI would be increased. Since F_m'/F_m values were in the crr2 mutant and WT alike it therefore strongly indicates that the amount of PSII centers and hence the performance of state transition was in mutant and WT alike. Instead, it suggests that the addition of FR light to low AL led to an increase in PGR5/PGRL1-dependent CEF in the crr2 mutant relative to WT.

Generally, in WT gl1, WT col, stn7, pph1, npq4, and pgr5 mutant plants Y(ND) levels showed a stronger instant increase when 70 µmol m-2 s-1 relative to when 13 µmol m-2 s-1 FR light was used (Fig. 44 A, B, C, D, E, G), indicative for a decrease in e- inflow at the donor side of PSI at 70 µmol m-2 s-1 relative to 13 µmol m-2 s-1 FR light. In contrast, the increase in Y(ND) levels in the crr2 mutant were at 13 µmol m-2 s-1 and at 70 µmol m-2 s-1 FR light at the same level and was resembling Y(ND) levels of WT plants that were supplemented with 70 µmol m-2 s-1 FR light (Fig. 44 E and F). Thus, Y(ND) levels could not be elevated further in the crr2 mutant when 70 µmol m-2 s-1 FR light relative to 13 µmol m-2 s-1 were used. This observation indicated that already with 13 µmol m-2 s-1 the capacity to decrease e- inflow at the donor side of PSI was saturated in the crr2 mutant. It can be speculated that in the crr2 mutant already AL led to a stronger decrease in e- inflow at most PSI centers relative to WT when for example

LEF was increased in the mutant. We, therefore, propose that the addition of FR light to low AL caused a rise in CEF (faster decrease in Y(ND) levels (Fig. 44 H)) as well as an increase in LEF in the crr2 mutant relative to WT. An increase in both CEF and LEF in the crr2 mutant relative to WT could originate from a difference in the mutant's thylakoid membrane structure. Interestingly, the crr2 mutant showed a mix of the stn7 mutant (increasing CEF) and the pph1 mutant (increasing LEF) phenotype, which could result from more LHCII molecules binding towards PSII and PSI, leading to an increase in light absorption and e- turnover at both PSII and PSI.

3.2.3. Increasing light irradiance levels in dark-adapted crr2 and pgr5 mutant leaves

Next, we investigated how the lack of NDH-dependent CEF (in the crr2 mutant) and PGR5/PGRL1-dependent CEF (in the pgr5 mutant) was affecting the mutant‘s ability to adapt to increasing light intensities. For this purpose, light irradiance levels were increased every 30 seconds from LL to HL in dark-adapted plants, and parameters were determined through the application of a saturating pulse at the end of each light step. Additionally, FR light was added to test the plant's capacity to oxidize PSII and PSI under certain light irradiance levels.

Interestingly, between 11 and 240 µmol m-2 s-1 Q_A levels (measured through 1-qL) were decreased in the crr2 mutant relative to WT (Fig. 45 A), indicating that e- outflow at the acceptor side of PSII was increased in the mutant. Moreover, while between 11 and 27 µmol m-2 s- Y(ND) and Y(NA) levels were alike in the crr2 mutant and WT when more than 58 µmol m-2 s-1 were applied, Y(ND) levels were decreased, and Y(NA) levels were more elevated in the crr2 mutant relative to WT (Fig. 46 A and C). Thus, from 58 µmol m-2 s-1 e- inflow at the donor side of PSI was increased, e- outflow at the acceptor side of PSI was decreased and e- outflow at the acceptor side of PSII was increased in the crr2 mutant relative to WT (Fig. 48 A, C, and D). Additionally, when more than 100 µmol m-2 s-1 were used, the capacity to perform NPQ (measured through 1-F_m'/F_m or Y(NPQ)) was increased in the crr2 mutant relative to WT (Fig. 47 A and C and Fig. 48 B). In the crr2 mutant, an increased capacity to perform NPQ was

already observed in kinetic analysis when the mutant was illuminated for several minutes at 58 µmol m-2 s-1 (Fig. 40 C and F). During the recording of an LRE, the increase in NPQ was most pronounced when more than 131 µmol m-2 s-1 were applied in the crr2 mutant relative to WT (Fig. 48 B). Therefore, when NPQ was elevated, e- inflow at the donor side of PSI increased (decreased Y(ND) levels), while e- outflow at the acceptor side of PSI was decreased (increased Y(NA) levels). At the same time, e- outflow at the acceptor side of PSII was increased (decreased Q_A levels) in the crr2 mutant relative to WT (Fig. 48 A, C, and D). Thus, when exposed to a stepwise increase in light irradiance levels above 58 µmol m-2 s-1 or when illuminated for a prolonged time with lower light intensities (such as 58 µmol m-2 s-1) we observed more CEF and more LEF causing a rise in NPQ in the crr2 mutant relative to WT. In contrast, when increasing light levels with lower light intensities (below 58 µmol m-2 s-1) more LEF was performed in the crr2 mutant relative to WT. It can be speculated that in the crr2 mutant more light is absorbed at PSII and PSI, which is increasing the mutant's capacity to perform more LEF relative to WT. In addition, from 58 µmol m-2 s-1 without FR and from 100 µmol m-2 s-1 with FR light caused a decrease in the Y(ND) level and an increase in the Y(NA) levels, indicating that also more PGR5/PGRL1-dependent CEF was performed in the crr2 mutant when compared to WT. Interestingly, a rise in PGR5/PGRL1-dependent CEF did not interfere with the decrease in the Q_A level, hence the e- outflow rate at the acceptor side of PSII. Thus, both an increase in LEF and CEF could in the crr2 mutant be the reason for elevated NPQ levels relative to WT. Indeed, when above 100 µmol m-2 s-1 were used, AL supplementing with FR- light led to increased NPQ (measured through $1-F_m'/F_m$ and Y(NPQ)) in both WT and the crr2 mutant, while in the crr2 mutant observations showed that NPQ levels were already increased without adding FR light relative to WT without FR light (Fig. 48 B). Moreover, the supplementation of FR light caused a stronger decrease in Q_A levels, hence e- outflow at PSII in the crr2 mutant relative to WT during the whole LRE (Fig. 45 A). This observation agreed with our assumption that more LEF was performed in the crr2 mutant versus WT.

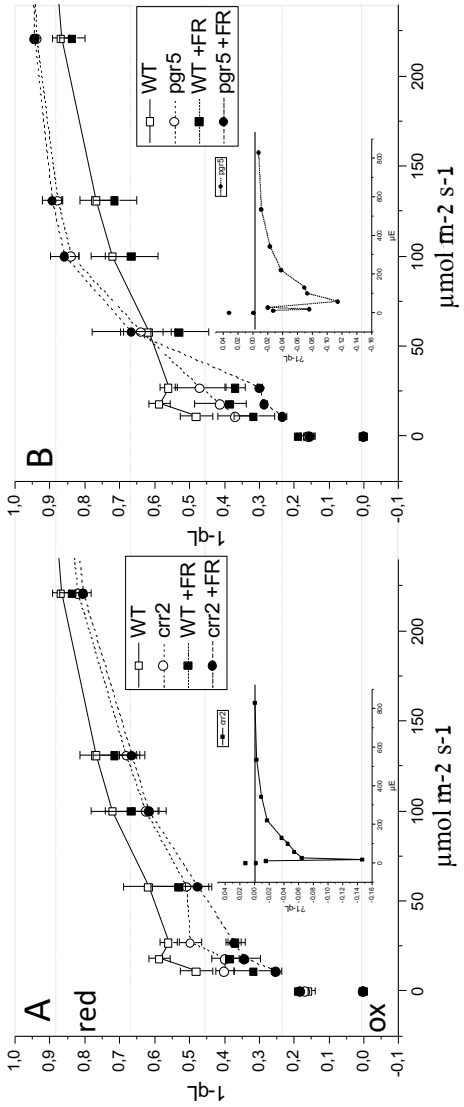

Figure 45. The oxidation state of PSII's acceptor side Q_A (1-qL) in *A. thaliana* mutant leaves A. crr2 and B. pgr5 compared to WT gl1 during the recording of a light-response experiment with increasing light irradiance levels determined via pulse-modulated spectroscopy. The graph in the inset shows the difference of measurements performed with AL minus measurements performed with AL supplemented with FR light (131 µmol m-2 s-1), subsequently, mutant difference graphs were subtracted from WT graphs. The x-axis refers to increasing light intensities (in µmol m-2 s-1) and the y-axis to normalized arbitrary units

(calculated according to method section 2.2.f). Plants were grown at 85 µmol m-2 s-1. Average values from three to five different plants are shown for each genotype and bars indicate standard deviation.

Therefore, it can be speculated that in the crr2 mutant the thylakoid membrane is composed of thinner grana stacks that are connected to the stroma thylakoid with more LHCII bound at PSI relative to WT resembling the pph1 mutant. An increase in LHCII molecules at PSI in the crr2 mutant relative to WT could be the consequence of or result of the lack of a functional NDH-PSI complex. On the one hand, e- outflow at the acceptor side of PSII is increased (stronger decrease in Q_A levels) suggesting that like in the pph1 mutant LEF is increased relative to WT. In addition, from 58 µmol m-2 s-1 e- inflow at the donor side was increased and e- outflow at the acceptor side of PSI was decreased in the crr2 mutant when compared to WT. It can be speculated that both LEF and CEF levels were increased when e- were shuttled from PSI directly towards the Cytb6f complex but not the PSII-served PQ pool. We hypothesize that this mode of CEF is PGR5/PGRL1-dependent. In WT, from 58 µmol m-2 s-1, Q_A levels were without FR light resembling the crr2 mutant measurements without FR light (Fig. 45 A and Fig, 48 A). Therefore, when leaves were illuminated for some minutes LEF levels were increased in WT and resembled levels in the crr2 mutant.

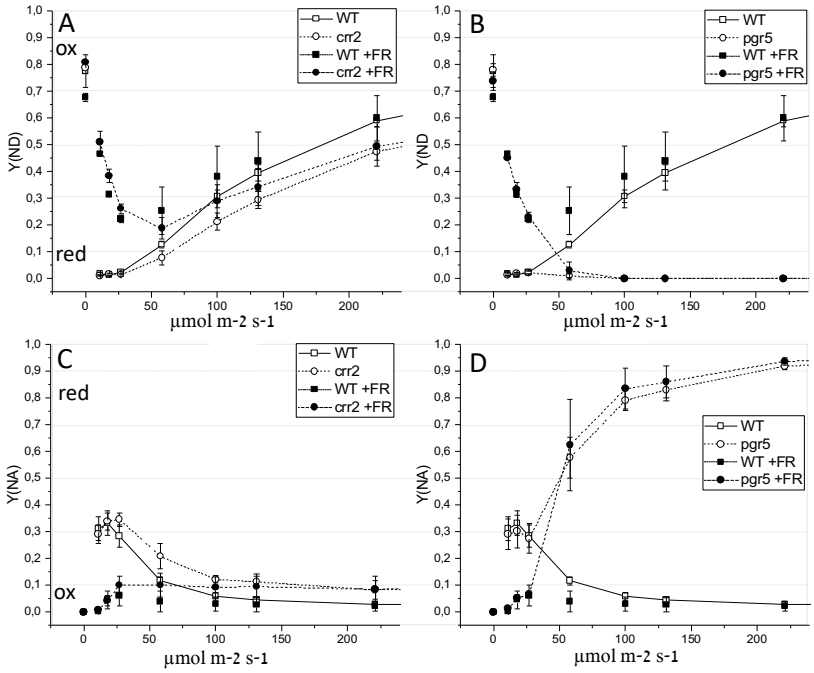

Figure 46. The oxidation state of PSI's donor and acceptor side in *A. thaliana* WT and crr2 and pgr5 mutant leaves during the recording of a light-response experiment with increasing light irradiance levels was determined via pulse-modulated spectroscopy. PSI donor side limitation Y(ND) in A. The crr2 and B. the pgr5 mutant and PSI acceptor side limitation in C. the crr2 and D. the pgr5 mutant during the recording of light-response experiment with increasing light irradiance levels were determined via pulse-modulated spectroscopy. The x-axis refers to increasing light intensities (in µmol m-2 s-1) and the y-axis to normalized arbitrary units (calculated according to method section 2.2.f). FR light at 131 µmol m-2 s-1 was supplemented. Plants were grown at 85 µmol m-2 s-1. Average values from three to five different plants are shown for each genotype and bars indicate standard deviation.

In contrast, in the pgr5 mutant Q_A levels were more decreased below 58 µmol m-2 s-1 and more increased from 100 µmol m-2 s-1 relative to WT (Fig. 45 B), indicating that e- outflow at the acceptor side was elevated at LL and decreased above growth light conditions. When Q_A levels were decreased, both Y(ND) and Y(NA) were like WT, while when Q_A was increased, Y(ND) was decreased and Y(NA) levels were significantly more increased in the pgr5 mutant relative to WT (Fig. 46 B and D), showing that e- inflow at the donor side of PSI was elevated, while e- outflow at its

acceptor side was decreased. It further suggests that in the pgr5 mutant at LL (11-27 µmol m-2 s-1) e- outflow in the metabolic pool via LEF was elevated relative to CEF, while above GL conditions LEF was downregulated when CEF was upregulated. It can be assumed that the mode of CEF in the pgr5 mutant is depending on the NDH-complex.

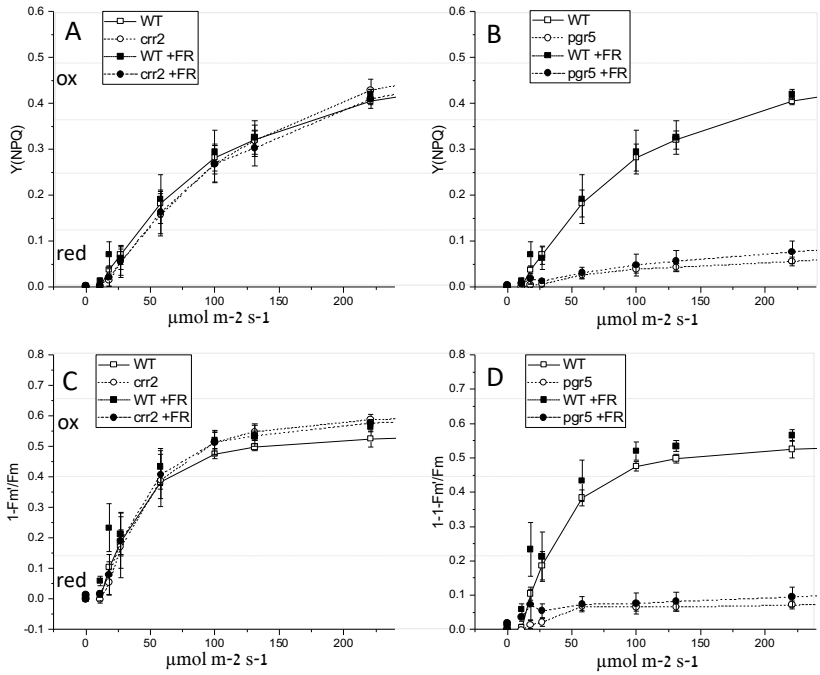

Figure 47. Chlorophyll fluorescence quench analysis in *A. thaliana* WT gl1, crr2, and pgr5 mutant leaves during the recording of a light-response experiment with increasing light irradiance levels was determined via pulse-modulated spectroscopy. The yield of non-photochemical quenching Y(NPQ) in A. crr2 and B. pgr5 mutants and the maximal fluorescence F_m' during light treatment normalized to the maximal fluorescence F_m after dark preincubation ($1-F_m'/F_m$) in C. crr2 and D. pgr5 mutants during the recording of light-response experiment with increasing light irradiance levels were determined via pulse-modulated spectroscopy. The x-axis refers to increasing light intensities (in µmol m-2 s-1) and the y-axis to normalized arbitrary units (calculated according to method section 2.2.f). FR light at 131 µmol m-2 s-1 was supplemented. Plants were grown at 85 µmol m-2 s-1. Average values from three to five different plants are shown for each genotype and bars indicate standard deviation.

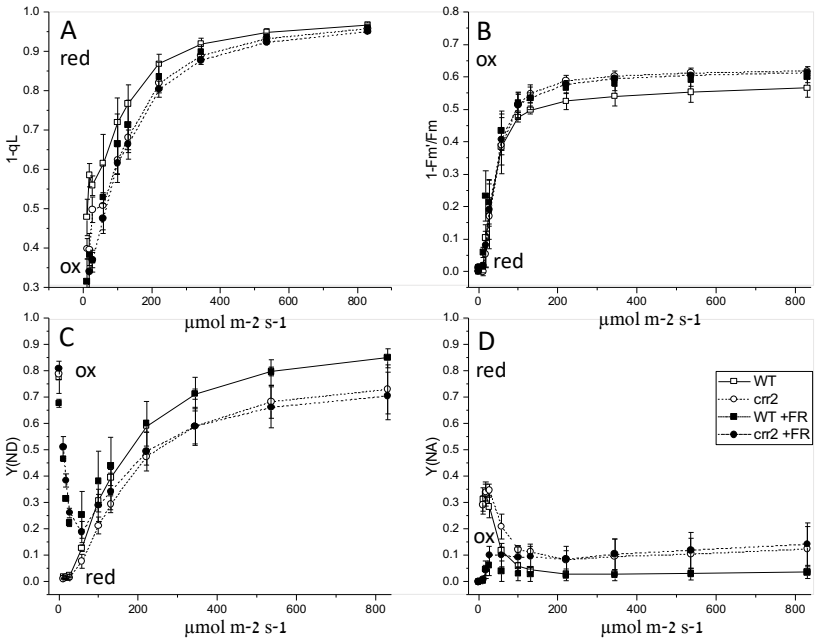

Figure 48. The oxidation state of PSII's acceptor side Q_A (1-qL) and PSI's donor and acceptor side and chlorophyll quench analysis during increasing light irradiance levels during the recording of a light-response experiment in WT (square) and crr2 (dot) *A. thaliana* leaves. A. Redox state of Q_A (1-qL), B. and the maximal fluorescence F_m' during light treatment normalized to the maximal fluorescence F_m after dark preincubation ($1-F_m'/F_m$), C. PSI donor side limitation Y(ND) and D. PSI acceptor side limitation Y(NA) were determined via pulse-modulated spectroscopy. The x-axis refers to increasing light intensities (in µmol m-2 s-1) and the y-axis to normalized arbitrary units (calculated according to method section 2.2.f). FR light at 131 µmol m-2 s-1 was supplemented. Plants were grown at 85 µmol m-2 s-1. Average values from three to five different plants are shown for each genotype and bars indicate standard deviation.

When Q_A levels were decreased at very low light (11-27 µmol m-2 s-1) (Fig. 45 B) and e- outflow at PSII elevated, it indicated that light was more equally absorbed at PSII and PSI in the pgr5 mutant relative to WT and e- were directly drawn off into the metabolic e- acceptor pool relative to WT. This interpretation would be following our finding that in the pgr5 mutant the capability to perform a state 2- to- state 1 was decreased relative to WT (paragraph 3.5). Hence, the mutant stayed more in a LEF-facilitating state 2. In detail, LEF would be favored in the pgr5 mutant being in state 2 – with phosphorylated LHCII molecules staying at PSI and the thylakoid membrane

containing thinner grana stacks that are fueling light absorption at PSII and PSI in an equal manner. Additionally, at low light intensities (11-27 µmol m-2 s-1), NPQ levels were decreased in the pgr5 mutant relative to WT (Fig. 47 B and D). This finding indicated that in the pgr5 mutant either a lower capacity to perform LEF and/or the lack of PGR5/PGRL1-dependent CEF was leading to a decrease in the proton gradient, subsequently lowering NPQ. Also, during high light irradiance levels, NPQ levels (measured through Y(NPQ) or 1-F_m'/F_m) were significantly decreased in the pgr5 mutant relative to WT (Fig. 47 B and D). However, from 100 µmol m-2 s-1 Q_A was increased, Y(ND) reduced, and Y(NA) levels were increased in the pgr5 mutant relative to WT (Fig. 45 B and Fig. 46 B and D), suggesting that e- outflow at the acceptor side of PSII and PSI was lowered, while e- inflow at the donor side of PSI was elevated. This observation indicated that at higher light intensities LEF was decreased and NDH-dependent CEF was elevated in the pgr5 mutant relative to WT. It can be speculated that a decrease in linear e- transport is causing a drop in the number of protons translocated inside the thylakoid lumen in the pgr5 mutant compared to WT. If fewer protons are translocated both the amount of ATP and the amount of metabolic e-acceptors in the chloroplasts are decreased. In contrast, in WT when PGR5/PGRL1-dependent CEF is operating under LL and HL conditions, more LEF can be performed and, NPQ is increased relative to the pgr5 mutant.

Moreover, the difference observed between the pgr5 mutant and WT in Q_A, and both Y(ND) and Y(NA), as well as NPQ levels, did not change when mutant and WT were supplemented with FR light (Fig. 45 B, Fig. 46 B and D and Fig. 47 B and D). Thus, FR light showed in the pgr5 mutant the same chlorophyll fluorescence phenotype as was observed with AL alone. It can be speculated that the absorption of light at PSI was already at its maxima in the pgr5 mutant and supplementing FR light made no difference. Additionally, the lack of PGR5/PGRL1-dependent CEF and a subsequently decreased capacity to perform LEF could decrease the impact FR light has on the pgr5 mutant.

3.3. The influence of dark- and light preincubation on e- transport modes in state transition mutants versus CEF-mutants

Next, we compared how the WT and mutant plants after dark or light preincubation adapted to 30 seconds of low-intensity light exposure (11 µmol m-2 s-1). We examined state transition mutants (stn7 and pph1 mutants) and CEF-mutants (crr2 and pgr5 mutants) to correlate changed light absorption at PSII and PSI through LHCII at PSII (in the stn7 mutant) or LHCII at PSI (in the pph1 mutant) and therewith coming e- transport changes when lacking PGR5/PGRL1-dependent (in the pgr5 mutant) or NDH-dependent CEF (in the crr2 mutant).

After dark- preincubation all plants showed a stronger increase in both Q_A (determined through 1-qL) and Y(NA) levels than when light-preincubated (Fig. 49 A, B, E, and F and Fig. 50 A, B, E and, F). Thus, when light-preincubated the opening of the metabolic e- acceptor pool was leading to an increase in e- outflow at the acceptor side of PSII and PSI via LEF.

Interestingly, when light-preincubated, Q_A levels were increased in the stn7 mutant relative to WT, indicating that e- outflow at the acceptor side of PSII was lowered and only the addition of FR light was able to decrease Q_A levels in the stn7 mutant like in WT (Fig. 49 B). In contrast, Y(NA) levels were after light preincubation in the stn7 mutant like WT with and without FR light, while Y(ND) levels were like WT without FR light but with FR light decreased relative to WT (Fig. 49 D and F). The latter showed that in the stn7 mutant with and without FR light, the e- inflow was increased at the donor side of PSI. In contrast, when dark-preincubated, Q_A, Y(ND), and Y(NA) were in WT and the stn7 mutant alike, whereas when FR light was supplemented, Q_A and Y(NA) levels were elevated and Y(ND) levels were decreased in the stn7 mutant relative to WT (Fig. 49 A, C, and E), indicating that FR light lowered e- outflow at both the acceptor side of PSII and PSI and enhanced e- inflow at the donor side of PSI. Therefore, observations indicated that after dark preincubation, in the stn7 mutant FR light decreased LEF and increased CEF relative to WT. When light-preincubated, the addition of FR light was decreasing both Q_A and Y(NA) levels in the stn7 mutant like

WT, hence increasing e- outflow at PSII‘s and PSI‘s acceptor side, while Y(ND) stayed more decreased and e- inflow at PSI‘s donor side elevated in the stn7 mutant relative to WT (Fig. 49 B and F). Thus, observations indicate that the addition of FR light was after both light preincubation and after dark preincubation keeping PSI’s donor side more strongly reduced (Y(ND) levels decreased) through the performance of CEF. A possible explanation for this phenomenon could be that in the stn7 mutant after both dark and light preincubation light is not equally absorbed and utilized at PSII and PSI, leading to a decrease in LEF. Under these conditions, adding FR light is causing an upregulation of CEF in the stn7 mutant relative to WT. Interestingly, after dark preincubation our data showed that when using AL more light was utilized at PSI relative to PSII, and CEF was increased in the stn7 mutant when compared to WT.

In contrast, when light-preincubated adding FR light caused Y(ND) levels to rise in the pph1 mutant relative to both WT and the stn7 mutant (Fig. 49 D), indicating that e- inflow at the donor side of PSI was decreased. Additionally, FR light caused Q_A and Y(NA) levels to decrease in mutants stn7 and pph1 and WT alike (Fig. 49 B and F). This observation indicated that when plants were light-preincubated, e- outflow from the acceptor side of PSII and PSI towards the metabolic acceptor pool via LEF was the same in WT, and the stn7 and pph1 mutant plants. However, opposite to WT and significantly to the stn7 mutant, in the pph1 mutant, the supplementation of FR light to low AL decreased e- inflow at the donor side of PSI. Thus, when adding FR light caused the turnover of CEF to be decreased relative to the performance of LEF in the pph1 mutant. Moreover, when dark-preincubated, Q_A levels were decreased in the pph1 mutant relative to WT, while both Y(NA) and Y(ND) were like in WT (Fig. 49 A, C, and E). This further showed that after dark preincubation, e- outflow from PSII was increased in the pph1 mutant relative to WT. Results indicated that after dark preincubation, phosphorylated LHCII at PSI was increasing LEF in the pph1 mutant when compared to WT. Moreover, adding FR light resulted in similar Q_A and both Y(ND) and Y(NA) values in the pph1 mutant and WT (Fig. 49 A, C, and E). Therefore, after dark preincubation when low AL was turned on and LHCII was phosphorylated and bound to PSI the capacity to perform LEF was elevated in the pph1 mutant relative

to WT. It can be speculated that light absorption and utilization were increased at both PSII and PSI relative to WT. The fact that the addition of FR light caused Q_A, Y(ND), and Y(NA) levels to be similar in WT and the pph1 mutant suggested that in WT less light was absorbed at PSI relative to the pph1 mutant due to a decrease in phosphorylated LHCII molecules at PSI.

To sum up, in the pph1 mutant when LHCII is bound at PSI leads to an increase in LEF and a decrease in CEF when compared to WT. It can be speculated that this is the case because the light is more equally absorbed at both photosystems in the pph1 mutant relative to WT. In contrast, when more light is utilized at PSI relative to PSII in the stn7 mutant, the addition of FR light causes after dark and light preincubation a stronger reduction in PSI's donor side (decreased Y(ND) levels) by increasing the performance of CEF relative to LEF. We conclude therefore that the distribution of light between PSII and PSI has a key regulatory function in switching between LEF and CEF.

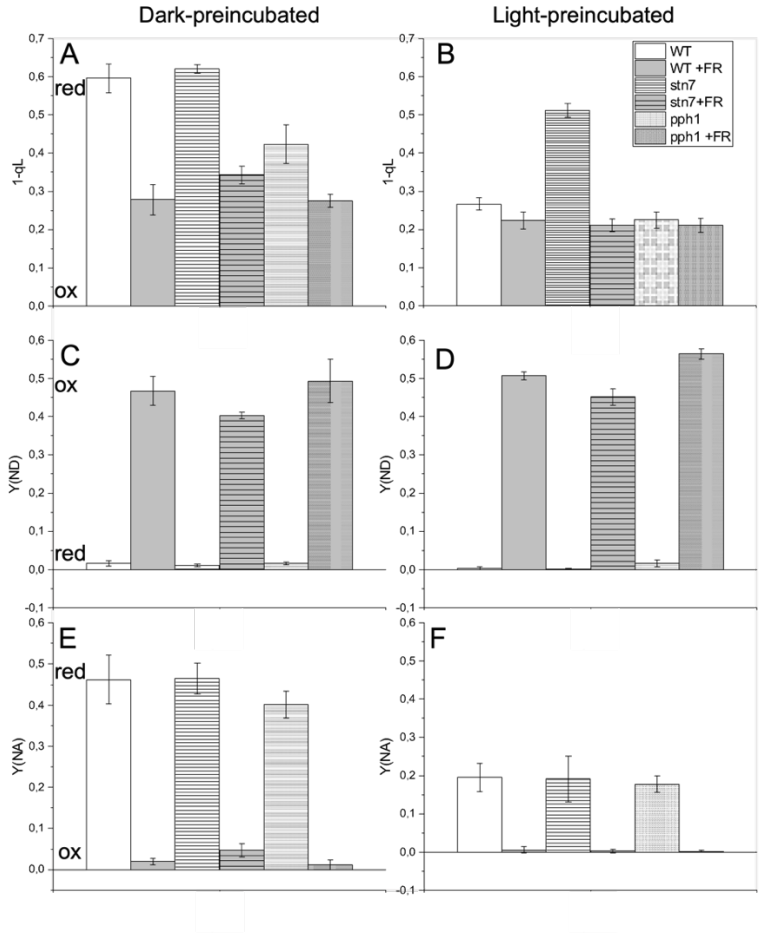

Figure 49. The oxidation state of PSII's acceptor side Q_A (1-qL) and PSI's donor and acceptor side in WT and stn7 and pph1 *A. thaliana* leaves. A. and B. Redox state of Q_A (1-qL), C. and D. PSI donor side limitation Y(ND) and E. and F. PSI acceptor side limitation Y(NA) were determined after dark or light preincubation via pulse-modulated spectroscopy. After dark or light preincubation, AL was turned on (11 µmol m-2 s-1). Additionally, low AL (11 µmol m-2 s-1) was supplemented with FR light at 131 µmol m-2 s-1. The x-axis refers to time (in min) and the y-axis to normalized arbitrary units (calculated according to method section 2.2.f). Plants were grown at 85 µmol m-2 s-1 1 and light-adapted at 8o µmol m-2 s-1. Average values from three to five different plants are shown for each genotype and bars indicate standard deviation.

Interestingly, dark-preincubated Q_A levels were decreased both with low AL and when low AL was supplemented with FR light in both crr2 and in pgr5 mutant plants relative to WT (Fig. 50 A), indicating that e- outflow was increased at the acceptor side of PSII

when one of the two main cyclic e- transport modes was missing. At the same time, Y(ND) and Y(NA) levels were with only AL in WT and both mutants alike (Fig. 50 C and E). However, when light-preincubated, Q_A levels were only decreased in the crr2 mutant but were increased in the pgr5 mutant relative to WT (Fig. 50 B), while Y(NA) values were decreased in both mutants relative to WT (Fig. 50 F). In the same way, as observed with Q_A levels, when light-preincubated, also Y(ND) levels were slightly elevated in the crr2 mutant and decreased in the pgr5 mutant relative to WT (Fig. 50 D), indicating that e- outflow at the acceptor side of PSII was decreased in the pgr5 mutant and increased in the crr2 mutant, while e- outflow at PSI was increased in both mutants and e- inflow at the donor side of PSI was decreased in the crr2 mutant and elevated in the pgr5 mutant. In conclusion, after dark preincubation when very low light was applied the capacity to perform LEF increased in both mutants, whereas after light preincubation CEF slightly increased in the pgr5 relative to the crr2 mutant, while LEF was increased in both pgr5 and crr2 mutants relative to WT. This observation indicated that when the NDH complex was missing (in the crr2 mutant) the plant increased when light- or dark-adapted its capacity to perform LEF relative to WT. In contrast, lacking PGR5/PGRL1-dependent CEF (in the pgr5 mutant) increased LEF at LL relative to WT when dark-preincubated and light-preincubated. In addition, when the pgr5 mutant was adapted to light it elevated CEF relative to the crr2 mutant.

Moreover, the addition of FR light caused when light pre-incubated Q_A levels and Y(NA) levels in the crr2 mutant to be like in WT, while Y(NA) levels were slightly elevated in the pgr5 mutant when compared to WT (Fig. 50 B and F). Additionally, the supplementation of FR light resulted in Y(ND) levels being decreased in the pgr5 mutant and elevated in the crr2 mutant relative to WT when FR light was added (Fig. 50 D). This finding suggested that with FR light e- inflow towards the donor side of PSI was elevated in the pgr5 mutant and decreased in the crr2 mutant, whereas e- outflow at the acceptor side of PSI was slightly decreased in the pgr5 mutant relative to WT and WT-like in the crr2 mutant. It can be speculated that after light preincubation more LEF is performed in the crr2 mutant, while more CEF is performed in the pgr5 mutant. The fact that LEF is upregulated in the crr2 mutant while CEF is enhanced in

the pgr5 mutant further implies that LEF and the mode of CEF could not work simultaneously but would work in competition with each other. It can be speculated that this type of CEF is feeding e- into the PQ pool, hence competing with e- supply from PSII. We propose that the type of CEF that is competing with LEF is NDH-dependent. Then, a reduction in LEF would favor NDH-dependent CEF in the pgr5 mutant, while a decrease in NDH-dependent CEF in the crr2 mutant would strengthen LEF. Hence, our observations indicated that after prolonged illumination NDH-dependent CEF is upregulated in the pgr5 mutant relative to WT.

Moreover, slightly increased Y(ND) levels after light preincubation in the pph1 mutant relative to WT, hence keeping e- inflow at PSI‘s donor side decreased could indicate that like in the crr2 mutant (when NDH-dependent CEF is lacking) also the *pph1* mutation causes a downregulation in NDH-dependent CEF. This could be due to increased binding of LHCII molecules to PSI centers, leading to a hindrance for the NDH-complex to bind PSI in turn downregulating NDH-dependent CEF. Alternatively, not the binding of LHCII or the NDH complex at PSI, but thylakoid membrane changes in the pph1 mutant could lead to the downregulation of NDH-dependent CEF. For example, in the pph1 mutant light could be more equally absorbed and utilized at PSII and PSI and LEF favored relative to WT. On the other hand, our findings indicated that NDH-dependent CEF is upregulated when the plant performs a low AL-induced state 2- to- state 1 transition. We, therefore, propose that since the pph1 mutant is locked in state 2 the mutant is not able like WT to dephosphorylate its LHCII molecules, change its thylakoid membrane, and increase the amount of light utilized at PSI relative to PSII to favor CEF over LEF.

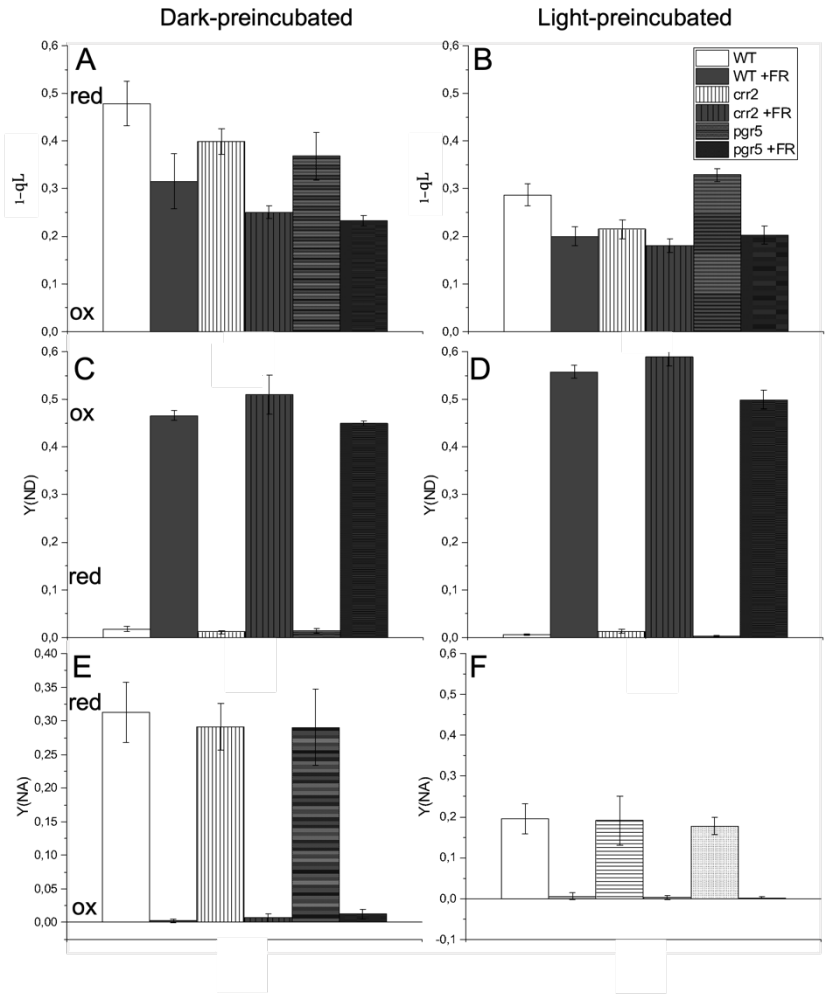

Figure 50. The oxidation state of PSII's acceptor side Q_A (1-qL) and PSI's donor and acceptor side in WT gl1 and crr2 and pgr5 *A. thaliana* leaves. A. and B. Redox state of Q_A (1-qL), C. and D. PSI donor side limitation Y(ND), and E. and F. PSI acceptor side limitation Y(NA) were determined after dark or light preincubation via pulse-modulated spectroscopy. After dark or light preincubation, AL was turned on (11 µmol m-2 s-1). Additionally, low AL (11 µmol m-2 s-1) was supplemented with FR light at 131 µmol m-2 s-1. The x-axis refers to time (in min) and the y-axis to normalized arbitrary units (calculated according to method section 2.2.f). Plants were grown at 85 µmol m-2 s-1 and light-adapted at 8o µmol m-2 s-1. Average values from three to five different plants are shown for each genotype and bars indicate standard deviation.

3.4. Free flow electrophoresis and second dimension Native-gel electrophoresis

3.4.1 Isolating protein complexes of the stroma thylakoids- in crr2 and pgr5 mutants

To study the composition of protein complexes in the stroma thylakoid membrane, chloroplasts were solubilized with digitonin. After the analysis was conducted with FFE in the first, and Native-PAGE in the second dimension, PSI complexes were isolated in WT from the cathode to the anode of FFE over the pH range 6.5-7.0 whereas in crr2 and pgr5 mutants PSI was separated from the pH 7 region at the cathode fractions (Fig. 51). Additionally, PSI complexes showed a specific fluorescence induction upon Native-PAGE relative to fluorescence analysis upon FFE separation (data not shown). The reason for the Native-PAGE specific increase in PSI fluorescence is unknown. However, it was observed that when LDS was supplemented to the cathode buffer during Native-PAGE a distinct LHCII band was visible (Fig. 51 and Fig. 52 A). This suggested that LHCII was released in the presence of LDS from PSI during Native-PAGE. It can be assumed that during FFE, LHCII was associated in a functional complex with PSI which efficiently quenched energy when excited and only upon Native-PAGE fluoresce. In addition to LHCII, PSI had bound LHCI and Cytb6f (Fig. 51 and Fig. 53). In the unstained gel when recording the fluorescence, we observed both in the crr2 and the pgr5 mutant and the WT the same number of PSI-Cytb6f complexes in the cathodic fractions (Fig. 51). However, in the crr2 mutant, the amount of disassembled LHCII complexes in the gel bottom increased relative to WT (Fig. 51; white arrows). Additionally, in the crr2 mutant significantly the formation of HMW complexes was enhanced relative to WT (Fig. 51; yellow box). Upon solubilization of the FFE fraction containing the HMW complexes with ß-DDM, PSI, and LHCII protein and to a smaller extent ATPase and PSII, which were detected by western blot detection against PSII's subunit D2 were released in WT, and in crr2 and pgr5 mutants (Fig. 54). The missing of large PSII and the presence of only the inner core of PSII complexes indicated that digitonin did not solubilize grana thylakoid membranes at large or that stroma thylakoids are at large devoid of large PSII complexes.

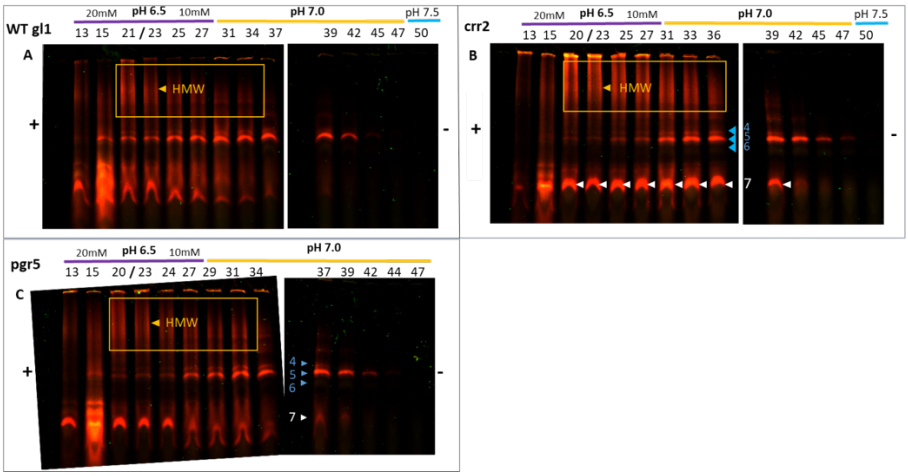

Figure 51. Separation of solubilized protein complexes of the stroma thylakoid membrane via LDS-Native-PAGE after FFE separation of A. WT gl1, B. crr2, and C. pgr5 *A. thaliana* plants. An equal amount of chloroplasts based on the chlorophyll content was solubilized with 16 mM digitonin and by FFE separated fractions were up-concentrated with 100K cut-off filters. For a better explanation of the methods working principle see section 2.2.c in material and methods. For an easier overview, pH and molarity of FFE buffers, the number of analyzed FFE fractions as well as the direction of electrical flow in the instrument (+/-) was added. Unstained gels were scanned at an excitation wavelength of 675/785 nm and emission of 700/800 nm. Yellow squares indicate HMW complexes and blue and white labeled protein complexes were analyzed via mass spectrometry (see Fig. 53 and Supplemental Table 1).

Additionally, the HMW complexes in the crr2 mutant were staying compared to WT much closer to the cathode (Fig. 51). The increase in HMW complexes in the crr2 mutant also correlated relative to WT with a rise in LHCII and PSII complexes (Fig. 51 and Fig. 55). Interestingly, after the supplementation of ß-DDM a higher degree of HMW complexes above 1000 kDa and more PSI and LHCII complexes were detected in the crr2 and the pgr5 mutant relative to WT (Fig. 54). This analysis indicated that the HMW complexes at the anode of FFE were composed of PSI complexes associated with a high quantity of mono- and trimeric LHC antenna proteins per PSI. Interestingly, when analyzing the unstained gel, in WT all protein bands clearly showed a stronger fluorescence relative to findings made in both crr2 and pgr5 mutants (comparing Fig. 51 unstained gel and Fig. 54; stained gel). This would suggest that crr2 and pgr5 mutants' fluorescence levels were decreased in the unstained gel due to a more

integrated binding of PSI toward LHC molecules and quenching the excitation energy more efficiently relative to WT.

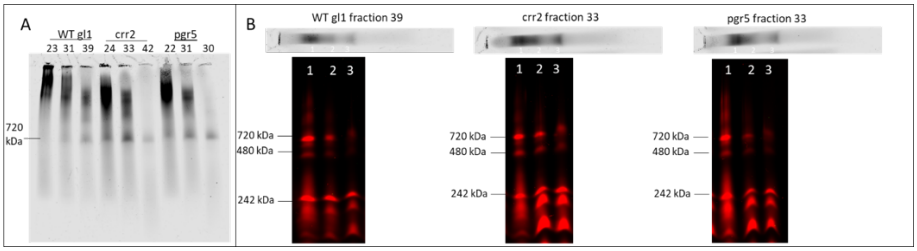

Figure 52. Analysis of the composition of native protein complexes by running Native-PAGE without LDS in the cathode buffer followed by a 2D-LDS-Native-PAGE after the second solubilization of protein bands from A. in ß-DDM. A. Native-PAGE analysis without LDS of selected fractions from WT gl1, crr2, and pgr5 *A. thaliana* plants were solubilized with 16 mM digitonin and up-concentrated with 100K cut-off filters. B. 2D-Native-PAGE with 80 µM LDS in cathode buffer after solubilizing protein bands derived from A. with 2mM ß-DDM. Gel images were recorded at excitation of 685 nm and emission at 700 nm.

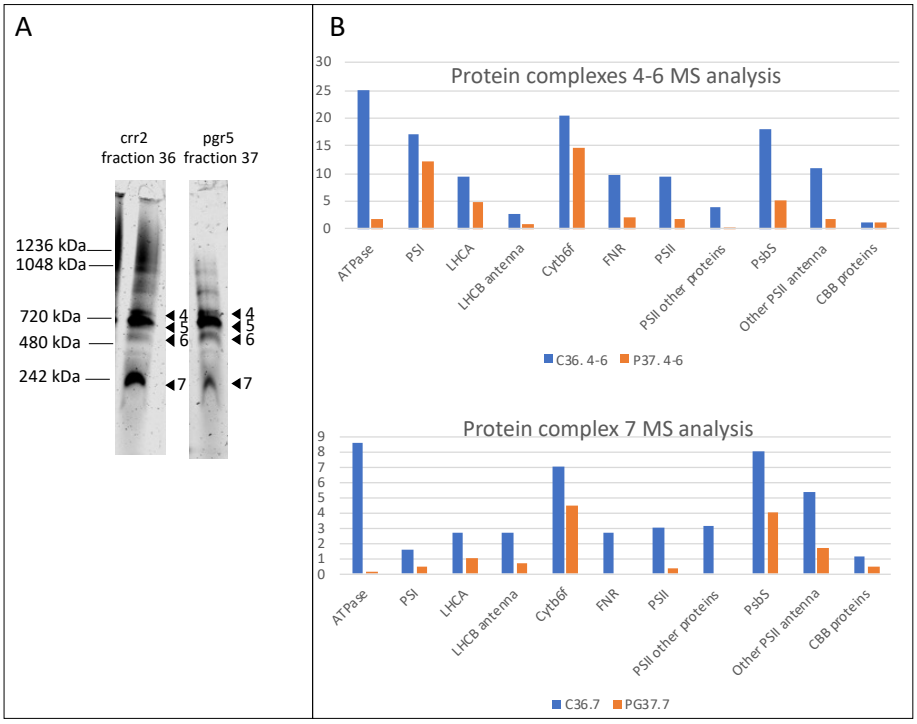

Figure 53. Mass spectrometry analysis of native protein complexes of the stroma thylakoid membrane separated via LDS-Native-PAGE after FFE separation. A. Native gel containing

separated fractions of crr2 and pgr5 stained with Coomassie and recorded at excitation 685 nm and emission at 700 nm. Bands used for mass spectrometry analysis were labeled with arrows and numbers. B. Total peptide count of protein bands labeled in A. Proteins identified in the crr2 mutant are labeled blue and proteins of the pgr5 mutant are labeled orange. A list of all identified proteins in the in here shown group results can be found in Supplemental Table 1.

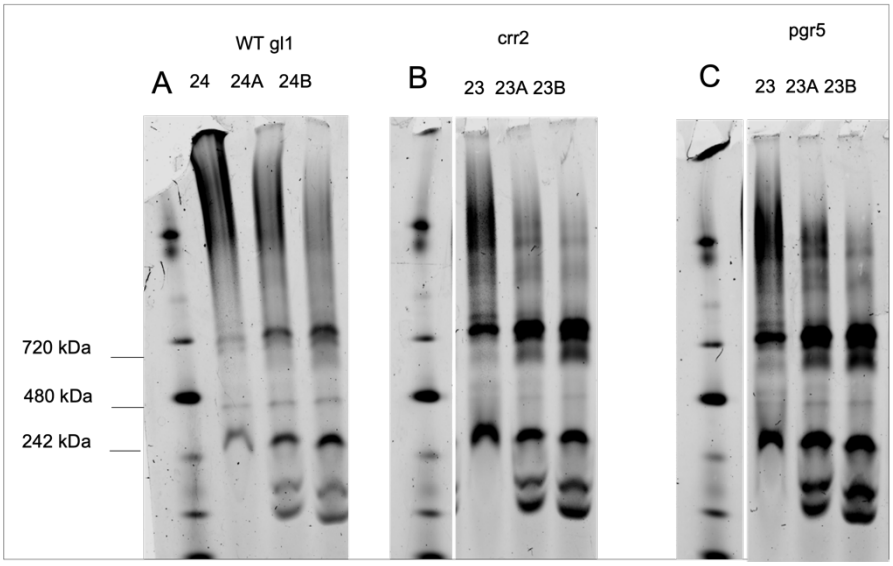

Figure 54. LDS-Native-PAGE after FFE separation of native protein complexes from A. WT gl1, B. crr2, and 3. pgr5. *A. thaliana* plants are solubilized with 16 mM digitonin and up-concentrated with 100K cut-off filters. Samples were additionally supplemented with (A) 1,25 mM ß-DDM and (B) 2,5 mM ß-DDM before loading on the gel. Stained gel was recorded at excitation of 685 nm and emission at 700 nm.

Moreover, preliminary data indicated that compared to WT in the crr2 mutant cathodic fractions correlated more with phosphorylated Lhcb1/2 molecules (Fig. 55). In the crr2 mutant, these cathodic fractions consisted of HMW and PSI-Cytb6f complexes (Fig. 55). Also, in the pgr5 mutant the amount of phosphorylated LHCII in the cathodic fractions containing PSI-Cytb6f complexes was enhanced relative to the WT (Fig. 55). In contrast, in the WT a rise in HMW complexes overlapped both with an increase in phosphorylated Lhcb1/2 and PSII complexes (Fig. 55). By that, the lower amount of HMW complexes in the pgr5 mutant correlated with a decrease in phosphorylated Lhcb1/2 and PSII protein relative to WT and the crr2 mutant (Fig. 51 and Fig. 55). Thus, it can be proposed that both the *crr2* and *pgr5* mutation influenced LHCII and its

subsequent binding to PSI-Cytb6f complexes. In addition, in the crr2 mutant, the composition of HMW complexes was drastically affected.

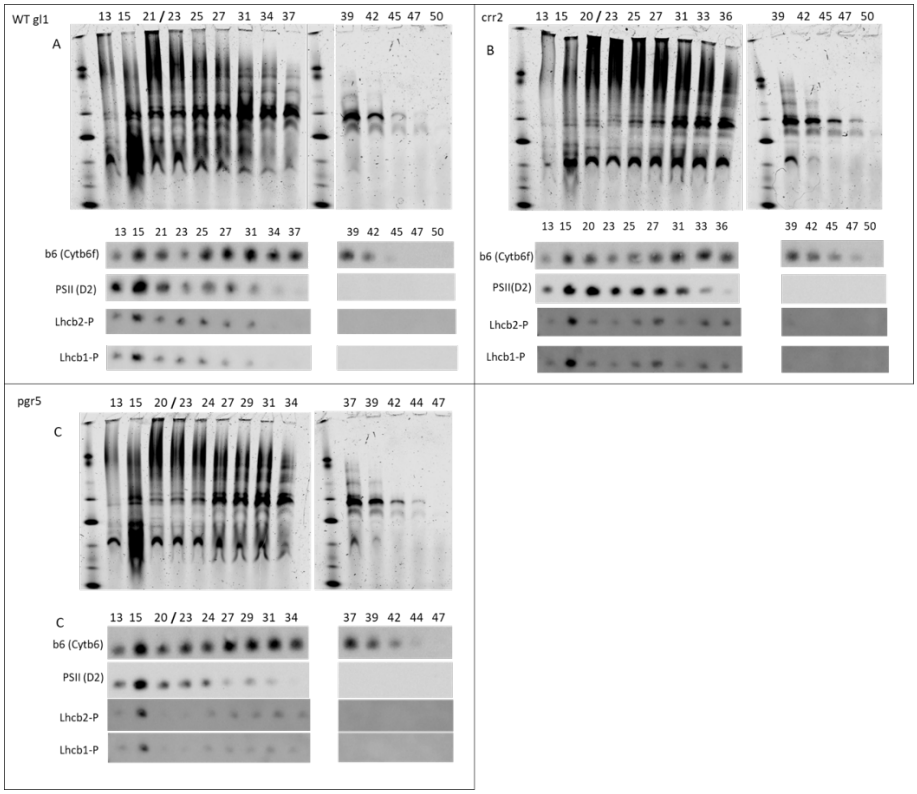

Figure 55. LDS-Native-PAGE after FFE separation of native protein complexes and Western blot analysis from A. WT gl1, B. crr2, and C. pgr5 *A. thaliana* plants solubilized with 16mM digitonin and up-concentrated with 100K cut-off filters. Gels were Coomassie stained and scanned at an excitation wavelength of 675nm and emission at 700nm. For Western blot antibodies against D2 (PSII), b6 (Cytb6f), phosphorylated Lhcb2 (Lhcb-2P), and phosphorylated Lhcb1-P) were used according to concentrations specified by the manufacturer.

Moreover, in the pgr5 mutant, the amount of HMW complexes was decreased relative to the crr2 mutant and looked like in WT (Fig. 51). When sequencing a cathodic PSI-Cytb6f complex containing fraction, in the pgr5 mutant we observed in general fewer proteins such as PSI, Cytb6f, PSII core complex, PsbS, Lhcb, and other PSII antenna proteins relative to the crr2 mutant (Fig. 53). However, the amount of ATPase molecules was significantly more decreased compared to the crr2 mutant, or

significantly more increased in the crr2 relative to the pgr5 mutant (Fig. 53). This further suggests that in agreement with less LEF capacity in the pgr5 mutant, leading to a decrease in ΔpH also the amount of photosynthetic protein complexes and especially the number of ATPase molecules in the stroma thylakoids was significantly lowered relative to the crr2 mutant (Fig. 53). Interestingly, while in the pgr5 mutant a drop in protein count was registered, protein complexes operating the CBB cycle were in both pgr5 and crr2 mutants equally present (Fig. 53 B). This observation suggested that while the number of protein complexes of the CBB stayed equal between pgr5 and crr2 mutants, photosynthetic complexes were decreased in the pgr5 relative to the crr2 mutant.

3.4.2 Isolation of proteins of the stroma thylakoids: in pph1 and stn7 mutant plants

Like protein analysis conducted in crr2 and pgr5 mutants (paragraph 3.9), the composition of protein complexes in the stroma thylakoid membrane in stn7 and pph1 mutant plants was analyzed by solubilizing chloroplasts with digitonin and separating protein complexes with FFE analysis in the first and Native-PAGE in the second dimension. While in WT PSI complexes were mostly isolated from the pH 7 region at the cathode fractions of FFE, in pph1 and stn7 mutants PSI was separated from the cathode to the anode over the pH range 6.5-7.0 (Fig. 56). As in the separations of WTgl1, crr2 and pgr5 mutants (Fig. 51), PSI complexes showed a specific fluorescence induction upon Native-PAGE relative to fluorescence analysis upon FFE separation. Again, it was observed that when LDS was supplemented to the cathode buffer during Native-PAGE a distinct LHCII band was visible suggesting that LHCII was released in the presence of LDS from PSI during Native-PAGE and that during pre-analysis by FFE LHCII was associated in a functional complex with PSI, which efficiently quenched energy and only upon Native-PAGE fluoresce (Fig. 57). In the pph1 mutant, an overall higher amount of HMW complexes and PSI-Cytb6f-LHCII complexes was identified throughout the FFE fractions, whereas in the stn7 mutant we observed a lower amount of HMW complexes and an increased amount of free PSI-Cytb6f-LHCII compared to WT (Fig. 56). This suggested that in the pph1 mutant the number of PSII-PSI-Cytb6f complexes that are found in a functional unit was increased, while the stn7

mutant decreased its amount. In the stn7 mutant, we found instead more PSI-Cytb6f complexes that were independent of HMW complexes and hence independent of PSII. Additionally, the pph1 mutant showed an increase in PSI-LHCII-Cytb6f complex that has a molecular shift of about 55 kDa relative to WT, which was absent in the stn7 mutant (Fig. 56). Interestingly, the stn7 mutant showed PSI-Cytb6f-LHCII complexes despite being depleted of kinase activity (Fig. 56 B). This finding implies that LHCII proteins can be bound to PSI centers without phosphorylation. This could suggest that unphosphorylated LHCII complexes bind at a different position than the phosphorylated state transition LHCII complex binds to.

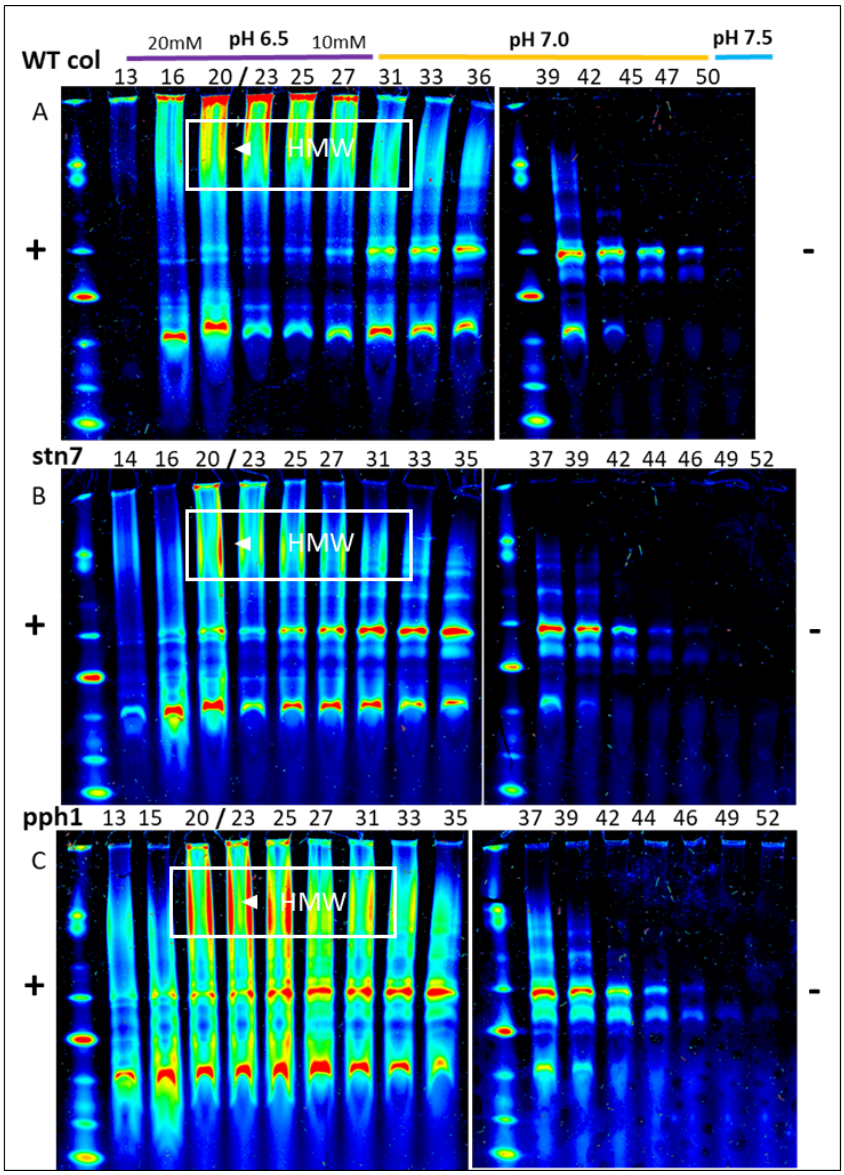

Figure 56. **Separation of solubilized protein complexes of the stroma thylakoid membrane via LDS-Native-PAGE after FFE separation of A. WT, B. stn7, and C. pph1 *A. thaliana* plants.** An equal amount of chloroplasts based on the chlorophyll content was solubilized with 16 mM digitonin and by FFE separated fractions were up-concentrated with 100K cut-off filters. For a better explanation of the methods working principle see section 2.2.c in material and methods. For an easier overview, pH and molarity of FFE buffers, the number of analyzed FFE fractions as well as the direction of electrical flow in the instrument (+/-) was added. Coomassie-stained gels were scanned at an excitation wavelength of 675 nm and emission at 700nm. White

squares indicate HMW complexes and were further analyzed via mass spectrometry (see Fig. 58 and Supplemental Table 2).

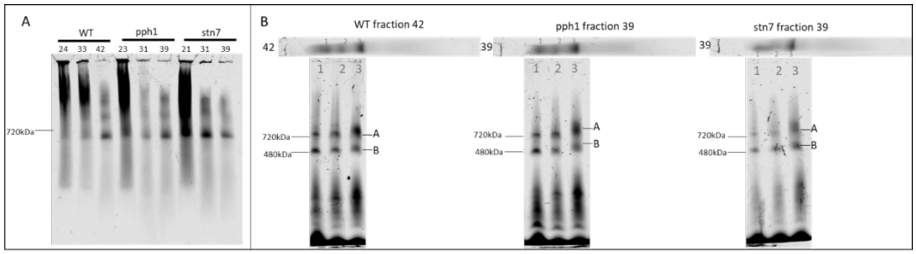

Figure 57. Analysis of the composition of native protein complexes by running Native-PAGE without LDS in the cathode buffer followed by a 2D-LDS-Native-PAGE after the second solubilization of protein bands from A. in ß-DDM. A. Native-PAGE analysis without LDS of selected fractions from WT col, and pph1 and stn7 *A. thaliana* plants were solubilized with 16 mM digitonin and up-concentrated with 100K cut-off filters. B. 2D-Native-PAGE with 80 µM LDS in cathode buffer after solubilizing protein bands derived from A. with 2 mM ß-DDM. Unstained gel images were recorded at excitation of 685 nm and emission at 700 nm.

Moreover, complexes with a very high molecular weight were separated specifically towards the anodic fractions during FFE (Fig. 56). These complexes were not able to enter the second-dimension gel and accumulated at the gel entry. Additionally, in the pph1 mutant and particularly in WT, a higher amount of HMW complexes accumulated relative to the stn7 mutant (Fig. 56; white squares). A higher fluorescence yield and protein concentration were recorded from these complexes in the pph1 mutant and especially WT, whereas in the stn7 mutant lower fluorescence and protein concentration were recorded (Fig. 56). The FFE fractions containing this HMW were analyzed separately by 2D NPAGE (Fig. 58). Analysis corroborated that HMW may contain solubilized membrane extracts containing PSII-LHCII-PSI-Cytb6f either as individual complexes or as a patch of photosynthetic supercomplexes. When breaking up HMW complexes though adding β-DDM, it was found that in WT, PSI in the anodic FFE fractions was nearly exclusively localized in the HMW complexes and hence in Native-PAGE analysis hardly any PSI complexes were determined in the anodic FFE fractions (Fig. 56 and Fig. 58). Interestingly, the HMW complexes were more stable in WT and the pph1 mutant relative to the stn7 mutant (Fig. 58). Hence, upon solubilization of the FFE fraction containing the HMW complexes with ß-DDM, PSI and LHCII protein were released in WT and the pph1 mutant; whereas in the stn7

mutant, most of the PSI and LHCII bound to PSI was already released during Native-PAGE without ß-DDM solubilization (Fig. 58). Interestingly, in the pph1 mutant after the supplementation of ß-DDM a higher degree of HMW complexes above 1000 kDa was visible relative to WT and the stn7 mutant (Fig. 58). In contrast, the addition of ß-DDM showed in the stn7 mutant a rise in HMW complexes between 800-1000 kDa relative to WT and the pph1 mutant (Fig. 58). Like in the crr2 and in the pgr5 mutant, in both state transition mutants as well as in the WT only a minority of PSII complexes was released that was shown by western blot detection against PSII's subunit D2 (Fig. 59). In concert with analysis conducted in the crr2 and in the pgr5 mutant, also in this analysis the absence of large PSII and the presence of only the inner core of PSII complexes indicated that digitonin did not solubilize grana thylakoid membranes at large or that stroma thylakoids are at large devoid of large PSII complexes.

This analysis indicated one more time that the HMW complexes at the anode of FFE were composed of PSI complexes associated with a high quantity of mono- and trimeric LHC antenna proteins per PSI. Additionally, stained gels showed the presence of ATPase in the HMW fractions (Fig. 58 B and C). Interestingly, HMW complexes from the stn7 mutant indicated in the native gel analysis the presence of a higher quantity of PSI-Cytb6f complexes relative to the pph1 mutant and WT (Fig. 58 A and B), which could not be verified via MS analysis (Fig. 58 C). When analyzing the unstained gel when excited at 685 nm it, therefore, suggests that in the stn7 mutant not the amount of PSI-Cytb6f complexes was increased but rather its fluorescence signal relative to WT. Additionally, in the anodic fraction, the total peptide count of proteins was compared between the stn7 and pph1 mutant. The WT was excluded from mass spectrometry analysis. In this analysis, proteins such as the NDH complex, Curvature thylakoid proteins (CURTs), Acclimation of photosynthesis to environment proteins (APE), Suppressor of quenching 1 protein (SOQ1), the enzyme Protochlorophyllide reductase (POR) and proteins of the CBB cycle were elevated in the stn7 mutant relative to the pph1 mutant (Fig. 58 C; other proteins in HMW complexes and Supplemental Table 2 for MS analysis).

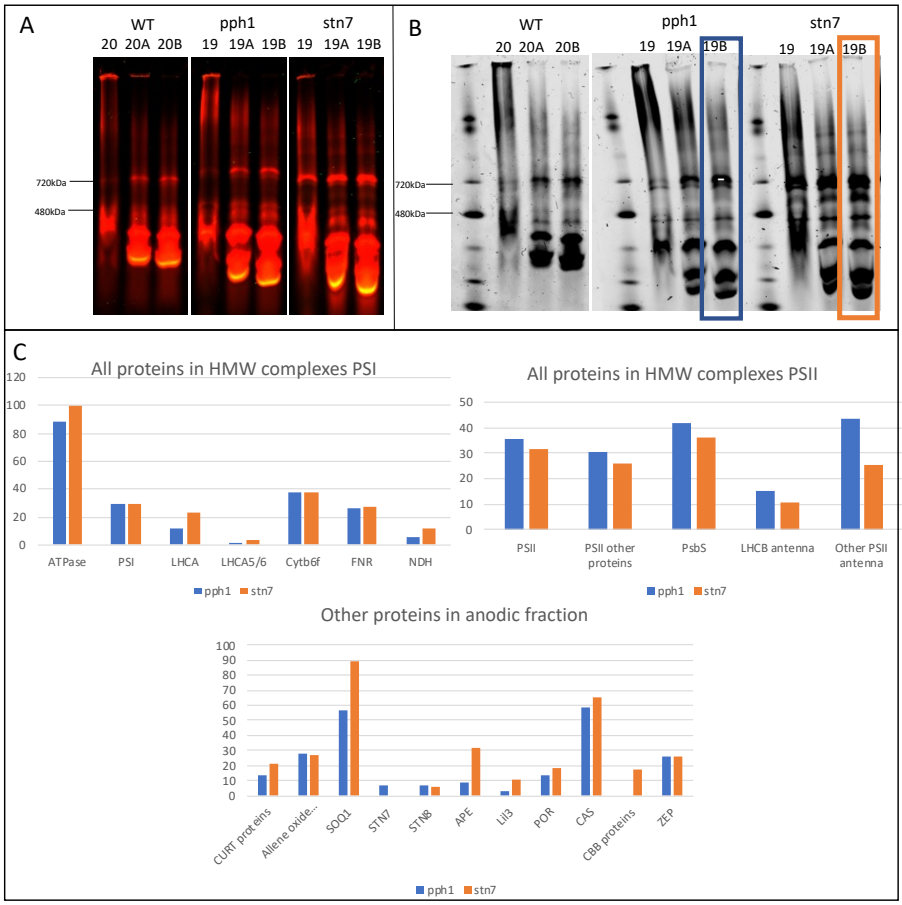

Figure 58. LDS-Native-PAGE after FFE separation of native protein complexes from WT, pph1, and stn7 *A. thaliana* plants solubilized with 16 mM Dig and up-concentrated with 100K cut-off filters. Samples were additionally supplemented with (A) 1,25 mM ß-DDM and in (B) 2,5 mM ß-DDM before loading on the gel. A. Unstained gel recorded at excitation 685 nm and emission at 700 nm. B. Coomassie-stained gel was recorded at excitation of 685 nm and emission at 700 nm. C. Total peptide count of protein bands supplemented with (B) 2,5 mM ß-DDM of pph1 19B (blue square) and stn7 19B (orange square) grouped in PSI-, PSII-related, and other proteins. A list of all identified proteins of the in here shown group results can be found in Supplemental Table 2.

In addition, the preliminary gel-blot analysis showed that more phosphorylated LHCII complexes were distributed in the HMW anodic FFE fractions in the pph1 mutant relative to the stn7 mutant, which showed none (Fig. 59). This would suggest that the

detergent had better access to solubilize membrane patches rich in phosphorylated LHCII in the pph1 mutant's stroma thylakoid structure. Therefore, we propose that the solubilization outcome depends to a very strong degree on the thylakoid membrane structure- namely the pph1 mutant having more wider grana stacks with fewer grana layers and thus more stroma thylakoids relative to the stn7 mutant which possess increased grana layers and thinner stacks. By this finding, the mutant overexpressing CurtA and increasing its grana stacks immensely[247] showed fewer HMW complexes relative to its corresponding WT (Fig. 60). Moreover, like in pph1 the increase in HMW complexes in the crr2 mutant relative to WTgl1 strongly suggests that in the crr2 mutant the fraction of stroma thylakoids was increased relative to WT.

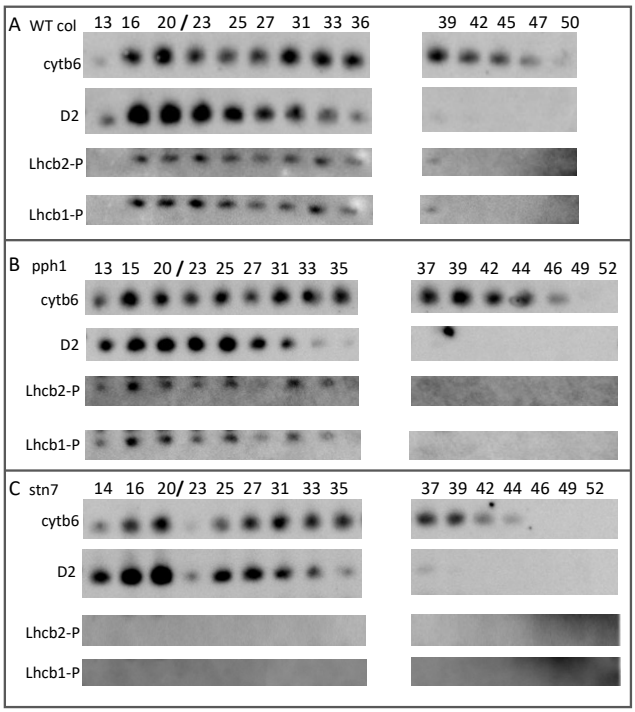

Figure 59. Western blot analysis from FFE fractions from A. WT gl1, B. pph1, and C. stn7 *A. thaliana* plants. The same amount of chloroplasts determined via chlorophyll concentration was solubilized with 16mM digitonin and up-concentrated with 100K cut-off filters. Antibodies against D2 (PSII), b6 (Cytb6f), phosphorylated Lhcb2 (Lhcb-2P), and phosphorylated Lhcb1-P) were used according to concentrations specified in materials and methods section 2.2.d.

In addition, in the WT and especially in the pph1 mutant an increase in PSI-LHCII-Cytb6f complex that has a molecular shift of about 55 kDa compared to the stn7 mutant was noticed (Fig. 56). Both in WT and the pph1 mutant Native-PAGE analysis showed a PSI-LHCII-Cytb6f complex with a higher molecular weight correlating with fractions that also contained phosphorylated LHCII (Fig. 56). In contrast, in the stn7 mutant, this complex, as well as phosphorylated LHCII, was not observed (Fig. 56 and Fig. 59). Moreover, the pph1 mutant showed phosphorylated Lhcb1/2 also in the very anodic fraction, where both WT and the stn7 mutant did not show any phosphorylated antenna (Fig. 59).

Thus, it can be proposed that the solubilization outcome in the stn7 and the pph1 mutant as well as the crr2 mutant- leads to more HMW complexes in the pph1 and the crr2 mutant, and more PSI-Cytb6f complexes in the stn7 mutant, were caused by differences in the grana and stroma thylakoid membrane structure.

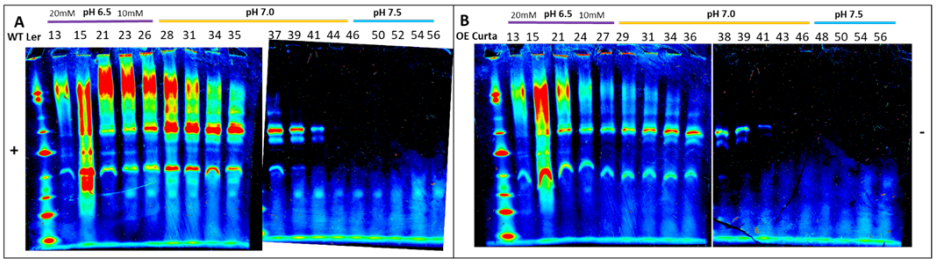

Figure 60. Separation of solubilized protein complexes of the stroma thylakoid membrane via LDS-Native-PAGE after FFE separation of A. WT Ler and B. OE CurtA plants. An equal amount of chloroplasts based on the chlorophyll content was solubilized with 16 mM digitonin and by FFE separated fractions were up-concentrated with 100K cut-off filters. For a better explanation of the methods working principle see section 2.2.c in material and methods. For an easier overview, pH and molarity of FFE buffers, the number of analyzed FFE fractions as well as the direction of electrical flow in the instrument (+/-) was added. Coomassie-stained gels were scanned at an excitation wavelength of 675 nm and emission at 700 nm.

4. Discussion

4.1. Comparing state transition, NPQ and CEF mutant(s) through chlorophyll fluorescence and absorption spectroscopy

4.1.1. State transition mutants stn7 and pph1, and the npq4 mutant

4.1.1.a. Disturbed light distribution between photosystems is changing e- transport modes in stn7, pph1, and npq4 mutant plants

Low-intensity AL settings were chosen to observe differences in e- transport modes comparing chlorophyll fluorescence and absorption changes obtained via pulse-modulated spectroscopy (PAM). The state transition mutants stn7, with LHCII bound at PSII, and the pph1 mutant, with phosphorylated LHCII bound at PSI, and the npq4 mutant missing qE, the fastest known form of NPQ were investigated. After dark preincubation, turning on low AL showed a higher relative contribution of e- flow through PSI (Y(I)) than through PSII (Y(II)) during the first minute in WT and the stn7 mutant (Fig. 26 A and B). In contrast, a more balanced e- flow of about a 1:1 ratio of Y(I)/Y(II) was observed in the pph1 and npq4 mutant plants (Fig. 26 A and B). Therefore, after dark preincubation, e- flow at PSI relative to e- flow at PSII was increased in the stn7 mutant and WT, which can be interpreted that after dark preincubation CEF was enhanced relative to LEF. When connecting our finding to recent membrane structure analysis, it further suggests that when PSII centers were embedded in more layers of grana thylakoid membrane after dark preincubation[3], light quanta were preferentially utilized at PSI centers through CEF in WT and the stn7 mutant. After a dark preincubation, the CBB cycle is not activated yet and LEF is not fully turned on at the onset of light. In this condition, CEF could be important for the formation of ΔpH leading to the synthesis of ATP without net formation of NADPH

and transient increase in NPQ[248,249]. Hereby, LEF and CEF can adjust the ATP/NADPH ratio according to their metabolic demand[250–252].

In the stn7 mutant and WT, Y(I) was rising during the first minute of illumination. The stn7 mutant showed a more strongly reduced PSI acceptor side (increased Y(NA) levels) and was keeping its PSI donor side more strongly reduced (decreased Y(ND) levels) relative to WT (Fig. 27 E and F), indicating that e- outflow at the acceptor side of PSI was decreased while inflow at its donor side was increased. This observation strongly indicated that at the onset of low AL, fewer e- were flowing into the metabolic pool in the stn7 mutant. Hence, LEF was decreased, and more e– were running in a cyclic mode keeping PSI‘s donor side more strongly reduced relative to WT. Moreover, at the onset of low AL, the transient increase in NPQ needed a longer time to relax in the stn7 mutant relative to WT and the pph1 mutant (Fig. 28 B and Fig. 29 B). This gives another hint that after dark preincubation and the onset of low AL, the increased performance of CEF in the stn7 mutant relative to WT caused a rise in the proton gradient, and hence elevated NPQ levels. Alternatively, this could mean that in the stn7 mutant a higher proton gradient across the thylakoid membrane is taking longer to dissolve due to a decrease in ATPase activity in the stn7 mutant when compared to WT. On the other hand, it can be speculated that ATP synthase molecules were slower activated in the stn7 mutant relative to WT. A stronger NPQ response could alternatively suggest that an increased number of LHCII bound at PSII in the stn7 mutant could lead to an increase in PsbS proteins. Then, an increase in PsbS could result in a stronger induction of qE in the stn7 mutant relative to WT at low AL. It has been shown that the amount of PsbS is adjusted by the plant to the growth light conditions and is reduced when plants are grown under low versus high light intensities[253]. It is believed that the plant makes sure through this adaptation mechanism that dissipated energy via NPQ does not limit photosynthesis. We were not able to draw any conclusion on this matter because we did not separate the grana region of the thylakoid membrane and only analyzed the stroma thylakoid membrane using digitonin solubilizing. In the stroma thylakoid membrane, we did not observe more PsbS in the stn7 mutant relative to the pph1 mutant (Fig. 58 C and Supplemental Table 2). On the

other hand, at the onset of low AL, NPQ was in the pph1 mutant like WT. Hence, we favor the hypothesis that a slower release in NPQ was caused by increased CEF in the stn7 mutant relative to WT and not by an increase in PsbS protein accumulating in the stn7 mutant.

In both pph1 and npq4 mutants, e- flow through PSII and PSI was more balanced at LL conditions relative to the stn7 mutant and WT (Fig. 26 A and B). It strongly suggests that the binding of LHCII at PSI was causing a more balanced e- flow between PSII and PSI during the first minutes of low AL in the pph1 mutant. During the onset of low AL, when the CBB cycle was activated and electrons were drained into the metabolic e- acceptor pool, PSII‘s and PSI‘s acceptor sides were oxidized. Hence, a more stable e- flow between PSII and PSI such as in the pph1 mutant strongly indicated that more LEF relative to CEF was performed when compared to both the stn7 mutant and WT. Moreover, the immediate onset of 11 µmol m-2 s-1 AL after dark preincubation resulted in stronger oxidation of PSII‘s acceptor side (faster decrease in Q_A levels) in the pph1 mutant relative to WT, which could only be compensated in WT through the addition of FR light (Fig. 49 A). Hence, this result can be interpreted that in the pph1 mutant, LEF was increased compared to WT. In case reduced Fd acceptor molecules would be capable of turning on CEF, LEF would be maintained in the pph1 mutant through enhanced oxidation of PSI‘s acceptor side by the stromal metabolic e- acceptor pool. Indeed, it has been shown that the redox state of the stroma affects the turnover of CEF and that a stronger reduction state enhances CEF around PSI[190,191]. Furthermore, it has been shown that different isoforms of Fd and FNR genes exist that encode either proteins devoted to LEF or CEF[254].

Interestingly, a more balanced e- flow between PSII and PSI was only established in the npq4 mutant by decreasing both e- turnover at PSII and PSI relative to the pph1 mutant (Fig. 25 A, B, C, and D). In npq4 and stn7 mutant plants, PSII‘s acceptor side was more strongly reduced (elevated Q_A levels) relative to WT (Fig. 26 A and D). Additionally, a more strongly reduced PSI‘s acceptor side in the npq4 mutant (increased Y(NA) levels) was leading to a slower increase in Y(I) relative to WT (Fig. 27 C and F). Thus, findings indicated that at the onset of low light in the npq4 mutant, the

performance of LEF was decreased relative to WT. After several minutes of illumination, e- flow through PSI was decreased in the npq4 mutant relative to WT and the two state transition mutants. This was determined through a drop in Y(I) when PSI's acceptor side was more strongly reduced (increased Y(NA) levels) while PSII's acceptor was only marginally more strongly reduced (slightly increased Q_A levels) (Fig. 26 A, C, and D and Fig. 27 C and F). A more strongly reduced PSI acceptor side could indicate that the performance of CEF is elevated in the npq4 mutant relative to WT. Since measurements at low AL with and without the supplementation of FR light showed that under these conditions more light was utilized at PSI in a cyclic manner in the stn7 mutant relative to WT (Fig. 35 A), it further suggests that this could also be the case in the npq4 mutant. It could indicate that like in the stn7 mutant, the *npq4* mutation is interfering with the plant's ability to balance light absorption between the photosystems. It has been proposed by others that the lack of PsbS is leading to an increase in CEF whereas PsbS's overexpression is decreasing the turnover of CEF, making the overexpressor more susceptible to PSI photoinhibition when illuminated for several hours at very high light relative to WT and the npq4 mutant[255]. Moreover, the npq4 mutant is known for its severe growth impairment when grown under fluctuating light intensities[65]. In the same way, the stn7 mutant suffered from a severe growth defect when grown under fluctuating light intensities[58] and field conditions[125]. Additionally, we observed that when plants were grown at stable growth light conditions, leaves were smaller in the stn7 and the npq4 mutant relative to the increased growth in the pph1 mutant (for the stn7 and pph1 mutants: supplemental figure 1; for the npq4 mutant data not shown). This further strengthens our finding that in the absence of PsbS and herewith of NPQ at PSII, the mutant has problems with balancing light absorption at PSII and PSI like in the stn7 mutant, which is resulting in a growth deficit both under constant and varying light conditions. Interestingly, with LHCII bound at PSI like in the pph1 mutant, the plant grows faster and thus shows a growth advantage. However, no data exists on the growth rates of the pph1 mutant under fluctuating light intensities. It was only proposed by Hepworth et al. 2021, after measuring an HL-induced decrease in the CO_2 fixation rate in the pph1 mutant relative

to WT that the pph1 mutant should show retarded growth when light intensities are fluctuating[2].

During the next minutes (3,5-20 min) of illumination with low AL, PSI's donor and acceptor sides were more strongly reduced in WT, and in the stn7, and npq4 mutant (Y(ND) levels decreased and Y(NA) levels increased). This was accompanied by a slowdown in the oxidation rate of PSII's acceptor side (Q_A levels increased), whereas in the pph1 mutant all three sides were more strongly oxidized (Fig. 27 A, B, and C). Moreover, after prolonged illumination with low AL supplemented with FR light, both the acceptor side of PSII (Q_A levels) and PSI as well as the donor side of PSI (Y(ND) and Y(NA) levels) were more strongly reduced in the stn7 mutant relative to WT, whereas the opposite was found in the pph1 mutant where both photosystems showed more strongly oxidized acceptor/donor molecule(s) relative to WT (Fig. 32 A, B, D, E). These observations give a very strong indication that the redox mechanism that leads to a stronger reduction of PSII and PSI by keeping the e- outflow at both acceptor sides decreased and e- inflow at the donor side of PSI increased in WT and the stn7 mutant, is not found in the pph1 mutant, and cannot be lifted in the stn7 mutant through the supplementation of FR light. In concert with findings made at 58 µmol m^{-2} s^{-1}AL, illuminating with 25 µmol m^{-2} s^{-1} after dark preincubation was causing a more strongly reduced acceptor side of both PSII (Q_A levels increased) and PSI (Y(NA) levels increased), and PSI's donor side (Y(ND) levels decreased) in the stn7 mutant, whereas all donor/acceptor molecules were more strongly oxidized in the pph1 mutant relative to WT (Fig. 32 and Fig. 33). Additionally, when FR light was added after 7 minutes of exposure to low AL (25 µmol m-2 s-1), FR was leading to a more strongly reduced PSII and PSI acceptor side (Q_A and Y(NA) levels increased) and more strongly reduced PSI donor side (Y(ND) levels decreased) in the stn7 mutant relative to WT (Fig. 33 A and Fig. 32 A and D), whereas Q_A in the pph1 mutant was like WT and PSI's acceptor and donor side were more strongly oxidized (Y(ND) increased and Y(NA) levels decreased) in the pph1 mutant when compared to WT (Fig. 33 B and Fig. 32 B and E). Thus, our observations at 25 µmol m-2 s-1 with and without the supplementation of FR light strengthened our findings made at 58 µmol m-2 s-1, which suggested that stronger

light utilization at PSI through CEF in the stn7 mutant increased e- inflow at the donor side of PSI and decreased e- outflow at the acceptor side of both PSII and PSI. In contrast, in the pph1 mutant when light is more equally utilized at PSII and PSI both photosystems are more strongly oxidized, and hence e- outflow increases and e- inflow at PSI‘s donor decreases. Hence, the binding of LHCII at PSI and the associated membrane changes in the pph1 mutant are boosting the mutant‘s capacity to perform LEF not only during the immediate onset of low AL light but also during the first minutes and during continuous illumination with low AL (with and without adding FR light). In contrast, in WT, the stn7, and the npq4 mutant plants, when after about two minutes of illumination with low AL after dark preincubation more light is utilized at PSI relative to PSII, this increases the proportion of CEF relative to LEF when compared to the pph1 mutant. Especially prolonged illumination with low AL and supplementation with FR light resulted in the strongest reduced PSII and PSI donor/acceptor molecules in the stn7 mutant, due to the strongest increase in the CEF to LEF ratio relative to WT and the npq4 mutant.

It has been hypothesized that in the stn7 mutant CEF is increased, whereas in the pph1 mutant LEF is enhanced[137]. However, this proposal was based on changes in grana membrane stacking leading to differences affecting the diffusion time of plastoquinol and plastocyanin from the grana to stromal lamellae thylakoids. The model proposed that in the stn7 mutant, the number of grana stacks is increased and that this is leading to greater partitioning between grana and stroma lamellae limiting the exchange of PQH_2 between the compartments. The elevated distance was suggested to poise the stromal lamellae PQ pool and accept e- from Fd^- either through enzymatic activity (such as the FQR or FNR) or through slow equilibration, facilitating CEF over LEF. How this is achieved has been a matter of strong debate. On the contrary, in the pph1 mutant smaller grana stacks were predicted to decrease the partitioning of e- carriers between grana and stroma lamellae causing enhanced LEF capacity[3,137]. However, after having conducted additional experiments, the same group extended their model about how e-transport is performed in the stn7 and the pph1 mutant. According to findings showing that the fixation of CO_2 was decreased in the stn7 mutant at LL and in the pph1 mutant

at HL relative to WT, Hepworth et al. 2021 proposed that LL exposure in the stn7 mutant and HL exposure in the pph1 mutant is causing a decrease in CEF, which is further decreasing LEF. Interestingly, NPQ was increased at LL in the stn7 mutant despite the stn7 mutant's proposed decreased capacity to perform CEF and LEF under LL conditions. Additionally, although CEF and LEF were proposed to be increased at LL in the pph1 mutant it did not show an increase in NPQ. This finding in the pph1 mutant was explained by the assumption that ATP was faster utilized and more LEF was performed leading to a decrease in NPQ relative to the stn7 mutant[2]. Additionally, in contradiction to our interpretations, CEF was proposed to be decreased under LL in the stn7 mutant while the donor side of PSI was more strongly reduced in the stn7 mutant relative to WT. However, HL-treatment in the pph1 mutant which was also proposed to decrease CEF did not cause a more strongly reduced PSI donor side in the pph1 mutant relative to WT[2]. This finding was interpreted to be caused by a faster PQ/PQH_2 diffusion rate under LL and HL conditions in the pph1 mutant than in the stn7 mutant due to differences in the mutant's grana morphology[2]. In conclusion, the authors did not see the same NPQ and Y(ND) trends under conditions when both mutants were supposed to decrease both CEF and LEF rates.

The findings made during the light-response experiments (LREs) let us conclude that Wood and Hepworth et al.'s interpretation of how e- transport is operated in the stn7 mutant and the pph1 mutant was a misinterpretation. When light intensities were increased during the recording of an LRE in the stn7 mutant, Q_A levels were increased, hence e- outflow at the acceptor side of PSII was decreased between 18 and 58 µmol m-2 s-1 and additionally increased Y(NA) levels indicated that also e- outflow at the acceptor side of PSI was decreased between 58 until 240 µmol m-2 s-1 relative to WT (Fig. 34 A and Fig. 35 D). Thus, with more LHCII at PSII in the stn7 mutant relative to WT, Q_A, and Y(NA) levels were only resembling WT when AL levels were increased, indicating that only when more light quanta were reaching the stn7 mutant it could mimic WT. This observation let us set up the hypothesis that after dark preincubation of both WT and the stn7 mutant, PSII centers are shielded from overexcitation, and that light is preferentially absorbed and utilized by PSI. In WT this

shielding mechanism was used at medium to high light intensities when applied after dark preincubation. In the stn7 mutant, already low AL levels were leading to light shielding of PSII. Hence, already low light intensities were more absorbed at PSI in the stn7 mutant when compared to WT and higher light intensities were needed in the stn7 mutant to resemble the WT measurements. Interestingly, Y(ND) levels were lower, hence e- inflow at the donor side of PSI increased in the stn7 mutant relative to WT during the whole LRE and could only resemble WT through the addition of FR light when AL was reaching GL conditions (>58 µmol m-2 s-1) (Fig. 35 A). This finding suggested that only when light intensities close to GL were used in the stn7 mutant, sufficient light was absorbed at PSII so that the addition of FR light caused PSI's donor side to resemble WT levels. Thus, only when the light intensity reached 58 µmol m-2 s-1, LEF could be increased in the stn7 mutant like in WT. In contrast, at LL (between 11 and 27 µmol m-2 s-1) more light was absorbed and utilized at PSI relative to PSII in the stn7 mutant, and the addition of FR light led to increased Q_A and lower Y(ND) levels, indicating that e- outflow at the acceptor side of PSII was decreased while e- inflow at the donor side of PSI was increased when compared to WT (Fig. 34 A and Fig. 35 A). Therefore, at lower light intensities when more light is absorbed at PSI relative to PSII in the stn7 mutant, the turnover of CEF is increased relative to WT. In contrast, the supplementation of FR light between 27 and 58 µmol m-2 s-1 caused a slight increase in Y(ND) levels and a decrease in Y(NA) levels in the pph1 mutant relative to WT, indicating that e- outflow at the acceptor side of PSI was increased and e- inflow at its donor side was decreased (Fig. 35 B and E). This can be interpreted that in the pph1 mutant more light was absorbed and also utilized at PSII relative to WT and that supplementing FR light and increasing light absorption at PSI was able to more strongly oxidize PSI's donor and acceptor side relative to WT through increasingly performing LEF in the mutant.

Therefore, our measurements showed that in stn7, npq4, and pph1 mutant plants when light quanta are absorbed differently at PSII and PSI, as represented through changes in the redox state of its e- acceptor (Q_A and Fd (or Y(NA)) and e- donor (Pc (or Y(ND)) molecule(s), the partitioning between LEF and CEF is affected. Additionally, when AL

intensities succeeded 240 µmol m-2 s-1, Y(ND) levels were lower in the stn7 mutant relative to WT (240 µmol m-2 s-1 Fig. 35 A; higher light intensities data not shown), indicating that e- inflow at the donor side of PSI was increased in the mutant under HL conditions. It is therefore concluded that CEF was increased relative to LEF in the stn7 mutant relative to WT. Also, increased NPQ levels in the stn7 mutant versus WT (240 µmol m-2 s-1 Fig. 36 A and D; higher light intensities data not shown) were interpreted to be a consequence of increased CEF.

Moreover, when WT and the npq4 mutant were illuminated for about 7 minutes at low AL (25 µmol m-2 s-1 and 58 µmol m-2 s-1), the decrease in Q_A levels, as well as the decrease Y(NA) levels and increase Y(ND) levels) was slowing down (Fig. 27 and Fig. 32 and Fig. 33 section 1). This observation indicated that in WT and the npq4 mutant upon prolonged illumination with low AL an adaptation mechanism was initiated, which decreased e- outflow from both PSII and PSI and in addition also increased e- inflow at the donor side of PSI. These observations strongly suggest that both in WT and the npq4 mutant more CEF relative to LEF is performed. In the stn7 mutant, the decrease of Q_A and Y(NA) and increase in Y(ND) levels was already halted after about -23 minutes of illumination, whereas in the pph1 mutant Q_A and Y(NA) continued to decrease and Y(ND) levels continued to increase and thus did not slow down like in WT, and in the npq4 and the stn7 mutant (Fig. 27 and Fig. 32 and Fig. 33 section 1). This indicated that e- outflow from the acceptor side of both PSII and PSI was increased and e- inflow at the donor side of PSI was decreased in the pph1 mutant relative to WT, and the npq4 and the stn7 mutant, which is suggesting that LEF was elevated relative to WT. These findings showed that the change that was happening in WT and the npq4 mutant was already performed in the stn7 mutant and decreased or was completely missing in the pph1 mutant. Also, the prolonged addition of FR light to low AL led in WT to a stronger decrease in Y(ND) levels (Fig. 32 A; section 2), indicating that e- inflow at the donor side of PSI was increased. This further gives evidence that the lowering of Y(ND) levels was not caused through stronger light absorption at PSII relative to PSI but through an increased e- turnover through PSI mediated by CEF. Therefore, we propose that during prolonged illumination with low AL, the WT and

npq4 mutant plants were performing a state 2- to- state 1 transition, with and without FR light supplementation, which was more resembling the stn7 mutant leading to an upregulation of CEF relative to LEF. Moreover, we suggest that the change in F_m‘/F_m values, which is indicative of the execution of NPQ when high AL was used, has a different function during continuous illumination with low or medium light intensities. During prolonged illumination of WT and the npq4 mutant with low AL, F_m‘/F_m values were first resembling the pph1 mutant and then were shifting towards values typical for the stn7 mutant (Fig. 29 C). In addition, during prolonged illumination with low AL in WT and the npq4 mutant also Q_A and Y(NA) levels increased, and Y(ND) levels decreased, indicating that e- outflow at the acceptor side of PSII and PSI was lowered and e- inflow at the donor side of PSI was elevated (Fig. 26 A, B and C). Therefore, we conclude that during the continuous illumination with low AL (with or without FR light) a state 2- to- state 1 transition is performed, leading to an increase in PSII centers that are fluorescing. Simultaneously a rise in CEF relative to LEF is happening in WT and the npq4 mutant, which is changing e- outflow/inflow rates at the acceptor/donor molecule(s) of PSII and PSI. Indeed, it was shown by Wood et al. 2018 that both low light and FR light were resulting in a thylakoid membrane with fewer but larger grana, which was interpreted to facilitate CEF[3].

Thus, our observations suggest that more grana layers (like in the stn7 mutant) or thinner grana layers which are better connected to the stroma thylakoid membrane (like in the pph1 mutant) are profoundly affecting the plant’s mode of e- transport through the induction of light absorption changes at PSII and PSI. Our model is independent of differences in the diffusion rates of PQ and PC and therefore disagrees with both theories suggested by Wood et al. 2019 and Hepworth et al. 2021. In contrast, in our model, the participation of PSII in e- transport is determined through changes in the thylakoid membrane protein complexes. Our measurements with AL and the supplementation of FR light suggest that if more LHCII is bound at PSII, and the layer of grana stacks increases (like in the stn7 mutant), light quanta are shielded from PSII, and instead more light is utilized by PSI, which in turn is facilitating CEF; whereas when grana stacks are thinner and better connected to the stroma lamellae (like in the

pph1 mutant), light is absorbed by both PSII and PSI; and e- transport favors LEF. If light utilization at PSII is decreased in the plant, the performance of CEF can step in to keep the donor side of PSI reduced and ATP synthesis running for the fixation of CO_2 from the atmosphere. It takes two e- from PQ to reduce PSI‘s donor side and keep CEF upregulated. In the stn7 mutant, that two e- can be delivered through less LEF, and more PGR5/PGRL1-dependent and NDH-dependent CEF. In the pph1 mutant, an increase in LEF could lead to a drainage of the PQ pool lowering the number of e- reaching PSI‘s donor side and hence causing a decrease in CEF. In the stn7 mutant, PSI and the Cytb6f complex can work separately from PSII. This would also explain why the stn7 mutant increased the number of PSI-Cytb6f complexes that were solubilized independently from PSII relative to WT and the pph1 mutant (Fig. 56). It further indicates that while PSII is reliant on PSI for LEF, PSI and the Cytb6f complex can work autonomously. This would give the PSI-Cytb6f complex a more ancient and important role in the evolution of e- transport and the origin of photosynthesis, leading the path to the world as we know it today. Also, the binding of LHCII antenna complexes to PSI in stn7 could be used to increase light utilization at PSI to elevate CEF (Fig. 56).

In the npq4 mutant, results at 25 µmol m-2 s-1 AL differed from measurements performed at 58 µmol m-2 s-1AL. At 25 µmol m-2 s-1AL, the oxidation of PSII‘s acceptor side showed a delay (slower decreasing Q_A levels) and PSI‘s acceptor side was only slightly more strongly reduced (slightly increased Y(NA) levels) relative to WT (Fig. 32 C and F and Fig. 33 C), indicating that e- outflow at the acceptor side of PSII and slightly at PSI was decreased. In contrast, at 58 µmol m-2 s-1 AL, both Q_A, and Y(NA) levels were like the stn7 mutant at LL indicating a significant decrease in e- outflow at the acceptor side of both PSII and PSI relative to WT (Fig. 27 A and C). This indicates that at 25 µmol m-2 s-1AL, light absorption was balanced more equally between PSII and PSI and more strongly facilitating LEF relative to findings made at 58 µmol m-2 s-1. In contrast, at 58 µmol m-2 s-1, more light was utilized at PSI relative to PSII, leading to a decrease in e- outflow at the acceptor side of PSII and PSI (increased Q_A and Y(NA) levels), strongly indicating that CEF was upregulated in the

npq4 mutant relative to WT. In agreement with this conclusion, low AL (25 µmol m-2 s-1AL) when supplemented with FR light resulted in stronger oxidation hence a decrease in e- inflow at the donor side of PSI (increased Y(ND) levels) in the npq4 mutant relative to WT (Fig. 32 C; section 2), indicating that when the light was absorbed more equally at PSII and PSI at 25 µmol m-2 s-1 compared to 58 µmol m-2 s-1more LEF relative to CEF was performed.

Supplementing FR light to low AL (25 µmol m-2 s-1AL) was causing the strongest increase in Y(ND) levels in the npq4 mutant compared to WT and the other mutants (Fig. 44 A and D). Accordingly, also a WT-like increase in Y(NA) levels throughout illumination, indicating that e- outflow at the acceptor side of PSI was decreased through increasing the ratio of CEF relative to LEF was missing in the npq4 mutant (Fig. 32 F). Results, therefore, suggest that in the npq4 mutant, when more LEF was performed at 25 µmol m-2 s-1 relative to WT, the initiation of a state 2- to- state 1 transition was not enhancing CEF over LEF like in WT. It can be speculated that under these conditions when LEF is favored, changes in the thylakoid membrane and protein complexes needed for the upregulation of CEF were less effective in the npq4 mutant relative to WT. However, when light levels were increased to 58 µmol m-2 s-1AL, more light was utilized at PSI relative to PSII, which caused an increase in CEF relative to LEF in the mutant. Our observations indicate that in the npq4 mutant the capacity to utilize light at PSII is more decreased at medium than at low AL intensities. This could be established by an increase in PSII centers in the grana lamellae in the npq4 mutant relative to a more PSII and PSI mixed stroma thylakoid membrane in WT. Unfortunately, up to now, no data on light-dependent thylakoid membrane changes exist in the npq4 mutant. We therefore conclude, under continuous illumination with 25 µmol m-2 s-1 light is more equally utilized at PSII and PSI and LEF favored, whereas at 58 µmol m-2 s-1 light is more utilized at PSI in the npq4 mutant when compared to WT. The finding is in contradiction to the overall thinking that in the absence of PsbS due to a lack of quenching, more light is utilized at PSII relative to PSI. Nevertheless, it appears as a useful adaptation of the mutant plant to increase light utilization at PSI and use CEF to avoid light damage at both photosystems.

Moreover, the recording of an LRE, in which light intensities were increased from 11 to 830 µmol m-2 s-1 AL every 30 seconds showed that under low AL LEF was decreased while CEF was in the npq4 mutant like WT. Only the supplementation of FR light was increasing cyclic e- turnover at PSI in the npq4 mutant when compared to WT. Interestingly, when more than 240 µmol m-2 s-1 was used e- outflow at the acceptor side of PSII was decreased (Q_A levels elevated) in the npq4 mutant relative to WT, and e- inflow at the donor side of PSI was decreased (Y(ND) levels increased) and e- outflow at the acceptor side of PSI was increased (Y(NA) levels decreased) in the npq4 mutant compared to WT (Fig. 36). It can be speculated that at HL both LEF and CEF were decreased in the npq4 mutant relative to WT. Similarly, to low AL conditions, the supplementing of FR from 240 µmol m-2 s-1 AL was increasing e- inflow at the donor side and decreased e- outflow at the acceptor side of PSI in the npq4 mutant relative to measurements without FR light and was leading to similar levels as observed in WT without FR light (Fig. 37). Thus, when in the npq4 mutant more than 240 µmol m-2 s-1 was applied the addition of FR light increased the performance of CEF relative to LEF when compared to measurements in the npq4 mutant without FR light. These findings indicated that when only AL (above 240 µmol m-2 s-1) was used, LEF was decreased while PSI stayed more strongly oxidized (e- inflow at donor decreased and e- outflow at the acceptor of PSI increased), whereas the addition of FR light caused an increase in CEF in the npq4 mutant relative to WT. Others have shown that under prolonged high-light treatment the npq4 mutant displayed less photoinhibition of PSII relative to the PsbS overexpressor strain due to an increase in CEF in the npq4 mutant[255]. In contrast, our LRE measurements indicated that when after dark preincubation stepwise increasing high-intensity light, LEF was decreased while e- outflow at the PSI side was increased in the npq4 mutant relative to WT. In addition, the same group showed that the npq4 mutant was producing at HL more O_2 radicals relative to both the WT and the PsbS-overexpressor strain[255]. It can be hypothesized that in our findings LEF is decreased in the npq4 mutant relative to WT because e- are preferentially transferred onto molecular O_2 (through the Mehler reaction), leading to increased e- outflow at PSI's acceptor while e- inflow at PSI's donor side was decreased. However, it stays elusive why increasing AL intensities

promote the Mehler reaction and e- are transferred onto O_2, while the addition of FR light, exciting PSI promotes CEF over LEF and/or the Mehler reaction.

4.2. CEF mutants pgr5 and crr2

4.2.1. In the absence of PGR5, LEF is favored and the switch from state 2 to state 1 is decreasing during the onset of low actinic light after dark preincubation

To further investigate which type of CEF is increased after dark preincubation and the onset of low AL as well as after prolonged illumination with low light intensities, we compared chlorophyll fluorescence and absorption spectra of stn7, pph1, and npq4 mutants with two mutants lacking proteins involved in cyclic e- transport, namely the pgr5 mutant- lacking PGR5 involved in PGR5/PGRL1-dependent CEF and the crr2 mutant- insufficient in the NDH complex- and hence NDH-dependent CEF.

When turning on low-intensity light, a slower outflow of e- into the metabolic pool was recorded in the pgr5 mutant, represented through a slower decrease of Y(NA) levels in the pgr5 mutant relative to WT (Fig. 39 C and Fig. 42 F). Also, in the pgr5 mutant, the transient increase in NPQ was significantly decreased relative to WT (Fig. 40 B and Fig. 43 G) and PSI‘s donor side was more strongly oxidized represented through increased Y(ND) levels relative to WT (Fig. 39 B and E), indicating that e- inflow at the donor side of PSI was decreased. These observations indicated that at the onset of low AL, when PGR5/PGRL1-dependent CEF was missing, fewer protons were translocated to the lumen leading to a smaller ΔpH in the pgr5 mutant relative to WT. Additionally, a decrease in Y(I) during the first minutes of illumination might indicate that CEF was decreased in the pgr5 mutant relative to WT, resulting in a smaller ΔpH in the pgr5 mutant. On the other hand, Y(II) levels in the pgr5 mutant were like in WT, and Q_A levels (measured through 1-qL) stayed at the same level in the pgr5 mutant and WT (Fig. 38 A and Fig. 39 A and D), indicating that e- outflow at the acceptor side of PSII, hence LEF was similar in mutant and WT.

Moreover, at the onset of light when in the pgr5 mutant Y(ND) levels did increase, Y(NA) levels decreased slower and continued after two minutes of illumination without

a WT-like increase before decreasing again, while Q_A levels decreased at an elevated rate in the pgr5 mutant relative to WT (Fig. 39 and Fig. 42 B, D and F). This observation strongly indicated that at the onset of low AL, e- flow differentiated in the pgr5 mutant from WT. It can be hypothesized that when missing a WT-like increase of Y(NA) levels after about two minutes of illumination and in addition showing a faster decrease of Q_A levels, hence increasing e- outflow at the acceptor side of both PSII and PSI in the pgr5 mutant relative to WT it was caused by a lack of PGR5/PGRL1-dependent CEF in the pgr5 mutant. This finding emphasizes that at the onset of light, after about two minutes of illumination the operation of PGR5/PGRL1-dependent CEF is causing the accumulation of H^+ molecules inside the thylakoid lumen in WT. In contrast, without PGR5/PGRL1-dependent CEF in the pgr5 mutant, protons do not accumulate to the same extent.

Additionally, when after dark preincubation light irradiance levels were increased during the recording of an LRE, above 100 µmol m-2 s-1, Q_A levels were increased, Y(ND) levels decreased and Y(NA) levels were increased in the pgr5 mutant relative to WT (Fig. 45 B and Fig. 46 B and D), indicating that e- outflow at the acceptor side of both PSII and PSI was decreased, while e- inflow at the donor side of PSI was elevated. This gives evidence that above growth light conditions, the capacity to perform LEF was decreased, whereas CEF was enhanced in the pgr5 mutant relative to WT. Interestingly, after dark-adaptation during the performance of an LRE below 27 µmol m-2 s-1, Q_A levels were decreased in the pgr5 mutant relative to WT with or without FR light (Fig. 45B), hence e- outflow at the acceptor side of PSII was elevated. This finding suggested that only at low AL levels, the capacity to perform LEF was increased in the pgr5 mutant relative to WT.

Moreover, at the onset of low light, a decrease in CEF and stronger performance in LEF in the pgr5 mutant relative to WT suggests that the mutant will need to find a different way to increase its ATP production to match the energy demands of the CBB cycle and produce enough e- acceptors for the operation of linear e- transport. It can therefore be hypothesized that in the pgr5 mutant, ATPase molecules might need to be constitutively activated. Constitutively activated ATPases would supply the pgr5 mutant constantly

with ATP during both darkness and when illuminated. If this was the case after dark preincubation at the onset of AL, no transient increase in NPQ could be observed because the proton gradient is already lowered by constitutively active ATPase molecules. It was shown previously that at the onset of low light, a mutant with a constitutively activated ATPase showed a lower proton gradient, which was displayed through a lower transient NPQ response[220]. This could explain the decrease in NPQ and drop in photosynthetic control at Cytb6f (decrease in Y(ND) levels) in the pgr5 mutant relative to WT. Moreover, evidence already exists in the literature that in the pgr5 mutant, the activity of ATPase complexes was not completely downregulated in the dark when compared to WT[193]. Therefore, in the pgr5 mutant a constitutively activated ATPase, which is causing a decrease in ΔpH at the onset of light could further explain the mutant's decreased transient rise in NPQ and increased e- flow through Cytb6f (after 2 minutes of illumination decreased Y(ND) levels (Fig. 39 B and C and Fig. 42 D)) when performing less photosynthetic control at Cytb6f relative to WT. Alternatively, a decrease in ΔpH in the pgr5 mutant could be caused by a lowering of H^+ molecules inside the thylakoid lumen when PGR5/PGRL1-dependent CEF was missing, and the mutant was depending not on LEF but on alternative e- pathways such as the Mehler reaction and/or NDH-dependent CEF, which could cause a lower proton-inflow at the onset of low AL.

Moreover, the pgr5 mutant showed when low AL was supplemented with FR light to initiate state transition a slower rate of transformation from state 2- to- state 1 relative to WT (Fig. 43 G and Fig. 44 G). This observation was in agreement with findings made in Mekala et al. (2015)[188], which showed that the pgr5 mutant is decreasingly dephosphorylating LHCII when exposed to HL relative to WT, hence decreasing the rate of performing a state 2- to- state 1 transition. Thus, at low AL, the pgr5 mutant seems to mimic the pph1 mutant, which is showing increased LEF capacity when LHCII stays bound to PSI and the grana thylakoid membrane showed decreased grana stacking leading to a better connection to the stroma region[137]. The similarity between the pph1 and the pgr5 mutant strengthened our previous assumption that in the pgr5 mutant when PGR5/PGRL1-dependent CEF is missing, the mutant tries to facilitate

LEF by staying stronger in state 2 relative to WT resulting in a pph1 mutant-like more equal absorption of light at both photosystems. Indeed, if the pgr5 mutant possesses a constitutive active ATPase, the mutant could only operate e- flow after darkness by staying in state 2 and facilitating LEF.

We further propose that in the pgr5 mutant, NDH-dependent CEF is only enhanced relative to WT when illuminated for a prolonged interval at low AL and not directly after dark preincubation at the onset of light. We observed that after prolonged illumination at low light, Q_A and Y(NA) levels were slightly increased relative to WT in the pgr5 mutant (Fig. 39 and Fig. 42B, D, and F), hence e- outflow at the acceptor side of PSII and PSI were decreased. It can be speculated that these observations resulted from a decrease in LEF and increase in CEF. However, Y(ND) levels were the same in the pgr5 mutant and WT, hence e- inflow at the donor side of PSI was the same. It suggests that under these conditions an upregulation of NDH-dependent CEF has no impact on PSI's donor side. Moreover, when leaves were preincubated with light close to growth light conditions, turning on very low light supplemented with FR light led to a more decreased Y(ND) in the pgr5 mutant when compared to WT, while both Q_A and Y(NA) were like WT (Fig. 50B, D and F), indicating that e- inflow at the donor side of PSI was increased in the mutant. The decrease in Y(ND) levels in the pgr5 mutant was especially visible after having adapted to growth light conditions when very low AL in addition to FR light was turned on (Fig. 50B). It indicated that in the pgr5 mutant when more light was utilized at PSI and/or LEF was significantly decreased at very low light, e- flow increased from the PQ pool towards PSI via CEF relative to WT. Hence, it can be speculated that under these light conditions NDH-dependent CEF was increased in the pgr5 mutant relative to WT.

On the contrary, in the crr2 mutant lacking the NDH complex, Y(ND) levels were increased, while both Q_A and Y(NA) levels were like WT (Fig. 50B, D and F), indicating that e- inflow at the donor side of PSI was decreased in the mutant. Therefore, it strongly suggests that LEF is increased in the crr2 mutant relative to the pgr5 mutant and WT. Furthermore, in both WT and the pgr5 mutant after prolonged illumination at low light, the decrease of Y(NA) level hence oxidation of PSI's acceptor side was

slowed down and Q_A levels were increased showing that e- outflow at the acceptor side of PSII was decreased (Fig. 39 A and Fig. 42 A and B). Therefore, also in WT, a change in e- outflow at PSII and PSI was observed which can be explained through the upregulation of NDH-dependent CEF. In agreement with this speculation, Wood et al.2018 proposed that at low light intensities, the thylakoid membrane dynamically changed towards more grana stacks, leading to an increase in CEF[3]. Therefore, our findings suggest that this type of CEF is actually NDH-dependent CEF and we can also conclude from our data that it needed a longer time before being activated and did not immediately switch on when the light was turned on after dark preincubation. In accordance with the literature, it was shown that when plants were treated with AA, which is inhibiting PGR5/PGRL1-dependent CEF, this caused Q_A levels to be increased and hence e- outflow at the acceptor side of PSII to be decreased through the upregulation of CEF at a later point relative to those not treated with AA. When PGR5/PGRL1-dependent CEF was missing through AA treatment, a delayed increase after prolonged illumination could therefore be caused through the activation of NDH-dependent CEF[208]. In our model, prolonged illumination at low AL facilitates NDH-dependent CEF. Based on our findings made through fluorescence and absorption spectroscopy in stn7, pph1, and npq4 mutants (discussed in 4.1.1. State transition mutants stn7 and pph1 and the npq4 mutant) we hypothesize that an increase in NDH-dependent CEF is facilitated through the formation of larger grana stacks. In our understanding, larger grana stacks are building a shield for incoming light at PSII leading to enhanced light utilization at PSI relative to PSII. Then, when more light is utilized at PSI relative to PSII more CEF is performed.

4.2.2. At the onset of low actinic light, more CEF was performed; while after prolonged illumination, depending on the light intensity, an enhancement in LEF and/or CEF was recorded in the crr2 mutant

At the onset of low AL (58 µmol m-2 s-1), during the first minute of illumination Y(ND) levels were decreased in the crr2 mutant relative to WT (Fig. 39 B), indicating that electron inflow at the donor side of PSI was increased in the mutant. This observation can be interpreted that in the crr2 mutant more CEF is performed relative

to WT because more light was absorbed or e- utilized at PSI relative to PSII. However, after about -23 minutes of illumination, Y(ND) levels were alike in the crr2 mutant and WT (Fig. 39 B), while Q_A and Y(NA) levels were increased in the crr2 mutant relative to WT (Fig. 39 A and C), showing that the e- outflow at the acceptor side of both PSII and PSI was decreased in the mutant. These observations indicated that at the onset of low light in the crr2 mutant the performance of PGR5/PGRL1-dependent CEF was elevated relative to WT. This could be the case if for example the mutant would after dark preincubation increase the thickness of its grana membranes, shielding more light from PSII and hence enhancing light utilization at PSI in the crr2 mutant relative to WT.

Interestingly, after about 7 minutes of illumination with low AL, Q_A levels were increased, hence e- outflow at the acceptor side of PSII decreased and NPQ levels were elevated in the crr2 mutant relative to WT (Fig. 39 A and Fig. 40 C). In addition, Y(NA) levels were increased but continued to resemble WT values during the following 5 minutes of illumination (Fig. 39 C). In WT, Y(NA) and Q_A levels stopped decreasing and subsequently continuously increased, thus switching from a mode facilitating e- outflow at both photosystems to a mode that decreases e- outflow. This finding was interpreted as a shift from state 2- to- state 1. Therefore, it can be speculated that in the crr2 mutant, when performing a transition from state 2 into state 1, this caused a decrease in Q_A levels, due to stronger e- flow from PSI towards the PQ pool through CEF when compared to WT. This could be initiated through increasing light absorption at PSI relative to PSII when compared to WT, leading to an increase in PGR5/PGRL1-dependent CEF in the crr2 mutant relative to WT. After prolonged illumination, Y(NA) levels were similar in the crr2 mutant and WT which is indicating that after having performed a state 2- to- state 1 transition, light absorption and coupled e- flow mechanisms in WT and the crr2 mutant were alike. However, NPQ levels were still increased in the crr2 mutant relative to WT, which suggested that the proton gradient was still increased in the mutant.

Interestingly, when illuminated for 7 minutes with 25 µmol m-2 s-1, NPQ was increased while Y(ND) levels were elevated and Y(NA) were decreased in the crr2

mutant relative to WT (Fig. 43 E vs. F and Fig. 42 C and E), indicating that e- inflow at the donor side of PSI was decreased, while e- outflow at the acceptor side of PSII was increased. Thus, at 25 µmol m-2 s-1, LEF was elevated in the crr2 mutant relative to WT. When LEF was increased in the crr2 mutant relative to WT, a stronger proton gradient could be formed causing an increase in NPQ. It strongly indicated that after dark preincubation when grana stacks are increased, 25 µmol m-2 s-1 are more equally absorbed at PSII and PSI, while 58 µmol m-2 s-1 are more absorbed by PSI leading to a rise in CEF.

Moreover, when FR light was added to 25 µmol m-2 s-1 AL, an increase in e- flow from PSI towards the PQ pool was noticed in the crr2 mutant relative to WT since through prolonged supplementation of FR light to AL light, the decrease of Y(ND) levels was accelerated, hence e- inflow at the donor side of PSI was increased in the crr2 mutant relative to WT (Fig. 44 E vs. F). That the rate of how fast e- were shuttled to the donor side of PSI was increased in the crr2 mutant relative to WT for several minutes could for example indicate that more LHCII molecules were shifted from PSI towards PSII during the performance of a state 2- to- state 1 transition, leading to a stronger e- flow from PSII towards PSI. However, at the same time, the fluorescence emission at PSII centers (measured through an increase in F_m'/F_m) was alike in the crr2 mutant and WT (Fig. 43 E vs. F). This observation indicated that in both WT and the crr2 mutant, the number of PSII centers, which were participating in the absorption of light when FR light was added stayed the same. Based on this last observation we suggest that Y(ND) was lowered in the crr2 mutant relative to WT which resulted from an increase in CEF, whereas state transition (from state 2- to- state 1) was performed to the same extent when compared to WT.

Moreover, in the crr2 mutant when adapted to low AL, adding 13 µmol m-2 s-1 FR light to low AL (25 µmol m-2 s-1) oxidized an equal amount of PSI as when 70 µmol m-2 s-1 FR light were added (Fig. 44 F). Both FR light intensities were leading to the same increase of Y(ND) levels in the crr2 mutant (Fig. 44 F). In contrast, in WT Y(ND) levels were increased with the addition of 70 µmol m-2 s-1 relative to 13 µmol m-2 s-1 FR light (Fig. 44 E). This observation strongly indicated that in the crr2 mutant the

addition of 13 µmol m-2 s-1 FR light has already reached all PSI centers which can lead to an increase in e- outflow at the acceptor side of PSI and decrease e- inflow at the donor side. Then, 70 µmol m-2 s-1 FR light did not make any difference to 13 µmol m-2 s-1 FR. It can be speculated that in the crr2 mutant when the light was more equally absorbed at PSII and PSI at low AL, adding more FR light (70 µmol m-2 s-1 FR) could not further increase the mutant's capacity to perform LEF relative to WT. For example, more LEF could be performed in the crr2 mutant like in the pph1 mutant if the thylakoid membrane possessed more stroma thylakoid membranes connected with thinner grana stacks when compared to WT plants.

Additionally, when conducting an LRE by increasing light irradiance levels, Q_A levels were always decreased in the crr2 mutant relative to WT (Fig. 45A), showing that e- outflow at the acceptor side of PSII was increased in the mutant, while PSI (Y(ND) and Y(NA) levels) in mutant and WT were alike from 11 to 27 µmol m-2 s-1 (Fig. 46). However, from 58 µmol m-2 s-1 Y(ND) levels were decreased, and Y(NA) levels were increased, hence e- inflow at the donor side of PSI increased and e- outflow at the acceptor side of PSII decreased and from 100 µmol m-2 s-1 also NPQ levels were enhanced in the crr2 mutant relative to WT (Fig. 46 A and C and Fig. 47 A and C). This observation indicated that in the crr2 mutant at all light intensities more LEF was performed relative to WT because Q_A levels were always decreased in the mutant. However, when more than 58 µmol m-2 s-1were applied in addition to increased LEF capacity also a rise in CEF was noticed in the crr2 mutant relative to WT, because e- inflow at PSI's donor side increased, while e- outflow at PSI decreased. Furthermore, from 100 µmol m-2 s-1 also NPQ levels were elevated in the crr2 mutant relative to WT (Fig. 48 B). It can be speculated that both an increase in CEF and LEF capacity in the crr2 mutant relative to WT increased the translocation of protons inside the lumen which showed an increase in NPQ above GL conditions because ATPase had reached its full potential leading thereafter to a rise in ΔpH. Moreover, when FR light was supplemented during the recording of LRE, it was not able to decrease Q_A levels, hence it was not capable of increasing e- outflow at the acceptor side of PSII relative to measurements without FR in the crr2 mutant like in WT (Fig. 45 A). This observation

was already seen at kinetic measurements with low AL, indicating that the influence of FR light increasing LEF was decreased in the crr2 mutant relative to WT. This could be the case if for example, the mutant can only increase CEF and not LEF through the addition of FR light. Indeed, while below 58 µmol m-2 s-1 Y(ND) and Y(NA) levels did not show any change through the supplementation of FR light from 58 µmol m-2 s-1 Y(ND) levels were slightly decreased and Y(NA) levels were slightly elevated in the crr2 mutant relative to WT supplemented with FR light (Fig. 46 A and C), indicating that FR light led to a marginal decrease in e- outflow at the acceptor side of PSI and instead caused a slight increase in e- inflow at the donor side of PSI. Thus, data suggest that at increased light levels (from 58 µmol m-2 s-1) through AL alone or by adding FR light CEF was elevated in the crr2 mutant relative to WT. Moreover, without the addition of FR light, Q_A levels stayed decreased, and hence e- outflow at PSII through LEF was elevated. This observation indicated that increased CEF in the crr2 mutant is not interfering with the mutant's capacity to perform LEF. It can be speculated that PGR5/PGRL1-dependent CEF uses a different mode to shuttle its e- towards PSI when compared to LEF, which is making it possible to run both modes simultaneously.

It was shown by Kono et al. (2017), that the addition of FR light during alternating low (30 µmol m-2 s-1) and very high light (1200 µmol m-2 s-1) in mutant plants insufficient in the NDH complex, was alleviating photodamage at PSI centers but could not alleviate photoinhibition to PSII centers when compared to measurements without the addition of FR light[256]. It has been suggested that less than 9% of absorbed FR light quanta are exciting PSII, and more than 91% are exciting PSI[257]. Thus, it can be speculated that in the crr2 mutant, the addition of FR was increasing LEF at LL and CEF at HL while LEF stayed increased. It can be speculated that at HL in crr2 CEF is protecting PSI centers but not PSII centers from photodamage. This strongly indicated that for the plant at HL it might be more important to protect PSI than PSII. Indeed, it was shown that damaged PSII centers can be renewed within several hours, whereas the degradation of damaged PSI centers and their replacement takes several days[258,259]. Since the crr2 mutant showed increased LEF and CEF relative to the WT it can therefore be speculated that at HL a decrease in both LEF and maybe also CEF as seen

in WT, through for example decreasing light utilization at PSII and PSI is making the WT plant more tolerant to light intensity changed when compared to the crr2 mutant plant.

4.2.3. PGR5/PGRL1-dependent CEF needs a more strongly reduced PQ pool, while NDH-dependent CEF needs a more oxidized PQ pool

We concluded that after prolonged illumination with 58 µmol m-2 s-1, NDH-dependent CEF was increased and LEF decreased in the pgr5 mutant, whereas PGR5/PGRL1-dependent CEF and LEF were enhanced in the crr2 mutant when compared to WT. After having made these observations, we propose that while PGR5/PGRL1-dependent CEF can be operated at the same time as LEF, NDH-dependent CEF can only be upregulated when LEF is decreased (as is the case during a state -2 state 1 transition).

Interestingly, when WT chloroplasts were treated with the inhibitor AA, which is inhibiting PGR5/PGRL1-dependent CEF, fluorescence levels were increasing at a decreased rate relative to experiments performed without AA[141]. The slower increase in fluorescence suggests that the reduction of the PQ pool when PGR5/PGRL1-dependent CEF was inhibited through AA was accomplished through NDH-dependent CEF. However, NDH-dependent CEF needed a longer time to activate and hence was only visible at a delayed time point. Additionally, through the supplementation of a higher concentration of AA fluorescence levels were increased at a slower rate but exceeded fluorescence levels of measurements without inhibitor, while a lower concentration of AA did not show such a fluorescence phenotype[141,162]. These observations therefore strongly indicated that when a higher concentration of AA was used, NDH-dependent CEF could be upregulated when for example PGR5/PGRL1-dependent CEF and in turn, LEF was more inhibited. Similarly, Jöet et al. 2001 showed that when WT leaves were treated with AA, the oxidation rate of PSII‘s acceptor side was decreased (Q_A levels elevated) relative to measurements without the inhibitor, which was indicating that less LEF was performed relative to WT. Hence, it can be further proposed that the lowering of PGR5/PGRL1-dependent CEF decreases LEF and enhances NDH-dependent CEF. Without PGR5/PGRL1-dependent CEF, when less

ATP is produced and LEF is decreased, the plant needs to change its e- flow mode to keep up its photosynthetic activity. Through this, the plant can ensure that at low AL intensities enough protons are translocated inside the lumen to keep up ATP synthesis and to fix CO_2 from the atmosphere. Hence, also the literature shows that a decrease in LEF is causing an upregulating in NDH-dependent CEF.

Moreover, a newer study by Kou et al. 2015 showed that during the measurements of LREs in pgr5 mutant plants treated with AA, P700 was more strongly oxidized, hence e- outflow at the acceptor side of PSI increased compared to measurements without the inhibitor[260]. This finding was interpreted by the authors that the binding of AA increased the Mehler reaction and/or plastid terminal oxidase (PTOX) reaction in the pgr5 mutant leading to a stronger e- outflow at the acceptor side of PSI[260]. However, on the opposite when lacking the NDH complex the supplementation with AA led to a significantly stronger reduction in P700 relative to measurements without the inhibitor[260], indicating that e- outflow at the acceptor side of PSI was decreased. This observation, therefore, suggests that the addition of AA resulted in a decrease in LEF in the crr2 mutant when lacking both CEF modes. In contrast, it can be speculated that the addition of AA in pgr5 led to an increase in NDH-dependent CEF, which was, in turn, decreasing the outflow of e- from the acceptor side of PSI relative to measurements without AA. To our understanding, when inhibiting PGR5/PGRL1-dependent CEF, this is leading to a decrease in LEF and could result in stronger oxidation of the PQ pool poising NDH-dependent CEF. In contrast, an upregulation of LEF which is leading to a more strongly reduced PQ pool would show decreased NDH-dependent CEF activity. Indeed, it was shown that when decreasing the capacity to perform LEF in the pgr5 mutant by decreasing CO_2 levels, the mutant increased the formation of NPQ. When LEF is decreased through cutting out CO_2, an increase in NPQ is most likely only possible through increasing NDH-dependent CEF relative to measurements where CO_2 is available and LEF can be performed[147]. Therefore, it is very likely that NDH-dependent CEF could be increased when LEF is decreased in the pgr5 mutant relative to WT, demonstrating that NDH-dependent CEF and LEF compete. Interestingly, in our observations in the crr2 mutant, both LEF and

PGR5/PGRL1-dependent are upregulated, which is suggesting that this type of CEF is not downregulated when LEF is increased. In contrast, PGR5/PGRL1 dependent CEF could upregulate LEF by keeping the PQ pool reduced, maintaining e- flow towards the Cytb6f complex, and further to PSI through increasing e- turnover through Cytb6f-PSI via CEF to protect PSI‘s donor side from overoxidation. We propose that after dark preincubation and under growth light conditions when the PQ pool is in a more reduced state relative to prolonged illumination at low AL, PGR5/PGRL1-dependent CEF is favored over NDH-dependent CEF, whereas after prolonged illumination with low AL when the PQ is more oxidized NDH-dependent CEF is favored over PGR5/PGRL1-dependent CEF. In our model, the switch between both modes of CEF is regulated by the redox state of the PQ pool.

4.2.4 Light distribution between PSII and PSI is controlling e- transport in all mutants

As discussed earlier, when conducting kinetics at 25 µmol m-2 s-1, the capacity to perform LEF after prolonged illumination was elevated in the crr2 mutant relative to WT, represented by increased Y(ND) and decreased Y(NA) levels (Fig. 42 C and E). In contrast, in WT the decrease in Q_A and Y(NA) and increase in Y(ND) levels were halted which can be interpreted that the capacity to perform LEF was decreased and CEF was elevated (Fig. 42 A, C, and E). Instead, in the crr2 mutant when the NDH complex is missing, the mutant increased under these low AL conditions LEF relative to WT. Thus, it suggests that after prolonged illumination with low AL in WT, NDH-dependent CEF competes with LEF. As already mentioned earlier, it can be speculated like in Wood et al.‘ s proposed model from 2018 that less e- outflow at the acceptor side of PSI was observed in WT, through adapting the thylakoid membrane to low light conditions by performing a state 2- to- state 1 transition and increasing the number of grana stacks[3]. Interestingly, in the stn7 mutant, both Q_A and Y(NA) levels stopped decreasing, and Y(ND) levels did not increase already after -23 minutes of illumination, whereas in the pph1 mutant, we observed the opposite (Fig. 27). Therefore, it shows that the *stn7* mutation – by decreasing LEF worked contrarily to the *crr2* mutation- by increasing LEF, while the *crr2* mutation resembled more the *pph1* mutation and both enhanced LEF. Moreover, when illuminating light-adapted stn7 and pph1 mutant

leaves with very low AL, the addition of FR caused Q_A and Y(NA) levels to be like in WT in both mutants, while Y(ND) levels were decreased in the stn7 mutant and elevated in the pph1 mutant relative to WT (Fig. 49 B, D, and F). Under the same experimental conditions, the treatment with FR light led also to a decrease in Y(ND) levels in the pgr5 mutant and to an increase in Y(ND) levels in the crr2 mutant relative to WT (Fig. 50 D and F). These observations indicate that when adapted to growth light conditions and treated with very low AL supplemented with FR light, the *stn7* mutation resembled the *pgr5* mutation, while the *pph1* mutation resembled the *crr2* mutation. Thus, when light-adapted and FR light was added in both the stn7 mutant and the pgr5 mutant CEF was increased, while in the pph1 and the crr2 mutants it was decreased relative to WT. Therefore, it can be speculated that in the stn7 mutant like in the pgr5 mutant, NDH-dependent CEF was upregulated relative to WT. In contrast, in the pph1 mutant when the capacity to perform LEF was increased NDH-dependent CEF was decreased. Then, if NDH-dependent CEF was decreased/missing, LEF was increased when leaves were at very low AL supplemented with FR light, which was resembled by an increase in e- outflow at the acceptor side of PSI and PSII and a decrease in e- inflow at the donor side of PSI. It can be speculated that in the pph1 and the crr2 mutant, the light was more equally absorbed and utilized at PSII and PSI relative to WT, while in the pgr5 and in the stn7 mutant after prolonged illumination with low AL more light was utilized at PSI relative to WT. Hence, it can be speculated that the structure of the thylakoid membrane is influencing e- transport modes in both state transition and CEF-mutants. Like in the stn7 and the pph1 mutant both the lack of PGR5/PGRL1- and of NDH-dependent CEF is leading to a change in light perception at PSII and PSI in the pgr5 and the crr2 mutant relative to WT.

4.3. Protein complexes of the stroma thylakoid membrane: comparing state transition and CEF mutants via IZE-FFE in the first and LDS-Native-PAGE in the second dimension

4.3.1. IZE-FFE and Native-PAGE vs. only Native-PAGE

Two different electrophoretic methods, FFE and Native-PAGE separation were applied to differentiate between the charge and molecular weight-specific mobility differences among protein complexes. Both methods separate protein complexes based on the mass to charge ratio. In FFE, the low viscosity and high mobility of the liquid phase were found to show hardly any interference with the mass and different molecular weight assembly states. Thus, separation was primarily based on the molecular charge state of complexes. For determination of the complexes' molecular weight, complexes were analyzed using Native-PAGE as a second-dimension separation termed 2D. Interestingly, complexes that separated with different mobility in 2D Native-PAGE separated with equal mobility in FFE separation (Fig. 51 and Fig. 56). This indicated that complexes determined upon Native-PAGE separation had been in a higher assembly state during FFE separation and that Native-PAGE separation exposed native complexes to disintegrating forces. In FFE, protein complexes of equal charge were separated in polydisperse distribution profiles with variable focal widths. During Native-PAGE, protein complexes were separated into bands. Complexes in one band are regarded to be homogenous for equal electrophoretic mobility in the gel matrix. Mobility in Native-PAGE is regarded to be based on an equal mass to charge ratio whereas separation of complexes in gel-electrophoresis is regarded to be dependent on the filtration of complexes weight by molecular dimension based on the correlation of molecular weight and diameter. Molecular weight is typically determined using reference proteins. However, a standard description of the electrophoretic process could not explain why FFE-separated complexes disintegrated in subcomplexes during Native-PAGE. For analysis, we concluded that bands that entered the gel and could be analyzed after separation in the gel-matrix had fulfilled the entry requirement of the

gel-matrix pores. In contrast, complexes that did not meet the requirement had accumulated at the interface of the gel and cathode buffer.

Our finding showed that several complexes with different molecular size-dependent mobility in Native-PAGE have localized at the same charge state-dependent mobility in FFE. This indicated that either several complexes of different molecular sizes in Native-PAGE showed the same charge state and hence all revealed the same mobility in FFE, or that one complex with a one-charge state that separated in FFE disintegrated into several complexes with specific molecular sizes during Native-PAGE. An observation supporting the latter was that the absence of the detergent LDS from the cathode buffer during Native-PAGE was leading to intact complexes with higher molecular weight (Fig. 52 A and Fig. 57 A). The nature of the disintegrating forces remained however unclear.

For separation by Native-PAGE, protein complexes transit from the liquid-phase cathode buffer to the gel-phase buffer residing in the gel-matrix. In this context, the formation of protein bands must be regarded as a property of the transition into the gel-matrix that restricts a continuation of the high mobility of protein complexes in the liquid phase. In this model, protein complexes show free-flow mobility before the liquid-gel junction is reached. At the junction, complexes accumulate and concentrate in bands. Only complexes that meet the gel-matrix entry requirement continue the flow through the gel-matrix as a concentrated band with lower mobility relative to the liquid phase. Protein complexes that concentrate at the liquid-gel junction decrease the pore diameter of the matrix, increase the concentration of protein complexes in the liquid phase, and increase the exclusion limit for protein complexes to enter the gel-matrix pores. The decrease in the size of the pores by the proteins at the gel entry restricts the electrophoretic flow of anions and the endo-osmotic flow of cations. This increases the electric field and hence the force on the charged sample and buffer ions increases. The entry of the complexes and the restriction of flow due to the decreasing pore size of the gel can be regarded as a key difference between FFE and Native-PAGE and the liquid-gel junction could be responsible for the disintegration of high molecular weight complexes during gel entry.

In the analysis, especially PSI was found to interact with Cytb6f, LHCII, and PSII (Fig. 53). ATPase was isolated as holo-complex composed of stromal head and membrane base motors, CF1 and CF0, or as CF1 alone, respectively (Supplemental Table 1 and 2). The CF0/CF1 ATPase holo complex emphasizes the gentle solubilization and separation of membrane protein complexes in this study. Some of the digitonin solubilized complexes were found to be too large for separation by Native-PAGE and had to be broken down into smaller complexes by secondary solubilization using ß-DDM to investigate the complex subunit-composition (Fig. 54 and Fig. 58 B). These high-molecular-weight complexes were termed HMW. Interestingly, the requirement for solubilization of HMW complexes was associated with the presence of PSII in the HMW complex indicating that digitonin-specific solubilization of the membrane lipids is influenced by a differential association of lipids with the different types of a membrane protein complex (Fig. 55 and Fig. 59).

4.3.2. IZE-FFE and the adaptation of the thylakoid membrane

When analyzing protein complexes of the stroma thylakoid membrane, it was striking that in the crr2 mutant, the formation of HMW complexes, separated at the anodic fractions during FFE was tremendously increased relative to WT gl1 and the pgr5 mutant, while in the pgr5 mutant, complex molecular weight distribution resembled WT gl1 (Fig. 51). In addition, in the crr2 mutant, the amount of LHCII was significantly increased relative to WT (Fig. 51 A and B). Pre-liminary gel blot analysis revealed that also the percentage of phosphorylated LHCII molecules and PSII complexes was increased in the crr2 mutant compared to WT (Fig. 55 A and B). This observation demonstrates that in the crr2 mutant when the NDH complex was missing, more LHCII molecules and PSII complexes were present as HMW complexes in the stroma thylakoid membrane relative to WT (Fig. 51 and Fig. 55 A and B). Moreover, the solubilization of the membranes from pph1 and stn7 mutants showed that more HMW complexes containing PSII, PSI, LHCII, and Cytb6f complexes were isolated from the anodic fractions upon FFE separation in the pph1 mutant than in WT and the stn7 mutant (Fig. 56). Indeed, like in the crr2 mutant, also in the pph1 mutant the amount of

phosphorylated LHCII and PSII in the stroma thylakoids was increased (Fig. 5 9A and C) indicating that the complexes became more accessible for digitonin solubilization. In the pph1 mutant, it was previously shown by transmission electron microscopy that grana stacks were thinner but more abundant leading to a larger stromal thylakoid membrane area relative to the stn7 mutant, which in contrast showed fewer grana stacks with an increased number of layers[137]. Based on structural data from the pph1 mutant[137], we, therefore, suggest that the solubilization of more HMW complexes in the crr2 mutant resulted from the presence of thinner grana stacks that were more abundant in number and thus increased the area of the stroma thylakoid membrane accessible by digitonin during the solubilization. By this hypothesis, FFE separations of the stroma thylakoid membrane of transgenic *A. thaliana* strain OE CurtA, which is overexpressing the membrane protein CURT 1A and in turn showed a significant increase in grana membrane relative to WT[247], significantly decreased the amount of HMW complexes relative to WT (Fig. 60). Therefore, our findings strongly suggest that by separating membrane protein complexes via IZE-FFE in the first dimension and Native-PAGE in the second, the dynamic changes in the thylakoid membrane are represented.

4.3.3. CEF mutants

In the crr2 mutant, more HMW complexes were solubilized relative to WT due to an increase in the stroma thylakoid membrane (Fig. 51 A and B). This potentially resulted from more phosphorylated LHCII molecules binding to PSI, causing the grana membrane to destack[3]. Since the NDH complex has been shown to bind to PSI[171,173], it strongly suggests that in the crr2 mutant, instead of NDH, an increased number of phosphorylated LHCII molecules were binding to PSI compared to WT. It is speculated that by this means, PSI complexes were stabilized when NDH was absent.

In the pgr5 mutant, the amount of HMW complexes in the stroma thylakoid was significantly reduced relative to the crr2 mutant (Fig. 51 B and C), thus leading to a general decrease in protein complexes when compared to the crr2 mutant (Fig. 53 B

and Supplemental Table 1). This is further indicating a general decrease in photosynthetic e- transport in the pgr5 mutant relative to the crr2 mutant. Especially, the amount of ATPase molecules was decreased relative to the crr2 mutant, indicating that either less ATPase is needed in the pgr5 mutant or more in the crr2 mutant (Fig. 53 B). It can be speculated that when in the pgr5 mutant, ATPases are constitutively activated a smaller number is needed in the chloroplasts. On the other hand, increasing both LEF and PGR5/PGRL1-dependent CEF in the crr2 mutant could require more ATPases relative to the pgr5 mutant. In contrast, the number of proteins operating in the CBB cycle, which were found in the anodic fractions separated through Native-PAGE after FFE separation determined via mass spectrometry were similar in both pgr5 and crr2 mutants (Fig. 53 B and Supplemental Table 1), indicating that while proteins of the e- transport chain differed in general, a similar concentration of proteins located in the stroma thylakoid membrane was separated. Additionally, preliminary data indicated that in the pgr5 mutant, more phosphorylated LHCII was residing in the stroma thylakoid membrane relative to WT (Fig. 55 A and C). In addition, it was shown that in the pgr5 mutant the shift from state 2- to- state 1 was decreased relative to WT (see paragraph 4.1.2.a.). Also, others showed that after HL treatment in the pgr5 mutant fewer LHCII molecules were dephosphorylated hence the switch from state 2- to- state 1 decreased when compared to WT[188]. If in the pgr5 mutant PGR5/PGRL1-dependent CEF is lost, more phosphorylated LHCII binding at PSI in the pgr5 mutant could be required to increase the capacity to perform LEF in the mutant. Like in the pph1 mutant, when LHCII is constantly phosphorylated, also in the pgr5 mutant a slower transition into state 1 from state 2 would keep more PSII centers connected to PSI to upregulate LEF.

Interestingly, while both pgr5 and crr2 mutants are showing more phosphorylated LHCII molecules relative to WT, only the crr2 but not the pgr5 mutant showed an increase in HMW complexes, hence stroma thylakoid membrane. Based on our PAM analysis it can be speculated that in the crr2 mutant when adapted to growth light, an increase in LHCII molecules leads to an increase in LEF. At the same time, after dark preincubation when an increased number of LHCII molecules is bound to PSII centers,

this could lead to an increase in grana stacks which in turn leads to the exclusion of PSII from linear e- transport, hence enhancing CEF. In contrast, in the pgr5 mutant, where we isolated a stroma thylakoid membrane that more resembles WT, our findings are suggesting that when PGR5/PGRL1-dependent CEF is missing, the mutant does not increase the amount of LHCII in its thylakoid membrane-like the crr2 mutant does. It can be speculated that in the crr2 mutant the lack of a functional NDH complex enables a rise in LHCII molecules binding to PSI. Indeed, it was hypothesized that the binding of NDH to PSI proceeds the full assembly of the NDH complex[261]. This could have, apart from initiating NDH-dependent CEF, also a stabilizing role for a functional operating PSI. It can further be speculated that after dark preincubation in the pgr5 mutant, when PGR5/PGRL1-dependent CEF is missing, grana stacks cannot be increased like in the crr2 and the stn7 mutant, as a stronger exclusion of PSII through an increased grana diameter would negatively affect the performance of LEF in the pgr5 mutant. Thus, also a switch from state 2- to- state 1 is decreased in the pgr5 mutant relative to WT. Instead, the pgr5 mutant appeared to keep more LHCII phosphorylated at PSI relative to WT and distribute incoming light quanta more equally between PSII and PSI, to stabilize LEF.

4.3.4. State transition mutants

The solubilization of the thylakoid membrane of the stn7 mutant resulted in an unphosphorylated LHCII stroma thylakoid membrane containing fewer HMW complexes, but more PSI-Cytb6f-LHCII complexes which were solubilized freely from PSII-containing HMW complexes relative to WT (Fig. 56 B). This finding was interesting, as the stn7 mutant, LHCII was despite of the absence of the phosphorylating kinase, still found in the stroma thylakoid membrane. This observation provided evidence that different pools of LHCII molecules, displaying different binding capacities to PSII and PSI could be present in the thylakoid despite the mutation. It could imply that LHCII complexes could bind accordingly to its phosphorylated/unphosphorylated state at different positions at PSI. Additionally, in a very recent model using Monte Carlo simulation, it was revealed that state transition is

unlikely to cause a large-scale shift of LHCII from the grana to the stroma lamellae and that light-harvesting capacity at PSI is more likely due to more efficient binding of LHCII towards PSI upon phosphorylation[262]. In the same way, LHCII that already resides in the grana may turn into functional PSII-LHCII clusters[262]. This proposes that unphosphorylated LHCII complexes binding to PSI might have a different function than the state transition LHCII complex. For example, an increase in light-harvesting capacity at PSI without changing the grana membrane in the stn7 mutant could boost the mutant's ability to perform CEF. Additionally, an increase in PSI-Cytb6f complexes which are operating independently of PSII in the stn7 mutant relative to WT could be useful in the stn7 mutant which possesses thicker grana stacks that are excluding more PSII centers from the participation in LEF. It can be further hypothesized that if LEF is decreased, the PQ pool is more reduced leading to an increase in PGR5/PGRL1-dependent CEF.

In contrast, as already mentioned above, in the pph1 mutant the amount of HMW complexes was significantly increased relative to WT and the stn7 mutant (Fig. 56). Moreover, when comparing the protein composition of anodic HMW complexes from FFE isolation between the pph1 and the stn7 mutant plants, the pph1 mutant showed a decrease in NDH complexes relative to the stn7 mutant (Fig. 58 C). Since both the pph1 and the crr2 mutant have significantly more phosphorylated LHCII molecules residing in their stroma thylakoid membrane compared to their corresponding WT, it might indicate that while in the crr2 mutant more LHCII is bound to PSI due to the lack of the NDH complex, in the pph1 mutant less NDH complex is bound to PSI due to an increase in phosphorylated LHCII binding at PSI.

4.4. Conclusive remarks

Conclusively, our data lays the foundation for a new hypothetic model (Fig. 61) of the regulation of e- transport, which is independent of the model based on the distance between grana- and stroma-located PQ pools[137]. Additionally, our hypothetical model disagrees with the hypothesis of light intensity-dependent suppression of CEF in the

state transition mutants stn7 and pph1 (namely CEF is suppressed at LL in the stn7 mutant and HL in the pph1 mutant causing under both conditions a decrease in LEF)[2]. Instead, our model assumes that an increase in grana stacks, which is permanently found in the stn7 mutant and after dark preincubation in the crr2 mutant, initiates an increase in PGR5/PGRL1-dependent CEF because the light is not as efficiently utilized at PSII the more LHCII is bound. We further hypothesize that an increase in LHCII at PSII is resulting in PSII being separated from the e- transport active compartment of the chloroplast. Hence, after dark preincubation at the onset of light when grana stacks are more separated from stroma thylakoids more light is absorbed and utilized at PSI relative to PSII and the plant increases PGR5/PGRL1-dependent CEF (Fig. 61 A1). Under these conditions, both PSII‘s acceptor side (Q_A levels increased) and PSI‘s acceptor side (Y(NA) levels increased) are reduced and PSI‘s donor side reduced (Y(ND) levels decrease) showing a drop in the outflow of e- from PSII and PSI into the metabolic pool and increase in e- inflow at the donor side of PSI (summary of all mutant phenotypes in table 8). In addition, we see that in the npq4 mutant, which is not able to turn on NPQ, e- turnover at PSI through PGR5/PGRL1-dependent CEF is increased. This is most likely performed through lowering e- transport at PSII by increasing the diameter of grana membrane stacks. This model is opposing the view that an increase in PSII-LHCII clusters is increasing the plant’s light-harvesting properties by lateral interactions[262]. On the opposite, when LHCII is phosphorylated and bound to PSI leading to increased interaction between PSI-rich stroma thylakoid membrane and PSII-rich grana stacks (such as found always in the pph1 mutant and after some minutes of illumination with low AL in both in the pgr5 and in the crr2 mutant), prolonged illumination at growth light conditions favors LEF over PGR5/PGRL1-dependent CEF (Fig. 61 A2). Then, Q_A and Y(NA) levels are decreased and e- outflow at the acceptor side of PSII and PSI increases, while Y(ND) levels are increased lowering e- inflow at the donor side of PSI by decreasing CEF.

As indicated in our hypothetical model (Fig. 61), we have found evidence that after dark preincubation at the onset of low, medium, or high AL, when the PQ pool is reduced, PGR5/PGRl1-dependent CEF is increased in stn7, npq4 and crr2 mutants

relative to WT, while NDH-dependent CEF comes into play when the PQ pool is oxidized such as it is the case in the stn7 and the pgr5 mutant plants after prolonged illumination with low AL. In our view, NDH-dependent CEF is turned on when the plant is illuminated for a longer time at lower limiting AL (below growth light conditions) when LEF is not working at full capacity (Fig.61. A3). Moreover, that PGR5/PGRL1-dependent CEF works under a reduced PQ pool, while NDH-dependent CEF needs an oxidized PQ pool could indicate that these two mechanisms return e- from PSI‘s acceptor side to the ETC at different junctions. If PGR5/PGRL1-dependent CEF is shuttling e- directly to Cytb6f it could bring e- back when the ETC would be in a reduced state, whereas NDH-dependent CEF when it is returning e- in a PSII-served PQ pool would need oxidized conditions to cycle e- towards Cytb6f and PSI. We further propose that even when the PQ pool is oxidized such as is the case in the pph1 mutant, NDH-dependent CEF is decreased because the NDH complex competes with phosphorylated LHCII to bind at PSI (Fig. 61 A2). Similarly, we see an increase in phosphorylated LHCII at PSI in the NDH-deprived crr2 mutant leading to a rise in LEF (Fig. 61 A2). Then, after dark preincubation and the onset of low to GL conditions, PGR5/PGRL1-dependent CEF decreases, and LEF increases in the pph1 mutant, due to a more strongly oxidized ETC relative to WT; whereas, in the crr2 mutant, in addition to LEF also PGR5/PGRL1-dependent CEF is increased because grana stacks are elevated (due to an increased number of LHCII molecules) and more strongly utilizing e- at PSI keeping the PQ pool more strongly reduced relative to the pph1 mutant. Indeed, when FR was added to low AL, a rise in PGR5/PGRL1-dependent CEF was observed in the crr2 mutant relative to WT because the ETC was in a more strongly reduced state. The experiments building the foundation for the outlined models (Fig. 61) are summarized below (table 8).

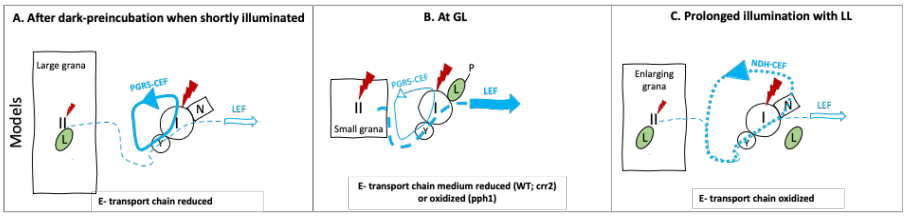

Figure 61. Hypothetical models for the regulation of e- transport after dark preincubation, after some minutes, and prolonged illumination under different light conditions. A. In plants dark-preincubated and at the onset of LL, GL, or HL, the diameter of grana stacks is increased, and the connection between grana and stroma thylakoids decreased resulting in stronger light absorption and utilization at PSI relative to PSII. Under these conditions, when LHCII is not phosphorylated and the ETC is in a reduced state PGR5/PGRL1-dependent CEF is elevated after short illumination (> 2min) relative to LEF. **B.** After short illumination with GL (about 2 min), grana stacks get smaller and the connection between grana and stroma thylakoid increases resulting in more balanced light absorption at PSII and PSI. Under these conditions, when LHCII gets phosphorylated and is binding to PSI, the ETC chain is more strongly oxidized compared to after dark preincubation, and LEF is increased relative to PGR5/PGRL1-dependent CEF. In the pph1 mutant, a more strongly oxidized ETC is suppressing PGR5/PGRL1-dependent CEF stronger, while in the crr2 mutant PGR5/PGRL1-dependent CEF is upregulated when the ETC is more strongly reduced relative to WT. **C.** After prolonged illumination at low limiting AL (below GL), grana stacks are increasing and the connection between grana and stroma thylakoids is decreasing leading to stronger light absorption at PSI relative to PSII. Under these conditions, LHCII is dephosphorylating again and decoupling from PSI. Then the ETC is in an oxidized state, and this results in a decrease in LEF and upregulation of NDH-dependent CEF. Experimental data obtained from PAM measurements with different mutant plants, which are laying the foundation for our proposed models can be found in table 8. Abbreviations: LHCII: light-harvesting complex II; LL: low light; GL: growth light; HL: high light; e-: electron ETC: electron transport chain, PSI: photosystem I; PSII: photosystem II.

Table 8. Findings observed in mutant phenotypes and figure guide for models A, B, and (Fig. 61.). Mutants labeled in green are proof for our assumed models, whereas red labeled mutants miss the phenotype.

Condition	Assumption	Mutant	Finding	Figure
Model A: After dark preincubation when shortly illuminate	Increase in PGR5/PGRL1-dependent CEF relative to LEF	stn7 mutant	Increase in light utilization at PSI (increase in Y(I)) relative to PSII when compared to the pph1 mutant; a slower decrease in Q_A (determined through 1-qL) in the stn7 mutant relative to WT and the pph1 mutant and PSI's donor side Y(ND) decreased, hence e- inflow at the donor side of PSI increased,	Fig.26. A and B Fig. Fig.27.A and D

d; or at HL			whereas PSI's acceptor side Y(NA) increased relative to WT, hence e-outflow at the acceptor side of PSII and PSI decreased; the addition of FR light to low AL (<58 µmol m-2 s-1) after darkness during the recording of an LRE causes increased Q_A and decreased Y(ND) levels LRE at HL causes an increase in NPQ and more decreased Y(ND) levels relative to WT	Fig.27. E and F Fig.34 A and Fig.34. A data not shown
		npq4 mutant	Q_A and Y(NA) levels increased, and Y(ND) levels decreased relative to WT LRE at HL: the addition of FR light causes decreased Y(ND) and increased Y(NA) levels relative to without adding FR light	Fig.27 A and D Fig.27B and E Fig.27C and F Fig.37 B and C
		crr2 mutant	Relative contribution of electron flow through PSI (Y(I)) was increased in WT and the crr2 relative to the pgr5 mutant; more increased Q_A levels relative to WT LRE at HL: Y(ND) levels are decreased, and Y(NPQ) levels increased relative to WT	Fig.38 B Fig.39A and D and Fig.42A Fig.48 C and B

		pgr5 mutant	The effective quantum yield at PSI (Y(I)) was significantly decreased relative to WT but the effective quantum yield at PSII (Y(II)) was WT-like, leading to a strongly decreased Y(I)/Y(II) ratio relative to WT; Y(ND) was decreased hence photosynthetic control at Cytb6f was decreased and in addition Y(NPQ) was significantly decreased in the pgr5 mutant relative to WT; after dark preincubation an increase in Y(NA) levels and a slower decrease in Q_A levels after two minutes of illumination seen in WT was missing in the pgr5 mutant indicating that in WT a halt in e- outflow at the acceptor side of PSII and PSI was depending on PGR5/PGRL1-dependent CEF	Fig.38 Fig.39B and E Fig.40 Fig.42B and F
	Increase in grana stacks not connected to PSI-located in stroma lamellae	stn7 mutant	A lower amount of HMW complexes and an increased amount of PSII-free PSI-Cytb6f-LHCII compared to WT	Fig.56 A and B
		OE CurtA mutant	A decrease in HMW complexes relative to WT	Fig.60
Model B: At GL	Increase in LEF relative to PGR5/PGRL1 -dependent CEF	pph1 mutant	Balanced e-flow of about a 1:1 ratio of Y(I)/Y(II); faster decrease in Q_A in the pph1 mutant relative to the stn7 mutant; Y(ND) levels elevated, hence e- supply at the donor side of PSI decreased, whereas PSI's	Fig.26 A and B Fig.27.A and D Fig.27. E and F

			acceptor side Y(NA) was decreased relative to the stn7 mutant; Q_A decreased like in WT, but Y(ND) was elevated, and Y(NA) decreased relative to WT, and the stn7 mutant	Fig.30, Fig.32, and Fig.33
	An increase in phosphorylated LHCII at PSI led to a better connection between stroma thylakoid membrane and grana stacks facilitating LEF	pph1 mutant	More phosphorylated LHCII complexes were distributed in the HMW anodic FFE fractions in the pph1 mutant relative to WT; phosphorylated Lhcb1/2 also in the very anodic fraction, where both WT and the stn7 mutant did not show any phosphorylated antenna	Fig.59
		crr2 mutant	Cathodic FFE fractions correlated stronger with phosphorylated Lhcb1/2 molecules relative to WT	Fig.55
		pgr5 mutant	More phosphorylated LHCII was residing in the stroma thylakoid membrane relative to WT	Fig.55 A and C
Model C: Prolonged illumination with LL	Increase in NDH-dependent CEF relative to LEF	stn7 mutant	After light adaptation to GL and turning on very low light (6 µmol m-2 s-1) Q_A levels were decreased relative to WT and the addition of FR light more strongly decreased Q_A levels but kept Y(ND) levels decreased relative to WT; At 25 µmol m-2 s-1 after prolonged illumination Q_A, Y(NA) were increased Y(ND) levels were significantly decreased	Fig,49 B and D Fig.32 A and D and Fig.33A

			compared to WT and the pph1 mutant	
		pgr5 mutant	After light adaptation to GL and turning on very low light (6 µmol m-2 s-1) through the addition of FR light, Y(ND) levels were decreased relative to WT	Fig.50 D
		pph1 mutant	After light adaptation to GL and turning on very low light (6 µmol m-2 s-1) through the addition of FR, Y(ND) levels were increased relative to WT; At 25 µmol m-2 s-1 after prolonged illumination, Y(NA) levels were lowered, and Y(ND) levels were significantly elevated compared to WT and the stn7 mutant	Fig.49 D Fig.32 B and E
		crr2 mutant	At 25 µmol m-2 s-1 after prolonged illumination, Y(NA) levels were decreased, and Y(ND) levels were significantly increased compared to WT and the pgr5 mutant	Fig.42C and E
	Lack/decrease in NDH-dependent CEF because less NDH complex bound to PSI instead more LHCII at PSI	crr2 mutant	Cathodic FFE fractions containing HMW complexes of PSII and PSI-Cytb6f complexes correlated stronger with phosphorylated Lhcb1/2 molecules	Fig.55
		pph1 mutant	In the anodic FFE fraction, the total peptide count of proteins such as NDH was decreased relative to the stn7 mutant	Fig.58 B and C

5. Supplements

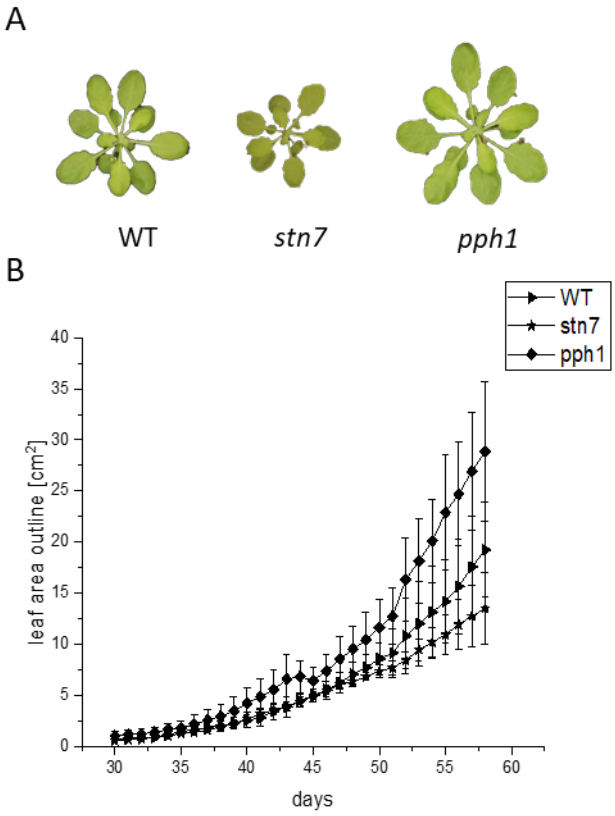

Supplemental Figure 1. Phenotypes of 7-week-old stn7 mutant, pph1 mutant, and WT *A. thaliana* plants grown under low light conditions (80- 90 µmol m-2 s-1) on an 8 h/16 h light/dark regime on day 49 (A). A growth curve was determined from leaf areas of 3 plants per phenotype for about 9 weeks after germination (B).

Supplements

Supplemental Table 1. List of identified proteins by mass spectrometry of FFE in the first dimension and Native-PAGE in the second dimension separated protein complexes of the crr2 mutant (fraction 36) and the pgr5 mutant (fraction 37) that were grouped in Fig. 53 B.

Grouped protein complexes	Single identified proteins (alternate ID)	Total unique peptide count			
		crr2	pgr5	crr2	pgr5
		complex 4-6		complex 7	
ATPase	atpA	39	4	12	0
	atpB	52	6	20	1
	atpD	13	0	4	0
	atpE	9	0	2	0
	atpF	23	1	9	0
	PDE334	18	1	6	0
	atpC	22	1	7	0
PSI	psaA	26	0	19	0
	psaB	16	1	13	0
	psaC	15	0	6	0
	psaD1	41	1	29	0
	PSAD2	6	0	4	0
	PSAE1	27	2	23	0
	PSAE2	11	0	10	0
	PSAF	20	6	16	3
	PSAL	11	2	9	0
	PSAN	12	4	4	1
	ycf4	4	3	1	1
LHCA	LHCA4	9	2	3	1
	LHCA1	10	3	6	0
	LHCA3	9	3	5	2
Cytb6f	petA	33	11	24	7
	petB	8	3	5	2
FNR	LFNR1	13	3	4	0
	LFNR2	10	2	2	0
	PGRL1A	6	3	0	0
PSII	psbA	8	2	2	0
	psbB	9	2	0	0
	psbC	14	5	3	2
	psbD	12	4	2	0

	PSBR	4	2	2	0
PSII other proteins	PSB33	14	6	1	0
	PSBO1	4	2	1	0
	PSBO2	0	0	0	0
	HCF136	0	6	0	0
	THF1 (Psb29)	3	3	0	0
PsbS	PsbS	18	8	5	4
LHCB antenna	LHCB1 (CB1A)	0	1	0	0
	Lhb1B1	0	1	0	0
	LHCB1 (CB1C)	1	1	0	0
	LHCB2	10	8	3	3
Other PSII antenna	LHCB4	5	2	2	0
	LHCB5	8	6	1	3
	LHCB4	8	3	0	1
	LHCB6	12	5	2	1
CBB proteins	GAPB	0	1	0	0
	RCA	2	4	0	0
	GAPC2	0	0	5	0
	GAPC1	0	0	1	0
	APE2	4	2	1	3

Supplemental Table 2. List of identified proteins by mass spectrometry of FFE in the first dimension and Native-PAGE in the second dimension separated protein complexes of the stn7 mutant (19B; orange square) and the pph1 mutant (19B; blue square) that were grouped in Fig. 58 C.

Grouped protein complexes	Single identified proteins (alternate ID)	Total unique peptide count	
		pph1	stn7
ATPase	atpA	125	135
	atpB	182	209
	atpD	45	57
	atpE	36	42
	atpF	76	80
	atpG	99	0
	PDE334	54	60
	atpC	0	118
PSI	psaA	42	42
	psaB	33	34
	psaC	18	23
	psaD1	56	69
	PSAD2	45	57
	PSAE1	27	29
	PSAE2	35	33
	PSAF	37	39
	PSAG	14	12
	PSAL	16	18
	PSAN	14	19
	ycf4	13	0
	PSAH1	0	0
	PSAH2	0	9
	PSAK	0	12
LHCA	LHCA4	9	14
	LHCA1	16	17
	LHCA3	11	10
LHCA5/6	LHCA6	1	0
	LHCA5	0	3

Cytb6f	petA	83	83
	petB	19	20
	petC	12	9
FNR	LFNR1	28	33
	LFNR2	22	19
	PGRL1A	28	32
NDH	PNSB2	9	19
	PNSB1	10	27
	PnsB4	3	8
	PNSL5	5	11
	PNSL3	5	9
	PNSL1	10	14
	PNSL2	4	6
	ndhK	6	12
	ndhM	4	11
	ndhS	13	25
	ndhN	2	8
	ndhU	2	12
	ndhI	2	4
	ndhD	1	0
	ndhH	8	16
	ndhJ	0	0
	ndhO	0	4
	NAD7	0	6
PSII	psbA	32	31
	psbB	89	61
	psbC	49	40
	psbD	32	29
	psbH	15	0
	PSBR	19	13
	psbE	15	15
PSII other proteins	PSB33	37	39
	PSBO1	69	53
	PSBO2	50	36
	HCF136	0	4
	THF1 (Psb29)	11	12
	PSB27-1	17	13

PsbS	PsbS	42	36
LHCB antenna	LHCB1 (CB1A)	15	17
	Lhb1B1	7	8
	LHCB1 (CB1C)	18	18
	LHCB2	21	0
	Lhb1B2	0	0
Other PSII antenna	LHCB4	35	19
	LHCB5	34	33
	LHCB4	34	0
	LHCB6	28	24
Curt proteins	CURT1A	27	30
	CURT1B	14	12
	CURT1C	1	0
Allene oxide cyclase/synthase	AOC2	17	27
	AOC1	3	5
	CYP74A	25	49
SOQ1	SOQ1	57	89
STN7	STN7	7	0
APE	APE1	19	40
	APE1	5	24
Lil3	Lil3	3	11
POR	PORA	0	0
	POR	16	24
	PORB	25	32
CAS	CAS	59	65
CBB proteins	RBCS-1A	0	15
	RBCS3B	0	12
	RBCS-1B	0	3
	rbcL	0	46
	GAPC2	0	13
	GAPC1	0	11
	GAPB	0	22
ZEP	ZEP	26	26

6. Literature references

1. Puthiyaveetil Sujith. A mechanism for regulation of chloroplast LHC II kinase by plastoquinol and thioredoxin. *FEBS Lett.* **585**, 1717–1721 (2011).

2. Hepworth, C. *et al.* Dynamic thylakoid stacking and state transitions work synergistically to avoid acceptor-side limitation of photosystem I. *Nat. Plants* **7**, 87–98 (2021).

3. Wood, W. H. J. *et al.* Dynamic thylakoid stacking regulates the balance between linear and cyclic photosynthetic electron transfer. *Nat. Plants* **4**, 116–127 (2018).

4. Cruz, J. A. *et al.* Plasticity in light reactions of photosynthesis for energy production and photoprotection. *J. Exp. Bot.* **56**, 395–406 (2005).

5. Robert E. Blankenship. Carbon Metabolism. in *Molecular Mechanisms of Photosynthesis* 171–203 (John Wiley & Sons, Ltd, 2002). doi:10.1002/9780470758472.ch9.

6. Moss, R. A. & Loomis, W. E. Absorption Spectra of Leaves. I. The Visible Spectrum. *Plant Physiol.* **27**, 370–391 (1952).

7. Merchant, S. & Sawaya, M. R. The light reactions: a guide to recent acquisitions for the picture gallery. *Plant Cell* **17**, 648–663 (2005).

8. Gómez, S. M., Nishio, J. N., Faull, K. F. & Whitelegge, J. P. The chloroplast grana proteome defined by intact mass measurements from liquid chromatography mass spectrometry. *Mol. Cell. Proteomics MCP* **1**, 46–59 (2002).

9. Kramer, D. M., Cruz, J. A. & Kanazawa, A. Balancing the central roles of the thylakoid proton gradient. *Trends Plant Sci.* **8**, 27–32 (2003).

10. Sacksteder, C. A., Kanazawa, A., Jacoby, M. E. & Kramer, D. M. The proton to electron stoichiometry of steady-state photosynthesis in living plants: A proton-pumping Q cycle is continuously engaged. *Proc. Natl. Acad. Sci. U. S. A.* **97**, 14283–14288 (2000).

11. Electrical evidence for the field indicating absorption change in bioenergetic membranes. *FEBS Lett.* **37**, 307–310 (1973).

12. Cruz, J. A., Sacksteder, C. A., Kanazawa, A. & Kramer, D. M. Contribution of electric field (Delta psi) to steady-state transthylakoid proton motive force (pmf) in vitro and in vivo. control of pmf parsing into Delta psi and Delta pH by ionic strength. *Biochemistry* **40**, 1226–1237 (2001).

13. Avenson, T. J., Cruz, J. A. & Kramer, D. M. Modulation of energy-dependent quenching of excitons in antennae of higher plants. *Proc. Natl. Acad. Sci. U. S. A.* **101**, 5530–5535 (2004).

14. Cramer, W. A., Hasan, S. S. & Yamashita, E. The Q cycle of cytochrome bc complexes: A structure perspective. *Biochim. Biophys. Acta BBA - Bioenerg.* **1807**, 788–802 (2011).

15. Cramer, W. A. & Zhang, H. Consequences of the structure of the cytochrome b6f complex for its charge transfer pathways. *14th Eur. Bioenerg. Conf.* **1757**, 339–345 (2006).

16. Smirnov, A. Y. & Nori, F. Modeling the Q-cycle mechanism of transmembrane energy conversion. *Phys. Biol.* **9**, 016011 (2012).

17. Robert E. Blankenship. Chemiosmotic Coupling and ATP Synthesis. in *Molecular Mechanisms of Photosynthesis* 157–170 (John Wiley & Sons, Ltd, 2002). doi:10.1002/9780470758472.ch8.

18. Avenson, T. J., Cruz, J. A., Kanazawa, A. & Kramer, D. M. Regulating the proton budget of higher plant photosynthesis. *Proc. Natl. Acad. Sci. U. S. A.* **102**, 9709 (2005).

19. Hahn, A., Vonck, J., Mills, D. J., Meier, T. & Kühlbrandt, W. Structure, mechanism, and regulation of the chloroplast ATP synthase. *Science* **360**, eaat4318 (2018).

20. Allen, J. Photosynthesis of ATP-electrons, proton pumps, rotors, and poise. *Cell* **110**, 273–276 (2002).

21. LIVINGSTON, A. K., KANAZAWA, A., CRUZ, J. A. & KRAMER, D. M. Regulation of cyclic electron flow in C3 plants: differential effects of limiting photosynthesis at ribulose-1,5-bisphosphate carboxylase/oxygenase and glyceraldehyde-3-phosphate dehydrogenase. *Plant Cell Environ.* **33**, 1779–1788 (2010).

22. Heckman, D. S. *et al.* Molecular evidence for the early colonization of land by fungi and plants. *Science* **293**, 1129–1133 (2001).

23. Sanderson, M. J. Molecular data from 27 proteins do not support a Precambrian origin of land plants. *Am. J. Bot.* **90**, 954–956 (2003).

24. RAVEN, J. A. Physiological correlates of the morphology of early vascular plants. *Bot. J. Linn. Soc.* **88**, 105–126 (1984).

25. Niklas, K. J. The influence of gravity and wind on land plant evolution. *Rev. Palaeobot. Palynol.* **102**, 1–14 (1998).

26. Ruban, A. V., Johnson, M. P. & Duffy, C. D. P. The photoprotective molecular switch in the photosystem II antenna. *Photosyst. II* **1817**, 167–181 (2012).

27. Horton, P. Optimization of light harvesting and photoprotection: molecular mechanisms and physiological consequences. *Philos. Trans. R. Soc. Lond. B. Biol. Sci.* **367**, 3455–3465 (2012).

28. Ruban, A. V. Nonphotochemical Chlorophyll Fluorescence Quenching: Mechanism and Effectiveness in Protecting Plants from Photodamage. *Plant Physiol.* **170**, 1903–1916 (2016).

29. Barber, J. Molecular Basis of the Vulnerability of Photosystem II to Damage by Light. *Funct. Plant Biol.* **22**, 201–208 (1995).

30. *Non-Photochemical Quenching and Energy Dissipation in Plants, Algae and Cyanobacteria*. (Springer Netherlands, 2014). doi:10.1007/978-94-017-903-21.

31. Krause, G. H. & Weis, E. Chlorophyll Fluorescence and Photosynthesis: The Basics. *Annu. Rev. Plant Physiol. Plant Mol. Biol.* **42**, 313–349 (1991).

32. Horton, P., Ruban, A. V. & Walters, R. G. REGULATION OF LIGHT HARVESTING IN GREEN PLANTS. *Annu. Rev. Plant Physiol. Plant Mol. Biol.* **47**, 655–684 (1996).

33. Demmig, B., Winter, K., Krüger, A. & Czygan, F. C. Photoinhibition and zeaxanthin formation in intact leaves : a possible role of the xanthophyll cycle in the dissipation of excess light energy. *Plant Physiol.* **84**, 218–224 (1987).

34. Li, X.-P. *et al.* A pigment-binding protein essential for regulation of photosynthetic light harvesting. *Nature* **403**, 391–395 (2000).

35. Sylak-Glassman, E. J. *et al.* Distinct roles of the photosystem II protein PsbS and zeaxanthin in the regulation of light harvesting in plants revealed by fluorescence lifetime snapshots. *Proc. Natl. Acad. Sci.* **111**, 17498 (2014).

36. Murata, N. Control of excitation transfer in photosynthesis V. Correlation of membrane structure to regulation of excitation transfer between two pigment systems in isolated spinach chloroplasts. *Biochim. Biophys. Acta BBA - Bioenerg.* **245**, 365–372 (1971).

37. Briantais, J.-M., Vernotte, C., Picaud, M. & Krause, G. H. A quantitative study of the slow decline of chlorophyll a fluorescence in isolated chloroplasts. *Biochim. Biophys. Acta BBA - Bioenerg.* **548**, 128–138 (1979).

38. Wraight, C. A. & Crofts, A. R. Energy-dependent quenching of chlorophyll alpha fluorescence in isolated chloroplasts. *Eur. J. Biochem.* **17**, 319–327 (1970).

39. Weis, E. & Berry, J. A. Quantum efficiency of Photosystem II in relation to 'energy'-dependent quenching of chlorophyll fluorescence. *Biochim. Biophys. Acta BBA - Bioenerg.* **894**, 198–208 (1987).

40. Genty, B., Briantais, J.-M. & Baker, N. R. The relationship between the quantum yield of photosynthetic electron transport and quenching of chlorophyll fluorescence. *Biochim. Biophys. Acta BBA - Gen. Subj.* **990**, 87–92 (1989).

41. Nilkens, M. *et al.* Identification of a slowly inducible zeaxanthin-dependent component of non-photochemical quenching of chlorophyll fluorescence generated under steady-state conditions in Arabidopsis. *Biochim. Biophys. Acta BBA - Bioenerg.* **1797**, 466–475 (2010).

42. Malnoë, A. *et al.* The Plastid Lipocalin LCNP Is Required for Sustained Photoprotective Energy Dissipation in Arabidopsis. *Plant Cell* **30**, 196 (2018).

43. Malnoë, A. Photoinhibition or photoprotection of photosynthesis? Update on the (newly termed) sustained quenching component qH. *Integr. Approach Photoinhibition Photoprotection Photosynth.* **154**, 123–133 (2018).

44. Powles, S. B. Photoinhibition of Photosynthesis Induced by Visible Light. *Annu. Rev. Plant Physiol.* **35**, 15–44 (1984).

45. PRASIL, O., ADIR, N. & OHAD, I. Dynamics of photosystem II : mechanism of photoinhibition and recovery process. *Dyn. Photosyst. II Mech. Photoinhibition Recovery Process* **11**, 295–348 (1992).

46. Aro, E.-M., Virgin, I. & Andersson, B. Photoinhibition of Photosystem II. Inactivation, protein damage and turnover. *Biochim. Biophys. Acta BBA - Bioenerg.* **1143**, 113–134 (1993).

47. Andersson, B. & Aro, E.-M. Photodamage and D1 Protein Turnover in Photosystem II. in *Regulation of Photosynthesis* (eds. Aro, E.-M. & Andersson, B.) 377–393 (Springer Netherlands, 2001). doi:10.1007/0-306-48148-0_22.

48. Nash, D., Miyao, M. & Murata, N. Heat inactivation of oxygen evolution in Photosystem II particles and its acceleration by chloride depletion and exogenous manganese. *Biochim. Biophys. Acta BBA - Bioenerg.* **807**, 127–133 (1985).

49. Sicher, R. C. Glycolaldehyde Inhibition of Photosynthetic Carbon Assimilation by Isolated Chloroplasts and Protoplasts. in *Advances in Photosynthesis Research: Proceedings of the VIth International Congress on Photosynthesis, Brussels, Belgium, August 1–6, 1983 Volume 3* (ed. Sybesma, C.) 413–416 (Springer Netherlands, 1984). doi:10.1007/978-94-017-4973-2_94.

50. Takahashi, S. & Murata, N. Glycerate-3-phosphate, produced by CO2

fixation in the Calvin cycle, is critical for the synthesis of the D1 protein of photosystem II. *Biochim. Biophys. Acta BBA - Bioenerg.* **1757**, 198–205 (2006).

51. Yang, X. *et al.* Genetic engineering of the biosynthesis of glycinebetaine enhances thermotolerance of photosystem II in tobacco plants. *Planta* **225**, 719–733 (2007).

52. Moon, B. Y., Higashi, S., Gombos, Z. & Murata, N. Unsaturation of the membrane lipids of chloroplasts stabilizes the photosynthetic machinery against low-temperature photoinhibition in transgenic tobacco plants. *Proc. Natl. Acad. Sci.* **92**, 6219 (1995).

53. Zhang, S. & Scheller, H. V. Photoinhibition of Photosystem I at Chilling Temperature and Subsequent Recovery in Arabidopsis thaliana. *Plant Cell Physiol.* **45**, 1595–1602 (2004).

54. Sejima, T., Takagi, D., Fukayama, H., Makino, A. & Miyake, C. Repetitive short-pulse light mainly inactivates photosystem I in sunflower leaves. *Plant Cell Physiol.* **55**, 1184–1193 (2014).

55. Tikkanen, M. & Grebe, S. Switching off photoprotection of photosystem I - a novel tool for gradual PSI photoinhibition. *Physiol. Plant.* **162**, 156–161 (2018).

56. Dall'Osto, L., Caffarri, S. & Bassi, R. A mechanism of nonphotochemical energy dissipation, independent from PsbS, revealed by a conformational change in the antenna protein CP26. *Plant Cell* **17**, 1217–1232 (2005).

57. Ruban, A. V. & Johnson, M. P. Dynamics of higher plant photosystem cross-section associated with state transitions. *Photosynth. Res.* **99**, 173–183 (2009).

58. Bellafiore, S., Barneche, F., Peltier, G. & Rochaix, J.-D. State transitions and light adaptation require chloroplast thylakoid protein kinase STN7. *Nature* **433**, 892–895 (2005).

59. Rintamäki, E., Martinsuo, P., Pursiheimo, S. & Aro, E.-M. Cooperative regulation of light-harvesting complex II phosphorylation via the plastoquinol and ferredoxin-thioredoxin system in chloroplasts. *Proc. Natl. Acad. Sci.* **97**, 11644 (2000).

60. Fernyhough, P., Foyer, C. H. & Horton, P. Increase in the level of thylakoid protein phosphorylation in maize mesophyll chloroplasts by decrease in the transthylakoid pH gradient. *FEBS Lett.* **176**, 133–138 (1984).

61. Cazzaniga, S., Dall' Osto, L., Kong, S.-G., Wada, M. & Bassi, R. Interaction between avoidance of photon absorption, excess energy dissipation and zeaxanthin synthesis against photooxidative stress in Arabidopsis. *Plant J. Cell Mol. Biol.* **76**,

568–579 (2013).

62. Baker, N. R. Photoinhibition of Photosynthesis. in *Light as an Energy Source and Information Carrier in Plant Physiology* (eds. Jennings, R. C., Zucchelli, G., Ghetti, F. & Colombetti, G.) 89–97 (Springer US, 1996). doi:10.1007/978-1-4613-0409-8_7.

63. Brooks, M. D., Sylak-Glassman, E. J., Fleming, G. R. & Niyogi, K. K. A thioredoxin-like/β-propeller protein maintains the efficiency of light harvesting in Arabidopsis. *Proc. Natl. Acad. Sci.* **110**, E2733 (2013).

64. Frenkel, M. *et al.* Improper excess light energy dissipation in Arabidopsis results in a metabolic reprogramming. *BMC Plant Biol.* **9**, 12 (2009).

65. Külheim, C., Ågren, J. & Jansson, S. Rapid Regulation of Light Harvesting and Plant Fitness in the Field. *Science* **297**, 91 (2002).

66. Suorsa, M. *et al.* Proton gradient regulation 5 Is essential for proper acclimation of arabidopsis photosystem I to naturally and artificially fluctuating light conditions. *Plant Cell* **24**, 2934–2948 (2012).

67. Krieger, A., Moya, I. & Weis, E. Energy-dependent quenching of chlorophyll a fluorescence: effect of pH on stationary fluorescence and picosecond-relaxation kinetics in thylakoid membranes and Photosystem II preparations. *Biochim. Biophys. Acta BBA - Bioenerg.* **1102**, 167–176 (1992).

68. Krieger, A. & Weis, E. The role of calcium in the pH-dependent control of Photosystem II. *Photosynth. Res.* **37**, 117–130 (1993).

69. Horton, P. & Ruban, A. V. Regulation of Photosystem II. *Photosynth. Res.* **34**, 375–385 (1992).

70. Ruban, A. V., Rees, D., Noctor, G. D., Young, A. & Horton, P. Long-wavelength chlorophyll species are associated with amplification of high-energy-state excitation quenching in higher plants. *Biochim. Biophys. Acta BBA - Bioenerg.* **1059**, 355–360 (1991).

71. Ruban, A. V. & Horton, P. Spectroscopy of non-photochemical and photochemical quenching of chlorophyll fluorescence in leaves; evidence for a role of the light harvesting complex of Photosystem II in the regulation of energy dissipation. *Photosynth. Res.* **40**, 181–190 (1994).

72. Briantais, J.-M. Light-harvesting chlorophyll a-b complex requirement for regulation of Photosystem II photochemistry by non-photochemical quenching. *Photosynth. Res.* **40**, 287–294 (1994).

73. Jahns, P. & Krause, G. H. Xanthophyll cycle and energy-dependent

fluorescence quenching in leaves from pea plants grown under intermittent light. *Planta* **192**, 176–182 (1994).

74. Lokstein, H., Härtel, H., Hoffmann, P., Woitke, P. & Renger, G. The role of light-harvesting complex II in excess excitation energy dissipation: An in-vivo fluorescence study on the origin of high-energy quenching. *J. Photochem. Photobiol. B* **26**, 175–184 (1994).

75. Ruban, A., Rees, D., Pascal, A. & Horton, P. Mechanism of DpH-dependent dissipation of absorbed excitation energy by photosynthetic membranes. II. The relationship between LHCII aggregation in vitro and qE in isolated thylakoids. *Biochim. Biophys. Acta* **1102**, 39–44 (1992).

76. Ruban, A. & Horton, P. Mechanism of DpH-dependent dissipation of absorbed excitation energy by photosynthetic membranes. I: Spectroscopic analysis of isolated light-harvesting complexes. *Biochim. Biophys. Acta* **1102**, 30–38 (1992).

77. Yamamoto, H. Y., Nakayama, T. O. M. & Chichester, C. O. Studies on the light and dark interconversions of leaf xanthophylls. *Arch. Biochem. Biophys.* **97**, 168–173 (1962).

78. Noctor, G., Ruban, A. V. & Horton, P. Modulation of ΔpH-dependent nonphotochemical quenching of chlorophyll fluorescence in spinach chloroplasts. *Biochim. Biophys. Acta BBA - Bioenerg.* **1183**, 339–344 (1993).

79. Ruban, A. V., Young, A. & Horton, P. Modulation of chlorophyll fluorescence quenching in isolated light harvesting complex of Photosystem II. *Biochim. Biophys. Acta BBA - Bioenerg.* **1186**, 123–127 (1994).

80. Ruban, A. V. & Horton, P. The Xanthophyll Cycle Modulates the Kinetics of Nonphotochemical Energy Dissipation in Isolated Light-Harvesting Complexes, Intact Chloroplasts, and Leaves of Spinach. *Plant Physiol.* **119**, 531 (1999).

81. Ruban, A. V., Young, A. J., Pascal, A. A. & Horton, P. The Effects of Illumination on the Xanthophyll Composition of the Photosystem II Light-Harvesting Complexes of Spinach Thylakoid Membranes. *Plant Physiol.* **104**, 227 (1994).

82. Ruban, A. V., Lee, P. J., Wentworth, M., Young, A. J. & Horton, P. Determination of the stoichiometry and strength of binding of xanthophylls to the photosystem II light harvesting complexes. *J. Biol. Chem.* **274**, 10458–10465 (1999).

83. Farber, A., Young, A. J., Ruban, A. V., Horton, P. & Jahns, P. Dynamics of Xanthophyll-Cycle Activity in Different Antenna Subcomplexes in the Photosynthetic Membranes of Higher Plants (The Relationship between Zeaxanthin Conversion and Nonphotochemical Fluorescence Quenching). *Plant Physiol.* **115**, 1609 (1997).

84. Ruban, A. V., Young, A. J. & Horton, P. Induction of Nonphotochemical Energy Dissipation and Absorbance Changes in Leaves (Evidence for Changes in the State of the Light-Harvesting System of Photosystem II in Vivo). *Plant Physiol.* **102**, 741–750 (1993).

85. Bilger, W. & Björkman, O. Relationships among violaxanthin deepoxidation, thylakoid membrane conformation, and nonphotochemical chlorophyll fluorescence quenching in leaves of cotton (Gossypium hirsutum L.). *Planta* **193**, 238–246 (1994).

86. Yamamoto, H. Y. & Kamite, L. The effects of dithiothreitol on violaxanthin de-epoxidation and absorbance changes in the 500-nm region. *Biochim. Biophys. Acta BBA - Bioenerg.* **267**, 538–543 (1972).

87. Dominici, P. *et al.* Biochemical properties of the PsbS subunit of photosystem II either purified from chloroplast or recombinant. *J. Biol. Chem.* **277**, 22750–22758 (2002).

88. Li, X.-P. *et al.* Regulation of photosynthetic light harvesting involves intrathylakoid lumen pH sensing by the PsbS protein. *J. Biol. Chem.* **279**, 22866–22874 (2004).

89. Crouchman, S., Ruban, A. & Horton, P. PsbS enhances nonphotochemical fluorescence quenching in the absence of zeaxanthin. *FEBS Lett.* **580**, 2053–2058 (2006).

90. Niyogi, K. K., Grossman, A. R. & Björkman, O. Arabidopsis Mutants Define a Central Role for the Xanthophyll Cycle in the Regulation of Photosynthetic Energy Conversion. *Plant Cell* **10**, 1121 (1998).

91. Andersson, J., Walters, R. G., Horton, P. & Jansson, S. Antisense Inhibition of the Photosynthetic Antenna Proteins CP29 and CP26: Implications for the Mechanism of Protective Energy Dissipation. *Plant Cell* **13**, 1193 (2001).

92. Kovács, L. *et al.* Lack of the Light-Harvesting Complex CP24 Affects the Structure and Function of the Grana Membranes of Higher Plant Chloroplasts. *Plant Cell* **18**, 3106 (2006).

93. Dall'Osto, L. *et al.* Two mechanisms for dissipation of excess light in monomeric and trimeric light-harvesting complexes. *Nat. Plants* **3**, 17033 (2017).

94. Townsend, A. J. *et al.* The causes of altered chlorophyll fluorescence quenching induction in the Arabidopsis mutant lacking all minor antenna complexes. *20th Eur. Bioenerg. Conf.* **1859**, 666–675 (2018).

95. Johnson, M. P. *et al.* Photoprotective Energy Dissipation Involves the Reorganization of Photosystem II Light-Harvesting Complexes in the Grana

Membranes of Spinach Chloroplasts. *Plant Cell* **23**, 1468 (2011).

96. Goral, T. K. *et al.* Light-harvesting antenna composition controls the macrostructure and dynamics of thylakoid membranes in Arabidopsis. *Plant J.* **69**, 289–301 (2012).

97. Ware, M. A., Giovagnetti, V., Belgio, E. & Ruban, A. V. PsbS protein modulates non-photochemical chlorophyll fluorescence quenching in membranes depleted of photosystems. *Recent Prog. Stud. Struct. Funct. Photosyst. II* **152**, 301–307 (2015).

98. Ruban, A. V. Adaptive Reorganisation of the Light Harvesting Antenna. in *Photosynthesis and Bioenergetics* 189–219 (WORLD SCIENTIFIC, 2017). doi:10.1142/9789813230309_0009.

99. Correa-Galvis, V., Poschmann, G., Melzer, M., Stühler, K. & Jahns, P. PsbS interactions involved in the activation of energy dissipation in Arabidopsis. *Nat. Plants* **2**, 15225 (2016).

100. Sacharz, J., Giovagnetti, V., Ungerer, P., Mastroianni, G. & Ruban, A. V. The xanthophyll cycle affects reversible interactions between PsbS and light-harvesting complex II to control non-photochemical quenching. *Nat. Plants* **3**, 16225 (2017).

101. Ilioaia, C., Johnson, M. P., Horton, P. & Ruban, A. V. Induction of efficient energy dissipation in the isolated light-harvesting complex of Photosystem II in the absence of protein aggregation. *J. Biol. Chem.* **283**, 29505–29512 (2008).

102. van Oort, B., van Hoek, A., Ruban, A. V. & van Amerongen, H. Equilibrium between quenched and nonquenched conformations of the major plant light-harvesting complex studied with high-pressure time-resolved fluorescence. *J. Phys. Chem. B* **111**, 7631–7637 (2007).

103. Krüger, T. P. J., Novoderezhkin, V. I., Ilioaia, C. & van Grondelle, R. Fluorescence spectral dynamics of single LHCII trimers. *Biophys. J.* **98**, 3093–3101 (2010).

104. Ruban, A. V. *et al.* Identification of a mechanism of photoprotective energy dissipation in higher plants. *Nature* **450**, 575–578 (2007).

105. Müller, M. G. *et al.* Singlet Energy Dissipation in the Photosystem II Light-Harvesting Complex Does Not Involve Energy Transfer to Carotenoids. *ChemPhysChem* **11**, 1289–1296 (2010).

106. Pascal, A. A. *et al.* Molecular basis of photoprotection and control of photosynthetic light-harvesting. *Nature* **436**, 134–137 (2005).

107. Ruban, A. V. Light harvesting control in plants. *FEBS Lett.* **592**, 3030–3039 (2018).

108. Rumberg, B. & Siggel, U. pH changes in the inner phase of the thylakoids during photosynthesis. *Naturwissenschaften* **56**, 130–132 (1969).

109. Tikhonov, A. N., Khomutov, G. B., Ruuge, E. K. & Blumenfeld, L. A. Electron transport control in chloroplasts. Effects of photosynthetic control monitored by the intrathylakoid pH. *Biochim. Biophys. Acta BBA - Bioenerg.* **637**, 321–333 (1981).

110. Nishio, J. N. & Whitmarsh, J. Dissipation of the Proton Electrochemical Potential in Intact Chloroplasts (II. The pH Gradient Monitored by Cytochrome f Reduction Kinetics). *Plant Physiol.* **101**, 89 (1993).

111. Hurry, V., Anderson, J. M., Badger, M. R. & Price, G. D. Reduced levels of cytochrome b 6/f in transgenic tobacco increases the excitation pressure on Photosystem II without increasing sensitivity to photoinhibition in vivo. *Photosynth. Res.* **50**, 159–169 (1996).

112. Kramer, D. M., Sacksteder, C. A. & Cruz, J. A. How acidic is the lumen? *Photosynth. Res.* **60**, 151–163 (1999).

113. Åkerlund, H.-E., Andersson, B., Persson, A. & Albertsson, P.-Å. Isoelectric points of spinach thylakoid membrane surfaces as determined by cross partition. *Biochim. Biophys. Acta BBA - Biomembr.* **552**, 238–246 (1979).

114. Jahns, P., Latowski, D. & Strzalka, K. Mechanism and regulation of the violaxanthin cycle: The role of antenna proteins and membrane lipids. *Biochim. Biophys. Acta BBA - Bioenerg.* **1787**, 3–14 (2009).

115. Noctor, G., Rees, D., Young, A. & Horton, P. The relationship between zeaxanthin, energy-dependent quenching of chlorophyll fluorescence, and trans-thylakoid pH gradient in isolated chloroplasts. *Biochim. Biophys. Acta BBA - Bioenerg.* **1057**, 320–330 (1991).

116. Mehler, E. L., Fuxreiter, M., Simon, I. & Garcia-Moreno, E. B. The role of hydrophobic microenvironments in modulating pKa shifts in proteins. *Proteins* **48**, 283–292 (2002).

117. Thurlkill, R. L., Grimsley, G. R., Scholtz, J. M. & Pace, C. N. Hydrogen Bonding Markedly Reduces the pK of Buried Carboxyl Groups in Proteins. *J. Mol. Biol.* **362**, 594–604 (2006).

118. Kromdijk, J. *et al.* Improving photosynthesis and crop productivity by accelerating recovery from photoprotection. *Science* **354**, 857 (2016).

119. Ruban, A. V. Crops on the fast track for light. *Nature* **541**, 36–37 (2017).

120. Pribil, M., Pesaresi, P., Hertle, A., Barbato, R. & Leister, D. Role of Plastid Protein Phosphatase TAP38 in LHCII Dephosphorylation and Thylakoid Electron Flow. *PLOS Biol.* **8**, e1000288 (2010).

121. Shapiguzov, A. *et al.* The PPH1 phosphatase is specifically involved in LHCII dephosphorylation and state transitions in Arabidopsis. *Proc. Natl. Acad. Sci.* **107**, 4782 (2010).

122. Lunde, C., Jensen, P. E., Haldrup, A., Knoetzel, J. & Scheller, H. V. The PSI-H subunit of photosystem I is essential for state transitions in plant photosynthesis. *Nature* **408**, 613–615 (2000).

123. Pesaresi, P. *et al.* Arabidopsis STN7 Kinase Provides a Link between Short- and Long-Term Photosynthetic Acclimation. *Plant Cell* **21**, 2402 (2009).

124. Rochaix, J.-D. Role of thylakoid protein kinases in photosynthetic acclimation. *FEBS Lett.* **581**, 2768–2775 (2007).

125. Frenkel, M., Bellafiore, S., Rochaix, J.-D. & Jansson, S. Hierarchy amongst photosynthetic acclimation responses for plant fitness. *Physiol. Plant.* **129**, 455–459 (2007).

126. Tikkanen, M., Grieco, M., Kangasjärvi, S. & Aro, E.-M. Thylakoid Protein Phosphorylation in Higher Plant Chloroplasts Optimizes Electron Transfer under Fluctuating Light. *Plant Physiol.* **152**, 723 (2010).

127. Grieco, M., Tikkanen, M., Paakkarinen, V., Kangasjärvi, S. & Aro, E.-M. Steady-State Phosphorylation of Light-Harvesting Complex II Proteins Preserves Photosystem I under Fluctuating White Light. *Plant Physiol.* **160**, 1896–1910 (2012).

128. Tikkanen, M. *et al.* State transitions revisited—a buffering system for dynamic low light acclimation of Arabidopsis. *Plant Mol. Biol.* **62**, 779 (2006).

129. Fernyhough, P., Foyer, C. & Horton, P. The influence of metabolic state on the level of phosphorylation of the light-harvesting chlorophyll-protein complex in chloroplasts isolated from maize mesophyll. *Biochim. Biophys. Acta BBA - Bioenerg.* **725**, 155–161 (1983).

130. Allen, J. F. Protein phosphorylation — Carburettor of photosynthesis? *Trends Biochem. Sci.* **8**, 369–373 (1983).

131. Cardol, P. *et al.* Impaired respiration discloses the physiological significance of state transitions in Chlamydomonas. *Proc. Natl. Acad. Sci.* **106**, 15979 (2009).

132. Bulté, L., Gans, P., Rebéillé, F. & Wollman, F.-A. ATP control on state transitions in vivo in Chlamydomonas reinhardtii. *Biochim. Biophys. Acta BBA - Bioenerg.* **1020**, 72–80 (1990).

133. Takahashi, H., Clowez, S., Wollman, F.-A., Vallon, O. & Rappaport, F. Cyclic electron flow is redox-controlled but independent of state transition. *Nat. Commun.* **4**, 1954 (2013).

134. Kyle, D. J., Staehelin, L. A. & Arntzen, C. J. Lateral mobility of the light-harvesting complex in chloroplast membranes controls excitation energy distribution in higher plants. *Arch. Biochem. Biophys.* **222**, 527–541 (1983).

135. Allen, J. F. State Transitions--a Question of Balance. *Science* **299**, 1530 (2003).

136. Rozak, P. R., Seiser, R. M., Wacholtz, W. F. & Wise, R. R. Rapid, reversible alterations in spinach thylakoid appression upon changes in light intensity. *Plant Cell Environ.* **25**, 421–429 (2002).

137. Wood, W. H. J., Barnett, S. F. H., Flannery, S., Hunter, C. N. & Johnson, M. P. Dynamic Thylakoid Stacking Is Regulated by LHCII Phosphorylation but Not Its interaction with PSI. *Plant Physiol.* **180**, 2152–2166 (2019).

138. Anderson, J. M., Horton, P., Kim, E.-H. & Chow, W. S. Towards elucidation of dynamic structural changes of plant thylakoid architecture. *Philos. Trans. R. Soc. B Biol. Sci.* **367**, 3515–3524 (2012).

139. Joliot, P. & Johnson, G. N. Regulation of cyclic and linear electron flow in higher plants. *Proc. Natl. Acad. Sci. U. S. A.* **108**, 13317–13322 (2011).

140. ARNON, D. I., ALLEN, M. B. & WHATLEY, F. R. Photosynthesis by Isolated Chloroplasts. *Nature* **174**, 394–396 (1954).

141. Munekage, Y. *et al.* PGR5 Is Involved in Cyclic Electron Flow around Photosystem I and Is Essential for Photoprotection in Arabidopsis. *Cell* **110**, 361–371 (2002).

142. DalCorso, G. *et al.* A Complex Containing PGRL1 and PGR5 Is Involved in the Switch between Linear and Cyclic Electron Flow in Arabidopsis. *Cell* **132**, 273–285 (2008).

143. Peltier, G., Aro, E.-M. & Shikanai, T. NDH-1 and NDH-2 Plastoquinone Reductases in Oxygenic Photosynthesis. *Annu. Rev. Plant Biol.* **67**, 55–80 (2016).

144. Yamamoto, H. & Shikanai, T. PGR5-Dependent Cyclic Electron Flow Protects Photosystem I under Fluctuating Light at Donor and Acceptor Sides. *Plant Physiol.* **179**, 588 (2019).

145. Hertle, A. P. *et al.* PGRL1 Is the Elusive Ferredoxin-Plastoquinone Reductase in Photosynthetic Cyclic Electron Flow. *Mol. Cell* **49**, 511–523 (2013).

146. Sugimoto, K. *et al.* A single amino acid alteration in PGR5 confers resistance to antimycin A in cyclic electron transport around PSI. *Plant Cell Physiol.* **54**, 1525–1534 (2013).

147. Nandha, B., Finazzi, G., Joliot, P., Hald, S. & Johnson, G. N. The role of PGR5 in the redox poising of photosynthetic electron transport. *Biochim. Biophys. Acta BBA - Bioenerg.* **1767**, 1252–1259 (2007).

148. Wang, C., Takahashi, H. & Shikanai, T. PROTON GRADIENT REGULATION 5 contributes to ferredoxin-dependent cyclic phosphorylation in ruptured chloroplasts. *Biochim. Biophys. Acta Bioenerg.* **1859**, 1173–1179 (2018).

149. TAGAWA, K., TSUJIMOTO, H. Y. & ARNON, D. I. Role of chloroplast ferredoxin in the energy conversion process of photosynthesis. *Proc. Natl. Acad. Sci. U. S. A.* **49**, 567–572 (1963).

150. Cardol, P., De Paepe, R., Franck, F., Forti, G. & Finazzi, G. The onset of NPQ and Deltamu(H)+ upon illumination of tobacco plants studied through the influence of mitochondrial electron transport. *Biochim. Biophys. Acta* **1797**, 177–188 (2010).

151. Heber, U. & Walker, D. Concerning a Dual Function of Coupled Cyclic Electron Transport in Leaves. *Plant Physiol.* **100**, 1621 (1992).

152. Allahverdiyeva, Y., Suorsa, M., Tikkanen, M. & Aro, E.-M. Photoprotection of photosystems in fluctuating light intensities. *J. Exp. Bot.* **66**, 2427–2436 (2015).

153. Okegawa, Y. & Motohashi, K. M-Type Thioredoxins Regulate the PGR5/PGRL1-Dependent Pathway by Forming a Disulfide-Linked Complex with PGRL1. *Plant Cell* **32**, 3866 (2020).

154. Okegawa, Y. *et al.* A Balanced PGR5 Level is Required for Chloroplast Development and Optimum Operation of Cyclic Electron Transport Around Photosystem I. *Plant Cell Physiol.* **48**, 1462–1471 (2007).

155. Yamamoto, H., Peng, L., Fukao, Y. & Shikanai, T. An Src Homology 3 Domain-Like Fold Protein Forms a Ferredoxin Binding Site for the Chloroplast NADH Dehydrogenase-Like Complex in Arabidopsis. *Plant Cell* **23**, 1480 (2011).

156. Ogawa, T. A gene homologous to the subunit-2 gene of NADH dehydrogenase is essential to inorganic carbon transport of Synechocystis PCC6803. *Proc. Natl. Acad. Sci.* **88**, 4275 (1991).

157. Mi, H., Endo, T., Ogawa, T. & Asada, K. Thylakoid Membrane-Bound, NADPH-Specific Pyridine Nucleotide Dehydrogenase Complex Mediates Cyclic Electron Transport in the Cyanobacterium Synechocystis sp. PCC 6803. *Plant Cell Physiol.* **36**, 661–668 (1995).

158. Burrows, P. A., Sazanov, L. A., Svab, Z., Maliga, P. & Nixon, P. J. Identification of a functional respiratory complex in chloroplasts through analysis of tobacco mutants containing disrupted plastid genes. *EMBO J.* **17**, 868 (1998).

159. Shikanai, T. *et al.* Directed disruption of the tobacco ndhB gene impairs cyclic electron flow around photosystem I. *Proc. Natl. Acad. Sci. U. S. A.* **95**, 9705–9709 (1998).

160. Endo, T., Shikanai, T., Takabayashi, A., Asada, K. & Sato, F. The role of chloroplastic NAD(P)H dehydrogenase in photoprotection. *FEBS Lett.* **457**, 5–8 (1999).

161. Hashimoto, M., Endo, T., Peltier, G., Tasaka, M. & Shikanai, T. A nucleus-encoded factor, CRR2, is essential for the expression of chloroplast ndhB in Arabidopsis. *Plant J. Cell Mol. Biol.* **36**, 541–549 (2003).

162. Munekage, Y. *et al.* Cyclic electron flow around photosystem I is essential for photosynthesis. *Nature* **429**, 579 (2004).

163. Tsuyama, M. & Kobayashi, Y. Reduction of the primary donor P700 of photosystem I during steady-state photosynthesis under low light in Arabidopsis. *Photosynth. Res.* **99**, 37–47 (2009).

164. Sazanov, L. A., Burrows, P. A. & Nixon, P. J. The chloroplast Ndh complex mediates the dark reduction of the plastoquinone pool in response to heat stress in tobacco leaves. *FEBS Lett.* **429**, 115–118 (1998).

165. Casano, L. M., Martín, M. & Sabater, B. Hydrogen Peroxide Mediates the Induction of Chloroplastic Ndh Complex under Photooxidative Stress in Barley. *Plant Physiol.* **125**, 1450 (2001).

166. Wang, P. *et al.* Chloroplastic NAD(P)H Dehydrogenase in Tobacco Leaves Functions in Alleviation of Oxidative Damage Caused by Temperature Stress. *Plant Physiol.* **141**, 465 (2006).

167. Yamori, W., Sakata, N., Suzuki, Y., Shikanai, T. & Makino, A. Cyclic electron flow around photosystem I via chloroplast NAD(P)H dehydrogenase (NDH) complex performs a significant physiological role during photosynthesis and plant growth at low temperature in rice. *Plant J.* **68**, 966–976 (2011).

168. Yamori, W., Shikanai, T. & Makino, A. Photosystem I cyclic electron flow

via chloroplast NADH dehydrogenase-like complex performs a physiological role for photosynthesis at low light. *Sci. Rep.* **5**, 13908 (2015).

169. Yamori, W., Makino, A. & Shikanai, T. A physiological role of cyclic electron transport around photosystem I in sustaining photosynthesis under fluctuating light in rice. *Sci. Rep.* **6**, 20147 (2016).

170. Nakano, H., Yamamoto, H. & Shikanai, T. Contribution of NDH-dependent cyclic electron transport around photosystem I to the generation of proton motive force in the weak mutant allele of pgr5. *Biochim. Biophys. Acta BBA - Bioenerg.* **1860**, 369–374 (2019).

171. Peng, L., Shimizu, H. & Shikanai, T. The Chloroplast NAD(P)H Dehydrogenase Complex Interacts with Photosystem I in Arabidopsis*. *J. Biol. Chem.* **283**, 34873–34879 (2008).

172. Peng, L., Fukao, Y., Fujiwara, M., Takami, T. & Shikanai, T. Efficient operation of NAD(P)H dehydrogenase requires supercomplex formation with photosystem I via minor LHCI in Arabidopsis. *Plant Cell* **21**, 3623–3640 (2009).

173. Peng, L. & Shikanai, T. Supercomplex Formation with Photosystem I Is Required for the Stabilization of the Chloroplast NADH Dehydrogenase-Like Complex in Arabidopsis. *Plant Physiol.* **155**, 1629 (2011).

174. Iwai, M. *et al.* Isolation of the elusive supercomplex that drives cyclic electron flow in photosynthesis. *Nature* **464**, 1210–1213 (2010).

175. Yadav, K. N. S. *et al.* Supercomplexes of plant photosystem I with cytochrome b6f, light-harvesting complex II and NDH. *Biochim. Biophys. Acta BBA - Bioenerg.* **1858**, 12–20 (2017).

176. Zhang, H., Whitelegge, J. P. & Cramer, W. A. Ferredoxin:NADP+ Oxidoreductase Is a Subunit of the Chloroplast Cytochrome b6fComplex *. *J. Biol. Chem.* **276**, 38159–38165 (2001).

177. Hald, S., Nandha, B., Gallois, P. & Johnson, G. N. Feedback regulation of photosynthetic electron transport by NADP(H) redox poise. *Biochim. Biophys. Acta BBA - Bioenerg.* **1777**, 433–440 (2008).

178. Stroebel, D., Choquet, Y., Popot, J.-L. & Picot, D. An atypical haem in the cytochrome b6f complex. *Nature* **426**, 413–418 (2003).

179. Joliot, P., Béal, D. & Joliot, A. Cyclic electron flow under saturating excitation of dark-adapted Arabidopsis leaves. *Biochim. Biophys. Acta BBA - Bioenerg.* **1656**, 166–176 (2004).

180. Courteille, A. *et al.* Thioredoxin m4 Controls Photosynthetic Alternative

Electron Pathways in Arabidopsis. *Plant Physiol.* **161**, 508 (2013).

181. Nikkanen, L. *et al.* Regulation of cyclic electron flow by chloroplast NADPH-dependent thioredoxin system. *Plant Direct* **2**, e00093 (2018).

182. Geigenberger, P. & Fernie, A. R. Metabolic control of redox and redox control of metabolism in plants. *Antioxid. Redox Signal.* **21**, 1389–1421 (2014).

183. Buchanan, B. B. The Path to Thioredoxin and Redox Regulation in Chloroplasts. *Annu. Rev. Plant Biol.* **67**, 1–24 (2016).

184. Serrato, A. J., Pérez-Ruiz, J. M., Spínola, M. C. & Cejudo, F. J. A novel NADPH thioredoxin reductase, localized in the chloroplast, which deficiency causes hypersensitivity to abiotic stress in Arabidopsis thaliana. *J. Biol. Chem.* **279**, 43821–43827 (2004).

185. Pérez-Ruiz, J. M. *et al.* Rice NTRC is a high-efficiency redox system for chloroplast protection against oxidative damage. *Plant Cell* **18**, 2356–2368 (2006).

186. Okegawa, Y. & Motohashi, K. Chloroplastic thioredoxin m functions as a major regulator of Calvin cycle enzymes during photosynthesis in vivo. *Plant J. Cell Mol. Biol.* **84**, 900–913 (2015).

187. Kono, M., Noguchi, K. & Terashima, I. Roles of the Cyclic Electron Flow Around PSI (CEF-PSI) and O-2Dependent Alternative Pathways in Regulation of the Photosynthetic Electron Flow in Short-Term Fluctuating Light in Arabidopsis thaliana. *Plant Cell Physiol.* **55**, 990–1004 (2014).

188. Mekala, N. R., Suorsa, M., Rantala, M., Aro, E.-M. & Tikkanen, M. Plants Actively Avoid State Transitions upon Changes in Light Intensity: Role of Light-Harvesting Complex II Protein Dephosphorylation in High Light. *Plant Physiol.* **168**, 721–734 (2015).

189. Endo, T., Shikanai, T., Sato, F. & Asada, K. NAD(P)H Dehydrogenase-Dependent, Antimycin A-Sensitive Electron Donation to Plastoquinone in Tobacco Chloroplasts. *Plant Cell Physiol.* **39**, 1226–1231 (1998).

190. Breyton, C., Nandha, B., Johnson, G. N., Joliot, P. & Finazzi, G. Redox Modulation of Cyclic Electron Flow around Photosystem I in C3 Plants. *Biochemistry* **45**, 13465–13475 (2006).

191. Okegawa, Y., Kagawa, Y., Kobayashi, Y. & Shikanai, T. Characterization of Factors Affecting the Activity of Photosystem I Cyclic Electron Transport in Chloroplasts. *Plant Cell Physiol.* **49**, 825–834 (2008).

192. Joet, T. *et al.* Involvement of a plastid terminal oxidase in plastoquinone oxidation as evidenced by expression of the Arabidopsis thaliana enzyme in tobacco.

J. Biol. Chem. **277**, 31623–31630 (2002).

193. Wang, C., Yamamoto, H. & Shikanai, T. Role of cyclic electron transport around photosystem I in regulating proton motive force. *SI Chloroplast Biog.* **1847**, 931–938 (2015).

194. Kanazawa, A. & Kramer, D. M. In vivo modulation of nonphotochemical exciton quenching (NPQ) by regulation of the chloroplast ATP synthase. *Proc. Natl. Acad. Sci.* **99**, 12789 (2002).

195. Yoshida, K., Terashima, I. & Noguchi, K. Up-Regulation of Mitochondrial Alternative Oxidase Concomitant with Chloroplast Over-Reduction by Excess Light. *Plant Cell Physiol.* **48**, 606–614 (2007).

196. Majeran, W., Olive, J., Drapier, D., Vallon, O. & Wollman, F.-A. The Light Sensitivity of ATP Synthase Mutants ofChlamydomonas reinhardtii. *Plant Physiol.* **126**, 421 (2001).

197. Rott, M. *et al.* ATP synthase repression in tobacco restricts photosynthetic electron transport, CO2 assimilation, and plant growth by overacidification of the thylakoid lumen. *Plant Cell* **23**, 304–321 (2011).

198. Fischer, S. & Gräber, P. Comparison of ΔpH- and Δφ-driven ATP synthesis catalyzed by the H+-ATPases from Escherichia coli or chloroplasts reconstituted into liposomes. *FEBS Lett.* **457**, 327–332 (1999).

199. Rantala, S. *et al.* PGR5 and NDH-1 systems do not function as protective electron acceptors but mitigate the consequences of PSI inhibition. *Biochim. Biophys. Acta BBA - Bioenerg.* **1861**, 148154 (2020).

200. Wang, C. & Shikanai, T. Modification of Activity of the Thylakoid H(+)/K(+) Antiporter KEA3 Disturbs ΔpH-Dependent Regulation of Photosynthesis. *Plant Physiol.* **181**, 762–773 (2019).

201. Yamamoto, H., Takahashi, S., Badger, M. R. & Shikanai, T. Artificial remodelling of alternative electron flow by flavodiiron proteins in Arabidopsis. *Nat. Plants* **2**, 16012 (2016).

202. Yamamoto, H. & Shikanai, T. Does the Arabidopsis proton gradient regulation5 Mutant Leak Protons from the Thylakoid Membrane? *Plant Physiol.* **184**, 421 (2020).

203. Vicente, J. B., Gomes, C. M., Wasserfallen, A. & Teixeira, M. Module fusion in an A-type flavoprotein from the cyanobacterium Synechocystis condenses a multiple-component pathway in a single polypeptide chain. *Biochem. Biophys. Res. Commun.* **294**, 82–87 (2002).

204. Munekage, Y. *et al.* Cytochrome b6f mutation specifically affects thermal dissipation of absorbed light energy in Arabidopsis. *Plant J.* **28**, 351–359 (2001).

205. Jahns, P., Graf, M., Munekage, Y. & Shikanai, T. Single point mutation in the Rieske iron-sulfur subunit of cytochrome b6/f leads to an altered pH dependence of plastoquinol oxidation in Arabidopsis. *FEBS Lett.* **519**, 99–102 (2002).

206. Sétif, P. Electron-transfer kinetics in cyanobacterial cells: Methyl viologen is a poor inhibitor of linear electron flow. *Biochim. Biophys. Acta BBA - Bioenerg.* **1847**, 212–222 (2015).

207. Oxborough, K. & Horton, P. Characterisation of the effects of Antimycin A upon high energy state quenching of chlorophyll fluorescence (qE) in spinach and pea chloroplasts. *Photosynth. Res.* **12**, 119–127 (1987).

208. Joët, T., Cournac, L., Horvath, E. M., Medgyesy, P. & Peltier, G. Increased Sensitivity of Photosynthesis to Antimycin A Induced by Inactivation of the Chloroplast ndhB Gene. Evidence for a Participation of the NADH-Dehydrogenase Complex to Cyclic Electron Flow around Photosystem I1. *Plant Physiol.* **125**, 1919–1929 (2001).

209. Mehler, A. H. Studies on reactions of illuminated chloroplasts: I. Mechanism of the reduction of oxygen and other hill reagents. *Arch. Biochem. Biophys.* **33**, 65–77 (1951).

210. Joliot, P. & Joliot, A. Cyclic electron flow in C3 plants. *14th Eur. Bioenerg. Conf.* **1757**, 362–368 (2006).

211. Rees, D. & Horton, P. The mechanisms of changes in Photosystem II efficiency in spinach thylakoids. *Biochim. Biophys. Acta BBA - Bioenerg.* **1016**, 219–227 (1990).

212. Noctor, G. & Horton, P. Uncoupler titration of energy-dependent chlorophyll fluorescence quenching and Photosystem II Photochemical yield in intact pea chloroplasts. *Biochim. Biophys. Acta BBA - Bioenerg.* **1016**, 228–234 (1990).

213. Takizawa, K., Cruz, J. A., Kanazawa, A. & Kramer, D. M. The thylakoid proton motive force in vivo. Quantitative, non-invasive probes, energetics, and regulatory consequences of light-induced pmf. *Biochim. Biophys. Acta* **1767**, 1233–1244 (2007).

214. Szabó, I., Bergantino, E. & Giacometti, G. M. Light and oxygenic photosynthesis: energy dissipation as a protection mechanism against photo-oxidation. *EMBO Rep.* **6**, 629–634 (2005).

215. Schuhmann, H. & Adamska, I. Deg proteases and their role in protein quality

control and processing in different subcellular compartments of the plant cell. *Physiol. Plant.* **145**, 224–234 (2012).

216. Ort, D. R. & Oxborough, K. In Situ Regulation of Chloroplast Coupling Factor Activity. *Annu. Rev. Plant Physiol. Plant Mol. Biol.* **43**, 269–291 (1992).

217. Kramer, D. M. & Crofts, A. R. Activation of the chloroplast ATPase measured by the electrochromic change in leaves of intact plants. *Biochim. Biophys. Acta BBA - Bioenerg.* **976**, 28–41 (1989).

218. Kramer, D. M. *et al.* Regulation of coupling factor in field-grown sunflower: A Redox model relating coupling factor activity to the activities of other thioredoxin-dependent chloroplast enzymes. *Photosynth. Res.* **26**, 213–222 (1990).

219. Kohzuma, K. *et al.* Thioredoxin-insensitive plastid ATP synthase that performs moonlighting functions. *Proc. Natl. Acad. Sci.* **109**, 3293 (2012).

220. Kohzuma, K. *et al.* The Role of Light-Dark Regulation of the Chloroplast ATP Synthase. *Front. Plant Sci.* **8**, 1248–1248 (2017).

221. Roberts, I. N., Lam, X. T., Miranda, H., Kieselbach, T. & Funk, C. Degradation of PsbO by the Deg Protease HhoA Is Thioredoxin Dependent. *PLOS ONE* **7**, e45713 (2012).

222. Finazzi, G. *et al.* A zeaxanthin-independent nonphotochemical quenching mechanism localized in the photosystem II core complex. *Proc. Natl. Acad. Sci. U. S. A.* **101**, 12375 (2004).

223. Kalituho, L., Beran, K. C. & Jahns, P. The Transiently Generated Nonphotochemical Quenching of Excitation Energy in Arabidopsis Leaves Is Modulated by Zeaxanthin. *Plant Physiol.* **143**, 1861 (2007).

224. Suorsa, M. *et al.* PGR5-PGRL1-Dependent Cyclic Electron Transport Modulates Linear Electron Transport Rate in Arabidopsis thaliana. *Mol. Plant* **9**, 271–288 (2016).

225. Porra, R. J., Thompson, W. A. & Kriedemann, P. E. Determination of accurate extinction coefficients and simultaneous equations for assaying chlorophylls a and b extracted with four different solvents: verification of the concentration of chlorophyll standards by atomic absorption spectroscopy. *Biochim. Biophys. Acta BBA - Bioenerg.* **975**, 384–394 (1989).

226. Strecker, V., Wumaier, Z., Wittig, I. & Schägger, H. Large pore gels to separate mega protein complexes larger than 10 MDa by blue native electrophoresis: isolation of putative respiratory strings or patches. *Proteomics* **10**, 3379–3387 (2010).

227. Kang, D., Suh, M.-K., & 강철훈. Highly Sensitive and Fast Protein Detection with Coomassie Brilliant Blue in Sodium Dodecyl Sulfate-Polyacrylamide Gel Electrophoresis. *Bull. Korean Chem. Soc.* **23**, 1511–1512 (2002).

228. Nesvizhskii, A. I., Keller, A., Kolker, E. & Aebersold, R. A statistical model for identifying proteins by tandem mass spectrometry. *Anal. Chem.* **75**, 4646–4658 (2003).

229. Oxborough, K. & Baker, N. R. Resolving chlorophyll a fluorescence images of photosynthetic efficiency into photochemical and non-photochemical components – calculation of qP and Fv-/Fm-; without measuring Fo-; *Photosynth. Res.* **54**, 135–142 (1997).

230. Maxwell, K. & Johnson, G. N. Chlorophyll fluorescence—a practical guide. *J. Exp. Bot.* **51**, 659–668 (2000).

231. Lazár, D. Chlorophyll a fluorescence induction1Dedicated to Docent Jan Nauš on the occasion of his 50th birthday.1. *Biochim. Biophys. Acta BBA - Bioenerg.* **1412**, 1–28 (1999).

232. Kramer, D. M., Johnson, G., Kiirats, O. & Edwards, G. E. New Fluorescence Parameters for the Determination of QA Redox State and Excitation Energy Fluxes. *Photosynth. Res.* **79**, 209 (2004).

233. Holzwarth, A. R., Lenk, D. & Jahns, P. On the analysis of non-photochemical chlorophyll fluorescence quenching curves: I. Theoretical considerations. *Biochim. Biophys. Acta BBA - Bioenerg.* **1827**, 786–792 (2013).

234. Krause, G. H. & Jahns, P. Non-photochemical Energy Dissipation Determined by Chlorophyll Fluorescence Quenching: Characterization and Function. in *Chlorophyll a Fluorescence: A Signature of Photosynthesis* (eds. Papageorgiou, G. C. & Govindjee) 463–495 (Springer Netherlands, 2004). doi:10.1007/978-1-4020-3218-9_18.

235. Krause, G. & Jahns, P. Pulse Amplitude Modulated Chlorophyll Fluorometry and its Application in Plant Science. in (2003).

236. Klughammer, C. & Schreiber, U. An improved method, using saturating light pulses, for the determination of photosystem I quantum yield via P700+-absorbance changes at 830 nm. *Planta* **192**, 261–268 (1994).

237. Klughammer, C. & Schreiber, U. Saturation Pulse method for assessment of energy conversion in PS I. *PAM Appl. Notes* **1**, (2008).

238. Kramer, D. M., Sacksteder, C. A. & Cruz, J. A. How acidic is the lumen? *Photosynth. Res.* **60**, 151–163 (1999).

239. Kramer, D. M., Cruz, J. A. & Kanazawa, A. Balancing the central roles of the thylakoid proton gradient. *Trends Plant Sci.* **8**, 27–32 (2003).

240. A. B. Ryzhikov, A. N. Tikhonov. Regulation of the speed of electron transfer in photosynthetic membranes of higher plants. *Biophysics* (1988).

241. Tikhonov, A. N. pH-Dependent regulation of electron transport and ATP synthesis in chloroplasts. *Photosynth. Res.* **116**, 511–534 (2013).

242. Tikhonov, A. N. The cytochrome b6f complex at the crossroad of photosynthetic electron transport pathways. *Photosynth. Res. Sustain.* **81**, 163–183 (2014).

243. Tikhonov, A.N.; Khomutov, G.B.; Ruuge, E.K. Electron transport control in chloroplasts. Effects of magnesium ions on the electron flow between two photosystems. *Photobiochem. Photobiophys.* (2013).

244. Butler, W. L. Energy Distribution in the Photochemical Apparatus of Photosynthesis. *Annu. Rev. Plant Physiol.* **29**, 345–378 (1978).

245. Pfündel, E. Estimating the contribution of Photosystem I to total leaf chlorophyll fluorescence. *Photosynth. Res.* **56**, 185–195 (1998).

246. Baker, N. R. Chlorophyll fluorescence: a probe of photosynthesis in vivo. *Annu. Rev. Plant Biol.* **59**, 89–113 (2008).

247. Armbruster, U. *et al.* Arabidopsis CURVATURE THYLAKOID1 Proteins Modify Thylakoid Architecture by Inducing Membrane Curvature. *Plant Cell* **25**, 2661–2678 (2013).

248. Johnson, G. N. Physiology of PSI cyclic electron transport in higher plants. *Biochim. Biophys. Acta BBA - Bioenerg.* **1807**, 384–389 (2011).

249. Yamori, W. & Shikanai, T. Physiological Functions of Cyclic Electron Transport Around Photosystem I in Sustaining Photosynthesis and Plant Growth. *Annu. Rev. Plant Biol.* **67**, 81–106 (2016).

250. Peter Horton. Interactions between electron transfer and carbon assimilation. in *Photosynthetic Mechanisms and the Environment* 135–187 (Elsevier).

251. Kramer, D. M., Avenson, T. J. & Edwards, G. E. Dynamic flexibility in the light reactions of photosynthesis governed by both electron and proton transfer reactions. *Trends Plant Sci.* **9**, 349–357 (2004).

252. Kramer, D. M. & Evans, J. R. The Importance of Energy Balance in Improving Photosynthetic Productivity. *Plant Physiol.* **155**, 70–78 (2011).

253. Ballottari, M., Dall'Osto, L., Morosinotto, T. & Bassi, R. Contrasting Behavior of Higher Plant Photosystem I and II Antenna Systems during Acclimation. *J. Biol. Chem.* **282**, 8947–8958 (2007).

254. Goss, T. & Hanke, G. The end of the line: can ferredoxin and ferredoxin NADP(H) oxidoreductase determine the fate of photosynthetic electrons? *Curr. Protein Pept. Sci.* **15**, 385–393 (2014).

255. Roach, T. & Krieger-Liszkay, A. The role of the PsbS protein in the protection of photosystems I and II against high light in Arabidopsis thaliana. *Biochim. Biophys. Acta BBA - Bioenerg.* **1817**, 2158–2165 (2012).

256. Kono, M., Yamori, W., Suzuki, Y. & Terashima, I. Photoprotection of PSI by Far-Red Light Against the Fluctuating Light-Induced Photoinhibition in Arabidopsis thaliana and Field-Grown Plants. *Plant Cell Physiol.* **58**, 35–45 (2017).

257. Pettai, H., Oja, V., Freiberg, A. & Laisk, A. Photosynthetic activity of far-red light in green plants. *Biochim. Biophys. Acta BBA - Bioenerg.* **1708**, 311–321 (2005).

258. Gollan, P. J., Lima-Melo, Y., Tiwari, A., Tikkanen, M. & Aro, E.-M. Interaction between photosynthetic electron transport and chloroplast sinks triggers protection and signalling important for plant productivity. *Philos. Trans. R. Soc. B Biol. Sci.* **372**, 20160390 (2017).

259. Scheller, H. V. & Haldrup, A. Photoinhibition of photosystem I. *Planta* **221**, 5–8 (2005).

260. Kou, J., Takahashi, S., Fan, D.-Y., Badger, M. R. & Chow, W. S. Partially dissecting the steady-state electron fluxes in Photosystem I in wild-type and pgr5 and ndh mutants of Arabidopsis. *Front. Plant Sci.* **6**, 758–758 (2015).

261. Kato, Y., Sugimoto, K. & Shikanai, T. NDH-PSI Supercomplex Assembly Precedes Full Assembly of the NDH Complex in Chloroplast. *Plant Physiol.* **176**, 1728 (2018).

262. Wood, W. H. J. & Johnson, M. P. Modeling the Role of LHCII-LHCII, PSII-LHCII, and PSI-LHCII Interactions in State Transitions. *Biophys. J.* **119**, 287–299 (2020).